

Universiteit
Leiden
The Netherlands

Vaccination and targeted therapy using liposomes : opportunities for treatment of atherosclerosis and cancer

Benne, N.

Citation
Benne, N. (2020, September 8). *Vaccination and targeted therapy using liposomes : opportunities for treatment of atherosclerosis and cancer*. Retrieved from https://hdl.handle.net/1887/136519

Version:	Publisher's Version
License:	Licence agreement concerning inclusion of doctoral thesis in the Institutional Repository of the University of Leiden
Downloaded from:	https://hdl.handle.net/1887/136519

Note: To cite this publication please use the final published version (if applicable).

Cover Page



Universiteit Leiden



The handle http://hdl.handle.net/1887/136519 holds various files of this Leiden University dissertation.

Author: Benne, N.
Title: Vaccination and targeted therapy using liposomes : opportunities for treatment of atherosclerosis and cancer
Issue Date: 2020-09-08

Vaccination and Targeted Therapy Using Liposomes

Opportunities for Treatment of Atherosclerosis and Cancer

Naomi Benne

Cover design: Naomi Benne

About the cover: NTA image of liposomes

Thesis lay-out: Naomi Benne

Printing: Ridderprint | www.ridderprint.nl

© Naomi Benne, 2020

ISBN: 978-94-6375-946-5

All rights reserved. No part of this book may be reproduced in any form or by any means without permission of the author.

Vaccination and Targeted Therapy Using Liposomes

Opportunities for Treatment of Atherosclerosis and Cancer

Proefschrift

Ter verkrijging van de graad van Doctor aan de Universiteit Leiden,
op gezag van Rector Magnificus prof. mr. C.J.J.M. Stolker,
volgens besluit van het College voor Promoties
te verdedigen op 8 september 2020
klokke 10:00 uur

Door

Naomi Benne
Geboren te Heemskerk
in 1993

Promotor: Prof. Dr. W. Jiskoot, Prof. Dr. J. Kuiper
Co-promotor: Dr. B. A. Slütter

Promotiecommissie:
Prof. Dr. H. Irth (chair)
Prof. Dr. J. A. Bouwstra (secretary)
Prof. Dr. E. Mastrobattista (Utrecht University, NL)
Prof. Dr. Y. Perrie (University of Strathclyde, UK)
Prof. Dr. W. van Eden (Utrecht University, NL)

The research described in this thesis was performed at the Division Biotherapeutics of the Leiden Academic Centre for Drug Research (LACDR), Leiden University (Leiden, The Netherlands).

Table of Contents

Chapter 1: General Introduction
3

Chapter 2: Orchestrating Immune Responses: How Size, Shape and Rigidity Affect the Immunogenicity of Particulate Vaccines
15

Chapter 3: Atomic Force Microscopy Measurements of Anionic Liposomes Reveal the Effect of Liposomal Rigidity on Antigen-Specific Regulatory T Cell Responses
51

Chapter 4: Anionic 1,2-Distearoyl-sn-Glycero-3-Phosphoglycerol (DSPG) Liposomes Induce Antigen-Specific Regulatory T Cells and Prevent Atherosclerosis in Mice
83

Chapter 5: Complement Receptor Targeted Liposomes Encapsulating the Liver X Receptor Agonist GW3965 Accumulate in and Stabilize Atherosclerotic Plaques
121

Chapter 6: An Accelerated Prime-Boost Strategy with cdiGMP-Containing Liposomes Induces Large and Long-Lasting CD8 T Cell Responses Against Neoepitopes and Eliminates Tumors in Mice
147

Chapter 7: General Discussion and Perspectives
173

Appendix: Dutch summary, curriculum vitae and list of publications
191

1

General Introduction

The immune system protects the body from infections by pathogens, such as viruses, bacteria and parasites, and sustains homeostasis. The immune system is broadly grouped into two branches: innate immunity and adaptive immunity. On the one hand, efficient elimination of pathogens requires fast recognition and clearance (phagocytosis), which is performed by immune cells of the innate immune system, such as macrophages and dendritic cells (DCs), which sense pathogens using pattern recognition receptors (PRRs)[1]. On the other hand, the adaptive immune system is involved with removing pathogens at later stages, using T and B lymphocytes which can recognize antigens. In this way, the adaptive immune system has a slower response time, but is more specific than the innate immune system and importantly has the ability to form immunological memory[2]. Antigen-presenting cells (APCs), such as DCs and macrophages, are essential for the interaction between the innate and adaptive immune system. This is due to these cells' ability to process pathogen-derived antigens after phagocytosis, and present parts of these antigens in the form of peptides on human leukocyte antigen (HLA) molecules, or major histocompatibility complex (MHC) class I or II molecules in the mouse. An antigenic peptide presented on such a molecule is then recognized by a T cell receptor (TCR), triggering an immune response; MHC-I and MHC-II activate $CD8^+$ and $CD4^+$ T cells, respectively[3]. $CD8^+$ T cells can kill target cells, such as cancer cells and cells that are infected[4]. Upon activation, they secrete interferon (IFN)-γ and tumor necrosis factor (TNF)-α, which are pro-inflammatory molecules that maintain the inflammatory environment[5,6]. These cytokines, in turn, can stimulate other immune cells, such as APCs and $CD4^+$ T cells[5]. $CD4^+$ T cells, also known as T helper (Th) cells, are important for their ability to positively or negatively regulate the magnitude of immune responses by interactions with B cells, $CD8^+$ T cells, and APCs. There are several types of $CD4^+$ T cell subsets that can arise from naïve $CD4^+$ T cells (Th0) depending on the inflammatory environment, including Th1, Th2, Th17 and regulatory T cells (Tregs) (Table 1)[7]. Th1 cells express the transcription factor T-bet and are induced by IFN-γ, interleukin (IL)-12 and IL-18[8,9]. Th1 cells, in turn, can secrete IFN-γ, TNF-α, and IL-2[7]. IL-2 is an important cytokine for T cell differentiation, as it can interact with all other $CD4^+$ T cell subtypes[10]. Th1 cells can also activate $CD8^+$ T cells and stimulate macrophages to become pro-inflammatory[11], generating a pro-inflammatory feedback loop. Th2 cells are activated by IL-4 and IL-33 and express the transcription factor Gata-3[12]. They produce IL-4, IL-5, and IL-13[11]. IL-4 induces B-cell class switching to immunoglobulin (Ig)E and suppresses Th1 responses[13]. IL-13 has similar effects to IL-4[14]. IL-5 supports B cell differentiation and enhances proliferation of eosinophils[15]. Th2 cells are thereby involved in allergic responses[12]. Th17 cells play an important role in auto-immune diseases and are vital for defense against extracellular bacterial and fungal infections[7]. They express RORγT and are induced by IL-6, IL-21, and transforming growth factor (TGF)-β. IL-6 is a pro-inflammatory cytokine[16], while TGF-β has inhibitory effects on immune cells, such as T cells, B cells, and macrophages[17]. IL-21 is implicated in several autoimmune diseases[18]. Th17 cells secrete IL-17, IL-21, IL-22, and IL-25[19]. IL17 and IL-25 are pro-inflammatory cytokines that act on many different cell types to stimulate the immune response[18]. IL-21 initiates an autoamplification loop for Th17 differentiation[18]. IL-22 is important for protection against infections[18]. Tregs are also induced by TGF-β, but in the absence of IL-6. They express the transcription factor FoxP3[20]. Tregs are important for the resolution of inflammation after infection, immune suppression, and immune homeostasis[21]. They

do so by producing the anti-inflammatory cytokines IL-10 and TGF-β[20]. Since both $CD8^+$ and $CD4^+$ T cells are important in the immune response, many diseases such as infection, allergy, cancer and autoimmune diseases involve an over- or under-active T cell response. In this thesis, we focus on two such diseases; atherosclerosis and cancer, which are the number 1 and 2 causes of death in the western world, respectively[22,23].

Table 1: Signature cytokines and function of selected $CD4^+$ T cell subsets.

$CD4^+$ T cell subset	Signature cytokines	Function
Th1	IFN-γ, TNF, IL-2	Fighting intracellular pathogens, cell-mediated inflammation, enhancing proinflammatory cytokine production
Th2	IL-4, IL-5, IL-13	Fighting helminth parasites, antibody-mediated inflammation
Th17	IL-17, IL-22, IL-21, IL-25	Fighting bacterial and fungal infections, recruitment of other immune cells, autoimmunity, enhancing proinflammatory cytokine production
Treg	IL-10, TGF-β	Suppressing other immune cells, maintaining immune tolerance, suppressing autoreactive T cells

Auto-immune diseases are examples of an over-active immune response, such as in a classic autoimmune disease like rheumatoid arthritis, but also in atherosclerosis[24-26]. Atherosclerosis is the predominant underlying pathology of cardiovascular disease which affects millions of people world-wide[22]. It is characterized by the accumulation of lipids in the form of low-density lipoprotein (LDL) in the subendothelial space in medium and large-sized arteries which leads to chronic inflammation[27]. This inflammation causes the modification of LDL to oxidized LDL (oxLDL), which attract immune cells such as monocytes[27]. Monocytes can differentiate into macrophages, and these, in turn, can phagocytose oxLDL, which leads to foam cell formation and plaque formation[28]. There are many different immune cells present in the atherosclerotic plaque, such as DCs, T and B lymphocytes[28,29]. While there is still debate about the specific role of T cells in atherosclerosis, it is generally accepted that Th1 cells progress the disease, while Tregs are protective[25,30]. Indeed, Tregs have abnormal activity in atherosclerosis[31]. Reestablishing immune homeostasis through induction of Tregs may, therefore, be an effective therapeutic approach[25].

As opposed to auto-immune diseases, cancer is an example of a disease associated with a dysfunctional pro-inflammatory immune response. Cancer is a major health concern, with approximately 1.7 million diagnoses and an estimated 600,000 deaths in the United States in the year 2019[23]. Cancer comprises a group of diseases involving abnormal sustained cell proliferation, replication, and survival. Benign cancers are contained and will not spread to other parts of the body, while malignant tumors have the potential to metastasize[32]. In cancer, T cells can recognize tumor-associated antigens[33,34]. These antigens can be tumor-associated antigens which are epitopes that are expressed on healthy cells but over-expressed on tumor cells[35]. Another type of tumor antigens are neoantigens. These result from non-synonymous somatic mutations that encode new amino acid residues, leading to new peptides that can be presented

on the cell surface of tumor cells[36]. However, the tumor can escape immune detection and attack by inducing immunosuppression. The main challenge in cancer treatment is, therefore, to induce strong pro-inflammatory $CD8^+$ and $CD4^+$ T cell responses to overcome this immune escape[37].

The goal of immunotherapy is to manipulate $CD4^+$ and $CD8^+$ T cell responses to either become more active to fight diseases such as infections or cancer[38], or to suppress the immune system in the case of auto-immune diseases or chronic inflammatory diseases[39]. Strategies include cytokine therapy[40], cell-based therapies (DCs[41] or T cells[42]) or the use of immune active drugs[43]. However, often these are non-specific, labor-intensive and expensive to make, quickly degraded or metabolized in the body, and/or have side effects at therapeutic doses[44-49]. Nanoparticulate drug delivery systems can overcome the limitations of immunotherapy; they can be designed to protect the drugs/biologicals and (indirectly) target specific immune cells, which allows for therapeutic efficacy, reduces the required dose and minimizes side-effects[50]. Nanoparticles can be made of different materials, such as polymers[51], metals[52], lipids[53], proteins[54], or a combination of the above. The choice of material depends on multiple factors, such as the properties of the cargo, the desired release rate of the cargo (i.e. sustained, delayed, burst), and the desired pharmacokinetics and biodistribution. Some of these materials have intrinsic immune effects[55], which makes them very interesting for use in immunotherapy. For instance, particles displaying the polymer poly(maleic anhydride-alt-1-octadecene)[56] or the anionic phospholipid phosphatidylglycerol[57] on their surface can induce tolerance. Conversely, particles composed of cationic phospholipids[58] or the polymer PC7A[59] can have strong pro-inflammatory effects. Furthermore, the physicochemical properties of the particles such as size, shape, rigidity (as reviewed in **chapter 2**), and charge[60] can affect the immune response. For example, small nano-sized particles show higher uptake by APCs and stronger cellular Th1 responses than larger particles[61].

Here we focus on liposomes because they have been FDA-approved for certain therapies[62], they can encapsulate a range of compounds, and their properties can be specifically tuned to induce immunogenicity or tolerance[53]. Liposomes are particles consisting of one or more lipid bilayers encapsulating an aqueous core. Both the liposomal composition and the formulation process determine the physicochemical properties of liposomes[53]. When using liposomes as a vaccine delivery system, their physicochemical properties can be tuned to obtain the desired immune response[63]. In this thesis, we prepared immune-suppressing liposomes to treat atherosclerosis, and immune-activating liposomes to treat cancer. Apart from APC uptake, liposomes can be functionalized with targeting molecules to be retained by other cell types or tissues. This allows for the delivery of drug substances into specific cells which may otherwise not be reached when using non-delivery approaches[64]. We used this approach to target liposomes to atherosclerotic plaques to deliver a drug substance to reverse foam cell formation.

Thesis Outline

Since liposomes are very versatile drug delivery systems, the research presented here focuses on using liposomes in two different treatment strategies; vaccination and delivery of a small molecule, and in two different disease models; cancer and atherosclerosis. For each of these treatment strategies, the liposomal formulation was tailored to obtain the desired therapeutic effect. **Chapter 2** reviews some of the most important physicochemical properties (size, shape, and rigidity) that determine the immunological effects of liposomes in the body. In **chapter 3** we present a detailed study on the effect of liposomal rigidity, as measured by atomic force microscopy, on antigen-specific Treg responses for anionic liposomes. In **chapter 4**, we show that our optimized anionic liposomes can induce potent antigen-specific Treg responses, and can be used to delay atherosclerosis progression in a mouse model. **Chapter 5** also focuses on liposomal treatment of atherosclerosis, but here liposomes were prepared to target to foam cells in atherosclerotic plaques to deliver a small molecule. **Chapter 6** again centers around using liposomes in immunotherapy; we used cationic liposomes in combination with an adjuvant to treat cancer in mice. Finally, we summarize the overall findings in **chapter 7** and discuss perspectives of using liposomes for vaccination and targeted drug delivery.

References

1 Akira, S., Uematsu, S. & Takeuchi, O. Pathogen recognition and innate immunity. *Cell* **124**, 783-801, doi:10.1016/j.cell.2006.02.015 (2006).

2 Iwasaki, A. & Medzhitov, R. Regulation of adaptive immunity by the innate immune system. *Science* **327**, 291-295, doi:10.1126/science.1183021 (2010).

3 Guermonprez, P., Valladeau, J., Zitvogel, L., Thery, C. & Amigorena, S. Antigen presentation and T cell stimulation by dendritic cells. *Annu Rev Immunol* **20**, 621-667, doi:10.1146/annurev.immunol.20.100301.064828 (2002).

4 Zhang, N. & Bevan, M. J. CD8(+) T cells: foot soldiers of the immune system. *Immunity* **35**, 161-168, doi:10.1016/j.immuni.2011.07.010 (2011).

5 Schroder, K., Hertzog, P. J., Ravasi, T. & Hume, D. A. Interferon-gamma: an overview of signals, mechanisms and functions. *J Leukoc Biol* **75**, 163-189, doi:10.1189/jlb.0603252 (2004).

6 Idriss, H. T. & Naismith, J. H. TNF alpha and the TNF receptor superfamily: structure-function relationship(s). *Microscopy research and technique* **50**, 184-195, doi:10.1002/1097-0029(20000801)50:3<184::AID-JEMT2>3.0.CO;2-H (2000).

7 Raphael, I., Nalawade, S., Eagar, T. N. & Forsthuber, T. G. T cell subsets and their signature cytokines in autoimmune and inflammatory diseases. *Cytokine* **74**, 5-17, doi:10.1016/j.cyto.2014.09.011 (2015).

8 Brunda, M. J. Interleukin-12. *J Leukoc Biol* **55**, 280-288, doi:10.1002/jlb.55.2.280 (1994).

9 Gracie, J. A., Robertson, S. E. & McInnes, I. B. Interleukin-18. *J Leukoc Biol* **73**, 213-224, doi:10.1189/jlb.0602313 (2003).

10 Liao, W., Lin, J. X. & Leonard, W. J. IL-2 family cytokines: new insights into the complex roles of IL-2 as a broad regulator of T helper cell differentiation. *Curr Opin Immunol* **23**, 598-604, doi:10.1016/j.coi.2011.08.003 (2011).

11 Romagnani, S. Th1/Th2 cells. *Inflammatory bowel diseases* **5**, 285-294, doi:10.1097/00054725-199911000-00009 (1999).

12 Walker, J. A. & McKenzie, A. N. J. TH2 cell development and function. *Nat Rev Immunol* **18**, 121-133, doi:10.1038/nri.2017.118 (2018).

13 Choi, P. & Reiser, H. IL-4: role in disease and regulation of production. *Clin Exp Immunol* **113**, 317-319, doi:10.1046/j.1365-2249.1998.00690.x (1998).

14 Wynn, T. A. IL-13 effector functions. *Annu Rev Immunol* **21**, 425-456, doi:10.1146/annurev.immunol.21.120601.141142 (2003).

15 Kouro, T. & Takatsu, K. IL-5- and eosinophil-mediated inflammation: from discovery to therapy. *International Immunology* **21**, 1303-1309, doi:10.1093/intimm/dxp102 (2009).

16 Kimura, A. & Kishimoto, T. IL-6: Regulator of Treg/Th17 balance. *European Journal of Immunology* **40**, 1830-1835, doi:10.1002/eji.201040391 (2010).

17 Li, M. O., Wan, Y. Y., Sanjabi, S., Robertson, A. K. & Flavell, R. A. Transforming growth factor-beta regulation of immune responses. *Annu Rev Immunol* **24**, 99-146, doi:10.1146/annurev.immunol.24.021605.090737 (2006).

18 Korn, T., Bettelli, E., Oukka, M. & Kuchroo, V. K. IL-17 and Th17 Cells. *Annual Review of Immunology* **27**, 485-517, doi:10.1146/annurev.immunol.021908.132710

(2009).
19 Damsker, J. M., Hansen, A. M. & Caspi, R. R. Th1 and Th17 cells: adversaries and collaborators. *Ann N Y Acad Sci* **1183**, 211-221, doi:10.1111/j.1749-6632.2009.05133.x (2010).
20 Mallat, Z., Ait-Oufella, H. & Tedgui, A. Regulatory T-cell immunity in atherosclerosis. *Trends Cardiovasc Med* **17**, 113-118, doi:10.1016/j.tcm.2007.03.001 (2007).
21 Sakaguchi, S., Yamaguchi, T., Nomura, T. & Ono, M. Regulatory T cells and immune tolerance. *Cell* **133**, 775-787, doi:10.1016/j.cell.2008.05.009 (2008).
22 Wang, H. *et al.* Global, regional, and national life expectancy, all-cause mortality, and cause-specific mortality for 249 causes of death, 1980–2015: a systematic analysis for the Global Burden of Disease Study 2015. *The Lancet* **388**, 1459-1544, doi:10.1016/s0140-6736(16)31012-1 (2016).
23 Siegel, R. L., Miller, K. D. & Jemal, A. Cancer statistics, 2019. *CA Cancer J Clin* **69**, 7-34, doi:10.3322/caac.21551 (2019).
24 Clemente-Casares, X. *et al.* Expanding antigen-specific regulatory networks to treat autoimmunity. *Nature* **530**, 434-440, doi:10.1038/nature16962 (2016).
25 Foks, A. C., Lichtman, A. H. & Kuiper, J. Treating atherosclerosis with regulatory T cells. *Arterioscler Thromb Vasc Biol* **35**, 280-287, doi:10.1161/ATVBAHA.114.303568 (2015).
26 van Herwijnen, M. J. *et al.* Regulatory T cells that recognize a ubiquitous stress-inducible self-antigen are long-lived suppressors of autoimmune arthritis. *Proc Natl Acad Sci U S A* **109**, 14134-14139, doi:10.1073/pnas.1206803109 (2012).
27 Pirillo, A., Norata, G. D. & Catapano, A. L. LOX-1, OxLDL, and atherosclerosis. *Mediators Inflamm* **2013**, 152786, doi:10.1155/2013/152786 (2013).
28 Tabas, I. & Lichtman, A. H. Monocyte-Macrophages and T Cells in Atherosclerosis. *Immunity* **47**, 621-634, doi:10.1016/j.immuni.2017.09.008 (2017).
29 Libby, P. Inflammation in atherosclerosis. *Arterioscler Thromb Vasc Biol* **32**, 2045-2051, doi:10.1161/ATVBAHA.108.179705 (2012).
30 Douna, H. & Kuiper, J. Novel B-cell subsets in atherosclerosis. *Curr Opin Lipidol* **27**, 493-498, doi:10.1097/MOL.0000000000000335 (2016).
31 Hansson, G. K. & Hermansson, A. The immune system in atherosclerosis. *Nat Immunol* **12**, 204-212, doi:10.1038/ni.2001 (2011).
32 Hanahan, D. & Weinberg, R. A. Hallmarks of cancer: the next generation. *Cell* **144**, 646-674, doi:10.1016/j.cell.2011.02.013 (2011).
33 Grivennikov, S. I., Greten, F. R. & Karin, M. Immunity, inflammation, and cancer. *Cell* **140**, 883-899, doi:10.1016/j.cell.2010.01.025 (2010).
34 Coulie, P. G., Van den Eynde, B. J., van der Bruggen, P. & Boon, T. Tumour antigens recognized by T lymphocytes: at the core of cancer immunotherapy. *Nat Rev Cancer* **14**, 135-146, doi:10.1038/nrc3670 (2014).
35 Johnson, L. A. *et al.* Gene therapy with human and mouse T-cell receptors mediates cancer regression and targets normal tissues expressing cognate antigen. *Blood* **114**, 535-546, doi:10.1182/blood-2009-03-211714 (2009).
36 Lu, Y. C. & Robbins, P. F. Cancer immunotherapy targeting neoantigens. *Semin Immunol* **28**, 22-27, doi:10.1016/j.smim.2015.11.002 (2016).
37 Whiteside, T. L. Inhibiting the inhibitors: evaluating agents targeting cancer immunosuppression. *Expert Opin Biol Ther* **10**, 1019-1035, doi:10.1517/14712

598.2010.482207 (2010).
38 Naran, K., Nundalall, T., Chetty, S. & Barth, S. Principles of Immunotherapy: Implications for Treatment Strategies in Cancer and Infectious Diseases. *Front Microbiol* **9**, 3158, doi:10.3389/fmicb.2018.03158 (2018).
39 Feldmann, M. & Steinman, L. Design of effective immunotherapy for human autoimmunity. *Nature* **435**, 612-619, doi:10.1038/nature03727 (2005).
40 Hansbro, P. M., Kaiko, G. E. & Foster, P. S. Cytokine/anti-cytokine therapy - novel treatments for asthma? *Br J Pharmacol* **163**, 81-95, doi:10.1111/j.1476-5381.2011.01219.x (2011).
41 Palucka, K. & Banchereau, J. Cancer immunotherapy via dendritic cells. *Nat Rev Cancer* **12**, 265-277, doi:10.1038/nrc3258 (2012).
42 Roncarolo, M. G. & Battaglia, M. Regulatory T-cell immunotherapy for tolerance to self antigens and alloantigens in humans. *Nat Rev Immunol* **7**, 585-598, doi:10.1038/nri2138 (2007).
43 Cheever, M. A. Twelve immunotherapy drugs that could cure cancers. *Immunol Rev* **222**, 357-368, doi:10.1111/j.1600-065X.2008.00604.x (2008).
44 Coutinho, A. E. & Chapman, K. E. The anti-inflammatory and immunosuppressive effects of glucocorticoids, recent developments and mechanistic insights. *Mol Cell Endocrinol* **335**, 2-13, doi:10.1016/j.mce.2010.04.005 (2011).
45 Barr, T. A. *et al.* B cell depletion therapy ameliorates autoimmune disease through ablation of IL-6-producing B cells. *J Exp Med* **209**, 1001-1010, doi:10.1084/jem.20111675 (2012).
46 Chatenoud, L. & Bluestone, J. A. CD3-specific antibodies: a portal to the treatment of autoimmunity. *Nat Rev Immunol* **7**, 622-632, doi:10.1038/nri2134 (2007).
47 Baldo, B. A. Side effects of cytokines approved for therapy. *Drug Saf* **37**, 921-943, doi:10.1007/s40264-014-0226-z (2014).
48 Hofmann, L. *et al.* Cutaneous, gastrointestinal, hepatic, endocrine, and renal side-effects of anti-PD-1 therapy. *Eur J Cancer* **60**, 190-209, doi:10.1016/j.ejca.2016.02.025 (2016).
49 Bamoulid, J. *et al.* The need for minimization strategies: current problems of immunosuppression. *Transpl Int* **28**, 891-900, doi:10.1111/tri.12553 (2015).
50 Tibbitt, M. W., Dahlman, J. E. & Langer, R. Emerging Frontiers in Drug Delivery. *J Am Chem Soc* **138**, 704-717, doi:10.1021/jacs.5b09974 (2016).
51 Rao, J. P. & Geckeler, K. E. Polymer nanoparticles: Preparation techniques and size-control parameters. *Prog Polym Sci* **36**, 887-913, doi:10.1016/j.progpolymsci.2011.01.001 (2011).
52 Kelly, K. L., Coronado, E., Zhao, L. L. & Schatz, G. C. The Optical Properties of Metal Nanoparticles: The Influence of Size, Shape, and Dielectric Environment. *The Journal of Physical Chemistry B* **107**, 668-677, doi:10.1021/jp026731y (2003).
53 Pattni, B. S., Chupin, V. V. & Torchilin, V. P. New Developments in Liposomal Drug Delivery. *Chem Rev* **115**, 10938-10966, doi:10.1021/acs.chemrev.5b00046 (2015).
54 Hawkins, M. J., Soon-Shiong, P. & Desai, N. Protein nanoparticles as drug carriers in clinical medicine. *Adv Drug Deliv Rev* **60**, 876-885, doi:10.1016/j.

addr.2007.08.044 (2008).
55 Song, W., Musetti, S. N. & Huang, L. Nanomaterials for cancer immunotherapy. *Biomaterials* **148**, 16-30, doi:10.1016/j.biomaterials.2017.09.017 (2017).
56 Carambia, A. *et al.* Nanoparticle-based autoantigen delivery to Treg-inducing liver sinusoidal endothelial cells enables control of autoimmunity in mice. *Journal of Hepatology* **62**, 1349-1356, doi:https://doi.org/10.1016/j.jhep.2015.01.006 (2015).
57 Benne, N. *et al.* Anionic 1,2-distearoyl-sn-glycero-3-phosphoglycerol (DSPG) liposomes induce antigen-specific regulatory T cells and prevent atherosclerosis in mice. *J Control Release* **291**, 135-146, doi:10.1016/j.jconrel.2018.10.028 (2018).
58 Heuts, J. *et al.* Cationic Liposomes: A Flexible Vaccine Delivery System for Physicochemically Diverse Antigenic Peptides. *Pharm Res* **35**, 207, doi:10.1007/s11095-018-2490-6 (2018).
59 Luo, M. *et al.* A STING-activating nanovaccine for cancer immunotherapy. *Nat Nanotechnol* **12**, 648-654, doi:10.1038/nnano.2017.52 (2017).
60 Kulkarni, S. A. & Feng, S. S. Effects of particle size and surface modification on cellular uptake and biodistribution of polymeric nanoparticles for drug delivery. *Pharm Res* **30**, 2512-2522, doi:10.1007/s11095-012-0958-3 (2013).
61 Benne, N., van Duijn, J., Kuiper, J., Jiskoot, W. & Slutter, B. Orchestrating immune responses: How size, shape and rigidity affect the immunogenicity of particulate vaccines. *J Control Release* **234**, 124-134, doi:10.1016/j.jconrel.2016.05.033 (2016).
62 Bobo, D., Robinson, K. J., Islam, J., Thurecht, K. J. & Corrie, S. R. Nanoparticle-Based Medicines: A Review of FDA-Approved Materials and Clinical Trials to Date. *Pharmaceut Res* **33**, 2373-2387, doi:10.1007/s11095-016-1958-5 (2016).
63 Aguilar, J. C. & Rodriguez, E. G. Vaccine adjuvants revisited. *Vaccine* **25**, 3752-3762, doi:10.1016/j.vaccine.2007.01.111 (2007).
64 Accardo, A. & Morelli, G. Review peptide-targeted liposomes for selective drug delivery: Advantages and problematic issues. *Biopolymers* **104**, 462-479, doi:10.1002/bip.22678 (2015).

2

Orchestrating immune responses: how size, shape and rigidity affect the immunogenicity of particulate vaccines

Authors and affiliations

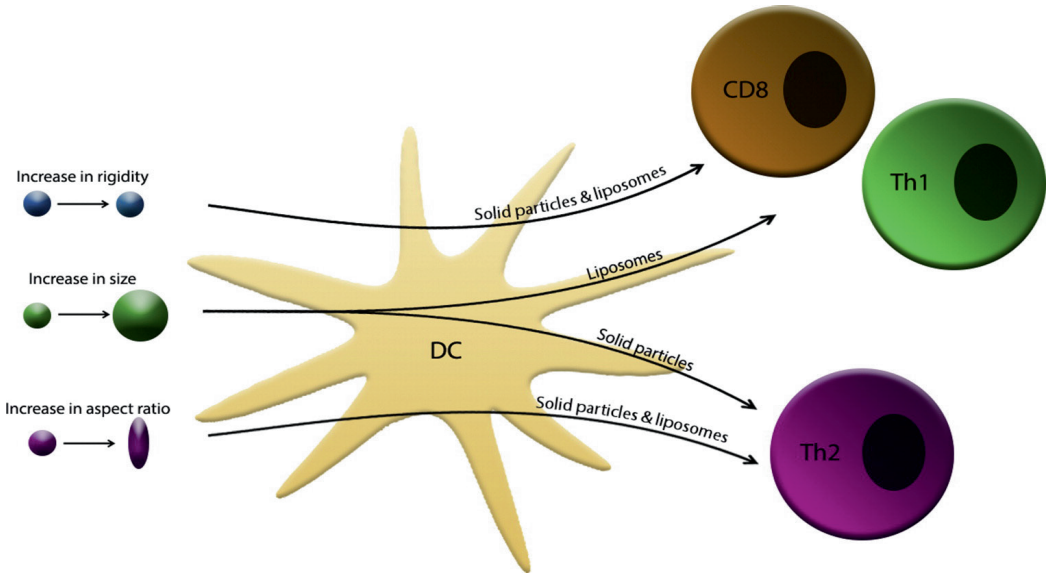
Naomi Benne[1,3*], Janine van Duijn[2,3*], Johan Kuiper[2,3], Wim Jiskoot[1,3], Bram Slütter[1,2,3]

[1] Division of Drug Delivery Technology, Leiden Academic Centre for Drug Research, Leiden University, Leiden, the Netherlands
[2] Division of Biopharmaceutics, Leiden Academic Centre for Drug Research, Leiden University, Leiden, the Netherlands
[3] Cluster BioTherapeutics, Leiden Academic Centre for Drug Research, Leiden University, Leiden, the Netherlands

* Authors contributed equally

Journal of Controlled Release, Volume 234, 28 July 2016, Pages 124-34.
doi: 10.1016/j.jconrel.2016.05.033

Graphical Abstract



Abstract

Particulate carrier systems are promising drug delivery vehicles for subunit vaccination as they can enhance and direct the type of T cell response. In order to develop vaccines with optimal immunogenicity, a thorough understanding of parameters that could affect the strength and quality of immune responses is required. Pathogens have different dimensions and stimulate the immune system in a specific way. It is therefore not surprising that physicochemical characteristics of particulate vaccines, such as particle size, shape, and rigidity, affect multiple processes that impact their immunogenicity. Among these processes are the uptake of the particles from the site of administration, passage through lymphoid tissue and the uptake, antigen processing and activation of antigen-presenting cells. Herein, we systematically review the role of the size, shape and rigidity of particulate vaccines in enhancing and skewing T cell response and attempted to provide a “roadmap” for rational vaccine design.

Introduction

The implementation of vaccines has proven to be an affordable and effective strategy to prevent disease. Concerted vaccine efforts in the 20th century have resulted in the reduced occurrence or even elimination of infectious diseases[1,2]. The first generation of successful vaccines was composed of weakened (attenuated) or inactivated pathogens. Despite their enormous success, some problems arise when using these types of vaccines. Firstly, there is a risk of genetic exchanges with other viruses, which may restore the virulence of live attenuated vaccines[3]. Secondly, due to their complex nature, these vaccines can induce adverse effects such as fever[4-6]. To circumvent these issues, subunit vaccines, containing only the antigen(s) against which the immune response must be targeted, have become more commonly used. These types of vaccines lead to superior safety profiles at the expense of decreased immunogenicity, due to the lack of pathogen-associated molecular patterns (PAMPs). Therefore, these vaccines require the addition of adjuvants[7] and/or the use of a particulate delivery system. The advantages of particulate delivery systems entail the protection of the integrity of antigens until they are delivered to antigen presenting cells (APCs)[8] and co-localisation of adjuvant and antigen to the same APCs, which limits systemic exposure to the adjuvant and thereby minimises adverse effects[9]. Furthermore, uptake of particulate matter by APCs induces an inflammatory response, contributing to the adjuvanticity[10].

Several classes of particulate vaccines have been developed which have been reviewed in great detail[11]. Interestingly, not only the composition of the particle affects its immunogenicity and a growing number of reports has covered the effect of particle size on vaccine efficiency. More recently, several publications reported the effect of particulate vaccine shape or rigidity on immunogenicity. This is probably due to the fact that techniques to alter and characterise particle shape and rigidity were developed later than those for particle size. There are several ways to alter size, shape, and rigidity. The size of particles is controlled by manufacturing conditions such as extrusion for vesicles[12], centrifugation for vesicles or solid particles[13,14], and emulsification conditions for polymeric particles[15]. The shape of particles can be altered by mechanical stretching[16] or by producing particles in a mould[17]. Rigidity, a measure of the particle's ability to retain its shape under mechanical stress can be manipulated for instance by varying the density of cross-linking in polymer hydrogel particles, by incorporating cholesterol in liposomes or by increasing shell layer thickness in capsules[18-20].

In this review, we discuss how particle size, shape, and rigidity affect biodistribution, cellular uptake, antigen presentation and the resulting immune response in murine models (unless stated otherwise), where appropriate as a function of the route of administration. We acknowledge that more parameters, such as surface charge, particle composition, biodegradability or the inclusion adjuvants are important characteristics that affect immunogenicity. However, the effect of these parameters has been extensively described elsewhere[21-30]. In addition, vaccines equipped with targeting ligands and adjuvants may induce immunological effects solely based on their physicochemical parameters[31].

Particle Size

Particle distribution

Vaccination aims to mimic a pathogenic infection and induce immunological memory for possible future encounters. For a vaccine to elicit an immune response, effective delivery of antigens from the site of injection to secondary lymphoid tissue, where APCs, B- and T cells reside, is the first requirement. Antigens can directly drain to lymphoid organs (such as spleen or lymph nodes, LNs) through the interstitial fluid and the collecting lymphoid vessels. Alternatively, particulate vaccine can be taken up by APCs at the site of injection and subsequently travel through the lymphatic system to interact with T and B cells that reside in the LNs[32,33].

The size of particulate vaccines plays a crucial role in their transport to the LNs. Upon intradermal injection, interstitial flow (drainage of fluids from the interstitial space) transports small, non-liposomal nanoparticles (<50 nm) more efficiently into lymphatic capillaries and draining LNs than particles larger than 100 nm. Smaller particles are hypothesised to be convected much easier through the interstitial flow, whereas larger particles require active transport by tissue-resident dendritic cells (DCs) to shuttle them to the LN. These smaller particles show increased retention in the LNs, due to efficient uptake by resident LN DCs[34-36]. Of note, for larger-sized particles (>50 nm), the efficiency of DC migration towards the draining LNs creates an extra parameter that might affect the quantity of antigen that is able to reach the LNs[37].

The effect of size on antigen distribution is also evident for liposomal formulations. Oussoren and colleagues reported a negative correlation between lymphatic uptake and liposome size in rats upon s.c. injection[38]. Interestingly, small 40 nm sized liposomes were poorly retained by the LNs compared to larger (>400 nm) liposomes. This was due to more efficient phagocytosis of larger liposomes, as macrophage-depleted LNs showed reduced LN localisation of large liposomes[39]. Small liposomes are possibly less affected, since they can be taken up by multiple cell types in the LNs via endocytic pathways other than phagocytosis, such as pinocytosis. This, of course, will also affect the immunogenicity of these particles as a lower percentage will reach APCs.

Different routes of administration encounter different barriers for the antigen to reach secondary lymphoid tissue. Thereby, different tissues contain different subsets of DCs, such as Langerhans cells in the skin, CD103+ DCs in connective tissue and mucosal DCs in the gut. The type of DC to which the antigen is delivered may influence the skewing of the immune response, but this is outside the scope of this review[40]. A study using orally dosed biodegradable polylactic acid (PLA) microparticles ranging from 1–26 µm in diameter showed that the uptake of these particles into intestinal lymphoid structures referred to as Peyer's patches, increased with increasing particle size up to 11 µm, and decreased again hereafter[41]. Microspheres smaller than 5 µm were subsequently translocated via the lymphatic system from the Peyer's patches to the spleen, whereas larger particles remained in the Peyer's patches in the jejunum. The authors suggested that uptake by phagocytes of particles larger than 10 µm was less likely to occur, explaining the decrease in splenic localisation when microparticle size exceeds this limit. Extending the size into the nanometre range, it was shown that oral administration of nanometre-sized particles results in higher uptake in the rat intestine than microparticles[42,43]. Nanoparticles are taken up more efficiently by the intestinal

epithelial cells and are able to penetrate deeper into the Peyer's patches, which make them more efficient than microparticles for oral delivery[14]. Thus, it appears that for optimal gut barrier passage, particulate vaccines should be designed to have a size in the nanometre range.

Concerning nasal delivery, it has been reported that migration of non-liposomal particles across the nasal mucosa of rats increases with decreasing particle size, resulting in stronger immunoglobulin G (IgG) and IgA responses, which are markers for general and mucosal immune responses, respectively[44]. Possibly, nanoparticles can permeate the epithelial lining more efficiently than microparticles, resulting in enhanced immunity as shown in rats and mice[13,45,46].

Overall, it can be concluded that smaller sized particles (<50 nm) can directly drain and penetrate deeper into the LNs. However, larger sized particles are retained more efficiently in the LNs, which emphasises the need for studies that find the optimal particle size to ensure efficient lymphatic drainage as well as retention. Furthermore, the route of administration can affect the distribution and should be considered in vaccine design as well.

Cellular uptake

An important step towards inducing a potent immune response is the uptake antigen-containing particles by APCs. APCs are continuously probing their environment for the presence of pathogens or danger-related signals, which enables them to internalise pathogens or other antigens and process them into peptides. Extracellular fluid, which may contain small antigens, is continuously taken up by APCs through macropinocytosis. Larger particles are generally internalised via phagocytosis due to binding to receptors on the plasma membrane of APCs, which triggers actin assembly and drives particle engulfment. All resulting vesicles travel to endosomes within the APC where their content is processed[47,48].

Conceivably, due to their exceptional capacity for macropinocytosis, DCs appear to preferentially take up nanoparticles. Studies in DC lines and DCs derived from human mononuclear cells have shown an inverse correlation between particle size and internalisation for particles of different compositions ranging from 20 µm to 150 nm[49-51]. Shima et al. have shown that 40, 100 and 200 nm sized poly(γ-glutamic acid) particles also show excellent uptake by DCs in vivo in the LNs upon s.c. administration. Interestingly, they report that the number of DCs that have taken up the 40 nm particles is twice as high as the number of DCs that have taken up the 200 nm particles while the relative amount of antigen taken up was three times as high for 200 nm particles compared to the 40 nm particles. This suggests that smaller-sized nanoparticles are taken up more efficiently, but larger-sized nanoparticles can deliver a greater amount of antigen to APCs[52]. In a study comparing uptake of polystyrene particles ranging from 20 nm – 1 µm in lung-draining LN upon intranasal administration, it was reported that smaller (<50 nm) particles were preferentially taken up by LN-resident DCs[53].

Examining the behaviour of particles in the extremely small size ranges, le Guével et al. produced gold nanoparticles of 12 nm and nanoclusters (clusters of gold atoms) of 2 nm in size[54]. Comparing the number of particles per human derived DC, the nanoclusters showed a higher uptake compared to the nanoparticles. However, only the nanoparticles induced DC maturation and subsequent Th1 mediated immunity.

Of interest, nanoclusters have a higher diffusion capacity than the nanoparticles. This suggests the nanoparticles are taken up by receptor-mediated endocytosis, which is less efficient than diffusion, resulting in lower uptake, but the particles taken up via this process are able to induce immunity.

Of note, the mechanism of antigen delivery has been reported to differ between nano- and microparticles. Here we discuss the consequences of particle size on uptake, however, it must be noted that attachment of microparticles to the APCs, without endocytosis of the delivery system, appears to be sufficient to deliver the antigen to the APCs[55,56].

Antigen presentation and APC activation

Following antigen uptake by APCs, these cells need to become activated by the recognition of PAMPs using pattern recognition receptors (PRRs)[57]. Effective processing leading to robust antigen presentation are required to induce potent immune responses. After uptake, antigen loaded particles are deposited in the endosome, where the particle and antigen are broken down by enzymatic degradation upon acidification of the endosome, resulting in short peptide sequences. These small protein fragments are loaded upon major histocompatibility complex (MHC) class II molecules, leading to CD4+ T cell activation. Alternatively, particles can be modified to facilitate endosomal escape, after which the antigenic peptide can reach the cytosol and, after proteasomal degradation, are loaded upon MHC class I molecules, thereby inducing CD8+ T cells. This process referred to as cross-presentation, can occur via two pathways: the presently described 'phagosome to cytosol pathway' and via the 'vacuolar pathway' in which antigens are loaded onto MHC class I molecules within the phagosome, which is not necessarily TAP-dependent[58-60].

Nanoparticles appeared to be efficient at inducing class I antigen presentation in vitro, whereas microparticles induced almost no MHC class I antigen presentation[61]. Particles larger than 500 nm were delivered into phagosomes, which subsequently fused with early endosomes, whereas smaller (<200 nm) particles localised rapidly into late endosomes which fused with lysosomes. MHC class II complexes were recruited to both compartments, but delivery to the prelysosomal (early) compartment was shown to be more efficient in processing and presenting an encapsulated antigen. Consequently, the larger particles (>500 nm) produced enhanced CD4+ T cell activation compared to smaller particles[12]. It has been suggested that the accumulation of nanoparticles within the lysosomes may have caused lysosomal overload, which resulted in defective lysosomal degradation, which may explain the reduced MHC class II antigen-presenting capacity[62].

Considering cross-presentation, it was suggested that particles in the nanometre size range induced MHC class I presentation via the phagosome-to-cytosol pathway, whereas the larger micrometre-sized particles were processed via the vacuolar pathway, which yielded relatively fewer MHC class I complexes[60]. Together, these studies provide strong evidence for a size-dependent effect of both liposomal and non-liposomal particles on endosomal antigen processing and subsequent presentation.

Skewing immune responses

Pathogens can infect host cells via various routes, occupy different compartments (intracellular or extracellular) and cause acute or chronic infections. Therefore, clearance of pathogens requires a specific approach. CD8+ T cells play a seminal role in detecting and clearing intracellular pathogens as they recognise infected cells by through specific epitopes presented upon MHC class I molecules, upon which they exert inflammatory and cytotoxic functions[63,64]. CD4+ T cells recognize MHC class II via their T cell receptor (TCR) and can be subdivided into different classes, the principal of which are T helper 1 (Th1), Th2 and T-regulatory (Treg) cells, characterised by the expression of T-bet, GATA-3, and FoxP3, respectively. Th1 cells produce inflammatory cytokines and are major producers of interferon-γ (IFN-γ) and TNF-α, which are pivotal for cell-mediated immunity (e.g. macrophage activation, CD8+ T cell help). The Th2 subset is characterised by a different cytokine profile, including cytokines such as interleukin 4 (IL-4), IL-5, IL-10 and IL-13 and are associated with the induction of humoral (antibody-mediated) immunity. Finally, Treg cells are a tolerogenic subset that suppresses inflammatory responses through secretion of anti-inflammatory cytokines (e.g. IL-10, TGF-β)[65].

As clearing a pathogen requires a specific type of immune response, skewing of the response after immunisation is an important aspect that particles can influence. As the size of a particulate vaccine affects the extent of MHC class I or MHC class II presentation, this directly influences effective CD8+ and CD4+ T cell priming. However, the size of particles also appears to influence the type CD4+ T cell that is induced. Nanoparticles (ranging in size from 100-600 nm) induce the most prominent activation of DCs (as measured by CD80 expression) compared to micro-sized particles. As a result, nanoparticles generated the highest antigen-specific CD8+ T cell response and a higher proportion of IgG2a antibodies relative to IgG1 antibodies, which indicates skewing towards a Th1 phenotype. Other studies showed that particles of 40-50 nm in size are most potent in inducing IFN-γ mediated Th1 immunity compared to particles in the 100 nm range, which induced stronger IL-4 responses. It has been suggested that smaller (<100 nm) particles may enter APCs through one of the mechanisms used by viruses, such as clathrin-coated pit-mediated uptake, which may induce a stronger Th1 immune response[66,67]. This suggests there is an optimal particle size of around 50 nm that triggers Th1 responses.

Microparticles (2-8 μm) were not taken up but instead attached to the surface of the APC, releasing their antigen into the cell in both mouse and rat models. This favoured IL-4 secretion and showed a higher IgG1/IgG2a ratio and higher antibody titres. Thereby, microparticles upregulated MHC class II expression, whereas nanoparticles induced more MHC class I. This suggests that nanoparticles induce a Th1 type immune response while microparticles induce a Th2 type response[49,55,68][49]. There appears to be an upper size limit for effective Th2 response; 5 μm poly(lactic-co-glycolic) acid (PLGA) microspheres containing hepatitis B surface antigen in pulmonary immunisation in rats induced higher antibody titres compared to larger (12 μm) PLGA particles, which could be due to less efficient uptake or adherence of particles that are larger in size than DCs[56]. Thus, the optimal size for inducing Th2 responses is approximately 1-5 μm.

Thus far we have seen a trend that smaller solid (polymeric or gold) particles induce stronger Th1 and CD8-mediated responses, whereas larger particles seem to skew towards a Th2 and B cell mediated response (Figure 1). Lipid vesicles, however, have

been reported to show an opposite trend; small (<200 nm) liposomes appear to induce Th2 mediated immunity, whereas larger liposomes skew towards Th1 responses[12,69,70].

The reason for the apparently contradictory effects observed for liposomal and non-liposomal particles could be explained by the differences in lysosomal degradation rates. Tran and colleagues studied the intracellular trafficking of 50 nm, 500 nm or 3 µm particles and showed that OVA conjugated to 50 nm polystyrene beads was rapidly exposed to an acidic environment in the lysosome[71]. This led to fast degradation of the antigen in the lysosome and, therefore, inefficient presentation. Furthermore, antigens bound to 500 nm and 3 µm particles remained in a less acidic environment within the phagosomes for a longer period of time, resulting in more efficient MHC class I presentation.

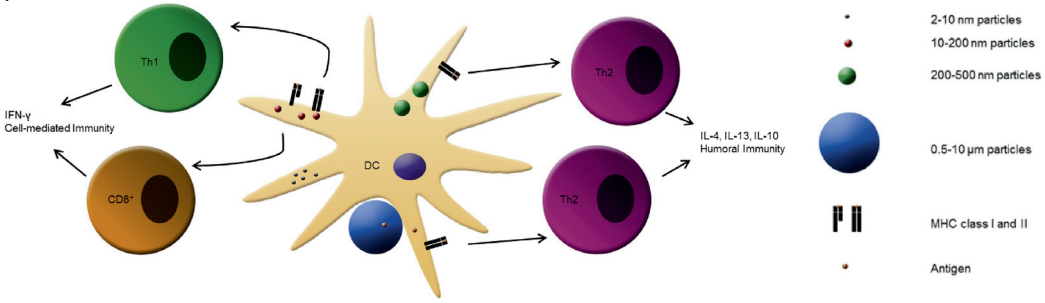


Fig. 1. Schematic overview of the effect of non-liposomal particle size on inducing T cell immunity. Ultra-small particles (2–10 nm) are taken up very efficiently by APCs but are poorly immunogenic. 10–200 nm nanoparticles are most efficient at inducing Th1 and CD8-mediated immunity, whereas larger 200–500 nm nanoparticles tend towards Th2 mediated responses. Microparticles adhere to the cell membrane and release antigen into the cell, which is presented upon MHC class II molecules and skews the immune response towards Th2 mediated responses.

Particle shape

Particle distribution

Besides particle size, shape is an important parameter influencing the immune response. A common way of characterising particle shape is by using the ratio between the height and width of the particle, denoted as the aspect ratio (AR). Huang et al. reported that the shape of mesoporous silica nanoparticles affects the biodistribution of these particles after intravenous (i.v.) administration in mice[72]. Both short-rod-shaped particles (185 nm, low AR) and long-rod particles (720 nm, high AR) were trapped in the spleen and liver. However, compared to the short-rod particles, the long-rod particles were more prominent in the spleen. Furthermore, short-rod particles were cleared faster from the body by urine and faeces than long-rod particles. Likely, the shape of the particles affects the ability for uptake by tissue-resident cells, which in turns affects the biodistribution and retention ability in the tissues. However, a size effect cannot be excluded in this experiment[72]. Injected filomicelles, micelles with a tubular shape (high AR), remained in circulation in rats and mice for up to one week[73]. Short tubular micelles were cleared from the circulation within two days. Filomicelles longer than 3 µm could not be taken up by human macrophages, whereas shorter filomicelles could be taken up via phagocytosis. The authors suggest that longer circulation time of the long filomicelles can be explained by the theory that they are stretched out by the blood flow, thereby

minimising interactions with phagocytes and the blood vessel wall. Shorter cylinders will be less affected by the blood flow and interact more with phagocytes, resulting in more efficient uptake and thus faster clearance from the circulation. However, it must be noted that these particles were injected i.v. and therefore, this study focused on the uptake from the circulation, instead of lymphatic trafficking[73]. Upon oral administration of mesoporous silica nanoparticles, different effects were observed; decreasing ARs (5, 1.75 and 1) of the particles resulted in increased absorption by the small intestine, whereas urinary secretion was decreased[74]. Indeed, particles with the smallest AR showed the highest content in the spleen compared to the other particles, which were mainly deposited in the liver, lungs and kidneys. These results suggest that upon oral administration, spherical particles will exhibit a more favourable biodistribution profile than non-spherical ones, emphasising that the route of administration is an important parameter influencing the effect of particle properties on immunogenicity.

Cellular uptake

Similar to particle size, particle shape also plays a major role in the uptake of particulate vaccines by APCs. Non-spherical long-rod polystyrene particles stretched from 3 μm spheres were shown to exhibit negligible phagocytosis in a macrophage cell line, as observed by time-lapse imaging[75]. Moreover, spherical particles of similar size were internalised efficiently by macrophages. Spheres and rods of 1 μm in size showed the same differential phagocytosis as 3 μm spheres and rods. The authors suggested that macrophages cannot take up the rod-like particles, as the shape is mostly flat and only contains curvatures on extreme ends, which hinders phagocytosis. Niikura et al. tested macrophage uptake of gold particles of different shapes; spheres of 20 nm and 40 nm in diameter, 40 nm x 10 nm rods (AR = 4) and 40 x 40 x 40 nm cubes[76]. Interestingly, rod-shaped particles appeared to be taken up more efficiently by macrophages than spherical or cubic particles (with cubic particles being the least effective), but in fact, the spherical particles had more efficient uptake per weight. Sharma et al. produced initially spherical polystyrene particles that were stretched to either prolate ellipsoids (high AR) or oblate ellipsoids (lower AR)[77]. The phagocytosis efficiency was in the order of oblate ellipsoids>>spheres>prolate ellipsoids. Even though oblate ellipsoids did not have the highest cell attachment, almost 90% of the attached particles were internalised, compared to 50% of the prolate ellipsoids and 70% of spheres. The combination of relatively high attachment and internalisation gives oblate ellipsoids a clear advantage for phagocytosis. Champion et al. reported that the particle shape at the point of cell contact dictated whether or not phagocytosis was initiated[78] (Figure 2). Polystyrene particles were fabricated in the shapes of spheres, oblate ellipsoids, prolate ellipsoids, elliptical discs, rectangular discs or flying saucer shapes. The orientation of the particle towards the phagocyte was of great importance in Fc receptor-mediated phagocytosis by macrophages. Actin polymerisation in the shape of a cup occurs beneath the particle, which then forms an actin ring that forces the membrane along the particle surface until it is engulfed. When this initial actin attachment forms on the flat side of a particle, the formation of the actin ring is not supported. The contact angle between the membrane normal and the particle, therefore, is an important determinant of the internalisation efficiency. Particles for which this angle is small are phagocytosed more efficiently, as only gradual expansion of the actin ring is required, which is a metabolically intensive

process. If the contact angle is too large, the cell will spread across the surface of the particle but cannot internalise it. Therefore, the uptake of (near) spherical particles is always favourable, whereas that of rod-shaped particles depends on the likelihood of the particle approaching at a favourable contact angle, thereby negatively influencing the uptake of such particles (Figure 2). Indeed, Huang et al. manufactured mesoporous silica nanoparticles of different lengths and ARs; 100 nm spherical (AR = 1), 240 nm short rod (AR = 2) and 450 nm long rod (AR = 4)[79]. Incubation with human melanoma cells showed the formation of well-organised F-actin bundles for the particles with ARs 1 and 2. However, F-actin was disorganised for cells incubated with the particles with an AR of 4. This may explain why near-spherical particles are taken up more effectively as described in the aforementioned papers.

Yi and Gao created a theoretical model for membrane wrapping of particles of different shapes[80]. Keeping rigidity constant, they found that longer and thinner rods require more energy for cellular wrapping than more spherical particles. Furthermore, non-spherical particles undergo an orientation change during wrapping, which also contributes to increased energy expenditure. Both in vitro and in silico models suggest that spherical and slightly ellipsoidal nanoparticles are most efficiently taken up due to favourable energy expenditure during actin membrane wrapping. It can also be noted that small spheres inherently require less polymerisation of the actin cytoskeleton, compared to larger spheres; hence, less energy is expended in this process. This might explain the preferential uptake of smaller compared to larger spheres.

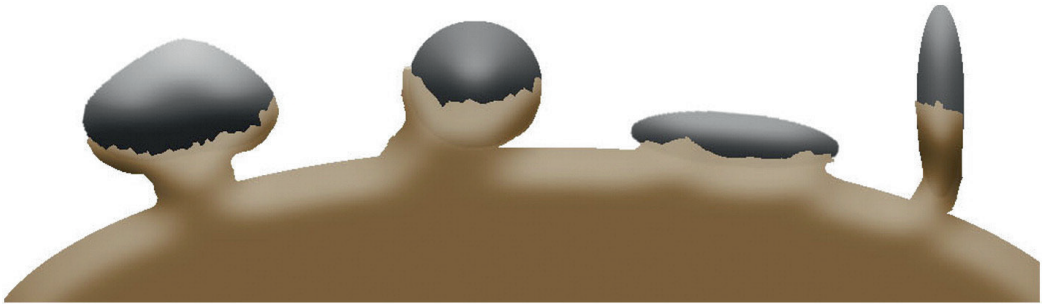


Fig. 2. Cellular uptake of a flexible sphere, rigid sphere and rigid rod approaching the cellular membrane at a perpendicular or tangential angle. The rigid sphere is taken up more efficiently than the flexible sphere; while the membrane envelopes both particles, the flexible particle deforms leading to slower uptake. For rod-shaped particles, the angle at which the particle approaches the cell is important; when the particle arrives at a tangential angle, it would require too much energy to form an actin cup around the particle leading to no uptake. Therefore, an orientation change is needed, which also requires high energy expenditure. The rigid rod approaching the cell at a perpendicular angle requires much less energy to be taken up.

Antigen presentation and APC activation

The effect of particle shape on antigen presentation is currently poorly described. In one study, rod-shaped gold particles (40 nm long, AR = 4) coated with West Nile virus induced production of IL-1β and IL-18 in bone marrow-derived DCs; these cytokines are secreted upon inflammasome activation. It is known that lysosomal rupture can induce inflammasome activation and indeed, rod-shaped particles were able to escape from the lysosome into the cytosol, suggesting lysosomal rupture could have occurred. In

contrast, spherical and cubical particles induced production of tumour necrosis factor-α (TNF-α), IL-6 and IL-12, which are not associated with inflammasome activation[76]. Mathaes et al. reported that both nano- (150 nm) and micro-sized (1.5 μm) spherical PLGA particles induced stronger activation of DCs as measured by upregulation of CD83 and CD86 than similar sized, non-spherical, stretched particles[50]. As these molecules provide important co-stimulatory signals during antigen presentation, this finding may suggest that spherical particles result in more efficient antigen presentation. However, more research is required to study this relationship.

Skewing immune responses

Recent observations suggest particle shape directly influences the type of immune response. In the aforementioned study by Niikura et al., spherical 40 nm gold particles coated with antigen derived from West Nile virus, induced superior levels of West Nile-specific IgG as compared to cubical and rod-shaped particles of similar size[76]. Kumar et al. performed an elegant study in which they used spherical polystyrene ovalbumin conjugated particles of 190 and 520 nm in diameter, which they stretched into rod-shaped particles of 380 and 1530 nm in length[16]. They found that the 190 nm spheres were most potent at inducing IgG2a antibody responses, whereas the 1530 nm rods induced the highest IgG1 antibody responses. Moreover, they showed that the small spheres were most potent at inducing IFN-γ responses, whereas IL-4 was consistently produced in all groups. From this, it can be concluded that the smaller sized nanoparticles are more effective than larger particles are inducing Th1 and CD8+ T cells, and this effect is most pronounced when these small particles are spherical. In contrast, the larger sized nanoparticles are more potent at inducing Th2 responses, which are most effective when using rod-shaped particles.

Particle Rigidity

Particle distribution

Apart from size and shape, rigidity can also affect the biodistribution and elimination rate of particles. Merkel et al. produced red blood cell mimics (RBCM); hydrogels containing particles of a similar shape, size (6 μm) and rigidity as compared to RBCs[81]. By altering the rigidity, they observed that circulation time was inversely correlated with rigidity, with the most rigid RBCMs being eliminated much faster than the least rigid ones. This was likely due to the less rigid particles being able to reach areas with constricted blood flow, increasing circulation times. Similarly, “soft” polyethylene glycol (PEG) based hydrogel nanoparticles were made which had a longer distribution half-life (rate of particle distribution from plasma into tissues) and elimination half-life (rate of particle clearance from plasma) than rigid particles[82]. Analysis of tissues after 30 min and 12 hours showed that soft particles were found at a higher concentration in almost all tissues (spleen, kidney, heart, lungs, brain, and blood) except for the liver. The differences in biodistribution were attributed to the longer circulation time of the soft nanoparticles, which led to increased retention in organs with high blood flow. Possibly, the soft nanoparticles were degraded in the liver, explaining their reduced retention in this tissue. Moreover, it was found that more rigid particles accumulated in the capillaries in the lungs while the less rigid particles avoided lung filtration and instead were found

mostly in the spleen, suggesting that more rigid particles become trapped in the first tissue with microvasculature they encounter[81].

It was found that liposomes containing phosphatidylcholine (PC) with a high transition temperature (i.e., high rigidity) injected i.v. remained in the blood for a longer period of time than similar liposomes containing PC with a low transition temperature. This was combined with a decreased uptake in the liver and spleen[83,84]. Similar results were observed by Senior et al. who hypothesised that longer circulation was due to less interaction between the liposomes and high-density lipoprotein in the blood[85]. There is evidence that ApoA-I and ApoA-II on high-density lipoprotein react with PC and cholesterol-containing liposomes, which results in faster clearance[86]. After i.m. injection, rigid cationic liposomes remained at the site of injection longer than less rigid ones. This corresponded with higher amounts of non-rigid liposomes found in the draining LNs[87]. In contrast, Kaur et al. observed no effects of cholesterol content (which also affects rigidity) in cationic liposomes on drainage from the site of injection or transport to LNs after i.m. injection[88]. It appears that similar to particles of increasing size, lymphatic trafficking of particles with increasing rigidity will be hindered by a decreased ability to navigate through narrow lymphatic vessels.

Cellular uptake

To understand the importance of particle rigidity on cellular uptake, one must first examine the interplay between the cell membrane and the particle. The first theoretical model of adhesive wrapping of a vesicle by the cell membrane was created by Yi et al.[89]. They theorised that the degree of wrapping was dependent on adhesion energy between the vesicle and the cell surface, vesicle size, the surface tension of the cell membrane upon contact with the vesicle, and the difference in rigidity of the cell membrane and the vesicle. They concluded that rigid particles are in general more easily wrapped by the cell membrane due to cell membrane deformation by the particles and that flexible particles spread out more across the cell membrane. This was supported by molecular dynamics simulations by Sun et al.[90]. Experimentally, Beningo and Wang reported that macrophages preferentially phagocytosed 1-6 μm-sized rigid particles over softer particles due to rigid particles stimulating actin filament assembly in macrophages[91]. The previously described RBCM hydrogels also showed minimal (<10%) uptake by human umbilical vein endothelial cells, probably due to a combination of low rigidity and large (6 μm) particle size[81]. Similarly, Anselmo et al. found that PEG-based rigid particles had significantly higher uptake than flexible particles (both spheres of 200 nm) in an endothelial brain cell line (bEnd.3), an epithelial tumour cell line (4T1) and macrophages (J774)[82]. As previously stated, phagocytosis by macrophages is important for retention of particles in the LNs, which improves the overall immunogenicity of the particles[39]. Similarly, cationic gel-state liposomes with higher cholesterol contents (i.e., lower rigidity) showed reduced uptake by THP-1 macrophages[88] and gel-state liposomes consisting of high transition temperature lipids had increased APC uptake compared to fluid-state liposomes made up of low transition temperature lipids[87]. Generally, it can be stated that rigid particles are most efficiently taken up, whereas more flexible particles are deformed by the membrane, resulting in increased energy expenditure and consequently reduced uptake (Figure 2).

Antigen presentation and APC activation

Once a particle has been taken up by a cell, intracellular processing can also be affected by rigidity. Hartmann et al. produced microcapsules of about 4 µm with varying shell thickness that altered their rigidity[92]. By observing uptake and acidification of the microcapsules in HeLa cells, they found that more rigid capsules had longer endosomal processing times and reached the lysosome later than more flexible capsules. Unfortunately, it was not reported how this affects the efficiency of antigen processing. Cui et al. prepared capsules of around 1 µm composed of polyglycolic acid (PGA) cross-linked to the adjuvant CpG[93]. They altered rigidity by increasing the cross-linker concentration. Incubation with plasmacytoid DC (pDCs) showed increased particle association to pDCs with increasing rigidity. The authors also showed a rigidity-dependent increase in pDC activation as measured by CD86 and CD40 levels. Thus, the effect of rigidity on uptake by macrophages and DCs may have important implications for immunity. In the case of liposomes, Christensen et al. showed that more rigid cationic liposomes injected i.m. resulted in increased activation of DCs in draining lymph nodes, as measured by CD40 and CD86 upregulation[87].

To our knowledge, no reports have been published that specifically examine antigen presentation as a function of particle rigidity. However, since antigen presentation is largely dependent on particle uptake by APCs, and it was shown above that rigid particles are more likely to be taken up, we suggest rigid particles shall have more efficient antigen presentation. Thereby, it can be speculated that the shorter endosomal processing time of rigid particles shall enhance antigen stability and lead to more efficient MHC presentation compared to flexible particles. This will mainly affect MHC class II epitopes as they require endosomal processing, whereas MHC class I epitopes are derived from the cytosol.

Skewing immune responses

Several studies have shown that particle rigidity can affect the skewing of the immune response. In two studies by the same group, the immune response was measured in mice after immunisation with liposomes composed of phospholipids with different transition temperatures. They found that liposomes containing high transition temperature lipids elicited higher antibody responses[94,95]. A similar rigidity effect on antibody[96,97] and T-cell responses[98,99] has been found by other groups. There is some evidence that reducing liposome rigidity by the addition of cholesterol or by selecting lipids with lower phase transition temperatures leads to reduced Th1 responses after i.m. immunisation. In contrast to the above mentioned studies, the authors state that there is no measurable effect of particle rigidity on Th2 or antibody responses. However, this was hypothesised to be due to reduced APC uptake of non-rigid liposomes from the site of injection[87,88].

Arnal and colleagues reported that the presence of virulence factors in Bordetella pertussis increased rigidity; a non-infectious mutant deficient of filamentous haemagglutinin (FHA) had lower rigidity[100]. The authors postulate that FHA increases the rigidity of the cell, specifically by creating rigid nanodomains that could enhance the adhesion of B. pertussis to cells. Studying different strains of Lactobacillus and Bifidobacterium, Mokrozub et al. found that Lactobacillus strains with elastic cell walls were more effectively digested by macrophages in vitro and enhanced their ability to

produce nitric oxide and accumulate reactive oxygen species. However, the more rigid strains had higher IL-12 and IFN-γ production (Th1 immune response). In the case of Bifidobacterium strains, uptake of the more rigid strains increased macrophage effector functions while also enhancing IFN-γ production[101]. The authors hypothesise that strains with more rigid cell walls remain viable within macrophages longer, prolonging cytokine production. For viruses, it was shown in two separate papers by Kol et al. that rigidity differs between the immature (non-infectious, viral budding) and mature (infectious, entry into cells) stage, for both murine leukaemia virus (MLV) and human immunodeficiency virus (HIV) (about 100 nm in size). In the case of MLV, the mature form of the virus is more rigid. Conversely, immature HIV is much more rigid than mature HIV, suggesting that a more flexible viral structure is beneficial for cell entry[102,103]. It can be concluded that, for lipid vesicles, immunisation with more rigid particles results in higher antibody and T-cell responses. Studies that examine the effect of particle rigidity on the immune response would be extremely valuable to further understanding and the role of this parameter in vaccine design.

Summary and conclusions

Here we reviewed how the immunogenicity of particulate vaccines is directed by their shape, size, and rigidity. Clearly, the choice of the optimal physicochemical parameters depends on multiple factors, such as the route of administration, which immune cells are targeted and what type of immune response is preferred. Importantly, in most of the studies discussed here, not only the shape, size or rigidity of the particles differ, but other parameters are also (indirectly) altered. Particle shape and rigidity are especially closely related, since highly deformable particles can alter their shape during circulation or cellular uptake. Additionally, differences in rigidity measurements and calculations can result in different definitions of “soft” or “rigid” particles. We strongly plead for systematic investigations where only one particle parameter is changed and all others are kept constant. This will help to accurately define the relationship between particle size or shape and the immunogenicity of particulate vaccines.

This review suggests it is important to take the physicochemical characteristics of particulate vaccines into account in order to induce maximal antigen responses. For instance, what may be a favourable characteristic for, e.g., transport towards the LN may not be ideal for inducing the desired skewing of the immune response. Therefore, the choice of particle size, shape and rigidity must involve a careful consideration of the effects of these on all of the events influencing the immunogenicity. Figure 3 could function as a “roadmap” and when the desired immunologic outcome is known, it might provide a model for rational vaccine development.

For instance, the development of a CD8+ T cell activating vaccine (e.g. cancer vaccines), may be most efficient when a small (<200 nm), rigid, elliptical non-liposomal nanoparticle is used. The elliptical shape, as well as rigidity, will ensure efficient uptake by APCs and a size smaller than 200 nm will skew the immune response towards Th1 and CD8+ T cell immunity. Alternatively, the development of a Th2 directed vaccine (e.g. hepatitis B vaccines), could benefit most from a small (<200 nm), spherical, slightly more flexible liposomal particulate formulation. Since liposomes show opposite trends compared to non-liposomal formulations in skewing immune responses, this will ensure a Th2 directed response. Thereby, the uptake of this particle by APCs will still be efficient

due to the small size. As rigid bacterial strains and liposomes are known to skew the immune response towards type 1 immunity, it could be desirable to use a more flexible particle. However, more energy is needed for uptake of soft particles, which may have a negative influence on the antigen presentation. Thus, depending on the application, one could also choose to use a larger, non-liposomal particle. Micro-sized particles are known to tether to the membrane of APCs and deliver their antigens without being internalised. This also results in skewing towards a Th2-mediated immunity.

Overall, it appears that small, rigid, near spherical nanoparticles are the most favourable particles to reach APCs in the LNs and induce strong immune responses. The exact size can be tailored based on the type of particle used, to skew towards either Th1 or Th2 mediated immunity. Due to the scarcity of research, particularly in the field of shape and rigidity, more studies will inevitably contribute to a more thorough understanding of how these parameters influence the immune response. This knowledge, in turn, will be of great importance for the rational design of more efficient vaccines, especially for diseases for which there is currently no vaccine, such as HIV, cancer or tuberculosis.

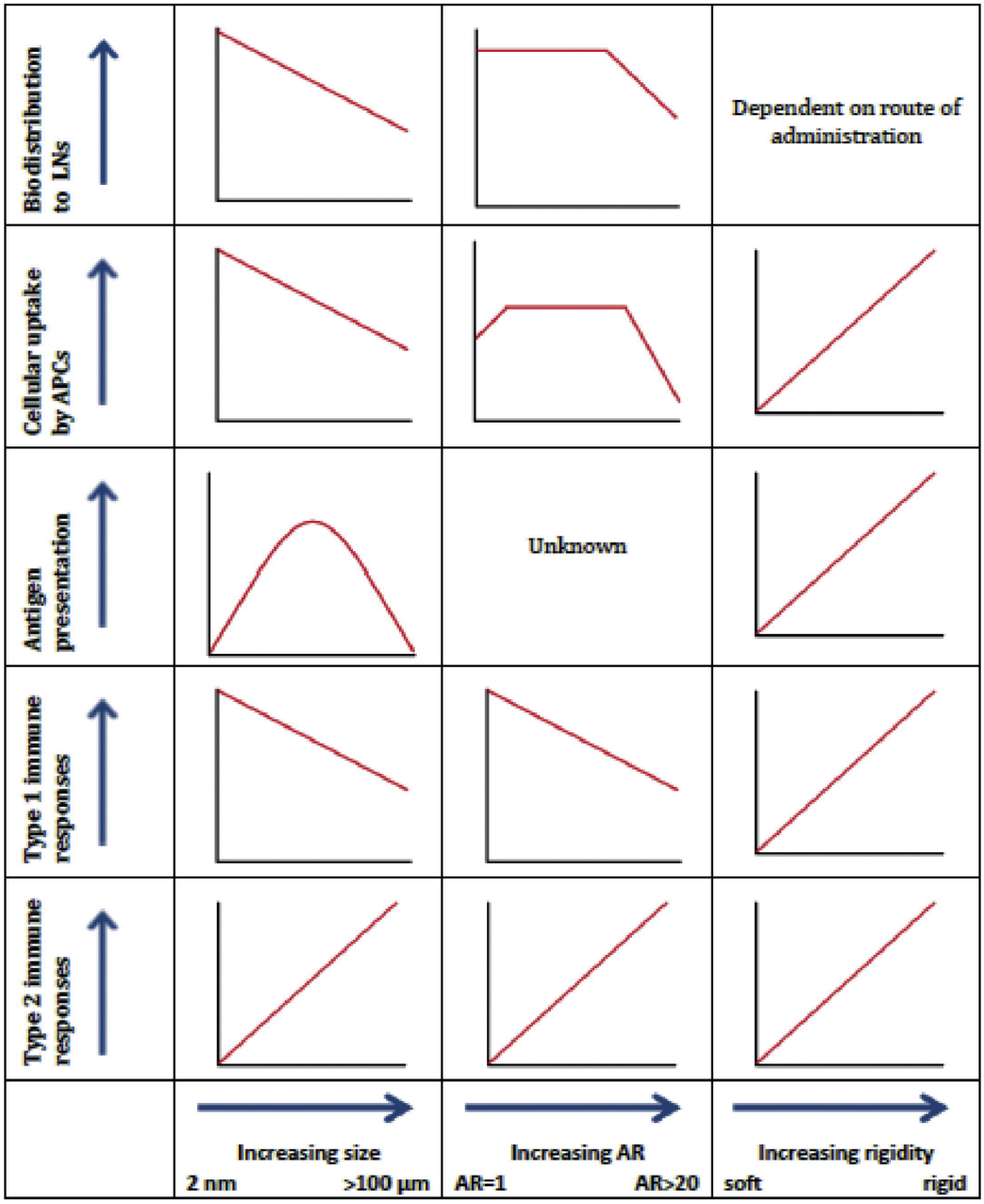


Fig. 3. Summary of the general trends of the effects of shape, size and rigidity on different parameters affecting the immunogenicity of particulate vaccines. The height of the red line represents the efficiency per parameter. Size ranges from left to right from ultra-small (2 nm) to large (> 100 µm) microparticles. Shape ranges from left to right from spherical (AR = 1) to long filomicelles (AR > 20). Rigidity ranges from left to right from very elastic particles to non-deformable particles.

References

1 Smith, K. A. Smallpox: can we still learn from the journey to eradication? Indian J Med Res 137, 895-899 (2013).

2 Milstien, J. B. & Gibson, J. J. Quality control of BCG vaccine by WHO: a review of factors that may influence vaccine effectiveness and safety. Bull World Health Organ 68, 93-108 (1990).

3 Guillot, S. et al. Natural genetic exchanges between vaccine and wild poliovirus strains in humans. J Virol 74, 8434-8443 (2000).

4 Donnelly, S., Loscher, C. E., Lynch, M. A. & Mills, K. H. Whole-cell but not acellular pertussis vaccines induce convulsive activity in mice: evidence of a role for toxin-induced interleukin-1beta in a new murine model for analysis of neuronal side effects of vaccination. Infect Immun 69, 4217-4223, doi:10.1128/iai.69.7.4217-4223.2001 (2001).

5 Murphy, T. V. et al. Intussusception among Infants Given an Oral Rotavirus Vaccine. New England Journal of Medicine 344, 564-572, doi:doi:10.1056/NEJM200102223440804 (2001).

6 Cherkasova, E. A. et al. Long-term circulation of vaccine-derived poliovirus that causes paralytic disease. J Virol 76, 6791-6799 (2002).

7 Moyle, P. M. & Toth, I. Modern subunit vaccines: development, components, and research opportunities. ChemMedChem 8, 360-376, doi:10.1002/cmdc.201200487 (2013).

8 Slutter, B. et al. Conjugation of ovalbumin to trimethyl chitosan improves immunogenicity of the antigen. J Control Release 143, 207-214, doi:10.1016/j.jconrel.2010.01.007 (2010).

9 O'Hagan, D. T. & Singh, M. Microparticles as vaccine adjuvants and delivery systems. Expert Rev Vaccines 2, 269-283 (2003).

10 Sharp, F. A. et al. Uptake of particulate vaccine adjuvants by dendritic cells activates the NALP3 inflammasome. Proc Natl Acad Sci U S A 106, 870-875, doi:10.1073/pnas.0804897106 (2009).

11 De Temmerman, M.-L. et al. Particulate vaccines: on the quest for optimal delivery and immune response. Drug Discovery Today 16, 569-582, doi:http://dx.doi.org/10.1016/j.drudis.2011.04.006 (2011).

12 Brewer, J. M., Pollock, K. G., Tetley, L. & Russell, D. G. Vesicle size influences the trafficking, processing, and presentation of antigens in lipid vesicles. J Immunol 173, 6143-6150 (2004).

13 Vila, A. et al. PLA-PEG particles as nasal protein carriers: the influence of the particle size. Int J Pharm 292, 43-52, doi:10.1016/j.ijpharm.2004.09.002 (2005).

14 Shakweh, M., Besnard, M., Nicolas, V. & Fattal, E. Poly (lactide-co-glycolide) particles of different physicochemical properties and their uptake by peyer's patches in mice. Eur J Pharm Biopharm 61, 1-13, doi:10.1016/j.ejpb.2005.04.006 (2005).

15 Cohen, J. A. et al. T-cell activation by antigen-loaded pH-sensitive hydrogel particles in vivo: the effect of particle size. Bioconjug Chem 20, 111-119, doi:10.1021/bc800338n (2009).

16 Kumar, S., Anselmo, A. C., Banerjee, A., Zakrewsky, M. & Mitragotri, S. Shape and

size-dependent immune response to antigen-carrying nanoparticles. J Control Release 220, 141-148, doi:10.1016/j.jconrel.2015.09.069 (2015).
17 Gratton, S. E. et al. Nanofabricated particles for engineered drug therapies: a preliminary biodistribution study of PRINT nanoparticles. J Control Release 121, 10-18, doi:10.1016/j.jconrel.2007.05.027 (2007).
18 Nakano, K., Tozuka, Y., Yamamoto, H., Kawashima, Y. & Takeuchi, H. A novel method for measuring rigidity of submicron-size liposomes with atomic force microscopy. Int J Pharm 355, 203-209, doi:10.1016/j.ijpharm.2007.12.018 (2008).
19 Best, J. P., Cui, J., Mullner, M. & Caruso, F. Tuning the mechanical properties of nanoporous hydrogel particles via polymer cross-linking. Langmuir 29, 9824-9831, doi:10.1021/la402146t (2013).
20 Sun, H. et al. The role of capsule stiffness on cellular processing. Chem Sci 6, 3505-3514, doi:10.1039/c5sc00416k (2015).
21 Albanese, A., Tang, P. S. & Chan, W. C. The effect of nanoparticle size, shape, and surface chemistry on biological systems. Annu Rev Biomed Eng 14, 1-16, doi:10.1146/annurev-bioeng-071811-150124 (2012).
22 Watson, D. S., Endsley, A. N. & Huang, L. Design considerations for liposomal vaccines: influence of formulation parameters on antibody and cell-mediated immune responses to liposome associated antigens. Vaccine 30, 2256-2272, doi:10.1016/j.vaccine.2012.01.070 (2012).
23 Wang, J., Byrne, J. D., Napier, M. E. & DeSimone, J. M. More effective nanomedicines through particle design. Small 7, 1919-1931, doi:10.1002/smll.201100442 (2011).
24 Geijtenbeek, T. B. H. & Gringhuis, S. I. Signalling through C-type lectin receptors: shaping immune responses. Nat Rev Immunol 9, 465-479 (2009).
25 Kawai, T. & Akira, S. The role of pattern-recognition receptors in innate immunity: update on Toll-like receptors. Nat Immunol 11, 373-384, doi:10.1038/ni.1863 (2010).
26 Alving, C. R. Liposomes as carriers of antigens and adjuvants. Journal of Immunological Methods 140, 1-13, doi:http://dx.doi.org/10.1016/0022-1759(91)90120-5 (1991).
27 Zaks, K. et al. Efficient immunization and cross-priming by vaccine adjuvants containing TLR3 or TLR9 agonists complexed to cationic liposomes. J Immunol 176, 7335-7345 (2006).
28 Smith, D. M., Simon, J. K. & Baker, J. R., Jr. Applications of nanotechnology for immunology. Nat Rev Immunol 13, 592-605, doi:10.1038/nri3488 (2013).
29 Moon, J. J., Huang, B. & Irvine, D. J. Engineering nano- and microparticles to tune immunity. Adv Mater 24, 3724-3746, doi:10.1002/adma.201200446 (2012).
30 Kamaly, N., Xiao, Z., Valencia, P. M., Radovic-Moreno, A. F. & Farokhzad, O. C. Targeted polymeric therapeutic nanoparticles: design, development and clinical translation. Chem Soc Rev 41, 2971-3010, doi:10.1039/c2cs15344k (2012).
31 Moyer, T. J., Zmolek, A. C. & Irvine, D. J. Beyond antigens and adjuvants: formulating future vaccines. The Journal of clinical investigation 126, 799-808, doi: doi:10.1172/JCI81083 (2016).
32 Banchereau, J. & Steinman, R. M. Dendritic cells and the control of immunity.

Nature 392, 245-252 (1998).
33 von Andrian, U. H. & Mempel, T. R. Homing and cellular traffic in lymph nodes. Nat Rev Immunol 3, 867-878, doi:http://www.nature.com/nri/journal/v3/n11/suppinfo/nri1222_S1.html (2003).
34 Reddy, S. T. et al. Exploiting lymphatic transport and complement activation in nanoparticle vaccines. Nat Biotech 25, 1159-1164, doi:http://www.nature.com/nbt/journal/v25/n10/suppinfo/nbt1332_S1.html (2007).
35 Reddy, S. T., Rehor, A., Schmoekel, H. G., Hubbell, J. A. & Swartz, M. A. In vivo targeting of dendritic cells in lymph nodes with poly(propylene sulfide) nanoparticles. J Control Release 112, 26-34, doi:10.1016/j.jconrel.2006.01.006 (2006).
36 Manolova, V. et al. Nanoparticles target distinct dendritic cell populations according to their size. Eur J Immunol 38, 1404-1413, doi:10.1002/eji.200737984 (2008).
37 Martín-Fontecha, A. et al. Regulation of Dendritic Cell Migration to the Draining Lymph Node: Impact on T Lymphocyte Traffic and Priming. The Journal of Experimental Medicine 198, 615-621, doi:10.1084/jem.20030448 (2003).
38 Oussoren, C., Zuidema, J., Crommelin, D. J. & Storm, G. Lymphatic uptake and biodistribution of liposomes after subcutaneous injection. II. Influence of liposomal size, lipid compostion and lipid dose. Biochim Biophys Acta 1328, 261-272 (1997).
39 Oussoren, C. et al. Lymphatic uptake and biodistribution of liposomes after subcutaneous injection . IV. Fate of liposomes in regional lymph nodes. Biochim Biophys Acta 1370, 259-272, doi:10.1016/s0005-2736(97)00275-7 (1998).
40 Merad, M., Sathe, P., Helft, J., Miller, J. & Mortha, A. The Dendritic Cell Lineage: Ontogeny and Function of Dendritic Cells and Their Subsets in the Steady State and the Inflamed Setting. Annual review of immunology 31, 10.1146/annurev-immunol-020711-074950, doi:10.1146/annurev-immunol-020711-074950 (2013).
41 Tabata, Y., Inoue, Y. & Ikada, Y. Size effect on systemic and mucosal immune responses induced by oral administration of biodegradable microspheres. Vaccine 14, 1677-1685, doi:10.1016/s0264-410x(96)00149-1 (1996).
42 Jani, P., Halbert, G. W., Langridge, J. & Florence, A. T. The uptake and translocation of latex nanospheres and microspheres after oral administration to rats. The Journal of pharmacy and pharmacology 41, 809-812 (1989).
43 Desai, M. P., Labhasetwar, V., Amidon, G. L. & Levy, R. J. Gastrointestinal uptake of biodegradable microparticles: effect of particle size. Pharm Res 13, 1838-1845 (1996).
44 Schroeder, H. W. & Cavacini, L. Structure and Function of Immunoglobulins. The Journal of allergy and clinical immunology 125, S41-S52, doi:10.1016/j.jaci.2009.09.046 (2010).
45 Jung, T. et al. Tetanus toxoid loaded nanoparticles from sulfobutylated poly(vinyl alcohol)-graft-poly(lactide-co-glycolide): evaluation of antibody response after oral and nasal application in mice. Pharm Res 18, 352-360 (2001).
46 Slütter, B. et al. Antigen−Adjuvant Nanoconjugates for Nasal Vaccination: An Improvement over the Use of Nanoparticles? Molecular Pharmaceutics 7, 2207-

2215, doi:10.1021/mp100210g (2010).
47 Mellman, I. & Steinman, R. M. Dendritic Cells: Specialized and Regulated Antigen Processing Machines. Cell 106, 255-258, doi:http://dx.doi.org/10.1016/S0092-8674(01)00449-4 (2001).
48 Trombetta, E. S. & Mellman, I. Cell biology of antigen processing in vitro and in vivo. Annual review of immunology 23, 975-1028, doi:10.1146/annurev.immunol.22.012703.104538 (2005).
49 Joshi, V. B., Geary, S. M. & Salem, A. K. Biodegradable particles as vaccine delivery systems: size matters. AAPS J 15, 85-94, doi:10.1208/s12248-012-9418-6 (2013).
50 Mathaes, R., Winter, G., Siahaan, T. J., Besheer, A. & Engert, J. Influence of particle size, an elongated particle geometry, and adjuvants on dendritic cell activation. Eur J Pharm Biopharm 94, 542-549, doi:10.1016/j.ejpb.2015.06.015 (2015).
51 Foged, C., Brodin, B., Frokjaer, S. & Sundblad, A. Particle size and surface charge affect particle uptake by human dendritic cells in an in vitro model. Int J Pharm 298, 315-322, doi:10.1016/j.ijpharm.2005.03.035 (2005).
52 Shima, F., Uto, T., Akagi, T., Baba, M. & Akashi, M. Size effect of amphiphilic poly(γ-glutamic acid) nanoparticles on cellular uptake and maturation of dendritic cells in vivo. Acta Biomaterialia 9, 8894-8901, doi:http://dx.doi.org/10.1016/j.actbio.2013.06.010 (2013).
53 Blank, F. et al. Size-Dependent Uptake of Particles by Pulmonary Antigen-Presenting Cell Populations and Trafficking to Regional Lymph Nodes. American Journal of Respiratory Cell and Molecular Biology 49, 67-77, doi:10.1165/rcmb.2012-0387OC (2013).
54 le Guével, X. et al. Nanoparticle size influences the proliferative responses of lymphocyte subpopulations. RSC Advances 5, 85305-85309, doi:10.1039/c5ra16164a (2015).
55 Kanchan, V. & Panda, A. K. Interactions of antigen-loaded polylactide particles with macrophages and their correlation with the immune response. Biomaterials 28, 5344-5357, doi:10.1016/j.biomaterials.2007.08.015 (2007).
56 Thomas, C., Gupta, V. & Ahsan, F. Particle size influences the immune response produced by hepatitis B vaccine formulated in inhalable particles. Pharm Res 27, 905-919, doi:10.1007/s11095-010-0094-x (2010).
57 Janeway, C. A., Jr. & Medzhitov, R. Innate immune recognition. Annual review of immunology 20, 197-216, doi:10.1146/annurev.immunol.20.083001.084359 (2002).
58 Villadangos, J. A. & Schnorrer, P. Intrinsic and cooperative antigen-presenting functions of dendritic-cell subsets in vivo. Nat Rev Immunol 7, 543-555 (2007).
59 Varkouhi, A. K., Scholte, M., Storm, G. & Haisma, H. J. Endosomal escape pathways for delivery of biologicals. Journal of Controlled Release 151, 220-228, doi:http://dx.doi.org/10.1016/j.jconrel.2010.11.004 (2011).
60 Mant, A., Chinnery, F., Elliott, T. & Williams, A. P. The pathway of cross-presentation is influenced by the particle size of phagocytosed antigen. Immunology 136, 163-175, doi:10.1111/j.1365-2567.2012.03558.x (2012).
61 Silva, A. L. et al. Poly-(lactic-co-glycolic-acid)-based particulate vaccines: Particle uptake by dendritic cells is a key parameter for immune activation. Vaccine 33,

847-854, doi:http://dx.doi.org/10.1016/j.vaccine.2014.12.059 (2015).
62 Seydoux, E. et al. Size-dependent accumulation of particles in lysosomes modulates dendritic cell function through impaired antigen degradation. Int J Nanomedicine 9, 3885-3902, doi:10.2147/ijn.s64353 (2014).
63 Nolz, J. C. Molecular mechanisms of CD8+ T cell trafficking and localization. Cellular and Molecular Life Sciences 72, 2461-2473, doi:10.1007/s00018-015-1835-0 (2015).
64 Tscharke, D. C., Croft, N. P., Doherty, P. C. & La Gruta, N. L. Sizing up the key determinants of the CD8+ T cell response. Nat Rev Immunol 15, 705-716, doi:10.1038/nri3905 (2015).
65 Geginat, J. et al. The CD4-centered universe of human T cell subsets. Seminars in Immunology 25, 252-262, doi:http://dx.doi.org/10.1016/j.smim.2013.10.012 (2013).
66 Mottram, P. L. et al. Type 1 and 2 immunity following vaccination is influenced by nanoparticle size: formulation of a model vaccine for respiratory syncytial virus. Mol Pharm 4, 73-84, doi:10.1021/mp060096p (2007).
67 Fifis, T. et al. Size-dependent immunogenicity: therapeutic and protective properties of nano-vaccines against tumors. J Immunol 173, 3148-3154 (2004).
68 Li, X., Sloat, B. R., Yanasarn, N. & Cui, Z. Relationship between the size of nanoparticles and their adjuvant activity: data from a study with an improved experimental design. Eur J Pharm Biopharm 78, 107-116, doi:10.1016/j.ejpb.2010.12.017 (2011).
69 Mann, J. F. et al. Lipid vesicle size of an oral influenza vaccine delivery vehicle influences the Th1/Th2 bias in the immune response and protection against infection. Vaccine 27, 3643-3649, doi:10.1016/j.vaccine.2009.03.040 (2009).
70 Henriksen-Lacey, M., Devitt, A. & Perrie, Y. The vesicle size of DDA:TDB liposomal adjuvants plays a role in the cell-mediated immune response but has no significant effect on antibody production. J Control Release 154, 131-137, doi:10.1016/j.jconrel.2011.05.019 (2011).
71 Tran, K. K. & Shen, H. The role of phagosomal pH on the size-dependent efficiency of cross-presentation by dendritic cells. Biomaterials 30, 1356-1362, doi:10.1016/j.biomaterials.2008.11.034 (2009).
72 Huang, X. et al. The Shape Effect of Mesoporous Silica Nanoparticles on Biodistribution, Clearance, and Biocompatibility in Vivo. ACS Nano 5, 5390-5399, doi:10.1021/nn200365a (2011).
73 Geng, Y. et al. Shape effects of filaments versus spherical particles in flow and drug delivery. Nat Nanotechnol 2, 249-255, doi:10.1038/nnano.2007.70 (2007).
74 Li, L. et al. Biodistribution, excretion, and toxicity of mesoporous silica nanoparticles after oral administration depend on their shape. Nanomedicine: Nanotechnology, Biology and Medicine 11, 1915-1924, doi:http://dx.doi.org/10.1016/j.nano.2015.07.004 (2015).
75 Champion, J. A. & Mitragotri, S. Shape induced inhibition of phagocytosis of polymer particles. Pharm Res 26, 244-249, doi:10.1007/s11095-008-9626-z (2009).
76 Niikura, K. et al. Gold nanoparticles as a vaccine platform: influence of size and shape on immunological responses in vitro and in vivo. ACS Nano 7, 3926-3938,

doi:10.1021/nn3057005 (2013).
77 Sharma, G. et al. Polymer particle shape independently influences binding and internalization by macrophages. J Control Release 147, 408-412, doi:10.1016/j.jconrel.2010.07.116 (2010).
78 Champion, J. A. & Mitragotri, S. Role of target geometry in phagocytosis. Proceedings of the National Academy of Sciences of the United States of America 103, 4930-4934, doi:10.1073/pnas.0600997103 (2006).
79 Huang, X., Teng, X., Chen, D., Tang, F. & He, J. The effect of the shape of mesoporous silica nanoparticles on cellular uptake and cell function. Biomaterials 31, 438-448, doi:10.1016/j.biomaterials.2009.09.060 (2010).
80 Yi, X. & Gao, H. Phase diagrams and morphological evolution in wrapping of rod-shaped elastic nanoparticles by cell membrane: a two-dimensional study. Phys Rev E Stat Nonlin Soft Matter Phys 89, 062712, doi:10.1103/PhysRevE.89.062712 (2014).
81 Merkel, T. J. et al. Using mechanobiological mimicry of red blood cells to extend circulation times of hydrogel microparticles. Proc Natl Acad Sci U S A 108, 586-591, doi:10.1073/pnas.1010013108 (2011).
82 Anselmo, A. C. et al. Elasticity of nanoparticles influences their blood circulation, phagocytosis, endocytosis, and targeting. ACS Nano 9, 3169-3177, doi:10.1021/acsnano.5b00147 (2015).
83 Gabizon, A. & Papahadjopoulos, D. Liposome formulations with prolonged circulation time in blood and enhanced uptake by tumors. Proc Natl Acad Sci U S A 85, 6949-6953, doi:10.1073/pnas.85.18.6949 (1988).
84 Allen, T. M., Hansen, C. & Rutledge, J. Liposomes with prolonged circulation times: factors affecting uptake by reticuloendothelial and other tissues. Biochim Biophys Acta 981, 27-35, doi:10.1016/0005-2736(89)90078-3 (1989).
85 Senior, J. & Gregoriadis, G. Stability of small unilamellar liposomes in serum and clearance from the circulation: the effect of the phospholipid and cholesterol components. Life Sci 30, 2123-2136, doi:10.1016/0024-3205(82)90455-6 (1982).
86 Wroblewska, M., Czyzewska, M., Wolska, A., Kortas-Stempak, B. & Szutowicz, A. Apo A-II participates in HDL-liposome interaction by the formation of new pre-beta mobility particles and the modification of liposomes. Biochim Biophys Acta 1801, 1323-1329, doi:10.1016/j.bbalip.2010.08.005 (2010).
87 Christensen, D. et al. A cationic vaccine adjuvant based on a saturated quaternary ammonium lipid have different in vivo distribution kinetics and display a distinct CD4 T cell-inducing capacity compared to its unsaturated analog. J Control Release 160, 468-476, doi:10.1016/j.jconrel.2012.03.016 (2012).
88 Kaur, R. et al. Effect of incorporating cholesterol into DDA:TDB liposomal adjuvants on bilayer properties, biodistribution, and immune responses. Mol Pharm 11, 197-207, doi:10.1021/mp400372j (2014).
89 Yi, X., Shi, X. & Gao, H. Cellular uptake of elastic nanoparticles. Phys Rev Lett 107, 098101, doi:10.1103/PhysRevLett.107.098101 (2011).
90 Sun, J. et al. Tunable rigidity of (polymeric core)-(lipid shell) nanoparticles for regulated cellular uptake. Adv Mater 27, 1402-1407, doi:10.1002/adma.201404788 (2015).
91 Beningo, K. A. & Wang, Y. L. Fc-receptor-mediated phagocytosis is regulated by

mechanical properties of the target. J Cell Sci 115, 849-856 (2002).
92 Hartmann, R., Weidenbach, M., Neubauer, M., Fery, A. & Parak, W. J. Stiffness-dependent in vitro uptake and lysosomal acidification of colloidal particles. Angew Chem Int Ed Engl 54, 1365-1368, doi:10.1002/anie.201409693 (2015).
93 Cui, J. et al. Mechanically tunable, self-adjuvanting nanoengineered polypeptide particles. Adv Mater 25, 3468-3472, doi:10.1002/adma.201300981 (2013).
94 Yasuda, T., Dancey, G. F. & Kinsky, S. C. Immunogenicity of liposomal model membranes in mice: dependence on phospholipid composition. Proc Natl Acad Sci U S A 74, 1234-1236, doi:10.1073/pnas.74.3.1234 (1977).
95 Dancey, G. F., Yasuda, T. & Kinsky, S. C. Effect of liposomal model membrane composition on immunogenicity. J Immunol 120, 1109-1113 (1978).
96 Kersten, G. F., van de Put, A. M., Teerlink, T., Beuvery, E. C. & Crommelin, D. J. Immunogenicity of liposomes and iscoms containing the major outer membrane protein of Neisseria gonorrhoeae: influence of protein content and liposomal bilayer composition. Infect Immun 56, 1661-1664 (1988).
97 Bakouche, O. & Gerlier, D. Enhancement of immunogenicity of tumour virus antigen by liposomes: the effect of lipid composition. Immunology 58, 507-513 (1986).
98 Garnier, F., Forquet, F., Bertolino, P. & Gerlier, D. Enhancement of in vivo and in vitro T cell response against measles virus haemagglutinin after its incorporation into liposomes: effect of the phospholipid composition. Vaccine 9, 340-345, doi:10.1016/0264-410x(91)90061-a (1991).
99 Mazumdar, T., Anam, K. & Ali, N. Influence of phospholipid composition on the adjuvanticity and protective efficacy of liposome-encapsulated Leishmania donovani antigens. J Parasitol 91, 269-274, doi:10.1645/GE-356R1 (2005).
100 Arnal, L. et al. Adhesin contribution to nanomechanical properties of the virulent Bordetella pertussis envelope. Langmuir 28, 7461-7469, doi:10.1021/la300811m (2012).
101 capital Em, C. V. V. et al. The role of beneficial bacteria wall elasticity in regulating innate immune response. EPMA J 6, 13, doi:10.1186/s13167-015-0035-1 (2015).
102 Kol, N. et al. A stiffness switch in human immunodeficiency virus. Biophys J 92, 1777-1783, doi:10.1529/biophysj.106.093914 (2007).
103 Kol, N. et al. Mechanical properties of murine leukemia virus particles: effect of maturation. Biophys J 91, 767-774, doi:10.1529/biophysj.105.079657 (2006).

Table 1: Overview of studies referenced in this review. Particle characteristics, animal or cell model, administration route (where appropriate), studied parameters and studied effects are specified for each article.

Particle characteristics	Model	Administration route	Parameter studied	Effect observed	Ref
Spherical; neutral, poloxamer 407-stabilised poly(propylene sulphide)	BALB/c and C57BL6 mouse	i.d.	Size	Distribution	1
Spherical; neutral; PEG-poly(propylene sulphide)	BALB/c mouse	s.c.	Size	Distribution	2
Spherical; anionic; polystyrene	C57BL/6 mouse	i.c.	Size	Distribution	3
Spherical; anionic; egg PC:egg phosphatidylglycerol(PG):cholesterol (10:1:4 molar ratio) liposomes	Wistar rat	s.c.	Size	Distribution	4
Spherical; neutral; egg PC:cholesterol (6:1 molar ratio)	Wistar rat	s.c.	Size	Distribution	5
Spherical; anionic; polystyrene	Sprague-Dawley rat	oral	Size	Distribution	6
Spherical; anionic; PLGA (50:50, MW 100,000)	Sprague-Dawley rat	*In situ* intestinal tissue loop	Size	Distribution	7
Spherical; anionic; PLA (MW 7,000)	BALB/c mouse	oral	Size	Distribution	8
Spherical; anionic; PLGA (75:25, MW 98,000)	CD1 mouse	oral	Size	Distribution	9
Spherical; neutral; PLA-PEG (31:69, MW 28,000)	Sprague-Dawley rat	intranasal	Size	Distribution	10
Spherical; cationic; N-trimethyl chitosan:tripolyphosphate (10:1.7 weight ratio)	BALB/c mouse	intranasal	Size	Distribution	11
Spherical; anionic; γ-PGA-g-phenylalanine (MW 380,000, 50:50)	C57BL/6j mouse	s.c.	Size	Distribution, cell uptake, APC activation	12

Spherical; anionic; carboxyl-modified polystyrene	BALB/c mouse	intranasal	Size	Distribution, cell uptake, APC activation	13
Spherical; anionic; poly(sulfobutyl-vinyl alcohol)-g-PLGA (50:50 MW 221,000)	BALB/c mouse	oral, intranasal, i.p.	Size, administration route	Distribution, immune response	14
Spherical; anionic; PLGA (50:50, MW 24,000)	C57BL/6 mouse	i.p.	Size	Cell uptake, APC activation, immune response	15
Spherical and elliptical; anionic; polystyrene	JAWSII DC cell line	-	Size, shape	Cell uptake, APC activation	16
Spherical; anionic and cationic; polystyrene	Human monocyte derived DCs	-	Size	Cell uptake	17
Spherical; anionic; PLA (MW 45,000)	Wistar rat	i.m.	Size	Cell uptake, antigen presentation, immune response	18
Spherical; neutral; glutathione-conjugated gold	Human monocyte derived DCs	-	Size	Cell uptake, APC activation, immune response	19
Spherical; anionic; PLGA (50:50, MW 43,500 and 4,500)	Sprague-Dawley rat	pulmonary	Size, weight	Cell uptake, immune response	20
Spherical; anionic; PLGA (50:50 MW 5,000 and 75:25 MW 4,000)	C57BL/6 mouse	s.c.	Size	Cell uptake, immune response	21
Spherical; anionic; monopalmitoyl glycerol:cholesterol:dicetyl phosphate (DCP) (5:4:1 molar ratio) liposomes	BALB/c or CBA/ca mouse derived macrophages	-	Size	Antigen presentation, cell uptake	22

Spherical; anionic; carboxyl-modified polystyrene	BALB/c and C57BL/6 mouse	i.d.	Size	Cell uptake, immune response	23
Spherical; anionic; carboxyl-modified polystyrene	C57BL/6 mouse	i.d.	Size	Distribution, immune response	24
Spherical; anionic; soy lecithin:glycerol monostearate (7:1 weight ratio)	C57BL/6 mouse	s.c.	Size	Distribution, antigen presentation, cell uptake, immune response	25
Spherical; anionic; monopalmitoyl glycerol:cholesterol:D-CP (5:4:1 molar ratio) liposomes	BALB/c mouse, ferret	oral, i.m.	Size, administration route	Immune response	26
Spherical; cationic; dimethyldioctadecylammonium (DDA): trehalose dibehenate (TDB) (5:1 weight ratio) liposomes	BALB/c mouse	i.m.	Size	Distribution, cell uptake, immune response	27
Elliptical (AR 1.5 and 5); cationic; tetraethyl orthosilicate mesoporous silica	ICR mouse	i.v.	Shape	Distribution	28
Filamental; neutral; PEG-polyethylethylene or PEG-polycaprolactone	Sprague-Dawley rat, C57BL/6 mouse	i.v.	Shape, size	Distribution, cell uptake	29
Elongated (AR >20); anionic; polystyrene	Rat alveolar macrophage	-	Shape, size	Cell uptake	30
Spherical, cubic and rod-like (AR 4); anionic; gold	C3H/HeN Jc1 mouse	i.p.	Shape, size	Cell uptake, APC activation, immune response	31
Spherical, oblate elliptical, prolate elliptical; anionic; polystyrene	RAW264.7 macrophage	-	Shape, size	Cell uptake	32

Spherical, oblate elliptical, prolate elliptical, elliptical disk, rectangular disk, UFO-shaped; anionic; polystyrene	Rat alveolar macrophage	-	Shape, size	Cell uptake	33
Spherical, short rod (AR 2), long rod (AR 4); cationic; tetraethyl orthosilicate mesoporous silica	A375 human melanoma	-	Shape	Cell uptake	34
Spherical, rod-shaped (AR 3 and 7); anionic; carboxyl-modified polystyrene	BALB/c mouse	s.c.	Shape, size	Cell uptake, immune response	35
Discoid; anionic; 2-hydroxyethyl acrylate and 2-carboxyethyl acrylate cross-linked with PEG-diacrylate hydrogel	BALB/c mouse	i.v.	Rigidity	Distribution, cell uptake	36
Spherical; anionic; PEG-diacrylate and 2-carboxyethyl acrylate hydrogel	BALB/c mouse	i.v.	Rigidity	Distribution, cell uptake	37
Spherical; anionic; polyacrylamide	Murine BMDC	-	Rigidity	Cell uptake	38
Spherical; cationic; poly(sodium 4-styrenesulphonate):poly(allylamine hydrochloride) (MW 70,000 and 56000) and dextran sulphate:poly-L-arginine (MW 40,000 and 15-70,000) capsules	A549 cells, HeLa cells, SH-SY5Y cells, HUVECs and human monocyte-derived macrophages and DCs	-	Rigidity	Cell uptake	39
Spherical; anionic; PGA (MW 3-15,000 and 45,000) capsules	PBMCs	-	Rigidity	Cell uptake, APC activation	40
Spherical; neutral and anionic; several liposomes containing egg PG, egg PC, cholesterol, monosialoganglioside, dipalmitoyl (DP)PG and distearoyl (DS)PC	Swiss-Webster mouse	i.v.	Rigidity	Distribution	41
Spherical; neutral and anionic; several liposomes containing egg PC, sphingomyelin (SM), DSPC, phosphatidylinositol, phosphatidic acid, DPPG, PS and monosialoganglioside,	ICR mouse	i.v., i.p., s.c.	Rigidity	Distribution	42

Spherical: neutral; liposomes containing egg PC, egg SM, DSPC and cholesterol	T.O. mouse	i.v. and i.p.	Rigidity	Distribution	43
Spherical; cationic; DDA:TDB (1.98:0.25 molar ratio) and dimethyldioleoylammonium:TDB liposomes	C67BL/6 and BALB/c mouse	i.m.	Rigidity	Distribution, cell uptake, APC activation, immune response	44
Spherical; cationic; DDA:TDB:cholesterol (8:1:0, 8:1:2 and 8:1:4 molar ratio) liposomes	C67BL/6 and BALB/c mouse	i.m.	Rigidity	Distribution, cell uptake, immune response	45
Spherical; anionic; various PC:cholesterol:DCP:dinitrophenyl-aminocaproyl phosphatidylethanolamine (PE) (2:1.5:0.2:0.1 molar ratio)	AKR mouse	i.p.	Rigidity	Immune response	46
Spherical; neutral, anionic or cationic; various PC and PE, DCP and stearylamine liposomes	AKR mouse	i.p.	Rigidity	Immune response	47
Spherical; anionic; PC:cholesterol:PG, DPPC:cholesterol:DPPG, DSPC:cholesterol:DSPG liposomes of various molar ratios	Cpb:SE mouse	s.c.	Rigidity	Immune response	48
Spherical; anionic; various PC/PE, DPPG/DCP and cholesterol (7:2:1 molar ratio) liposomes	W/Fu rat	s.c.	Rigidity	Immune response	49
Spherical; anionic; cholesterol:DCP:DLPC or cholesterol:DCP:DSPC (1:2:7 molar ratio) liposomes	BALB/c mouse	s.c.	Rigidity	Immune response	50
Spherical; neutral; various PC:cholesterol (7:2 molar ratio) liposomes	Hamster	i.p.	Rigidity	Immune response	51

References

1 Reddy, S. T. et al. Exploiting lymphatic transport and complement activation in nanoparticle vaccines. Nat Biotech 25, 1159-1164, doi:http://www.nature.com/nbt/journal/v25/n10/suppinfo/nbt1332_S1.html (2007).

2 Reddy, S. T., Rehor, A., Schmoekel, H. G., Hubbell, J. A. & Swartz, M. A. In vivo targeting of dendritic cells in lymph nodes with poly(propylene sulfide) nanoparticles. J Control Release 112, 26-34, doi:10.1016/j.jconrel.2006.01.006 (2006).

3 Manolova, V. et al. Nanoparticles target distinct dendritic cell populations according to their size. Eur J Immunol 38, 1404-1413, doi:10.1002/eji.200737984 (2008).

4 Oussoren, C., Zuidema, J., Crommelin, D. J. & Storm, G. Lymphatic uptake and biodistribution of liposomes after subcutaneous injection. II. Influence of liposomal size, lipid compostion and lipid dose. Biochim Biophys Acta 1328, 261-272 (1997).

5 Oussoren, C. et al. Lymphatic uptake and biodistribution of liposomes after subcutaneous injection . IV. Fate of liposomes in regional lymph nodes. Biochim Biophys Acta 1370, 259-272, doi:10.1016/s0005-2736(97)00275-7 (1998).

6 Jani, P., Halbert, G. W., Langridge, J. & Florence, A. T. The uptake and translocation of latex nanospheres and microspheres after oral administration to rats. The Journal of pharmacy and pharmacology 41, 809-812 (1989).

7 Desai, M. P., Labhasetwar, V., Amidon, G. L. & Levy, R. J. Gastrointestinal uptake of biodegradable microparticles: effect of particle size. Pharm Res 13, 1838-1845 (1996).

8 Tabata, Y., Inoue, Y. & Ikada, Y. Size effect on systemic and mucosal immune responses induced by oral administration of biodegradable microspheres. Vaccine 14, 1677-1685, doi:10.1016/s0264-410x(96)00149-1 (1996).

9 Shakweh, M., Besnard, M., Nicolas, V. & Fattal, E. Poly (lactide-co-glycolide) particles of different physicochemical properties and their uptake by peyer's patches in mice. Eur J Pharm Biopharm 61, 1-13, doi:10.1016/j.ejpb.2005.04.006 (2005).

10 Vila, A. et al. PLA-PEG particles as nasal protein carriers: the influence of the particle size. Int J Pharm 292, 43-52, doi:10.1016/j.ijpharm.2004.09.002 (2005).

11 Slütter, B. et al. Antigen−Adjuvant Nanoconjugates for Nasal Vaccination: An Improvement over the Use of Nanoparticles? Molecular Pharmaceutics 7, 2207-2215, doi:10.1021/mp100210g (2010).

12 Shima, F., Uto, T., Akagi, T., Baba, M. & Akashi, M. Size effect of amphiphilic poly(γ-glutamic acid) nanoparticles on cellular uptake and maturation of dendritic cells in vivo. Acta Biomaterialia 9, 8894-8901, doi:http://dx.doi.org/10.1016/j.actbio.2013.06.010 (2013).

13 Blank, F. et al. Size-Dependent Uptake of Particles by Pulmonary Antigen-Presenting Cell Populations and Trafficking to Regional Lymph Nodes. American Journal of Respiratory Cell and Molecular Biology 49, 67-77, doi:10.1165/rcmb.2012-0387OC (2013).

14 Jung, T. et al. Tetanus toxoid loaded nanoparticles from sulfobutylated poly(vinyl alcohol)-graft-poly(lactide-co-glycolide): evaluation of antibody response after

oral and nasal application in mice. Pharm Res 18, 352-360 (2001).
15 Joshi, V. B., Geary, S. M. & Salem, A. K. Biodegradable particles as vaccine delivery systems: size matters. AAPS J 15, 85-94, doi:10.1208/s12248-012-9418-6 (2013).
16 Mathaes, R., Winter, G., Siahaan, T. J., Besheer, A. & Engert, J. Influence of particle size, an elongated particle geometry, and adjuvants on dendritic cell activation. Eur J Pharm Biopharm 94, 542-549, doi:10.1016/j.ejpb.2015.06.015 (2015).
17 Foged, C., Brodin, B., Frokjaer, S. & Sundblad, A. Particle size and surface charge affect particle uptake by human dendritic cells in an in vitro model. Int J Pharm 298, 315-322, doi:10.1016/j.ijpharm.2005.03.035 (2005).
18 Kanchan, V. & Panda, A. K. Interactions of antigen-loaded polylactide particles with macrophages and their correlation with the immune response. Biomaterials 28, 5344-5357, doi:10.1016/j.biomaterials.2007.08.015 (2007).
19 le Guével, X. et al. Nanoparticle size influences the proliferative responses of lymphocyte subpopulations. RSC Advances 5, 85305-85309, doi:10.1039/c5ra16164a (2015).
20 Thomas, C., Gupta, V. & Ahsan, F. Particle size influences the immune response produced by hepatitis B vaccine formulated in inhalable particles. Pharm Res 27, 905-919, doi:10.1007/s11095-010-0094-x (2010).
21 Silva, A. L. et al. Poly-(lactic-co-glycolic-acid)-based particulate vaccines: Particle uptake by dendritic cells is a key parameter for immune activation. Vaccine 33, 847-854, doi:http://dx.doi.org/10.1016/j.vaccine.2014.12.059 (2015).
22 Brewer, J. M., Pollock, K. G., Tetley, L. & Russell, D. G. Vesicle size influences the trafficking, processing, and presentation of antigens in lipid vesicles. J Immunol 173, 6143-6150 (2004).
23 Mottram, P. L. et al. Type 1 and 2 immunity following vaccination is influenced by nanoparticle size: formulation of a model vaccine for respiratory syncytial virus. Mol Pharm 4, 73-84, doi:10.1021/mp060096p (2007).
24 Fifis, T. et al. Size-dependent immunogenicity: therapeutic and protective properties of nano-vaccines against tumors. J Immunol 173, 3148-3154 (2004).
25 Li, X., Sloat, B. R., Yanasarn, N. & Cui, Z. Relationship between the size of nanoparticles and their adjuvant activity: data from a study with an improved experimental design. Eur J Pharm Biopharm 78, 107-116, doi:10.1016/j.ejpb.2010.12.017 (2011).
26 Mann, J. F. et al. Lipid vesicle size of an oral influenza vaccine delivery vehicle influences the Th1/Th2 bias in the immune response and protection against infection. Vaccine 27, 3643-3649, doi:10.1016/j.vaccine.2009.03.040 (2009).
27 Henriksen-Lacey, M., Devitt, A. & Perrie, Y. The vesicle size of DDA:TDB liposomal adjuvants plays a role in the cell-mediated immune response but has no significant effect on antibody production. J Control Release 154, 131-137, doi:10.1016/j.jconrel.2011.05.019 (2011).
28 Huang, X. et al. The Shape Effect of Mesoporous Silica Nanoparticles on Biodistribution, Clearance, and Biocompatibility in Vivo. ACS Nano 5, 5390-5399, doi:10.1021/nn200365a (2011).
29 Geng, Y. et al. Shape effects of filaments versus spherical particles in flow and drug delivery. Nat Nanotechnol 2, 249-255, doi:10.1038/nnano.2007.70 (2007).

30 Champion, J. A. & Mitragotri, S. Shape induced inhibition of phagocytosis of polymer particles. Pharm Res 26, 244-249, doi:10.1007/s11095-008-9626-z (2009).
31 Niikura, K. et al. Gold nanoparticles as a vaccine platform: influence of size and shape on immunological responses in vitro and in vivo. ACS Nano 7, 3926-3938, doi:10.1021/nn3057005 (2013).
32 Sharma, G. et al. Polymer particle shape independently influences binding and internalization by macrophages. J Control Release 147, 408-412, doi:10.1016/j.jconrel.2010.07.116 (2010).
33 Champion, J. A. & Mitragotri, S. Role of target geometry in phagocytosis. Proceedings of the National Academy of Sciences of the United States of America 103, 4930-4934, doi:10.1073/pnas.0600997103 (2006).
34 Huang, X., Teng, X., Chen, D., Tang, F. & He, J. The effect of the shape of mesoporous silica nanoparticles on cellular uptake and cell function. Biomaterials 31, 438-448, doi:10.1016/j.biomaterials.2009.09.060 (2010).
35 Kumar, S., Anselmo, A. C., Banerjee, A., Zakrewsky, M. & Mitragotri, S. Shape and size-dependent immune response to antigen-carrying nanoparticles. J Control Release 220, 141-148, doi:10.1016/j.jconrel.2015.09.069 (2015).
36 Merkel, T. J. et al. Using mechanobiological mimicry of red blood cells to extend circulation times of hydrogel microparticles. Proc Natl Acad Sci U S A 108, 586-591, doi:10.1073/pnas.1010013108 (2011).
37 Anselmo, A. C. et al. Elasticity of nanoparticles influences their blood circulation, phagocytosis, endocytosis, and targeting. ACS Nano 9, 3169-3177, doi:10.1021/acsnano.5b00147 (2015).
38 Beningo, K. A. & Wang, Y. L. Fc-receptor-mediated phagocytosis is regulated by mechanical properties of the target. J Cell Sci 115, 849-856 (2002).
39 Hartmann, R., Weidenbach, M., Neubauer, M., Fery, A. & Parak, W. J. Stiffness-dependent in vitro uptake and lysosomal acidification of colloidal particles. Angew Chem Int Ed Engl 54, 1365-1368, doi:10.1002/anie.201409693 (2015).
40 Cui, J. et al. Mechanically tunable, self-adjuvanting nanoengineered polypeptide particles. Adv Mater 25, 3468-3472, doi:10.1002/adma.201300981 (2013).
41 Gabizon, A. & Papahadjopoulos, D. Liposome formulations with prolonged circulation time in blood and enhanced uptake by tumors. Proc Natl Acad Sci U S A 85, 6949-6953, doi:10.1073/pnas.85.18.6949 (1988).
42 Allen, T. M., Hansen, C. & Rutledge, J. Liposomes with prolonged circulation times: factors affecting uptake by reticuloendothelial and other tissues. Biochim Biophys Acta 981, 27-35, doi:10.1016/0005-2736(89)90078-3 (1989).
43 Senior, J. & Gregoriadis, G. Stability of small unilamellar liposomes in serum and clearance from the circulation: the effect of the phospholipid and cholesterol components. Life Sci 30, 2123-2136, doi:10.1016/0024-3205(82)90455-6 (1982).
44 Christensen, D. et al. A cationic vaccine adjuvant based on a saturated quaternary ammonium lipid have different in vivo distribution kinetics and display a distinct CD4 T cell-inducing capacity compared to its unsaturated analog. J Control Release 160, 468-476, doi:10.1016/j.jconrel.2012.03.016 (2012).
45 Kaur, R. et al. Effect of incorporating cholesterol into DDA:TDB liposomal adjuvants on bilayer properties, biodistribution, and immune responses. Mol

Pharm 11, 197-207, doi:10.1021/mp400372j (2014).
46 Yasuda, T., Dancey, G. F. & Kinsky, S. C. Immunogenicity of liposomal model membranes in mice: dependence on phospholipid composition. Proc Natl Acad Sci U S A 74, 1234-1236, doi:10.1073/pnas.74.3.1234 (1977).
47 Dancey, G. F., Yasuda, T. & Kinsky, S. C. Effect of liposomal model membrane composition on immunogenicity. J Immunol 120, 1109-1113 (1978).
48 Kersten, G. F., van de Put, A. M., Teerlink, T., Beuvery, E. C. & Crommelin, D. J. Immunogenicity of liposomes and iscoms containing the major outer membrane protein of Neisseria gonorrhoeae: influence of protein content and liposomal bilayer composition. Infect Immun 56, 1661-1664 (1988).
49 Bakouche, O. & Gerlier, D. Enhancement of immunogenicity of tumour virus antigen by liposomes: the effect of lipid composition. Immunology 58, 507-513 (1986).
50 Garnier, F., Forquet, F., Bertolino, P. & Gerlier, D. Enhancement of in vivo and in vitro T cell response against measles virus haemagglutinin after its incorporation into liposomes: effect of the phospholipid composition. Vaccine 9, 340-345, doi:10.1016/0264-410x(91)90061-a (1991).
51 Mazumdar, T., Anam, K. & Ali, N. Influence of phospholipid composition on the adjuvanticity and protective efficacy of liposome-encapsulated Leishmania donovani antigens. J Parasitol 91, 269-274, doi:10.1645/GE-356R1 (2005).

3

Atomic Force Microscopy Measurements of Anionic Liposomes Reveal the Effect of Liposomal Rigidity on Antigen-Specific Regulatory T Cell Responses

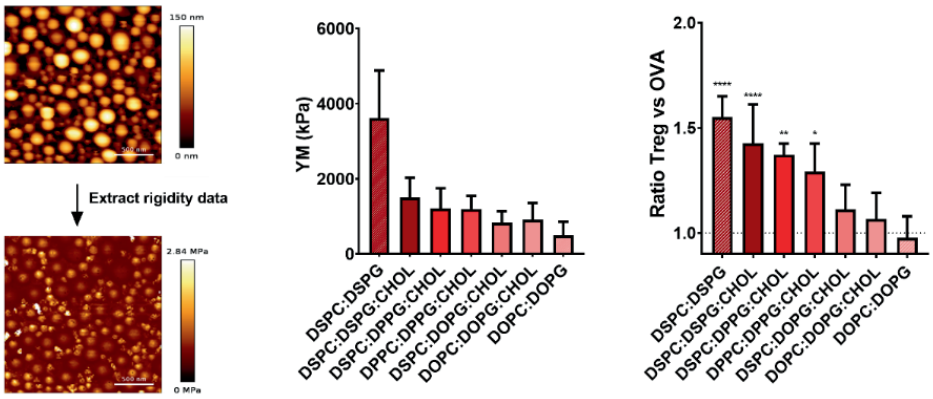
Authors and affiliations

Naomi Benne[a], Romain J. T. Leboux[a], Marco Glandrup[a], Janine van Duijn[a], Fernando Lozano Vigario[a], Malene Aaby Neustrup[a], Stefan Romeijn[a], Federica Galli[b], Johan Kuiper[a], Wim Jiskoot[a], Bram Slütter[a]*

[a] Division of BioTherapeutics, Leiden Academic Centre for Drug Research, Leiden, the Netherlands
[b] Leiden Institute of Physics, Leiden, the Netherlands

Journal of Controlled Release, Volume 318, February 2020, Pages 246-55
doi: 10.1016/j.jconrel.2019.12.003

Graphical Abstract



Abstract

Regulatory T cells (Tregs) are vital for maintaining a balanced immune response and their dysfunction is often associated with auto-immune disorders. We have previously shown that antigen-loaded anionic liposomes composed of phosphatidylcholine (PC) and phosphatidylglycerol (PG) and cholesterol can induce strong antigen-specific Treg responses. We hypothesized that altering the rigidity of these liposomes while maintaining their size and surface charge would affect their capability of inducing Treg responses. The rigidity of liposomes is affected in part by the length and saturation of carbon chains of the phospholipids in the bilayer, and in part by the presence of cholesterol. We used atomic force microscopy (AFM) to measure the rigidity of anionic OVA_{323}-containing liposomes composed of different types of PC and PG, with or without cholesterol, in a molar ratio of 4:1(:2) distearoyl (DS)PC:DSPG (Young's modulus (YM) 3611 ± 1271 kPa), DSPC:DSPG:CHOL (1498 ± 531 kPa), DSPC:dipalmitoyl (DP)PG:CHOL (1208 ± 538), DPPC:DPPG:CHOL (1195 ± 348 kPa), DSPC:dioleoyl (DO)PG:CHOL (825 ± 307 kPa), DOPC:DOPG:CHOL (911 ± 447 kPa), and DOPC:DOPG (494 ± 365 kPa). Next, we assessed if rigidity affects the association of liposomes to bone marrow-derived dendritic cells (BMDCs) *in vitro.* Aside from DOPC:DOPG liposomes, we observed a positive correlation between liposomal rigidity and cellular association. Finally, we show that rigidity positively correlates with Treg responses *in vitro* in murine DCs and *in vivo* in mice. Our findings underline the suitability of AFM to measure liposome rigidity and the importance of this parameter when designing liposomes as a vaccine delivery system.

Introduction

Regulatory T cells (Tregs) are important for the resolution of inflammation after infection, immune suppression, and immune homeostasis[1]. They do so by producing anti-inflammatory cytokines[2], consuming pro-inflammatory interleukin 2 (IL-2) and interrupting effector T cell metabolism[3]. A reduction in the number or the dysfunction of Tregs has been implicated in many diseases, including type 1 diabetes, rheumatoid arthritis, and multiple sclerosis[4]. Due to their immunosuppressive capacity, inducing Tregs is an attractive approach for immunotherapy in inflammatory and auto-immune diseases. Approaches to induce tolerance include oral administration of disease-specific antigens[5], as well as the use of tolerogenic nanoparticles (reviewed by Kishimoto and Maldonado[6]). Many of these tolerogenic nanoparticles co-encapsulate antigens with ligands to enhance tolerance or inhibit effector responses, such as CD22[7] or rapamycin[8,9], respectively. However, it is possible to use "bare" particles that exploit natural tolerogenic processes, generally by targeting scavenger receptors[10]. When using such nanoparticles, their physicochemical properties determine their efficiency to induce antigen-specific Treg responses. For instance, cationic particles are superior to anionic particles when comparing the efficiency of their association to APCs, as well as induction of pro-inflammatory responses[11], whereas we and other groups have shown that anionic nanoparticles like PG-containing liposomes are more efficient at inducing tolerance[12,13]. Besides the surface charge, particle size has also been shown to affect liposome-APC interactions and subsequent induction of antigen-specific Tregs. For example, nano-sized particles are taken up more efficiently by APCs than micron-sized particles, leading to stronger APC activation and subsequent immune responses[14]. Finally, the rigidity of nanoparticles is another important parameter for the induction of T cell responses[15,16], however, to our knowledge, it is unknown whether Treg responses are similarly affected by this parameter. The rigidity of a particle, expressed here as YM, describes the deformation of an entire particle and is not the same as the intrinsic deformation property of the material(s) that the particle is made of. Rigid particles were previously shown to be more efficiently taken up by macrophages compared to soft particles[17], and rigid liposomes were able to induce stronger DC activation *in vivo*[18]. Furthermore, rigid liposomes led to higher levels of antigen presentation on MHC-II in DCs[19]. Finally, increasing liposomal rigidity has been shown to result in increased humoral and cellular immune responses[20-22].

Here, we aimed to study the relationship between liposomal rigidity and induced antigen-specific Treg responses. Liposomal rigidity is related to, but not the same as, the rigidity of the lipid bilayer. Bilayer rigidity is strongly dependent on the transition temperature (T_m) of the constituent phospholipids. Below the T_m, phospholipid bilayers are in a relatively rigid gel state, whereas above the Tm they are in a (much less rigid) liquid disordered state[23]. Analytical techniques such as differential scanning calorimetry (DSC)[24] are commonly used to determine the average Tm of liposomal bilayers. However, these techniques do not measure the absolute rigidity of bilayers, let alone of liposomal particles. Moreover, bilayers containing substantial amounts of cholesterol (CHOL) lack a clear Tm[25], making the use of these analytical techniques less useful. In the present study, we employed atomic force microscopy (AFM), as this technique allows for simultaneous imaging and rigidity measurement of individual liposomes, whether or not they contain CHOL[26]. Here we present an AFM-based method to measure the YM of a range of anionic

liposomes, by immobilizing them on (3-aminopropyl)triethoxysilane (APTES)-modified silicon plates. Moreover, we show that liposomal rigidity is positively correlated with Treg responses against a loaded antigen *in vitro* and *in vivo*.

Materials and Methods

Materials

The phospholipids 1,2-distearoyl-sn-glycero-3-phosphocholine (DSPC), 1,2-dipalmitoyl-sn-glycero-3-phosphocholine (DPPC), 1,2-dioleoyl-sn-glycero-3-phosphocholine (DOPC), 1,2-distearoyl-sn-glycero-3-phosphoglycerol (DSPG), 1,2-dipalmitoyl-sn-glycero-3-phosphoglycerol (DPPG), 1,2-dioleoyl-sn-glycero-3- phosphoglycerol (DOPG), and 1,2-dipalmitoyl-sn-glycero-3-phosphoethanolamine-N-(lissamine rhodamine B sulfonyl) (DPPE-Rho) were purchased from Avanti Polar Lipids (Alabaster, AL, USA). Cholesterol (CHOL), APTES, acetic acid, N,N'-diisopropyl carbodiimide (DIC), and triisopropyl silane were purchased from Sigma-Aldrich (Zwijndrecht, the Netherlands). The ovalbumin-derived peptide OVA_{323} (ISQAVHAAHAEINEAGR) was purchased from Invivogen (San Diego, California, USA). Tentagel R-RAM resin was purchased from Rapp Polymere (Tübingen, Germany). Amino acids were supplied by Novabiochem (Merck, Darmstadt, Germany). Dimethylformamide (DMF), trifluoracetic acid (TFA), piperidine, pyridine, and acetonitrile were purchased from Biosolve (Valkenswaard, the Netherlands). Oxyma was supplied by Carl Roth (Karlsruhe, Germany). DCM was purchased from Honeywell (Fisher, Landsmeer, the Netherlands). Diethyl ether was acquired from VWR (Amsterdam, the Netherlands). Polycarbonate track-etched membranes with a pore size of 400 nm and 200 nm were obtained from Millipore (Kent, UK).

For cell culture, Ca^{2+}- and Mg^{2+}-free phosphate-buffered saline (PBS), Iscove's Modified Dulbecco's Medium (IMDM), Roswell Park Memorial Institute Medium (RPMI 1640), L-glutamine, and penicillin/streptomycin were purchased from Lonza (Basel, Switzerland). Fetal calf serum (FCS) was purchased from PAA Laboratories (Ontario, Canada). β-mercaptoethanol was purchased from Sigma-Aldrich (Zwijndrecht, the Netherlands). Granulocyte-macrophage colony-stimulating factor (GM-CSF) was purchased from PeptroTech (London, UK).

The antibodies CD45.1-PE-Dazzle594 (A20), Thy1.2-PE-Cy7 (53-2.1), Gata-3-PE (16E10A23), T-bet-APC (4B10), IL-17A-AF488 (TC11-18H10.1), and CD11c-PerCP-Cy5.5 (N418) were purchased from Biolegend (CA, USA). FOXP3-eFluor450 (FJK-16S), CD25-AF488 (PC61.5), Ki-67-FITC (SolA15), fixable viability dye-APC-eFluor780, IL-10-PerCP-Cy5.5 (JES5-16E3), IFNγ-APC (XMG1.2), and FOXP3/transcription factor staining kit were purchased from eBioscience (Thermofisher Scientific, MA, USA). CD4-V500 (RM4-5) was purchased from BD Biosciences (CA, USA).

Preparation of OVA_{323}-AF488

The OVA_{323} peptide with the sequence ISQAVHAAHAEINEAGRGC was synthesized using a Liberty Blue microwave-assisted peptide synthesizer. Synthesis was performed on a 0.1 mmol scale with a low-loading (0.18 mmol/g) Tentagel® R-RAM resin. Amino acid activation was performed using DIC as the activator and oxyma as a base, and Fmoc-deprotection was performed with 20% piperidine in DMF. The resin was washed five times with DMF and five times with dichloromethane. To protect the N-terminal amine, the peptide was reacted with 5% v/v acetic acid anhydride and 6% pyridine v/v in DMF for 1 hour at room temperature. Subsequently, cleavage from the resin was performed using a mixture of TFA:triisopropyl silane:water, 38/1/1 v/v/v. The peptide was precipitated using ice-cold diethyl ether. The precipitate was collected by centrifugation before resuspension in

water:acetonitrile 4/1 v/v, after which the acetonitrile was evaporated and the remaining aqueous solution was lyophilized overnight. Purification was performed by RP-HPLC on a Kinetic Evo C18 column with a Shimadzu system comprising two LC-8A pumps and an SPD-10AVP UV-Vis detector. The collected fractions were analyzed using LC-MS and pure fractions were pooled, the organic solvent was evaporated and the peptide solution was lyophilized overnight. To obtain fluorescently labeled OVA_{323}, the peptide was incubated for 48 hours at 4°C with AlexaFluor 488 C_5 maleimide (ThermoFisher Scientific, Landsmeer, Netherlands) at pH 7.4 (100 mM HEPES buffer). The purified fluorescent peptide was obtained by RP-HPLC and mass was confirmed by LC-MS.

Liposome preparation

Liposomes were prepared using the thin film dehydration-rehydration method, as described previously[27]. Briefly, phospholipids with or without CHOL (10 mg/mL, 1 mL) were dissolved in chloroform and mixed in a 50 mL round-bottom flask at a molar ratio of 4:1(:2) PC:PG(:CHOL). The chloroform was evaporated under vacuum in a rotary evaporator (Rotavapor R-210, Büchi, Switzerland) for 1 hour at 40°C. The resulting lipid film was rehydrated with 250 µg OVA_{323} dissolved in 1 mL Milli-Q water and homogenized using glass beads. The liposome dispersion was snap-frozen in liquid nitrogen, followed by freeze-drying overnight (Christ alpha 1–2 freeze-dryer, Osterode, Germany). The freeze-dried lipid cake was slowly rehydrated using 10 mM sodium phosphate buffer (PB), pH 7.4. Two volumes of 500 µL and one volume of 1,000 µL PB were successively added, with intervals of 30 min between each addition. The mixture was vortexed well between each hydration step, and the resulting dispersion was left to rehydrate for at least 1 hour. The multilamellar vesicles were sized by high-pressure extrusion (LIPEX Extruder, Northern Lipids Inc., Canada) by passing the dispersion four times through stacked 400-nm and 200-nm pore size membranes (Whatman® NucleporeTM, GE Healthcare, Little Chalfont, UK). The resulting liposomes were assumed to be unilamellar. Homogenization, rehydration, and extrusion were performed at a temperature above the T_m of the phospholipids. To separate non-encapsulated OVA_{323} from the liposomes, liposomes were washed in a Vivaspin 2 centrifuge membrane concentrator (MWCO 300 kDa, Sartorius, Göttingen, Germany) by centrifugation at 524 g and 4°C. To prepare fluorescently labeled liposomes, 0.1 mol% of PC was replaced with DPPE-Rho. To prepare liposomes with fluorescently labeled OVA_{323}, 10% of the OVA_{323} was replaced with OVA_{323}-AF488. Liposomes were stored at 4°C and used for further experiments within 2 weeks.

Liposome characterization

The Z-average diameter and polydispersity index (PDI) of the liposomes were measured by dynamic light scattering (DLS) using a NanoZS Zetasizer (Malvern Ltd., Malvern, UK). The same instrument was used to measure ζ-potential by laser Doppler electrophoresis. The liposomes were diluted 100-fold in PB to a total volume of 1 mL for these measurements. Particle concentration was measured using nanoparticle tracking analysis (NTA), as described previously[28], for optimal AFM measurements. Liposomes were diluted in PB to a particle concentration between 10^7 and 10^9 particles/mL based on the DLS attenuation. NTA measurements were performed using a NanoSight LM20 (NanoSight, Amesbury, UK). Capture time was 60 seconds, the camera shutter was set to 1500 ms, and gain to 680. To determine the concentration of loaded OVA_{323}, the

peptide was extracted from liposomes using a modified Bligh-Dyer method, as described previously[29]. Briefly, 100 µL of aqueous liposomal dispersion or a known concentration of free peptide as control was mixed with 250 µL methanol and 125 µL chloroform and vortexed. Then, 250 µL of 0.1 M HCl and 125 µL chloroform were added and the mixture was vortexed and subsequently centrifuged for 5 min at 524 g to separate the two phases. The upper phase was collected and analyzed by RP- UPLC. Sample injections were 10 µL and the column used was a 1.7 µm BEH C18 column (2.1 x 50 mm, Waters ACQUITY UPLC, Waters, MA, USA). Column and sample temperatures were 40°C and 4°C, respectively. The mobile phases were Milli-Q water with 0.1% TFA (solvent A) and acetonitrile with 0.1% TFA (solvent B). For separation, the mobile phases were applied in a linear gradient from 5% to 95% solvent B over 5 minutes at a flow rate of 0.370 mL/min. Peptides were detected by absorbance at 214 nm using an ACQUITY UPLC TUV detector (Waters ACQUITY UPLC, Waters, MA, USA).

Preparation of APTES-modified silicon plates

To allow for imaging of anionic liposomes, (negatively charged) silicon plates were modified with APTES, to obtain a positively charged surface, as described previously[30]. Briefly, the plates were washed with acetone and methanol and dried in a vacuum oven (Binder, Germany) for 30 minutes at 50°C. The plates were incubated in a solution of 3/7 v/v H_2O_2/H_2SO_4 at 120°C to remove any organic contaminants and to hydroxylize the silicon surface. The plates were then washed with water and dried for 30 minutes in a vacuum oven. The plates were incubated overnight in 2% v/v APTES in toluene, washed thoroughly with toluene to remove any excess APTES, and subsequently washed with methanol, and dried in a vacuum oven at 175°C. Lastly, a curing step for the hydrolysis of residual ethoxy groups was performed at 120°C for 30 minutes followed by incubation in Milli-Q water at 40°C for 2 hours after which the plates were washed with methanol and stored in a vacuum oven at 175°C until use. The smoothness of the APTES-modified plates was confirmed using AFM in QI mode. A sharp cantilever (Oltespa, Opus, Bulgaria) with a nominal spring constant of 2 N/m, a nominal resonance frequency of 70 kHz and a tip radius of <7 nm was used to image the surface of the plates. The sample tilt was corrected using the JPK Data Processing software v6.1.79 flattening function. Images were extracted using Gwyddion v2.50 and the heights of structures on the plates were determined. The roughness of the plates was expressed as root mean square (RMS)[31], and plates used had RMS values between 0.6 and 3 nm, which was deemed to have minimal interference and to favor adsorption of liposomes[32].

Sample preparation for AFM measurements

APTES-modified plates were attached to glass microscope slides using Reprorubber® (Thin Pour Kit, Flexbar Machine Corporation, USA). A small glass ring with a diameter of 15 mm and a height of 3 mm was attached on the plate to form a small basin. Next, 200 µL of liposomal formulation (particle concentrations of about 10^{12} – 10^{13} particles/mL, as measured by NTA) was applied to the plate and incubated at room temperature for 5 min. The plate was gently washed with PB without exposure of the plate to air to remove free liposomes.

Scanning electron microscopy (SEM) of cantilevers

The cantilever tip radius of the HSC-20 cantilever (Team Nanotec, Germany) was assessed

by SEM using an FEI Nova nanoSEM 200. Imaging was performed in high vacuum mode at 15 kV and a spot of 4.0 at a tilt of 45°. Images were captured at 200,000-fold magnification and the radius of the cantilever tip was determined using the SEM software.

AFM measurements

To image the liposomes a JPK Nanowizard 3 (JPK Instruments AG, Berlin, Germany) was used. Measurements were performed at 25 ± 1°C in QI mode. The AFM probe used was a Team Nanotec (Germany) HSC-20 hemispherical cone-shaped tip cantilever with gold-reflective coating and metal carbide coating on the tip side, with a nominal spring constant of 0.2 N/m, a nominal resonance frequency of 15 kHz and a tip radius of 35 nm, as determined by SEM. The cantilever was calibrated using contact-based calibration and thermal tuning. For calibration, the setpoint was 0.1 V on approach with a dynamic baseline. Imaging of the liposomes was performed with a z-length 200 nm and a set point between 0.5 – 0.85 nN. The area of the image was 2 x 2 µm at a resolution of 128 x 128 pixels with a pixel rate of 20 msec/pixel. Scan line artifacts were removed, line fitting was applied to the images, and sample tilt was corrected. Liposomes with a height below 40 nm were excluded from the analysis to prevent interference from the substrate. Force vs. height curves were measured for each pixel of the AFM image. After subtracting the cantilever deflection, the force vs. tip-sample separation (or distance) curves were fitted using the Hertz/Sneddon model[33] for a hemispherical cantilever tip according to the following equation:

$$F = \frac{4\sqrt{R}}{3}\frac{E}{1-\nu^2}\delta^{\frac{3}{2}} \qquad \text{(equation 1)}^{34}$$

where F is the force as measured by AFM, R is the tip radius as measured by SEM, E is the YM, ν is Poisson's ratio, set to 0.5 for soft materials such as liposomes[35], and δ is the indentation of the sample, also measured by AFM. The YM was determined for the center of the liposomes.

Raw data images and force vs. height curves were processed using JPK Data Processing software v6.1.70. Data from the images were extracted using Gwyddion v2.50. Between 31 and 450 liposomes were analyzed per formulation (Figure 1A).

BMDC culture

Bone marrow was isolated from the tibias and femurs of wild-type (WT) C57BL/6 mice. A single-cell suspension of bone marrow cells was obtained by straining over a 70 µm cell strainer (Greiner Bio-One B.V., Alphen aan den Rijn, NL). Cells were cultured for 10 days in complete IMDM (cIMDM) which contains IMDM supplemented with 2 mM L-glutamine, 8% v/v FCS, 100 U/mL penicillin/streptomycin, and 50 µM β-mercaptoethanol at 37˚C and 5% CO_2 in 95-mm Petri dishes (Greiner Bio-One B.V., Alphen aan den Rijn, NL) and 20 ng/mL GM-CSF. The medium was refreshed every other day.

Liposome or antigen association to BMDCs

BMDCs were cultured as described above. After 10 days of culture, BMDCs were plated in F-bottom 96-well plates (Greiner Bio-One B.V., Alphen aan den Rijn, Netherlands) at 50,000 cells/well. To measure association (either by uptake or adsorption) of liposomes to BMDCs, liposomes prepared with 0.1 mol% Rho-DPPE or controls (non-fluorescent

liposomes or medium) were added at a concentration of 20 µg/mL lipids in supplemented IMDM. To measure OVA_{323} association to DCs, liposomes encapsulating fluorescently labeled OVA_{323} were added to a concentration of 0.1 µg/mL OVA_{323}. Cells were incubated for 4 hours at 37˚C and 5% CO_2. Subsequently, excess liposomes were removed by washing the cells several times with cIMDM, and cells were incubated overnight. Cells were stained with a fluorescent antibody against CD11c-PerCP-Cy5.5 (N418) and fixable viability dye-APC-eFluor780 and subsequently analyzed by flow cytometry (CytoFLEX S, Beckman Coulter, CA, USA). The presence of the fluorescent label in DCs indicated the association of either liposomes or peptide by BMDCs. Data were analyzed with FlowJo software V10 (Treestar, OR, USA).

In vitro Treg induction by liposome-pulsed BMDCs

BMDCs were cultured as described above, plated to 50,000 cell/well in a 96-well F-bottom plate, and pulsed for 4 hours with liposomes or controls in cIMDM. Spleens from OT-II mice were strained through a 70 µm cell strainer to obtain a single-cell suspension. Erythrocytes were lysed using ammonium-chloride-potassium (ACK) lysis buffer (0.15 M NH_4Cl, 1 mM $KHCO_3$, 0.1 mM Na_2EDTA; pH 7.3). $CD4^+$ T cells were isolated using a $CD4^+$ T cell isolation kit (Miltenyi Biotec B.V., Leiden, Netherlands) according to the manufacturer's protocol. After exposure, BMDCs were washed with cIMDM to remove free liposomes, and 100,000 $CD4^+$ T cells/well were added to the BMDCs. Co-cultures were incubated for 72 hours in RPMI 1640 medium supplemented with 2 mM L-glutamine, 10% v/v FCS, 100 U/mL penicillin/streptomycin, and 50 µM β-mercaptoethanol. Cells were stained for Thy1.2-PE-Cy7, CD4-V500, viability-APC-eFluor780, FOXP3-eFluor450, and Ki-67-FITC, and analyzed by flow cytometry (CytoFLEX S, Beckman Coulter, CA, USA). Data were analyzed using FlowJo software V10 (Treestar, OR, USA).

Animals

C57BL/6 and OT-II transgenic mice on a C57BL/6 background were purchased from Jackson Laboratory (CA, USA), bred in-house under standard laboratory conditions, and provided with food and water *ad libitum*. All animal work was performed in compliance with the Dutch government guidelines and the Directive 2010/63/EU of the European Parliament. Experiments were approved by the Ethics Committee for Animal Experiments of Leiden University.

Adoptive transfer

Eleven-week-old female C57BL/6 mice were randomized into 4 groups based on weight. On day 0, all mice received 500,000 $CD45.1^+CD4^+$ T cells splenocytes isolated from a female OT-II transgenic mouse *via* the tail vein. On day 1, mice were immunized intravenously (i.v.) with a single injection of DSPC:DSPG, DSPC:DSPG:CHOL, DOPC:DOPG or DOPC:DOPG:CHOL liposomes containing 1 nmol OVA_{323} in PBS, in a total volume of 200 µL *via* the tail vein. On day nine, mice were sacrificed by cervical dislocation and spleens were immediately removed. Spleens were processed as mentioned above and stained for CD4-V500, CD45.1-PE-Dazzle594, Thy1.2-PE-Cy7, viability-APC-eFluor780, CD25-AF488, Gata-3-PE, T-bet-APC, and FOXP3-eFluor450 and measured by flow cytometry (CytoFLEX S, Beckman Coulter, CA, USA). To measure cytokine production, splenocytes were stimulated ex vivo with OVA_{323} (10 µg/mL). After 1 hour brefeldin A (3 µg/mL) was

added and cells were incubated for a further 5 hours. Cells were subsequently stained for CD4-V500, CD45.1-PE-Dazzle594, Thy1.2-PE-Cy7, viability-APC-eFluor780, IFNγ-APC, IL-17A-AF 488, and IL-10-PerCP-Cy5.5, and analyzed by flow cytometry. Data were analyzed using FlowJo software V10 (Treestar, OR, USA).

Statistical analysis

Results were analyzed using one-way or two-way ANOVA, followed by Bonferroni's multiple comparisons test, performed using GraphPad Prism v 8.1.1 (GraphPad Software, CA, USA).

Results

Preparation of liposomes

Tregs are vital for maintaining immune homeostasis and are an attractive target for immunotherapy. We have previously demonstrated that liposomes prepared with DSPC, DSPG and CHOL in a molar ratio of 4:1:2 and loaded with an initial OVA_{323} concentration of 250 µg/ml induce strong antigen-specific Treg responses. In order to assess how the rigidity of these liposomes affects the Treg responses, we altered the rigidity of the liposomes by using phospholipids with different carbon chain-lengths (*e.g.* DSPC, di-18:0 PC vs. DPPC, di-16:0 PC), unsaturation in the lipid chain (*e.g.* DSPC, di-18:0 PC vs. DOPC, di-18:1 (Δ9-Cis) PC) or exclusion of CHOL (Table S1). The resulting liposomes were between 138 and 177 nm in size (Table 1). Exclusion of CHOL slightly, but significantly, reduced the size of the liposomes ($p<0.05$). All formulations were monodisperse, indicated by a PDI of about 0.1. As expected, because of the incorporation of an anionic PG phospholipid, all liposomes had a negative ζ-potential. The loading efficiency (LE) of the OVA_{323} was between 11.4 and 24.6%.

Table 1. Physicochemical characteristics of liposomal formulations.

Lipid composition (molar ratio)	Z-average ± SD (nm)	PDI ± SD	ζ-potential ± SD (mV)	LE (%)[a]	Phase state at room temperature
DSPC:DSPG:CHOL (4:1:2)	166.1 ± 8.5	0.09 ± 0.05	-48.0 ± 6.0	16.0 ± 8.5	Lo
DSPC:DPPG:CHOL (4:1:2)	177.3 ± 6.6	0.08 ± 0.03	-46.4 ± 9.5	15.8 ± 5.5	Lo
DPPC:DPPG:CHOL (4:1:2)	173.5 ± 10.6	0.08 ± 0.04	-46.2 ± 11.7	24.7 ± 10.2	Lo
DSPC:DOPG:CHOL (4:1:2)	168.1 ± 17.0	0.10 ± 0.05	-45.8 ± 4.9	13.9 ± 3.9	Lo
DOPC:DOPG:CHOL (4:1:2)	158.7 ± 14.7	0.12 ± 0.03	-43.4 ± 5.1	24.8 ± 12.8	Lo
DSPC:DSPG (4:1)	138.4 ± 13.2	0.10 ± 0.03	-39.7 ± 5.7	11.4 ± 6.2	Gel
DOPC:DOPG (4:1)	140.1 ± 4.9	0.13 ± 0.03	-44.9 ± 5.9	24.6 ± 12.9	Ld

[a] Percentage of OVA_{323} amount remaining in liposomes after purification compared to the initial amount. Lo= Liquid ordered, Ld= liquid disordered

Effect of lipid composition on liposome rigidity

To study the effect of lipid composition on the rigidity of the liposomes, we measured the YM of the anionic liposomes by AFM. Liposomes were successfully immobilized on APTES-modified silicon plates and were imaged in quantitative imaging (QI) mode (Figure 1 and Table S2). AFM confirmed the size and monodispersity measured by dynamic light scattering and allowed extraction of force-separation curves and determination of the YM of single liposomes (Figure 1A). The most rigid liposomes were

DSPC:DSPG liposomes, while the least rigid liposomes were DOPC:DOPG liposomes (Figure 1B). This was expected, since DSPC:DSPG bilayers are in a gel state, and DOPC:DOPG bilayers are in a liquid disordered state at 25°C (Table 1). For DSPC:DSPG liposomes, the addition of CHOL significantly reduced the YM (from 3611 ± 1271 kPa to 1498 ± 530 kPa, $p < 0.001$), while this was reversed for DOPC:DOPG liposomes (from 493 ± 365 kPa to 911 ± 447 kPa, $p = 0.0153$). Interestingly, we observed that replacing a small amount of a high-T_m phospholipid with a lower-T_m phospholipid has the same effect as replacing all phospholipids by a lower-T_m one. For instance, both DSPC:DPPG:CHOL (YM = 1159 ± 525 kPa), where DSPC has a higher T_m than DPPC, and DPPC:DPPG:CHOL liposomes (YM = 1211 ± 399 kPa) were significantly less rigid than DSPC:DSPG:CHOL liposomes (YM = 1498 ± 531 $p<0.005$), while not being significantly different from each other ($p > 0.99$). A similar effect was observed for DSPC:DOPG:CHOL and DOPC:DOPG:CHOL liposomes. Finally, we found that the T_m values and the molar ratio of the constituent lipids do not significantly correlate with the rigidity of the liposomes (Figure S1).

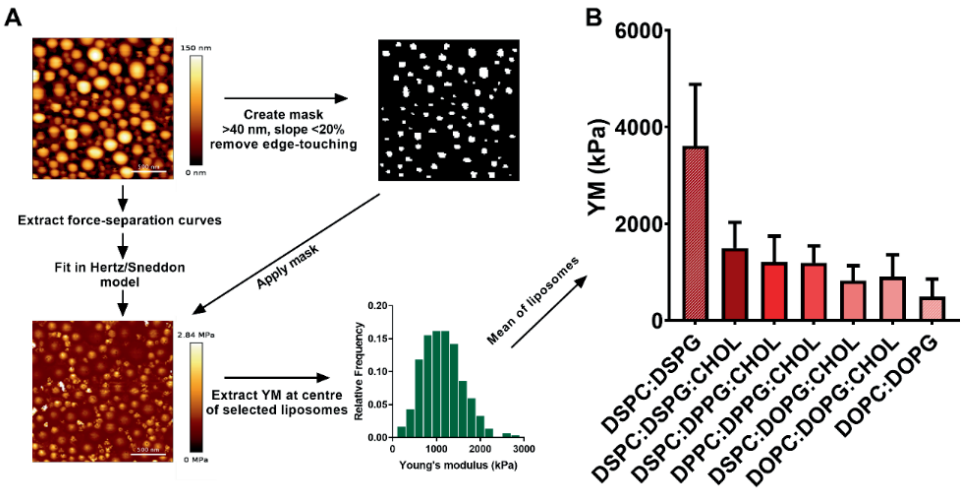


Figure 1. AFM measurements of liposomes. (A) Schematic overview of the AFM method used to determine the rigidity of liposomes. Liposomes were immobilized on APTES-modified silicon plates. The rigidity of the liposomes was measured using AFM in QI mode. AFM images were processed in JPK data processing software v6.1.70. Scan line artifacts were removed and images were corrected for baseline tilt. YM data per pixel was extracted by fitting each force-separation curve with the Hertz/Sneddon model resulting in a YM map. To remove the interference of the silicon substrate, a mask was created in Gwyddion 2.50, selecting a threshold of 40 nm with a slope of less than 20%. Liposomes touching the edges of the image were not included in the analysis. This mask was applied to the YM map, and YM data was extracted for each liposome. Only the center of each liposome was used to calculate the mean YM per formulation. Representative AFM images of DSPC:DPPG:CHOL liposomes. (B) Rigidity, expressed as YM, of the different liposomes. Data shown is mean values ± SD, n = 31 – 450. Significant differences as measured by one-way ANOVA are displayed in Table S3.

Effect of liposomal composition on liposome association to BMDCs and Treg responses *in vitro*

Next, we assessed how the rigidity of liposomes affects the uptake by APCs and the induction of Tregs by the APCs. To this end, we incorporated a fluorescently labeled phospholipid, Rho-DPPE, into the lipid bilayer and exposed BMDCs for 4 hours to these formulations (Figure 2A). For almost all formulations, we observed a positive trend between liposomal rigidity and association. Interestingly, the highest association was observed for the least rigid, DOPC:DOPG liposomes. It should be noted, however, that the DOPC:DOPG liposomes showed primarily passive association, indicated by high cell association at 4°C (Figure 2B), while all other liposomes showed negligible association at 4°C (Figure S2). Furthermore, DOPC:DOPG liposomes did not appear to effectively deliver their cargo; while the association of DSPC:DSPG liposomes led to a significant 7.5-fold increase in OVA_{323} association compared to free OVA_{323} (control), both DOPC:DOPG:CHOL and DOPC:DOPG liposomes did not increase OVA_{323} association compared to the control (Figure 2C).

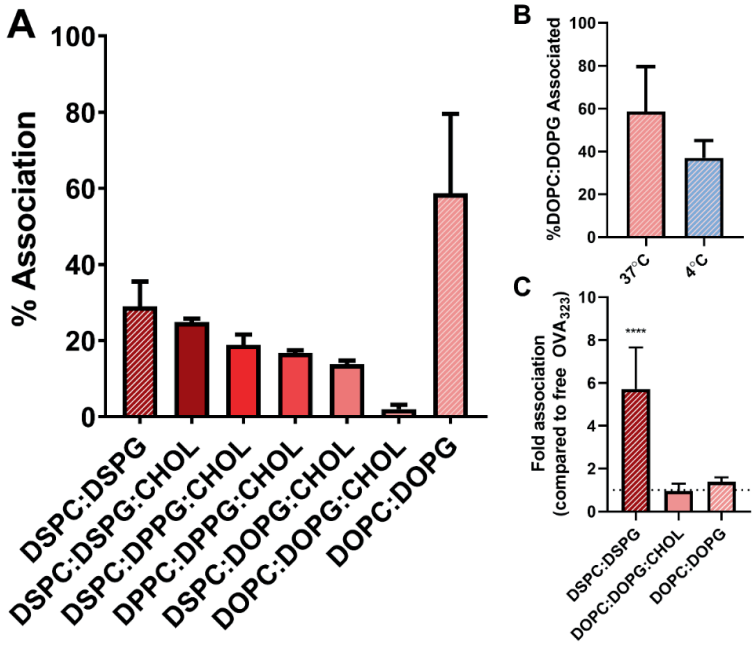


Figure 2. Liposomal association (uptake and/or adsorption) by BMDCs *in vitro*. (A) OVA_{323}-containing fluorescently labeled liposomes were incubated for 4 hours with BMDCs at 37°C. Liposomes were subsequently washed away and cells were incubated overnight before being analyzed *via* flow cytometry. % Association indicates the percentage of live BMDCs that are positive for the fluorescent label in the liposomes. (B) Association of OVA_{323}-containing fluorescently labeled DOPC:DOPG liposomes at 37°C vs. 4°C. (C) Association of encapsulated OVA_{323} to BMDCs. Fluorescently labeled OVA_{323} was encapsulated in liposomes and incubated for 4 hours with BMDCs at 37°C. Liposomes were subsequently washed away and cells were incubated overnight before being analyzed by flow cytometry. Association was normalized to % of BMDCs positive for fluorescently labeled OVA_{323} in the free OVA_{323} control. Graphs show mean ± SD, (A) n = 3, (B) n = 9, (C) n = 6. ****$p < 0.0001$, compared to free OVA_{323} determined by one-way ANOVA and Bonferroni's multiple comparisons test.

To determine whether the liposomal composition affected Treg responses, BMDCs were pulsed with liposomes for 4 hours, and subsequently co-cultured with OT-II CD4$^+$ T cells. After three days of incubation, induced Tregs were identified using flow cytometry (Figure 3A, B, and C). Among all tested OVA_{323}-containing liposomes, the DSPC:DSPG liposomes induced the strongest Treg responses, with a 1.6-fold increase in % FOXP3$^+$ population in live CD4$^+$Ki-67$^+$ T cell population compared to free OVA_{323}. Also DSPC:DSPG, DSPC:DSPG:CHOL, DSPC:DPPG:CHOL, and DPPC:DPPG:CHOL liposomes showed significantly higher Treg responses compared to free OVA_{323}. Furthermore, we observed a significant correlation between the liposomal rigidity (determined by AFM) and Treg responses (Figure 3D). Interestingly, there was no clear relationship between the association of liposomes with BMDCs and subsequent Treg responses (Figure 3E).

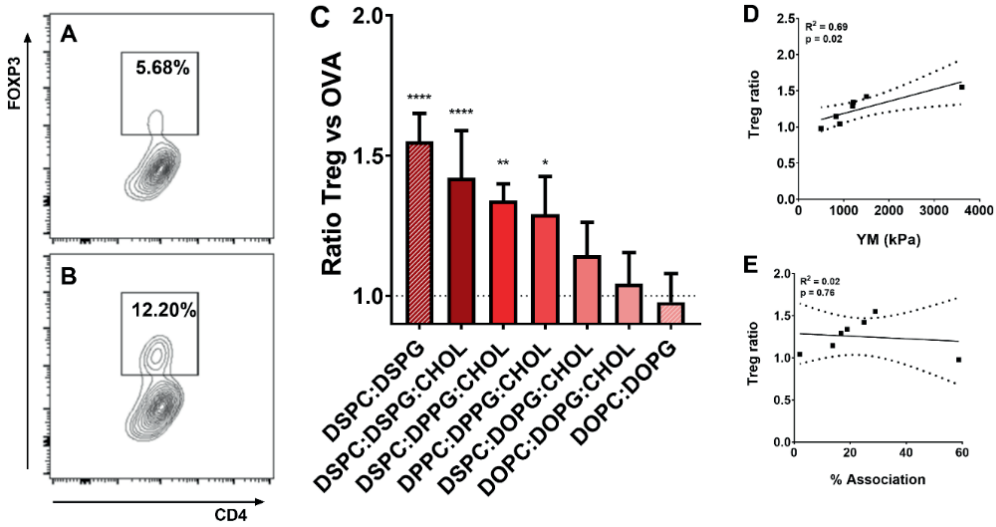


Figure 3: Induction of Tregs by OVA_{323}-loaded liposomes *in vitro*. BMDCs were pulsed for 4 hours with liposomes or controls and subsequently co-cultured for 72 hours with CD4$^+$ T cells isolated from OT-II splenocytes. Flow cytometry was used to measure FOXP3$^+$Ki-67$^+$CD4$^+$ T cells. Representative flow cytometry plots of FOXP3$^+$CD4$^+$ T cells in the live Ki-67$^+$CD4$^+$ T cell population of OT-II T cells cultured with (A) free OVA_{323} (0.1 µg/mL) and (B) OVA_{323}-loaded DSPC:DSPG liposomes (0.1 µg/mL OVA_{323}). (C) Summary Treg data of all liposomal formulations tested. Results were normalized to % FOXP3$^+$Ki-67$^+$CD4$^+$ T cells in the free OVA_{323} control. The dashed line at Y = 1 represents the free OVA_{323} control. The graph shows mean ± SD, n = 4. Linear correlations (95% CI) between (D) YM and Treg response ratio, and (E) % association and Treg response ratio. ****p < 0.0001, **p < 0.01. *p < 0.05, compared to free OVA_{323} determined by one-way ANOVA and Bonferroni's multiple comparisons test.

Effect of liposomal composition on Treg response *in vivo*

Next, we aimed to assess whether liposome rigidity affects Treg induction *in vivo*. An adoptive transfer mouse model using ovalbumin-specific OT-II T cells was used to study the induction of antigen-specific Treg responses by the liposomes *in vivo*. We selected the highest rigidity (DSPC:DSPG) and lowest rigidity liposomes (DOPC:DOPG) and their CHOL-containing counterparts. Both DSPC:DSPG and DSPC:DSPG:CHOL liposomes showed a significantly higher expansion of antigen-specific CD4$^+$ T cells than

the formulations containing DOPC and DOPG (DSPC:DSPG 7.3 ± 0.9%, DSPC:DSPG:CHOL 7.3 ± 2.6%, DOPC:DOPG:CHOL 4.1 ± 0.3%, and DOPC:DOPG 4.1 ± 0.7%, Figure 4A, B, C, D, and E). Moreover, in line with the *in vitro* results, the total percentage of antigen-specific Tregs within the $CD4^+$ T cell population was highest for DSPC:DSPG liposomes, and decreased with decreasing liposome rigidity (Figure 4F). We observed no differences in Th1 and Th2 responses between liposomal formulations (Figure S3). Furthermore, there were no differences in the production of IFNγ, IL-10 and IL-17A by splenocytes between liposomal formulations upon restimulation with OVA_{323} for 6 hours (Figure 4G, H and I), although we did find a significant increase in production of IL-10 in all groups comparing antigen-specific $CD4^+$ T cells to $CD45.1^-CD4^+$ T cells, suggesting liposomal vaccination induces functional Tregs.

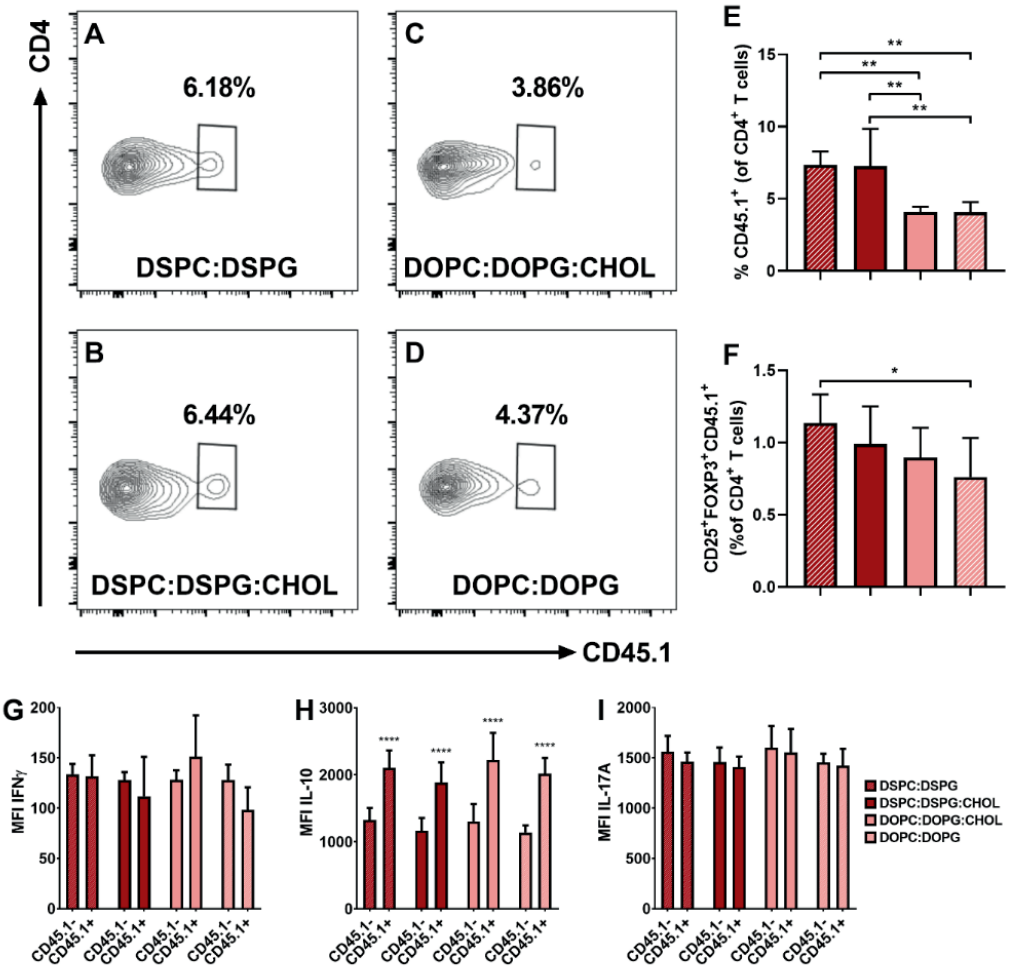


Figure 4. Expansion of OVA_{323} -specific Tregs in spleens of mice 8 days after i.v. injection of OVA_{323}-containing liposomes. Representative flow cytometry plots of OVA_{323}-specific $CD45.1^+CD4^+$ T cells in the spleen of a mouse injected with (A) DSPC:DSPG, (B) DSPC:DSPG:CHOL, (C) DOPC:DOPG:CHOL and (D) DOPC:DOPG liposomes containing OVA_{323}. (E) Percentage of $CD45.1^+$ cells in the $CD4^+$ T cell population. (F) % of $CD25^+FOXP3^+CD45.1^+$ Tregs in the $CD4^+$ T cell population. Graphs show mean ± SD, n = 8. *p < 0.05, **p < 0.01, compared to free OVA_{323} determined by one-way ANOVA and Bonferroni's multiple comparisons test. Intracellular (G) IFNγ, (H) IL-10, and (I) IL-17A staining in splenocytes restimulated with 10 µg/mL OVA323 peptide for 6 hours. ****p < 0.0001 comparing $CD45.1^+CD4^+$ T cells to $CD45.1^+CD4^+$ T cells. No significant differences found between liposomal formulations as measured by two way ANOVA with Bonferroni's post-test.

Discussion

The induction of antigen-specific Tregs through vaccination is an attractive approach for the treatment of autoimmune diseases. We and others have previously shown that nanoparticles, such as liposomes, can be used to induce these Tregs[10,13]. Generally, approaches to optimize such nanoparticles are focused on studying the effect of particle size and surface charge, while another important parameter, rigidity, is often overlooked[15]. This parameter is usually approximated by the phase properties of the lipid bilayers by analytical techniques such as DSC and Laurdan anisotropy. Besides the fact that these techniques only provide information about the bilayer of liposomes and thereby exclude other influencing factors, such as size, lamellarity, antigen content, and formulation excipients, there are other issues associated with these techniques. For instance, many liposomal formulations contain CHOL in the lipid bilayer, which compromises the suitability of techniques such as DSC[25], Fourier-transform infrared spectroscopy (FTIR)[36], and Laurdan anisotropy[37]. Furthermore, compounds encapsulated in liposomes can also interfere with DSC[38,39] and FTIR measurements[40]. Other analytical techniques such as measuring the ability of particles to be extruded[41,42] are indirect measurements of rigidity. Importantly, all of the aforementioned techniques can only measure the average properties of a batch of particles. In contrast, AFM is an excellent technique to accurately measure the rigidity of individual particles and is not hindered by the presence of other compounds, such as CHOL and antigen. To further confirm this, studies should be performed to compare AFM to other techniques that measure liposomal rigidity.

We observed that CHOL reduces DSPC:DSPG liposome rigidity, and increases DOPC:DOPG liposome rigidity. The lipid bilayers of liposomes can generally be classified into three physical states with increasing rigidity: liquid disordered (bilayers composed of low-T_m phospholipids), liquid ordered (bilayers composed of high- or low-T_m phospholipids containing at least 20 mol % CHOL) and gel state (bilayers containing high-T_m phospholipids). In the gel state, CHOL disrupts the tight packing of the lipids, while in the liquid disordered state, CHOL occupies space at the interfacial region near the membrane surface and replaces the hydrated CH_2 groups. As the acyl chains become dehydrated and straighten out, the packing becomes tighter and rigidity is, therefore, increased[43]. While bilayer state is not the same as liposomal rigidity, it is most likely one of the most important parameters that influence the rigidity of the liposomes. This is also in line with results from Takechi-Haraya *et al*. who used AFM to study the effect of CHOL on liposome rigidity[44].

From our study, it became clear that the introduction of lipid order mismatch significantly affects the rigidity of the liposomes. Mixing of lipids with different phase transitions in the absence of CHOL can lead to the formation of lipid domains (*e.g.* rigid domains and fluid domains), which could destabilize the bilayer packing, and thereby the rigidity of the liposomes[23]. We observed a significant decrease in rigidity of liposomes in the presence of a small amount of lower-T_m lipid (*e.g.* DSPC:DSPG:CHOL vs. DSPC:DPPG:CHOL, Table S3), which did not further decrease upon complete substitution (*e.g.* DSPC:DPPG:CHOL vs. DPPC:DPPG:CHOL). This suggests that the T_m values and the molar ratio of the constituent lipids are poor predictors of the rigidity of the liposomes (Figure S1).

Physicochemical properties of liposomes other than bilayer composition can

also affect their rigidity. For example, smaller liposomes, measured by AFM, are more rigid than larger liposomes[45]. This may be due to the different curvature of liposomes of different sizes, leading to more restricted molecular interactions between the lipids of smaller liposomes[46]. The charge of liposomes can also affect rigidity; neutral DOPC liposomes measured by AFM were shown to be more rigid than anionic DOPC:DOPG or cationic DOPC:DOTAP liposomes. This was hypothesized to be due to electrostatic repulsions causing structural destabilization of the lipid bilayer[47]. Due to technical limitations, the AFM measurements were performed at 25°C. Since temperature affects the phase state of the lipid bilayers, it also influences the rigidity of liposomes. However, the phase states of the used phospholipids are the same at 25°C and 37°C (Table S1), so the trends in YM at this physiologically more relevant temperature should be very similar to those observed at 25°C. Furthermore, a recent study found no difference in anionic liposome stiffness over the temperature range of 25-37°C[48]. Finally, antigen content may affect liposomal rigidity. In this study, we have generated liposomal formulations with similar size, antigen loading, and ζ-potential to allow an *in vitro* and *in vivo* assessment primarily based on liposome rigidity.

The liposomes we measured had a range of YM from about 500 kPa to almost 4 MPa (Figure 1B). For comparison, the YM of most mammalian cells was measured to be between 0.02 and 400 kPa [49] and that of cortical bone was reported to be about 20 GPa[50]. Moreover, we have used our AFM method to measure other anionic particle type, PLGA nanoparticles (Z-average diameter of 142.1 ± 1.1 nm, PDI of 0.073 ± 0.016, ζ-potential -49.7 ± 4.2 mV), which had a YM of 14.4 MPa ± 1.8 MPa. This illustrates that the range of rigidities of the liposomes is relatively small. This is especially true for the CHOL-containing liposomes, the rigidity of which ranged from about 800 kPa to 1500 kPa (Figure 1B). This was expected since their bilayers are all in the liquid disordered state. However, even such small differences in rigidity could be measured using our AFM method, and we could measure significant differences between formulations (Table S3), illustrating the strength of this technique.

We have reported the SD of YM values of all liposomes measured within a batch. The SD of YM was relatively high for each liposomal formulation. The high SD was not due to a lack of precision of the AFM measurements, as repeated measurements of the same liposomes showed very low variation (the difference between two measurements of the same DSPC:DSPG:CHOL:OVA_{323} liposomes was 2.8%, Table S4). Rather, it illustrates the variation in YM of the liposomes within a formulation, which is likely due to differences in size, lamellarity, and possibly antigen loading among different individual liposomes within the same batch. Variation in YM as measured in two different batches of DSPC:DSPG:CHOL:OVA_{323} liposomes was also very low (1467 ± 575 kPa vs. 1510 ± 514, Figure S4).

Based on previous reports we expected that the rigidity of the liposomes would positively correlate with their uptake by APCs since it requires less energy for a cell membrane to wrap around rigid particles[51]. It is known that phospholipid saturation has a significant effect on their fate in biological systems. For instance, dimethyldioctadecylammonium:trehalose 6,6'-dibehenate (DDA:TDB) liposomes showed higher retention at the site of injection and uptake by APCs *in vivo* compared to more fluid (as measured by DSC) dimethyldioleoylammonium (DODA):TDB liposomes[18]. Furthermore, CHOL content negatively correlated with uptake by THP-1-derived

macrophages[52]. In our study, almost all formulations show a positive trend between liposomal rigidity and APC association. However, DOPC:DOPG liposomes showed the highest association to BMDCs of all tested formulations (Figure 2A), which was not expected since these liposomes presented the lowest rigidity (Figure 1B). Their route of uptake could be different from that of the more rigid formulations. For instance, pure DOPC liposomes (YM of 45 kPa as measured by AFM) were hypothesized to fuse with cells[53]. The DOPC:DOPG liposomes showed high passive association (Figure 2B), and did not deliver their cargo to BMDCs (Figure 2C), explaining their inability to induce T cell responses (Figure 3C). There is evidence of an inverse relationship between liposomal rigidity and membrane permeability, as measured by calcein leakage[37]. So, it may be that the peptide had leaked out of the DOPC:DOPG and DOPC:DOPG:CHOL liposomes prior to BMDC association. This hypothesis is supported by our observation that a mixture of free OVA_{323} and empty DOPC:DOPG or DOPC:DOPG:CHOL liposomes showed the same amount of OVA_{323} association as encapsulated peptide (data not shown). Since we used fluorescently-labeled lipids and peptides, we cannot exclude the influence of the fluorophore itself on the measured association in BMDCs. However, since all formulations (aside from DOPC:DOPG liposomes) show almost no association of fluorophore when incubated at 4°C (Figure S2), the fluorophore itself likely has no effect on association.

We observed a clear correlation between the rigidity of the liposomes and the Treg responses they elicited *in vitro* and in *vivo* (Figure 3D, Figure 4F). While others have shown a link between increased rigidity and MHC-II presentation[19], and enhanced humoral and cellular responses[54,55], we are the first to report the effects of rigidity on Treg responses. This may have implications for the design of delivery systems aimed to enhance antigen-specific Treg responses.

In conclusion, we showed that liposomal rigidity as measured by our optimized AFM method is an important parameter in eliciting antigen-specific Treg responses *in vitro* and *in vivo*. Our findings may contribute to a better understanding of the factors driving Treg responses. Moreover, this paper may contribute to a rational design of liposomal as well as other nanoparticulate vaccine formulations aiming to enhance antigen-specific Treg responses for the treatment of autoimmune diseases.

References

1 Sakaguchi, S., Yamaguchi, T., Nomura, T. & Ono, M. Regulatory T cells and immune tolerance. *Cell* **133**, 775-787, doi:10.1016/j.cell.2008.05.009 (2008).

2 Mallat, Z., Ait-Oufella, H. & Tedgui, A. Regulatory T-cell immunity in atherosclerosis. *Trends Cardiovasc Med* **17**, 113-118, doi:10.1016/j.tcm.2007.03.001 (2007).

3 Keijzer, C., van der Zee, R., van Eden, W. & Broere, F. Treg inducing adjuvants for therapeutic vaccination against chronic inflammatory diseases. *Front Immunol* **4**, 245, doi:10.3389/fimmu.2013.00245 (2013).

4 Dominguez-Villar, M. & Hafler, D. A. Regulatory T cells in autoimmune disease. *Nat Immunol* **19**, 665-673, doi:10.1038/s41590-018-0120-4 (2018).

5 Faria, A. M. & Weiner, H. L. Oral tolerance: therapeutic implications for autoimmune diseases. *Clin Dev Immunol* **13**, 143-157, doi:10.1080/17402520600876804 (2006).

6 Kishimoto, T. K. & Maldonado, R. A. Nanoparticles for the Induction of Antigen-Specific Immunological Tolerance. *Front Immunol* **9**, 230, doi:10.3389/fimmu.2018.00230 (2018).

7 Macauley, M. S. *et al.* Antigenic liposomes displaying CD22 ligands induce antigen-specific B cell apoptosis. *J Clin Invest* **123**, 3074-3083, doi:10.1172/JCI69187 (2013).

8 Pang, L., Macauley, M. S., Arlian, B. M., Nycholat, C. M. & Paulson, J. C. Encapsulating an Immunosuppressant Enhances Tolerance Induction by Siglec-Engaging Tolerogenic Liposomes. *Chembiochem* **18**, 1226-1233, doi:10.1002/cbic.201600702 (2017).

9 Maldonado, R. A. *et al.* Polymeric synthetic nanoparticles for the induction of antigen-specific immunological tolerance. *Proc Natl Acad Sci U S A* **112**, E156-165, doi:10.1073/pnas.1408686111 (2015).

10 Rodriguez-Fernandez, S. *et al.* Phosphatidylserine-Liposomes Promote Tolerogenic Features on Dendritic Cells in Human Type 1 Diabetes by Apoptotic Mimicry. *Front Immunol* **9**, 253, doi:10.3389/fimmu.2018.00253 (2018).

11 Watson, D. S., Endsley, A. N. & Huang, L. Design considerations for liposomal vaccines: influence of formulation parameters on antibody and cell-mediated immune responses to liposome associated antigens. *Vaccine* **30**, 2256-2272, doi:10.1016/j.vaccine.2012.01.070 (2012).

12 Hunter, Z. *et al.* A biodegradable nanoparticle platform for the induction of antigen-specific immune tolerance for treatment of autoimmune disease. *ACS Nano* **8**, 2148-2160, doi:10.1021/nn405033r (2014).

13 Benne, N. *et al.* Anionic 1,2-distearoyl-sn-glycero-3-phosphoglycerol (DSPG) liposomes induce antigen-specific regulatory T cells and prevent atherosclerosis in mice. *J Control Release* **291**, 135-146, doi:10.1016/j.jconrel.2018.10.028 (2018).

14 Bachmann, M. F. & Jennings, G. T. Vaccine delivery: a matter of size, geometry, kinetics and molecular patterns. *Nat Rev Immunol* **10**, 787-796, doi:10.1038/nri2868 (2010).

15 Benne, N., van Duijn, J., Kuiper, J., Jiskoot, W. & Slutter, B. Orchestrating immune responses: How size, shape and rigidity affect the immunogenicity of particulate

vaccines. *J Control Release* **234**, 124-134, doi:10.1016/j.jconrel.2016.05.033 (2016).
16 Anselmo, A. C. & Mitragotri, S. Impact of particle elasticity on particle-based drug delivery systems. *Adv Drug Deliv Rev* **108**, 51-67, doi:10.1016/j.addr.2016.01.007 (2017).
17 Beningo, K. A. & Wang, Y. L. Fc-receptor-mediated phagocytosis is regulated by mechanical properties of the target. *J Cell Sci* **115**, 849-856 (2002).
18 Christensen, D. *et al.* A cationic vaccine adjuvant based on a saturated quaternary ammonium lipid have different in vivo distribution kinetics and display a distinct CD4 T cell-inducing capacity compared to its unsaturated analog. *J Control Release* **160**, 468-476, doi:10.1016/j.jconrel.2012.03.016 (2012).
19 Norling, K. *et al.* Gel Phase 1,2-Distearoyl-sn-glycero-3-phosphocholine-Based Liposomes Are Superior to Fluid Phase Liposomes at Augmenting Both Antigen Presentation on Major Histocompatibility Complex Class II and Costimulatory Molecule Display by Dendritic Cells in Vitro. *ACS Infect Dis*, doi:10.1021/acsinfecdis.9b00189 (2019).
20 Yasuda, T., Dancey, G. F. & Kinsky, S. C. Immunogenicity of liposomal model membranes in mice: dependence on phospholipid composition. *Proc Natl Acad Sci U S A* **74**, 1234-1236, doi:10.1073/pnas.74.3.1234 (1977).
21 Dancey, G. F., Yasuda, T. & Kinsky, S. C. Effect of liposomal model membrane composition on immunogenicity. *J Immunol* **120**, 1109-1113 (1978).
22 Bakouche, O. & Gerlier, D. Enhancement of immunogenicity of tumour virus antigen by liposomes: the effect of lipid composition. *Immunology* **58**, 507-513 (1986).
23 Mouritsen, O. G. & Jorgensen, K. Dynamical order and disorder in lipid bilayers. *Chem Phys Lipids* **73**, 3-25, doi:10.1016/0009-3084(94)90171-6 (1994).
24 Demetzos, C. Differential Scanning Calorimetry (DSC): a tool to study the thermal behavior of lipid bilayers and liposomal stability. *J Liposome Res* **18**, 159-173, doi:10.1080/08982100802310261 (2008).
25 Matsingou, C. & Demetzos, C. Calorimetric study on the induction of interdigitated phase in hydrated DPPC bilayers by bioactive labdanes and correlation to their liposome stability: The role of chemical structure. *Chem Phys Lipids* **145**, 45-62, doi:10.1016/j.chemphyslip.2006.10.004 (2007).
26 Spyratou, E., Mourelatou, E. A., Makropoulou, M. & Demetzos, C. Atomic force microscopy: a tool to study the structure, dynamics and stability of liposomal drug delivery systems. *Expert Opin Drug Deliv* **6**, 305-317, doi:10.1517/17425240902828312 (2009).
27 Varypataki, E. M., Benne, N., Bouwstra, J., Jiskoot, W. & Ossendorp, F. Efficient Eradication of Established Tumors in Mice with Cationic Liposome-Based Synthetic Long-Peptide Vaccines. *Cancer Immunol Res* **5**, 222-233, doi:10.1158/2326-6066.CIR-16-0283 (2017).
28 Filipe, V., Hawe, A. & Jiskoot, W. Critical evaluation of Nanoparticle Tracking Analysis (NTA) by NanoSight for the measurement of nanoparticles and protein aggregates. *Pharm Res* **27**, 796-810, doi:10.1007/s11095-010-0073-2 (2010).
29 Varypataki, E. M., van der Maaden, K., Bouwstra, J., Ossendorp, F. & Jiskoot, W. Cationic liposomes loaded with a synthetic long peptide and poly(I:C): a defined

adjuvanted vaccine for induction of antigen-specific T cell cytotoxicity. *AAPS J* **17**, 216-226, doi:10.1208/s12248-014-9686-4 (2015).

30 van der Maaden, K., Sliedregt, K., Kros, A., Jiskoot, W. & Bouwstra, J. Fluorescent nanoparticle adhesion assay: a novel method for surface pKa determination of self-assembled monolayers on silicon surfaces. *Langmuir* **28**, 3403-3411, doi:10.1021/la203560k (2012).

31 Howarter, J. A. & Youngblood, J. P. Optimization of silica silanization by 3-aminopropyltriethoxysilane. *Langmuir* **22**, 11142-11147, doi:10.1021/la061240g (2006).

32 Duarte, A. A. *et al.* Adsorption kinetics of DPPG liposome layers: a quantitative analysis of surface roughness. *Microsc Microanal* **19**, 867-875, doi:10.1017/S1431927613001621 (2013).

33 JPK Instruments AG Application Note.

34 Lin, D. C., Dimitriadis, E. K. & Horkay, F. Robust strategies for automated AFM force curve analysis--I. Non-adhesive indentation of soft, inhomogeneous materials. *J Biomech Eng* **129**, 430-440, doi:10.1115/1.2720924 (2007).

35 Liang, X., Mao, G. & Simon Ng, K. Y. Probing small unilamellar EggPC vesicles on mica surface by atomic force microscopy. *Colloids Surf B Biointerfaces* **34**, 41-51, doi:10.1016/j.colsurfb.2003.10.017 (2004).

36 Altunayar, C., Sahin, I. & Kazanci, N. A comparative study of the effects of cholesterol and desmosterol on zwitterionic DPPC model membranes. *Chem Phys Lipids* **188**, 37-45, doi:10.1016/j.chemphyslip.2015.03.006 (2015).

37 Takechi-Haraya, Y., Sakai-Kato, K. & Goda, Y. Membrane Rigidity Determined by Atomic Force Microscopy Is a Parameter of the Permeability of Liposomal Membranes to the Hydrophilic Compound Calcein. *AAPS PharmSciTech* **18**, 1887-1893, doi:10.1208/s12249-016-0624-x (2017).

38 Zhao, L., Feng, S. S., Kocherginsky, N. & Kostetski, I. DSC and EPR investigations on effects of cholesterol component on molecular interactions between paclitaxel and phospholipid within lipid bilayer membrane. *Int J Pharm* **338**, 258-266, doi:10.1016/j.ijpharm.2007.01.045 (2007).

39 Eloy, J. O. *et al.* Co-loaded paclitaxel/rapamycin liposomes: Development, characterization and in vitro and in vivo evaluation for breast cancer therapy. *Colloids Surf B Biointerfaces* **141**, 74-82, doi:10.1016/j.colsurfb.2016.01.032 (2016).

40 Toyran, N. & Severcan, F. Interaction between vitamin D2 and magnesium in liposomes: Differential scanning calorimetry and FTIR spectroscopy studies. *Journal of Molecular Structure* **839**, 19-27, doi:10.1016/j.molstruc.2006.11.005 (2007).

41 van den Bergh, B. A., Wertz, P. W., Junginger, H. E. & Bouwstra, J. A. Elasticity of vesicles assessed by electron spin resonance, electron microscopy and extrusion measurements. *Int J Pharm* **217**, 13-24, doi:10.1016/s0378-5173(01)00576-2 (2001).

42 Myerson, J. W. *et al.* Flexible Nanoparticles Reach Sterically Obscured Endothelial Targets Inaccessible to Rigid Nanoparticles. *Adv Mater* **30**, e1802373, doi:10.1002/adma.201802373 (2018).

43 Krause, M. R. & Regen, S. L. The structural role of cholesterol in cell membranes:

from condensed bilayers to lipid rafts. *Acc Chem Res* **47**, 3512-3521, doi:10.1021/ar500260t (2014).

44 Takechi-Haraya, Y. *et al.* Atomic Force Microscopic Analysis of the Effect of Lipid Composition on Liposome Membrane Rigidity. *Langmuir* **32**, 6074-6082, doi:10.1021/acs.langmuir.6b00741 (2016).

45 Delorme, N. & Fery, A. Direct method to study membrane rigidity of small vesicles based on atomic force microscope force spectroscopy. *Phys Rev E Stat Nonlin Soft Matter Phys* **74**, 030901, doi:10.1103/PhysRevE.74.030901 (2006).

46 Nakano, K., Tozuka, Y., Yamamoto, H., Kawashima, Y. & Takeuchi, H. A novel method for measuring rigidity of submicron-size liposomes with atomic force microscopy. *Int J Pharm* **355**, 203-209, doi:10.1016/j.ijpharm.2007.12.018 (2008).

47 Takechi-Haraya, Y., Goda, Y. & Sakai-Kato, K. Atomic Force Microscopy Study on the Stiffness of Nanosized Liposomes Containing Charged Lipids. *Langmuir* **34**, 7805-7812, doi:10.1021/acs.langmuir.8b01121 (2018).

48 Takechi-Haraya, Y., Goda, Y., Izutsu, K. & Sakai-Kato, K. Improved Atomic Force Microscopy Stiffness Measurements of Nanoscale Liposomes by Cantilever Tip Shape Evaluation. *Analytical Chemistry* **91**, 10432-10440, doi:10.1021/acs.analchem.9b00250 (2019).

49 Kuznetsova, T. G., Starodubtseva, M. N., Yegorenkov, N. I., Chizhik, S. A. & Zhdanov, R. I. Atomic force microscopy probing of cell elasticity. *Micron* **38**, 824-833, doi:10.1016/j.micron.2007.06.011 (2007).

50 Rho, J. Y., Ashman, R. B. & Turner, C. H. Young's modulus of trabecular and cortical bone material: ultrasonic and microtensile measurements. *J Biomech* **26**, 111-119, doi:10.1016/0021-9290(93)90042-d (1993).

51 Yi, X., Shi, X. & Gao, H. Cellular uptake of elastic nanoparticles. *Phys Rev Lett* **107**, 098101, doi:10.1103/PhysRevLett.107.098101 (2011).

52 Kaur, R. *et al.* Effect of incorporating cholesterol into DDA:TDB liposomal adjuvants on bilayer properties, biodistribution, and immune responses. *Mol Pharm* **11**, 197-207, doi:10.1021/mp400372j (2014).

53 Guo, P. *et al.* Nanoparticle elasticity directs tumor uptake. *Nat Commun* **9**, 130, doi:10.1038/s41467-017-02588-9 (2018).

54 Garnier, F., Forquet, F., Bertolino, P. & Gerlier, D. Enhancement of in vivo and in vitro T cell response against measles virus haemagglutinin after its incorporation into liposomes: effect of the phospholipid composition. *Vaccine* **9**, 340-345, doi:10.1016/0264-410x(91)90061-a (1991).

55 Mazumdar, T., Anam, K. & Ali, N. Influence of phospholipid composition on the adjuvanticity and protective efficacy of liposome-encapsulated Leishmania donovani antigens. *J Parasitol* **91**, 269-274, doi:10.1645/GE-356R1 (2005).

56 Zhang, Y. P., Lewis, R. N. & McElhaney, R. N. Calorimetric and spectroscopic studies of the thermotropic phase behavior of the n-saturated 1,2-diacylphosphatidylglycerols. *Biophys J* **72**, 779-793, doi:10.1016/s0006-3495(97)78712-5 (1997).

57 Biltonen, R. L. & Lichtenberg, D. The Use of Differential Scanning Calorimetry as a Tool to Characterize Liposome Preparations. *Chemistry and Physics of Lipids* **64**, 129-142, doi:Doi 10.1016/0009-3084(93)90062-8 (1993).

58 Ulrich, A. S., Sami, M. & Watts, A. Hydration of DOPC bilayers by differential scanning calorimetry. *Biochim Biophys Acta* **1191**, 225-230, doi:10.1016/0005-2736(94)90253-4 (1994).

59 Smaal, E. B., Nicolay, K., Mandersloot, J. G., de Gier, J. & de Kruijff, B. 2H-NMR, 31P-NMR and DSC characterization of a novel lipid organization in calcium-dioleoylphosphatidate membranes. Implications for the mechanism of the phosphatidate calcium transmembrane shuttle. *Biochim Biophys Acta* **897**, 453-466, doi:10.1016/0005-2736(87)90442-1 (1987).

Supplements

Table S1. T_m of phospholipids.

Lipid	Abbreviation	Structure	T_m (°C)	Ref
Neutral				
1,2-distearoyl-*sn*-glycero-3-phosphocholine	DSPC	di-18:0 PC	55	[56]
1,2-dipalmitoyl-*sn*-glycero-3-phosphocholine	DPPC	di-16:0 PC	41	[57]
1,2-dioleoyl-*sn*-glycero-3-phosphocholine	DOPC	di-18:1 (Δ9-Cis) PC	-17	[58]
Anionic				
1,2-distearoyl-*sn*-glycero-3-phospho-(1'-rac-glycerol)	DSPG	di-18:0 PG	55	[57]
1,2-dipalmitoyl-*sn*-glycero-3-phospho-(1'-rac-glycerol)	DPPG	di-16:0 PG	41	[57]
1,2-dioleoyl-*sn*-glycero-3-phospho-(1'-rac-glycerol)	DOPG	di-18:1 (Δ9-Cis) PG	-18	[59]

Table S2. Rigidity, expressed as YM, of liposomes determined by AFM, n = number of liposomes measured

Lipid composition (molar ratio)	YM ± SD (kPa)	n
DSPC:DSPG (4:1)	3611 ± 1271	450
DSPC:DSPG:CHOL (4:1:2)	1498 ± 531	281
DSPC:DPPG:CHOL (4:1:2)	1208 ± 538	243
DPPC:DPPG:CHOL (4:1:2)	1195 ± 348	170
DSPC:DOPG:CHOL (4:1:2)	825 ± 307	31
DOPC:DOPG:CHOL (4:1:2)	911 ± 447	63
DOPC:DOPG (4:1)	494 ± 365	149

Table S3. Significant differences between liposomal rigidities as measured by One-way ANOVA and Bonferroni's post-test. ****p < 0.0001, ***p < 0.001, **p < 0.01. *p < 0.05.

DOPC:DOPG:CHOL vs. DSPC:DOPG:CHOL	ns
DOPC:DOPG:CHOL vs. DSPC:DSPG:CHOL	****
DOPC:DOPG:CHOL vs. DPPC:DPPG:CHOL	ns
DOPC:DOPG:CHOL vs. DSPC:DPPG:CHOL	ns
DOPC:DOPG:CHOL vs. DOPC:DOPG	*
DOPC:DOPG:CHOL vs. DSPC:DSPG	****
DSPC:DOPG:CHOL vs. DSPC:DSPG:CHOL	***
DSPC:DOPG:CHOL vs. DPPC:DPPG:CHOL	ns
DSPC:DOPG:CHOL vs. DSPC:DPPG:CHOL	ns
DSPC:DOPG:CHOL vs. DOPC:DOPG	ns
DSPC:DOPG:CHOL vs. DSPC:DSPG	****
DSPC:DSPG:CHOL vs. DPPC:DPPG:CHOL	**
DSPC:DSPG:CHOL vs. DSPC:DPPG:CHOL	**
DSPC:DSPG:CHOL vs. DOPC:DOPG	****
DSPC:DSPG:CHOL vs. DSPC:DSPG	****
DPPC:DPPG:CHOL vs. DSPC:DPPG:CHOL	ns
DPPC:DPPG:CHOL vs. DOPC:DOPG	****
DPPC:DPPG:CHOL vs. DSPC:DSPG	****
DSPC:DPPG:CHOL vs. DOPC:DOPG	****
DSPC:DPPG:CHOL vs. DSPC:DSPG	****
DOPC:DOPG vs. DSPC:DSPG	****

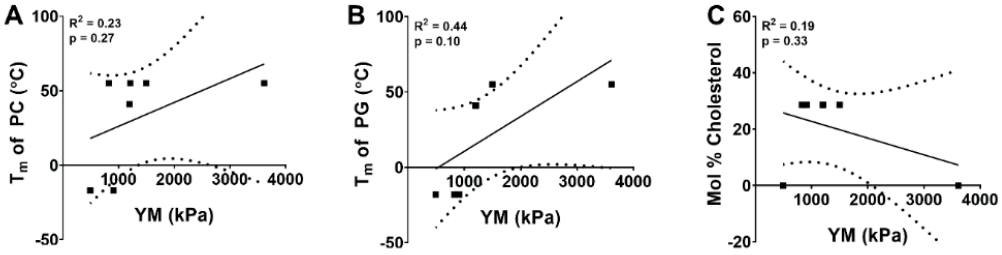


Figure S1. Linear correlations (95% CI) between YM and T_m of PC or PG, CHOL content, liposome size, liposome ζ-potential and LE of OVA_{323}. Correlations between (A) YM and T_m of PC, (B) YM and T_m of PG, (C) YM and mol % CHOL.

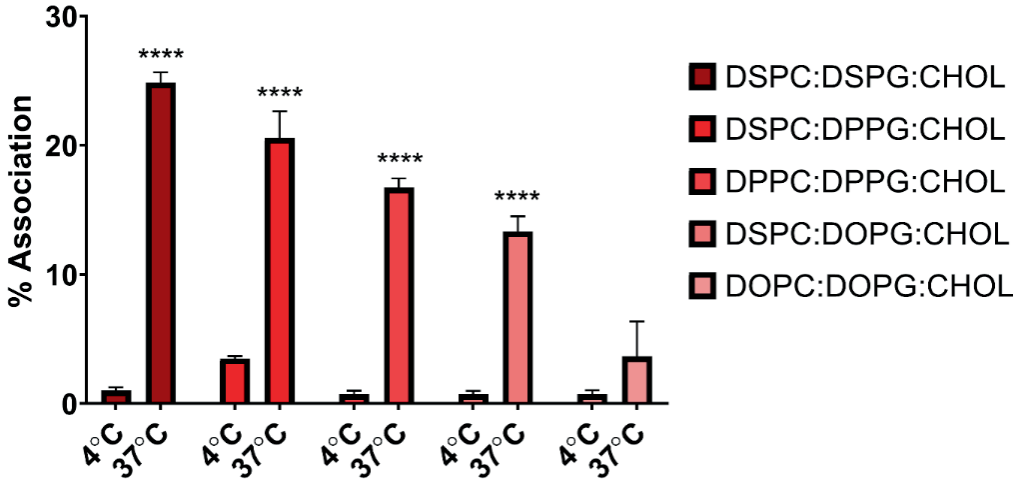


Figure S2. Liposomal association (uptake and/or adsorption) by BMDCs *in vitro*. OVA_{323}-containing fluorescently labeled liposomes were incubated for 4 hours with BMDCs at 4°C and 37°C. Liposomes were subsequently washed away and cells were incubated overnight before being analyzed *via* flow cytometry. % Association indicates the percentage of live BMDCs that are positive for the fluorescent label in the liposomes. Graph shows mean ± SD, n = 3. ****p < 0.0001, comparing 4°C to 37°C determined by two-way ANOVA and Bonferroni's multiple comparisons test.

Table S4. DSPC:DSPG:CHOL:OVA_{323} liposomes measured twice. Measurement 1 and 2 indicate repeated scans of the exact same liposomes.

Young's Modulus (kPa)	
Measurement 1	Measurement 2
1660.80	1651.40
1345.50	1643.60
2009.60	2393.20
1345.80	1731.60
957.60	1277.50
677.60	1229.10
857.90	784.50
1595.50	1394.40
636.00	792.30
1246.50	743.00
1842.50	1687.30
720.10	1128.00
1234.90	1886.80
1595.10	1229.20
1131.30	1038.60

1508.20	1324.50
1055.20	1406.50
1187.50	974.30
2258.40	1343.30
1226.00	1642.40
734.10	930.90
901.70	988.20
1385.20	1247.10
2038.90	1876.20
1854.40	1506.90
2111.80	2249.80
2949.30	2779.90
749.10	798.40
1253.40	1300.80
772.30	638.50
1607.90	2085.40
1626.90	1608.20
1604.00	1537.50
683.80	775.90
2214.00	2287.70
1562.20	1703.10
2994.10	3184.40
1706.60	1603.80
Average	
1443.20	1484.32

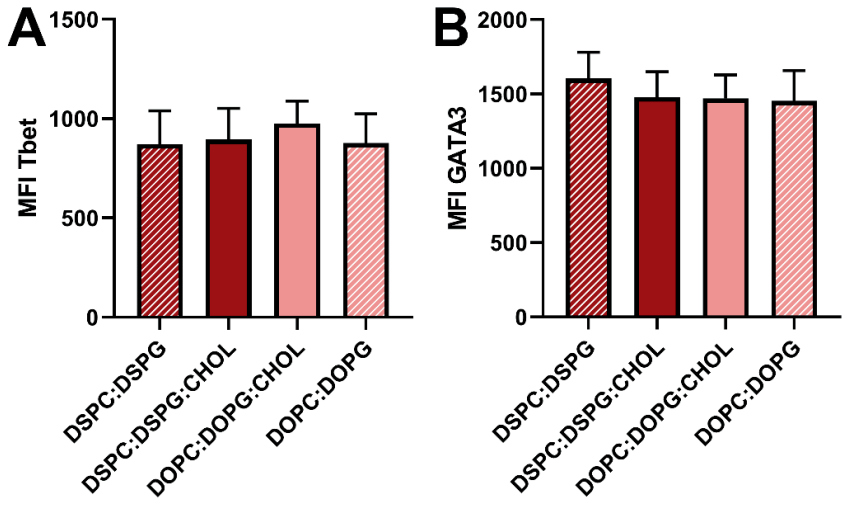


Figure S3. Th1 and Th2 responses in spleens of mice 8 days after i.v. injection of OVA_{323}-containing liposomes. (A) MFI Tbet and (B) MFI GATA3 of $CD45.1^{+}CD4^{+}$ T cells. Graphs show mean ± SD, n = 8. No significant differences between groups as analyzed by one-way ANOVA and Bonferroni's multiple comparisons test.

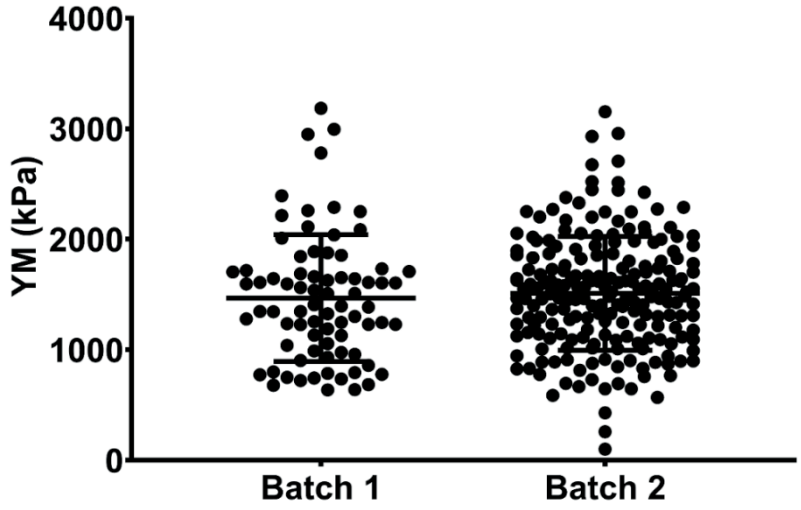


Figure S4. Comparison between two different batches of DSPC:DSPG:CHOL:OVA_{323} liposomes. Each point represents a liposome measurement. Graph shows mean ± SD. No significant difference found between both batches with unpaired two-tailed t-test. N = 77-204.

4

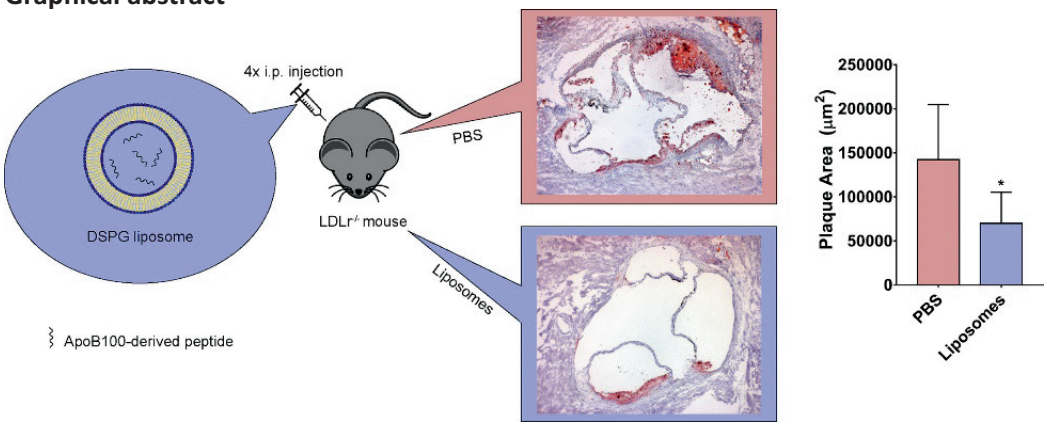
Anionic 1,2-Distearoyl-sn-glycero-3-phosphoglycerol (DSPG) liposomes induce antigen-specific regulatory T cells and prevent atherosclerosis in mice

Author names and affiliations
Naomi Benne[1], Janine van Duijn[1], Fernando Lozano Vigario[1], Romain J. T. Leboux[1], Peter van Veelen[2], Johan Kuiper[1], Wim Jiskoot[1], Bram Slütter[1]

[1]Divison of BioTherapeutics, Leiden Academic Center for Drug Research, Leiden, the Netherlands
[2]Center for Proteomics and Metabolomics, Leiden University Medical Center, Leiden, the Netherlands

Journal of Controlled Release, Volume 291, 10 December 2018, Pages 135-146.
doi: 10.1016/j.jconrel.2018.10.028

Graphical abstract



Abstract

Atherosclerosis is the predominant underlying pathology of many types of cardiovascular disease and is one of the leading causes of death worldwide. It is characterized by the retention of oxidized low-density lipoprotein (ox-LDL) in lipid-rich macrophages (foam cells) in the intima of arteries. Autoantigens derived from oxLDL can be used to vaccinate against atherosclerosis. However, a major challenge is the induction of antigen-specific Tregs in a safe and effective way. Here we report that liposomes containing the anionic phospholipid 1,2-distearoyl-sn-glycero-3-phosphoglycerol (DSPG) induce Tregs that are specific for the liposomes' cargo. Mechanistically, we show a crucial role for the protein corona that forms on the liposomes in the circulation, as uptake of DSPG-liposomes by antigen-presenting cells is mediated via complement component 1q (C1q) and scavenger receptors (SRs). Vaccination of atherosclerotic mice on a western-type diet with DSPG-liposomes encapsulating an LDL-derived peptide antigen significantly reduced plaque formation by 50% and stabilized the plaques, and reduced serum cholesterol concentrations. These results indicate that DSPG-liposomes have potential as a delivery system in vaccination against atherosclerosis.

Introduction

Atherosclerosis is a disease involving large and medium-sized arteries, which affects millions of people worldwide[1]. It is initiated by the retention of LDL in the subendothelial space of arteries, and subsequent oxidation and uptake of LDL (oxLDL) by infiltrating macrophages leading to foam cell formation[2]. In recent years, it has become clear that atherosclerosis is a chronic inflammatory disease. Cells of both the innate and adaptive immune system, such as macrophages, dendritic cells (DCs), T and B lymphocytes, are present in atherosclerotic plaques and are involved in the progression of the disease[3,4]. While there is still debate about the specific role of certain cell types in atherosclerosis, the general consensus is that T helper 1 (Th1) $CD4^+$ T cells are pro-atherogenic, while regulatory T and B cells (Tregs and Bregs, respectively) are protective[5,6]. Tregs are known to be vital for immune suppression, regulation, and resolution of inflammation after infection[7]. They form a subset of $CD4^+$ T cells that express the transcription factor forkhead box P3 (FOXP3) and the IL-2 receptor α chain (CD25). Tregs mediate tolerance by the production of the anti-inflammatory cytokines interleukin (IL)-10 and transforming growth factor (TGF)-β[8], consuming IL-2, interrupting effector T cell metabolism or even lysing effector T cells[9]. In many diseases, including atherosclerosis[10-12], Tregs have a reduced function or ability to proliferate. Current strategies for treatment of such disorders involve systemic suppression of inflammation with drugs or by selective cell depletion. However, these therapies can result in severe side effects, especially upon long-term treatment[13-15]. A more specific strategy would be to design a vaccine that induces specific tolerance through induction of Tregs that recognize the autoantigens involved in inflammatory diseases. LDL has been identified as the most relevant antigen in atherosclerosis, as it is important in the initiation of atherosclerosis[2,16]. Indeed, oxLDL-specific T cells have been found in human atherosclerotic plaques[17], and antibodies against ApoB100 (the apolipoprotein of LDL) have been identified in patients with cardiovascular disease[18-20]. LDL, ApoB100, ApoB100-derived peptides and antibodies against ApoB100-derived peptides have successfully been used as vaccine targets in mice[21-28].

While these studies show a reduction in atherosclerotic plaque formation in mice, only a few have been designed with the goal of inducing antigen-specific Tregs[29] or using complex formulations[24]. To our knowledge, there are no reports about the use of athero-protective antigens with advanced drug delivery formulations. Immunotherapy with so-called tolerogenic DCs (DCs pulsed *ex vivo* with antigens and IL-10 or TGF-β) or oxLDL-pulsed (apoptotic) DCs have been successful at inducing Tregs. However, these treatments are expensive, as they require *ex vivo* isolation and long-term culturing of DCs under GMP conditions[30-32]. Moreover, there is evidence that DCs induced in this way can lose their migratory and T cell activation potential or can even revert to a pro-inflammatory phenotype *in vivo*[33]. Therefore, there is a need for vaccine formulations that induce tolerogenic DCs and ApoB100-specific Tregs *in vivo*.

Liposomes are established delivery vehicles which can deliver a drug or antigen directly into the cell[34]. Moreover, their properties and contents can be fine-tuned to the therapy. For instance, it has been shown that anionic liposomes composed of phosphatidylserine (PS) resemble apoptotic cells (PS becomes exposed on the surface of apoptotic cells[35]). Through SR-mediated uptake by antigen-presenting cells, PS-containing liposomes mediate an anti-inflammatory effect in diabetic and edema mouse

models[36,37]. Furthermore, empty PS liposomes used in the treatment of atherosclerosis reduced plaque size and cellular content to a similar extent as injection of apoptotic cells[38]. In contrast, cationic liposomes are known to be pro-inflammatory, which is advantageous for vaccination against infectious diseases or the treatment of cancer[39,40].

Here we assessed whether we can use liposomal formulations to induce antigen-specific Tregs, and subsequently use these liposomes to encapsulate a newly identified ApoB100-derived peptide to provide protection against atherosclerosis. We report that phosphatidylglycerol (PG)-containing liposomes mediate a superior antigen-specific Treg response compared to the free antigen, PS liposomes or cationic liposomes. Moreover, we show that an SR-independent pathway for PG-containing liposomes mediates the induction of Tregs. Furthermore, we identified a major-histocompatibility complex (MHC)-II-restricted ApoB100-derived peptide using a peptidomics strategy, which, when encapsulated in DSPG liposomes, successfully reduced atherosclerotic plaque formation in an atherosclerosis mouse model.

Materials and Methods

Materials

The lipids 1,2-distearoyl-sn-glycero-3-phosphocholine (DSPC), 1,2-distearoyl-sn-glycero-3-phosphoglycerol (DSPG), 1,2-dipalmitoyl-sn-glycero-3-phospho-L-serine (DPPS), 1,2-dipalmitoyl-3-trimethylammonium-propane (DPTAP), and 1,2-dipalmitoyl-sn-glycero-3-phosphoethanolamine-N-(lissamine rhodamine B sulfonyl) (DPPE-Rho) were obtained from Avanti Polar Lipids (Alabaster, AL, USA). Cholesterol was purchased from Sigma-Aldrich (Zwijndrecht, the Netherlands). The ovalbumin-derived peptide OVA323 (ISQAVHAAHAEINEAGR) was obtained from Invivogen (San Diego, California, USA). The ApoB100-derived peptide p3500 (LSQEYSGSVANEANV) was synthesized by GenScript (Piscataway, New Jersey, USA). Polycarbonate track-etched membranes with a pore size of 400 nm and 200 nm were obtained from Millipore (Kent, UK).

For cell culture, Ca^{2+}- and Mg^{2+}-free phosphate-buffered saline (PBS), Iscove's Modified Dulbecco's Medium (IMDM), Roswell Park Memorial Institute Medium (RPMI 1640), L-glutamine, and penicillin/streptomycin were purchased from Lonza (Basel, Switzerland). Lipopolysaccharide (LPS) extracted from *Salmonella Typhosa*, phorbol 12-myristate 13-acetate (PMA), ionomycin, brefeldin A, β-mercaptoethanol, and polyinosinic acid (poly I) were purchased from Sigma-Aldrich (Zwijndrecht, the Netherlands). Granulocyte-macrophage colony-stimulating factor (GM-CSF) was purchased from PeptroTech (London, UK). Human C1q was purchased from Abcam (Cambridge, UK). Fetal calf serum (FCS) was purchased from GE Healthcare (Little Chalfont, UK). Human C1q-depleted serum and normal human serum were a generous gift from Dr. F. A. Ossendorp (Department of Immunohematology and Blood Transfusion, Leiden University Medical Centre).

The antibodies CD4-PerCP (RM4-5), Ly-6G (1A8) and NK1.1 (PK136) were purchased from BD Biosciences (NJ, USA). CD4-APC (GK1.5), CD4-FITC (GK1.5) and Thy1.2-PerCP-Cy5.5 (53-2.1) were purchased from Biolegend (CA, USA). CD11b-eFluor450 (M1/70), CD25-FITC (PC61.5), CD45.1-eFluor450 (A20), CD45.1-PE (A20), Fixable viability dye-APC-eFluor780, Fixable viability dye-eFluor506, FOXP3-eFluor450 (FJK-16s), IFNγ-PE (XMG1.2), IL-10-APC (JES5-16E3), IL-17A-PE (eBio17B7), IL-4-APC (11B11), Ki67-FITC (SolA15), Ly-6C-PerCP-Cy5.5 (HK1.4), Thy1.2-PE-Cy7 (53-2.1), and FOXP3/transcription factor staining kit were purchased from eBioscience (Thermofisher Scientific, MA, USA). CCR2-APC (#475301) was purchased from R&D systems (MN, USA).

For sodium dodecyl sulfate-polyacrylamide gel electrophoresis (SDS-PAGE) and Western blotting (WB), Laemmli sample buffer, Precision Plus Protein™ all blue prestained protein standards, Mini-PROTEAN® Tetra vertical electrophoresis cell, Mini Trans-Blot® cell, blot absorbent filter paper, and 4-20% Mini-PROTEAN® precast gels were purchased from Bio-Rad (Veenendaal, the Netherlands). Bovine serum albumin (BSA), Polysorbate 20, tris-glycine-SDS buffer 10x concentrate, tris(hydroxymethyl)aminomethane, glycine, and 3-amino-9-ethylcarbazole (AEC) staining kit were purchased from Sigma-Aldrich (Zwijndrecht, the Netherlands). Nitrocellulose membrane with a 0.45 µm pore size was obtained from GE Healthcare (Little Chalfont, UK). Mouse monoclonal biotinylated anti-C1q antibody (JL-1) was purchased from Abcam (Cambridge, UK). Streptavidin-horseradish peroxidase (HRP) was purchased from Thermofisher Scientific (MA, USA).

Optimal cutting temperature (OCT) formulation Tissue-Tek® was obtained from Sakura

Finetek (CA, USA). For immunohistochemical staining, Hematoxylin, Oil-Red-O, Sirius Red, and anti-rat IgG (whole molecule)–alkaline phosphatase antibody produced in goat were purchased from Sigma-Aldrich (Zwijndrecht, the Netherlands), rat anti-mouse macrophages/monocytes antibody (MOMA2) was purchased from Bio-Rad (Veenendaal, the Netherlands). 5-bromo-4-chloro-3-indolyl phosphate (BCIP)/nitro blue tetrazolium (NBT) substrate system buffer was purchased from DAKO (Agilent, CA, USA).

Animals

C57BL/6, OT-II transgenic, T-cell immunoglobulin- and mucin-domain-containing molecule 4 (TIM4)$^{-/-}$ and LDLr$^{-/-}$ mice on a C57BL/6 background were purchased from Jackson Laboratory (CA, USA), bred in-house under standard laboratory conditions, and provided with food and water *ad libitum*. LDLr$^{-/-}$ mice were fed a Western-type diet (WTD) containing 0.25% cholesterol and 15% cocoa butter (Special Diet Services, Essex, UK). All animal work was performed in compliance with the Dutch government guidelines and the Directive 2010/63/EU of the European Parliament. Experiments were approved by the Ethics Committee for Animal Experiments of Leiden University.

Bone marrow-derived dendritic cells (BMDCs)

Bone marrow was isolated from the tibias and femurs of C57BL/6 or TIM4$^{-/-}$ mice. A single-cell suspension of bone marrow cells was obtained by using a 70-µm cell strainer (Greiner Bio-One B.V., Alphen aan den Rijn, NL). The cells were cultured in IMDM (Lonza) supplemented with 2 mM L-glutamine, 8% (v/v) FCS, 100 U/mL penicillin/streptomycin (Lonza), and 50 µM β-mercaptoethanol (Sigma) at 37˚C and 5% CO_2 in 95 mm Petri dishes (Greiner Bio-One B.V., Alphen aan den Rijn, NL) and 20 ng/mL GM-CSF (PeproTech) for 10 days. Medium was refreshed every other day.

Immunoprecipitation

BMDCs were incubated with 10% serum from LDLr$^{-/-}$ mice on a WTD activated with 0.1 µg/mL LPS. Affinity-purification of MHC-II (I-Ab) molecules from BMDCs and subsequent peptide elution was performed as described previously[41]. Approximately 50 x 10^6 BMDCs were lysed in 0.5 mL lysis buffer (50 mM Tris-Cl pH 8.0, 150 mM NaCl, 5 mM Ethylenediaminetetraacetic acid (EDTA), 0.5% Zwittergent 3-12 (N-dodecyl-N,N-dimethyl-3-ammonio-1-propanesulfonate) and protease inhibitor (Complete, Roche Applied Science)) for 2 hours at 0°C [41]. Lysates were centrifuged for 10 min at 2500 × g and for 45 min at 31,000 x g to remove nuclei and other insoluble material, respectively. Lysates were passed through a 50 µL CL-4B Sepharose column (in a standard yellow tip equipped with a filter) to pre-clear the lysate and subsequently passed through a 50 µL column containing 125 µg pan class II (Y3P) IgG coupled to protein G Sepharose[41]. The Y3P column was subsequently washed with 250 µL of lysis buffer, 250 µL of low salt buffer (20 mM Tris-Cl pH 8.0, 120 mM NaCl), 100 µL of high salt buffer (20 mM Tris-Cl pH 8.0, 1 M NaCl), and finally with 250 µL of the low salt buffer. I-Ab and peptides were eluted with 250 µL of 10% acetic acid, diluted with 1 mL of 0.1% trifluoroacetic acid (TFA) and purified by SPE (Oasis HLB, Waters) by sequential elution with 20%, 30% and 40% acetonitrile in 0.1% TFA to recover MHC peptide molecules.

Mass spectrometry

MHC peptides were analyzed by using an Easy nLC1000 (Thermo, Bremen, Germany) coupled to a Q-Exactive mass spectrometer (Thermo). The injection was done onto a homemade pre-column (100 µm × 15 mm; Reprosil-Pur C18-AQ 3 µm, Dr. Maisch, Ammerbuch, Germany) and elution via a homemade analytical column (15 cm × 50 µm; Reprosil-Pur C18-AQ 3µm). The gradient was 0% to 30% solvent B (90% ACN/0.1% TFA) in 120 min. The analytical column was drawn to a tip of around 5 µm and acted as the electrospray needle of the MS source. The Q-Exactive mass spectrometer was operated in top10-mode. Parameters were as follows: full scan, 70,000 resolution, 3,000,000 AGC target, max fill time 20 ms; MS/MS, 35,000 resolution, 100,000 AGC target, 60 ms max fill time, 17,400 intensity threshold. Apex trigger was set to 1–5 s and allowed charges were 2–5. Proteome Discoverer version 2.1 was used for peptide and protein identification, using the mascot node for identification, using mascot version 2.2.04 with the UniProt/Mouse database (51,374 entries). Methionine oxidation (on methionine) and cysteinylation (on cysteine) were set as variable modification. Precursor ion mass tolerance was set to 10 ppm. MS/MS fragment tolerance was 20 mmu. ApoB100-derived peptides as proposed by the software are shown in Table S1 and were manually assessed. The identified ApoB100 peptides were screened *in silico* (www.IEDB.org) for their ability to bind to MHC-II (Table S2). The correct assignment of the candidate peptide of sequence LSQEYSGSVANEAN was confirmed by matching of the MS/MS spectrum of eluted peptide and its synthetic peptide counterpart (Figure S1).

Liposome preparation

Liposomes were prepared by using the thin film dehydration-rehydration method, as described previously[42]. Briefly, DSPC (T_m = 54.9°C[43]), a charged lipid (DSPG (T_m = 54.4°C[44]), DPPS (T_m = 55°C[45]), or DPTAP (T_m = 52.8°C[46])) and cholesterol were dissolved in chloroform and mixed in a round-bottom flask at a molar ratio of 4:1:2 DSPC:charged lipid:cholesterol to obtain a final lipid concentration of 10 mg/mL. The chloroform was evaporated in a rotary evaporator (Rotavapor R-210, Büchi, Switzerland) for 1 hour at 40°C. The lipid film was rehydrated with 250 µg OVA323 dissolved in 1 mL Milli-Q water and homogenized by rotation at 60°C by using glass beads. Next, the liposome dispersion was snap-frozen in liquid nitrogen, followed by freeze-drying overnight (Christ alpha 1–2 freeze-dryer, Osterode, Germany). The freeze-dried lipid cake was slowly rehydrated by using 10 mM phosphate buffer (PB), pH 7.4 at 60°C; two volumes of 500 µL and one volume of 1,000 µL PB were successively added, with intervals of 30 min between each addition. The mixture was vortexed well between each hydration step, and the resulting dispersion was kept at 60°C for at least 1 hour. The multilamellar vesicles were sized by high-pressure extrusion at 60°C (LIPEX Extruder, Northern Lipids Inc., Canada). To obtain monodisperse liposomes, the liposome mixture was passed four times through stacked 400 nm and 200 nm pore size membranes. To separate non-encapsulated OVA323 from the liposomes, liposomes were washed by using a Vivaspin 2 centrifuge membrane concentrator (MWCO 300 kDa, Sartorius, Göttingen, Germany). DSPG-containing liposomes encapsulating the ApoB100-derived peptide p3500 were prepared in the same way as OVA323 liposomes, where the lipid film was rehydrated with 250 µg p3500 dissolved in 1 mL Milli-Q water. To prepare fluorescently labeled liposomes, 0.5 mol% of DSPC was replaced with DPPE-Rho. Liposomes were stored at 4°C and used for further

experiments within 2 weeks.

Liposome characterization

The Z-average diameter (Z_{ave}) and polydispersity index (PDI) of the liposomes were measured by dynamic light scattering (DLS) using a NanoZS Zetasizer (Malvern Ltd., Malvern, UK). Zeta-potential was determined by using laser Doppler electrophoresis using the same instrument. For measurements, the liposomes were diluted 100-fold in 10 mM phosphate buffer at pH 7.4 to a total volume of 1 mL. To determine the concentration of loaded OVA323, the peptide was separated from liposomes by using a modified Bligh-Dyer method, as described previously[42]. Briefly, 100 µL of aqueous liposomal dispersion or a known concentration of free peptide as control was mixed with 250 µL methanol and 125 µL chloroform and vortexed briefly. 250 µL of 0.1 M HCl and 125 chloroform was added and the mixture was vortexed again. This was then centrifuged for 5 min at 1500 rpm to separate the water-methanol phase (containing the peptide) from the chloroform phase. The upper water-methanol phase was collected and analyzed by reversed phase UPLC (Waters ACQUITY UPLC, Waters, MA, USA). For this, 5 µL of the sample was injected into a 1.7 µm BEH C18 column (2.1 x 50 mm, Waters ACQUITY UPLC, Waters, MA, USA). The column temperature and the temperature of the sample were set at 40°C and 4°C respectively. The mobile phases were Milli-Q water with 0.1% TFA (solvent A) and acetonitrile with 0.1% TFA (solvent B). For detection, the mobile phases were applied in a linear gradient from 5% to 95% solvent B over 5 minutes at a flow rate of 0.370 mL/min. Peptides were detected by absorbance at 220 nm using an ACQUITY UPLC TUV detector (Waters ACQUITY UPLC, Waters, MA, USA).

Protein corona analysis

To characterize the formation of a protein corona on liposomes, liposomes were diluted to a lipid concentration of 0.1 mg/mL and incubated for 1 hour at 37°C with FCS or 10 µg/mL C1q in PB. Liposomes were washed three times and concentrated with a Vivaspin 500 centrifuge membrane concentrator (MWCO 1,000 kDa, Sartorius, Goettingen, Germany) to remove unbound proteins, leaving the 'hard' protein corona[47]. Size, PDI, and zeta-potential of liposomes were measured with a NanoZS Zetasizer (Malvern Ltd., Malvern, UK). SDS-PAGE was performed according to the manufacturer's instructions. Samples and MW standards were diluted 1:1 in reducing Laemmli buffer and 10 µL of sample was loaded per lane. Gels were stained with Coomassie Blue and analyzed by using a scanner (GS-900™, Bio-Rad, Veenendaal, the Netherlands) and Image Lab™ software (Bio-Rad, Veenendaal, the Netherlands). For WB for C1q, SDS-PAGE was first carried out as described above, and proteins were transferred by using the wet blotting method according to the manufacturer's instructions. Blots were blocked overnight at 4°C with PBS containing 2% BSA and 0.5% polysorbate 20. Subsequently, blots were incubated for 1 hour at room temperature with biotinylated anti-C1q antibody diluted 1000-fold in blocking buffer, followed by 1-hour incubation at room temperature with streptavidin-HRP diluted 1000-fold in blocking buffer. An AEC staining kit was used to develop the blots, and we analyzed blots with a scanner and Image Lab™ software.

Liposome uptake by BMDCs

BMDCs were cultured as described above. After 10 days of culture, 50,000 BMDCs were plated in 96-well plates (Greiner Bio-One B.V., Alphen aan den Rijn, Netherlands) and fluorescently labeled liposomes or controls were added at a concentration of 0.1 µg/mL OVA323 in different media. To block SR-mediated uptake, 250 µg/mL poly I was added. After 4 hours of incubation at 37˚C and 5% CO_2, excess liposomes were removed by washing the cells several times with IMDM. Cultures were supplemented with 20 ng/mL GM-CSF and incubated overnight. Cells were analyzed by flow cytometry (CytoFLEX S, Beckman Coulter, CA, USA). BMDCs were stained for CD11c and viability. The presence of the fluorescent label in the liposomes indicated uptake by BMDCs. Data were analyzed by using FlowJo software (Treestar, OR, USA).

***In vitro* Treg induction by liposome-pulsed BMDCs**

Wild-type (WT) or $TIM4^{-/-}$ BMDCs were cultured as described above, and activated for 4 hours with liposomes or controls in different media. Spleens were removed from OT-II mice and strained through a 70-µm cell strainer to obtain a single-cell suspension. Erythrocytes were lysed with Ammonium-Chloride-Potassium (ACK) lysis buffer (0.15 M NH_4Cl, 1 mM $KHCO_3$, 0.1 mM Na_2EDTA; pH 7.3). $CD4^+$ T cells were isolated using a $CD4^+$ T cell isolation kit (Miltenyi Biotec B.V., Leiden, Netherlands) according to the manufacturer's protocol. After incubation, BMDCs were thoroughly washed with PBS to remove any free liposomes, and 100,000 $CD4^+$ T cells were added to obtain a number ratio of 2:1 $CD4^+$ T cells:BMDCs. Co-cultures were cultured for 72 hours in complete RPMI 1640 medium supplemented with 2 mM glutamine, 10% FCS, 100 U/mL penicillin/streptomycin, and 50 µM β-mercaptoethanol. Cells were stained for Thy1.2, CD4, viability, FOXP3, and Ki67, and analyzed by flow cytometry (CytoFLEX S, Beckman Coulter, CA, USA). Data were analyzed by using FlowJo software (Treestar, OR, USA).

Analysis of antigen-specific $CD4^+$ T cell responses *in vivo*

12-week-old male C57BL/6 mice were randomized into 5 groups. On day 0, all groups received splenocytes isolated from a female OT-II transgenic mouse equivalent to 500,000 $CD45.1^+CD4^+$ T cells via the tail vein. On day 1, mice were immunized intravenously (i.v.) with a single injection of either PBS, 1 nmol free OVA323 in PBS, or liposomes containing 1 nmol OVA323 in PBS, in a total volume of 200 µl via the tail vein. Seven days after immunization, a small amount of blood was collected from the mice via the tail. Blood samples were lysed and stained for Thy1.2, CD4, CD45.1 and viability, and samples were analyzed by flow cytometry (Cytoflex S, Beckman Coulter, Indiana, USA). On day 8, mice were sacrificed by cervical dislocation and spleens and inguinal lymph nodes (iLNs) were immediately removed. Organs were processed and stained for CD4, CD45.1, Thy1.2, viability, Ki67, CD25 and FOXP3 and measured by flow cytometry. To measure cytokine production, splenocytes were stimulated *ex vivo* with PMA (50 ng/mL) and Ionomycin (500 ng/mL). After 1-hour brefeldin A (3 µg/mL) was added and cells were incubated for a further 5 hours. Cells were subsequently stained for Thy1.2, CD4, CD45.1, viability, IFN-γ, IL-17, IL-4 and IL-10 and analyzed by flow cytometry.

Analysis of atherosclerosis in mice

Eight- to 14-week-old male LDLr$^{-/-}$ mice were randomized into 3 groups of 9 mice. Mice were fed a WTD for 10 weeks to induce atherosclerosis. During this time, mice were immunized at week 0, 3, 6 and 9 via i.p. injection with either PBS, 10 nmol of free p3500 peptide in PBS, 0.5 mg DSPG-liposomes in PBS, or 0.5 mg DSPG-liposomes containing 10 nmol of p3500 in PBS, in a total volume of 200 µL. After 10 weeks, mice were euthanized by a subcutaneous injection (120 µL) of a cocktail containing ketamine (40 mg/mL), atropine (50 µg/mL), and sedazine (6.25 mg/mL). Mice were exsanguinated and perfused with PBS. For flow cytometry, aortas were harvested and cut into small pieces. These were then incubated for 30 min at 37°C with 450 U/mL collagenase I, 250 U/mL collagenase XI, 120 U/mL DNAse, and 120 U/mL hyaluronidase, and strained through a 70-µm cell strainer to obtain a single-cell suspension. Cells were stained for Thy1.2, CD4, CD8 and viability. Hearts were harvested and fixed frozen in OCT formulation at -80°C. Hearts were subsequently cryosectioned horizontally to the aortic axis and towards the aortic arch. Upon identification of the aortic root, defined by the trivalve leaflets, 10 µm sections were collected. Sections were stained for Oil-Red-O as previously described[48] to visualize lipid-rich plaques. Macrophages in the plaques were stained using MOMA2 staining as previously described[49]. Collagen in the plaques was stained using Sirius Red staining, as previously described[50]. All stainings were analyzed by microscopy using Leica QWin software on a Leica DM-RE microscope (Leica, Imaging Systems, UK). Briefly, the area stained positively for Oil-Red-O, expressed as µm^2, was determined for the section with the largest lesion, and the two flanking sections to estimate the average plaque size. The average percentage of macrophages in the plaque was determined by dividing the area positive for the MOMA2 staining by the total plaque area for the 3 largest subsequent sections. Sirius Red staining was visualized under polarized light[51], and the percentage of collagen was calculated by dividing the area positive for the Sirius Red staining by the total plaque area for the 3 largest subsequent sections. Blood samples were prepared for determination of serum cholesterol levels as previously described[30].

Statistical analysis

Results were analyzed using one-way or two-way ANOVA, followed by Bonferroni's multiple comparisons test and was performed using GraphPad Prism version 7.00 for Windows (GraphPad Software, CA, USA).

Results

Preparation of liposomes

Anionic liposomes are associated with tolerance induction[36,37], although it is unclear whether this is merely due to the negative charge or the specific anionic head group. In order to determine which anionic phospholipid would be most effective for the induction of antigen-specific Tregs, we prepared liposomes containing DSPG or DPPS, ensuring all other physicochemical characteristics like size, zeta-potential and rigidity remained similar. As a positive control for pro-inflammatory responses, we made DPTAP-containing liposomes. Liposomes were prepared with DSPC, charged lipids (DSPG, DPPS or DPTAP) and cholesterol at a molar ratio of 4:1:2 with an initial concentration of 250 µg/mL OVA323. The liposomes were around 165 nm in size and were monodisperse, with a PDI around 0.1 (Table 1). As expected, the zeta potential of the liposomes was negative for both anionic liposomal formulations and positive for the DPTAP liposomes. The loading efficiency (LE) of OVA323 was between 10-15% for the anionic liposomes and almost 30% for the cationic liposomes. The addition of a small amount of fluorescently labeled DPPE did not alter the liposomal properties (Table S3), and replacing OVA323 with the athero-specific ApoB100-derived peptide p3500 did not alter the properties of DSPG-liposomes (Table S4).

Table 1: Physicochemical properties of OVA323-containing liposomes composed of 4:1:2 molar ratio DSPC:charged lipid:chol.

Charged lipid	Z_{ave} (nm) [a]	PDI	Zeta-potential (mV)	% LE [b]
DSPG	167.3 ± 11.8	0.08 ± 0.04	-54.4 ± 5.5	10.6 ± 3.9
DPPS	165.4 ± 15.7	0.12 ± 0.05	-54.0 ± 6.4	14.7 ± 4.7
DPTAP	166.9 ± 14.9	0.09 ± 0.04	33.7 ± 3.7	27.6 ± 8.5

[a] Z-average diameter (Z_{ave}), mean ± SD, n = 12.

[b] %LE was calculated as the total amount of peptide before extrusion/total amount of peptide after purification * 100%.

Liposomes induce strong antigen-specific $CD4^+$ T cell responses in mice

To determine the effect of liposomes on antigen-specific $CD4^+$ T cell expansion *in vivo*, a single immunization with OVA323-containing liposomes or free OVA323 was performed in mice, which had received an adoptive transfer of OT-II splenocytes one day prior to immunization. All liposomal formulations induced proliferation of antigen-specific $CD45.1^+CD4^+$ T cells in the blood of mice just 7 days after immunization (Figure 1A, D, E, F, and G). In contrast, free OVA323 induced almost no antigen-specific $CD4^+$ T cell proliferation, comparable to PBS. We observed very similar results in the spleens and iLNs on day 8 (Figure 1B and C). The antigen-specific $CD4^+$ T cell proliferation induced by cationic liposomes tended to be increased, albeit not significant compared to OVA-specific $CD4^+$ T-cell responses induced by anionic liposomes (Figure S2).

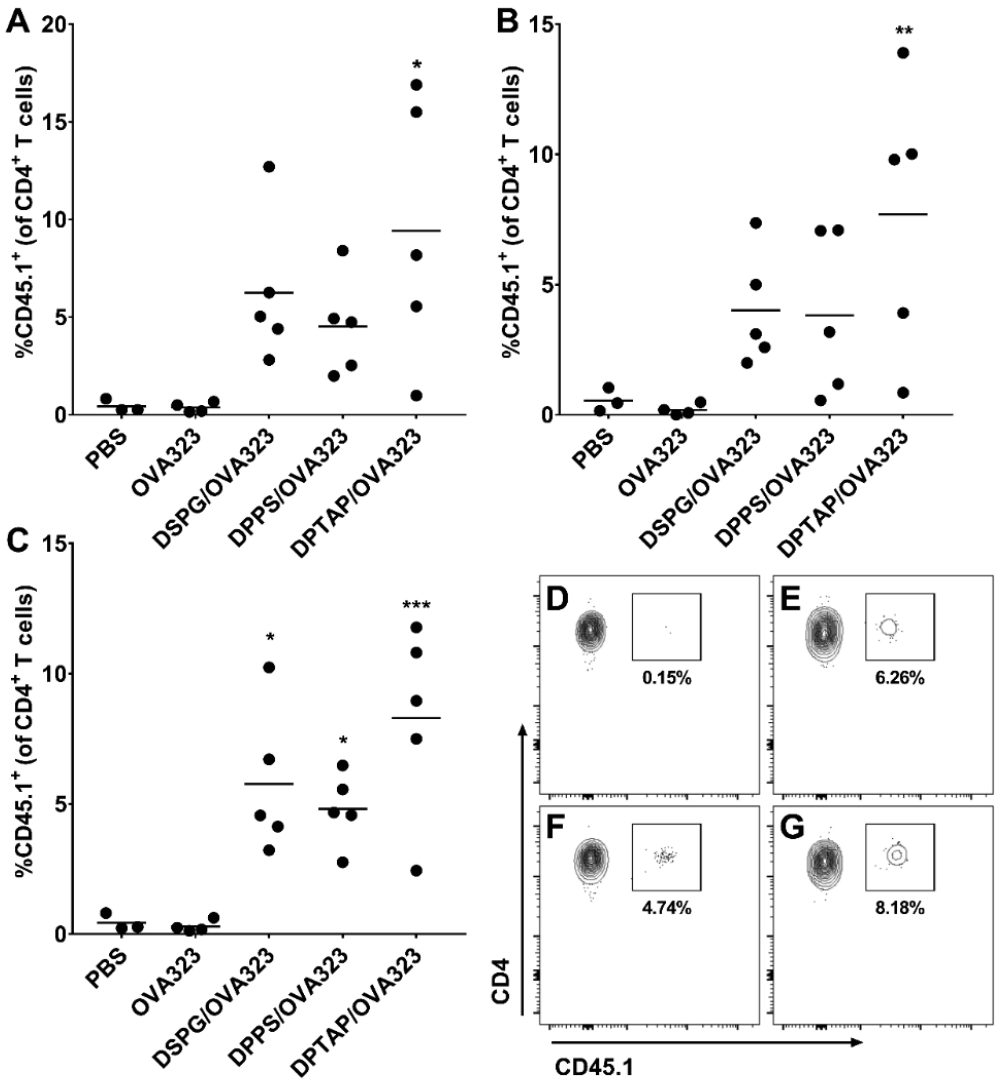


Figure 1: Expansion of OVA323-specific CD4⁺ T cells in blood, spleens, and iLNs of mice after i.v. injection of OVA323-containing liposomes. (A) CD45.1⁺ CD4⁺ T cells in blood (day 7), (B) inguinal LNs (day 8) and (C) spleen (day 8) of mice after immunization with DSPG-, DPPS-, or DPTAP-liposomes containing the OVA323 peptide, or PBS or free OVA323 peptide. Representative flow cytometry plots of pre-gated CD4⁺ T-cells in the blood mice 7 days after immunization with (D) free OVA323, (E) DSPG/OVA323-, (F) DPPS/OVA323-, and (G) DPTAP/OVA323-liposomes. *p < 0.05, **p < 0.01, compared to free OVA323 determined by one-way ANOVA and Bonferroni's multiple comparisons test. No significant differences were found between the different liposomal formulations. Representative example of 2 independent experiments.

DSPG-liposomes induce antigen-specific Tregs *in vivo*

To uncover the type of OVA323-specific $CD4^+$ T cells induced by the liposomes in mice, antigen-specific ($CD45.1^+CD4^+CD25^+FOXP3^+$) Tregs were measured by flow cytometry after immunization (Figure 2A, B, and C). We found comparable percentages of non-specific Treg populations ($CD45.1^-CD4^+CD25^+FOXP3^+$) in all mice (Figure S3). DSPG-liposomes encapsulating OVA323 induced the highest percentage of antigen-specific Tregs, which was significantly higher than the background Treg response after injection of free OVA323. Surprisingly, DPPS-liposomes were not as efficient at Treg induction as DSPG-liposomes, but they did show a non-significant increase in Tregs compared to free OVA323. DPTAP-liposomes did not alter Treg responses as compared to the background. We also measured antigen-specific intracellular cytokine responses by flow cytometry after restimulation with PMA and ionomycin (Figure 2D, E, F, and G). DPTAP-liposomes greatly increased pro-inflammatory cytokine production (interferon (IFN)-γ and IL-17) of the antigen-specific $CD4^+$ T cells, while both anionic liposomes induced almost no production of these cytokines. There were no differences in IL-4 or IL-10 production in any of the groups.

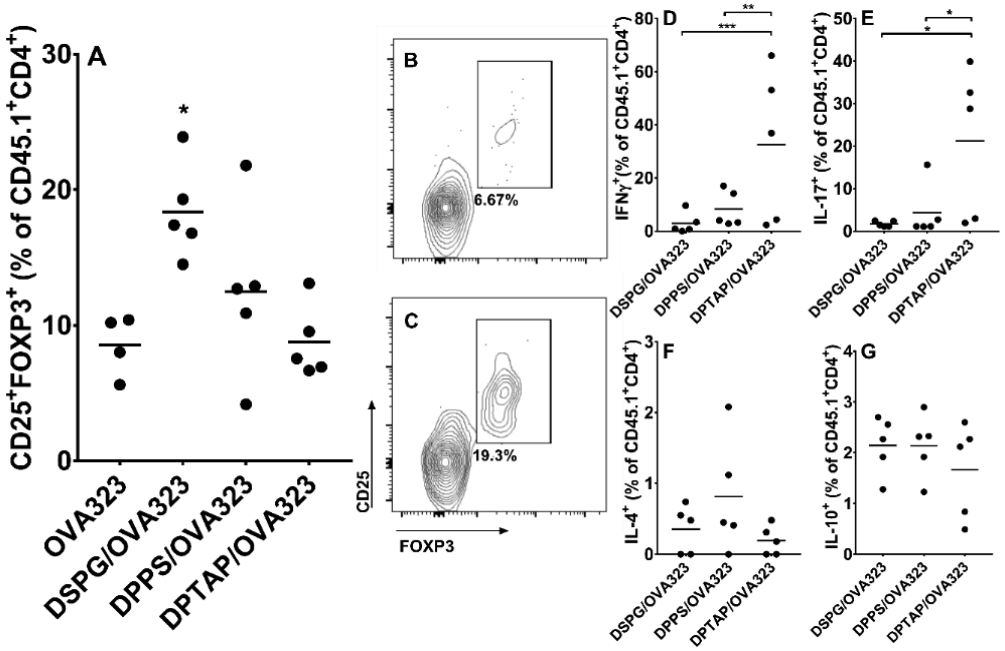


Figure 2: Induction of OVA323-specific immune responses in iLNs and spleens of mice 8 days after i.v. injection of OVA323-containing liposomes. (A) $CD25^+FOXP3^+CD4^+$ T cells from adoptive transfer of $CD4^+$ T cells from an OT-II mouse were detected in iLNs of WT mice after immunization with free OVA323, or DSPG-, DPPS- or DPTAP-liposomes containing OVA323 peptide. Representative flow cytometry plots of pre-gated $CD45.1^+CD4^+$ T-cells in the iLNs of a mouse 8 days after immunization with (B) DPTAP, or (C) DSPG liposomes. Splenocytes were incubated for 6 hours with PMA + ionomycin and brefeldin A, and subsequently, (D) IFNγ, (E) IL-17, (F) IL-4 and (G) IL-10 production by antigen-specific $CD45.1^+CD4^+$ T cells was analyzed by flow cytometry. Graphs show mean, *$p < 0.05$, **$p < 0.01$ determined by one-way ANOVA and Bonferroni's multiple comparisons tests. Representative of 2 independent experiments.

Anionic liposomes attract C1q from serum and are taken up by SRs

While both anionic liposomal formulations had similar physicochemical properties and could induce Tregs, DSPG-containing liposomes were clearly more potent. The cationic DPTAP liposomes induced no Tregs. We hypothesized that a protein corona around the liposomes could be responsible for the differences in *in vivo* immunological responses. To assess the formation of a protein corona, we incubated the anionic liposomes in FCS for 1 hour at 37°C and washed them to remove any unbound proteins, leaving the 'hard' protein corona. SDS-PAGE analysis showed that the liposomes attract proteins from FCS (Figure S4A). Several serum proteins can bind to nanoparticles, including complement proteins[52]. Of these complement proteins, C1q is especially interesting since it can bind to various receptors[53]. Notably, binding of C1q to PS on apoptotic cells leads to recognition and clearance by phagocytic cells via SRs[54-56]. To test whether the protein corona or C1q is important for uptake of liposomes by BMDCs and Treg induction, we measured uptake of fluorescently labeled liposomes by BMDCs in the absence of serum, or in medium containing either 8% FCS or C1q. We also assessed OT-II $FOXP3^{+}Ki67^{+}CD4^{+}$ T cell induction by these BMDCs. Both DSPG- and DPPS-liposomes showed an uptake of less than 10% in the absence of FCS or C1q, however, the uptake of DPPS-liposomes was around 10-fold lower in this condition (Figure 3A). Addition of C1q or FCS significantly increased uptake of both liposomes, with DSPG-liposomes showing significantly higher uptake than DPPS-liposomes in normal serum conditions at the concentration of lipids we examined (Figure 3A). For DSPG-liposomes, depletion of C1q from serum significantly reduced uptake, which was remedied by reconstituting C1q (Figure S5). Liposomes in the presence of serum significantly increased Treg induction compared to serum-free conditions (Figure 3B). The *in vitro* data supports the *in vivo* findings, i.e., in the presence of serum, both liposomes enhanced Treg induction compared to free OVA323, and DSPG liposomes were more potent. It should be noted that, although DCs can produce C1q[57], the short incubation time of 4 hours should not allow for a significant production of C1q. We also assessed whether TIM4, a known receptor for apoptotic cells that plays an important role in atherosclerosis[58], plays a role in mediating the uptake of our liposomes and induction of Tregs. However, $TIM4^{-/-}$ BMDCs showed no differences in liposome uptake and Treg induction compared to WT BMDC (Figure S6).

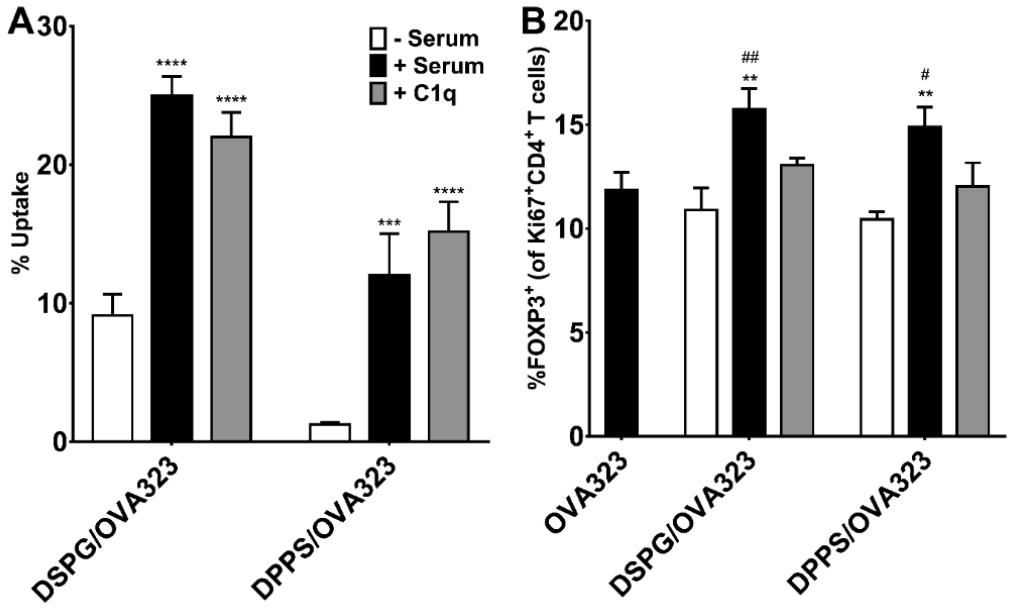


Figure 3: Effect of C1q and FCS on *in vitro* uptake by BMDCs and subsequent antigen-specific Treg induction. (A) Percentage of DCs which have taken up fluorescently labeled OVA323-loaded DSPG- or DPPS-containing liposomes after 4 hours incubation, as measured by flow cytometry. Cells were incubated with liposomes either in serum-free IMDM (white bars), in IMDM supplemented with FCS (black bars) or in IMDM supplemented with 10 µg/mL C1q (gray bars). (B) OT-II $FOXP3^+Ki67^+CD4^+$ T cells induced after 3 days co-culture with BMDCs exposed to conditions shown in (A). Graph shows mean ± SD (n = 3), * shows comparison to "- serum" condition within liposome group, # compares to free OVA323 + serum. ** $p < 0.01$, *** $p < 0.001$, **** $p < 0.0001$, # $p < 0.05$, ## $p < 0.01$ determined by one-way ANOVA and Bonferroni's multiple comparisons test.

Importantly, C1q is present in FCS and in the protein corona of both DSPG- and DPPS-liposomes, as measured by SDS and WB (Figure 4A, Figure S4B). To test the effect of FCS and C1q binding to the liposomes on their physicochemical properties, we incubated liposomes either with FCS in PB or with C1q in PB, washed them, and analyzed them using DLS. Either condition significantly increased the size of both DSPG- and DPPS-liposomes as compared to a protein-free medium. However, there were no signs of severe aggregation of liposomes, as the size remained below 200 nm for all groups (Figure 4B, E, and F). For both liposomal formulations, C1q binding moderately but significantly increased PDI and reduced the negative zeta-potential of the liposomes. FCS binding enhanced this effect even further (Figure 4C and D).

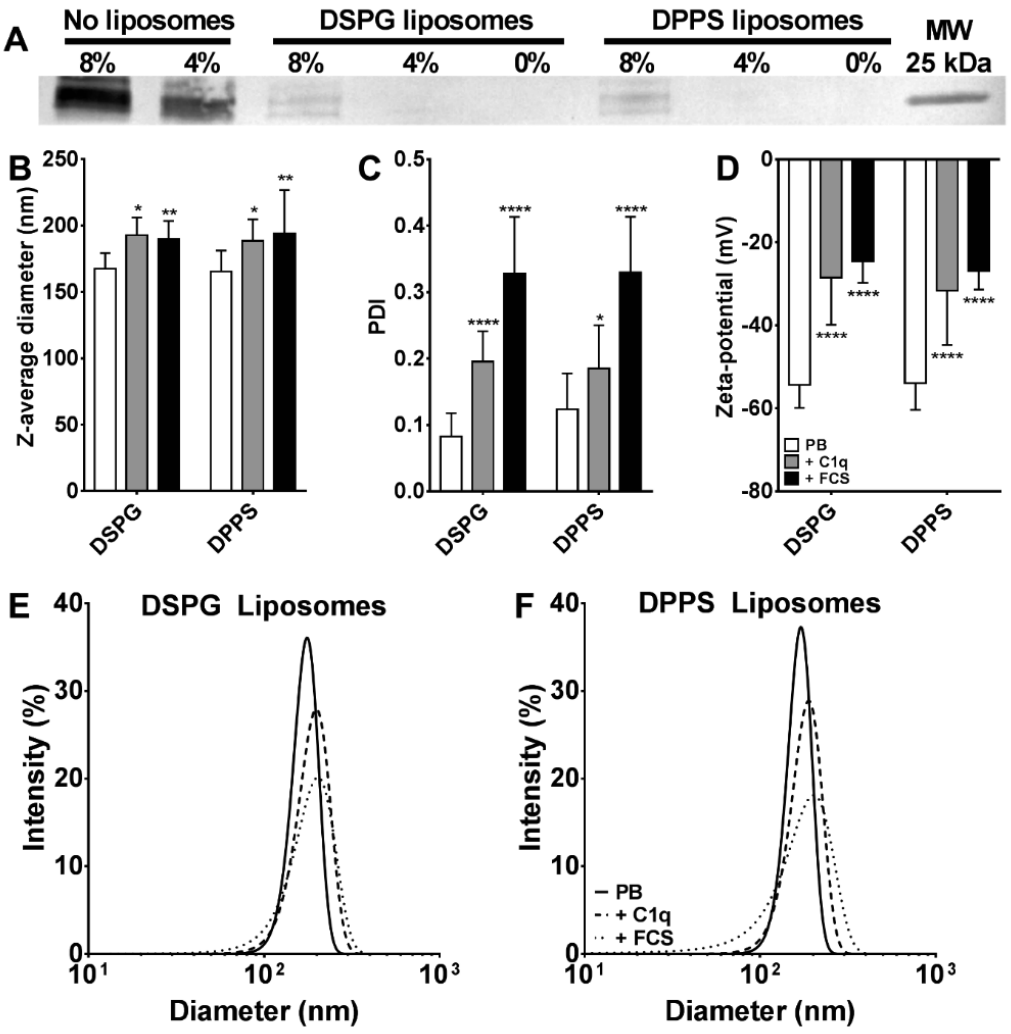


Figure 4: Binding of C1q and FCS components to DSPG- and DPPS-liposomes Liposomes were incubated with 8% or 4% FCS for 1 hour at 37°C and subsequently washed thoroughly to remove all unbound proteins, leaving only the protein corona. (A) WB of C1q after SDS-PAGE under reducing conditions. Percentages indicate the concentration (v/v) of FCS in PB. FCS in PB (no liposomes) was included as a control. Complete blot is shown in Figure S3. (B) Z-average diameter, (C) PDI, and (D) zeta-potential of samples in PB (white bars), with bound C1q (gray bars), or with bound FCS (black bars). (E and F) Representative Gaussian-smoothed intensity-weighted size distribution of DSPG- and DPPS-liposomes in PB (solid lines), with bound C1q (dashed lines) or with bound FCS (dotted lines). (F) Bar graphs show mean ± SD (n = 3) *p < 0.05, **p < 0.01, ****p < 0.0001, compared to PB, determined by two-way ANOVA and Bonferroni's multiple comparisons tests.

As C1q has been reported to mediate SR-mediated uptake, we evaluated the role of SR-mediated uptake of liposomes by BMDCs by measuring uptake of fluorescently labeled liposomes in the presence of poly I, a non-selective SR antagonist[59], in both medium containing 8% FCS or serum-free medium Blocking of SR-mediated uptake in the presence of serum reduced uptake of both DSPG- and DPPS-liposomes to the levels

of "- serum", indicating that SRs are responsible for the uptake of most of the liposomes by BMDCs under normal serum conditions (Figure 5). The addition of poly I did not alter the uptake of liposomes in serum-free conditions, suggesting that bare liposomes did not interact with SRs (Figure 5).

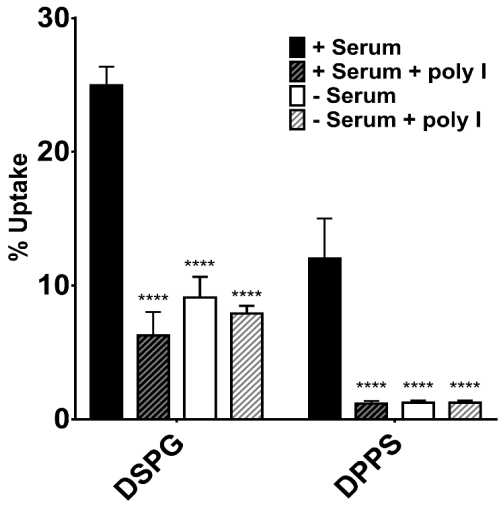


Figure 5: Effect of SR blocking on *in vitro* uptake of fluorescently labeled anionic liposomes encapsulating OVA323 by BMDCs. Percentage of DCs which have taken up fluorescently labeled OVA323-loaded DSPG- or DPPS-containing liposomes after 4 hours incubation, as measured by flow cytometry. Cells were incubated with liposomes in IMDM supplemented with FCS without SR blocking (black bars) or with SR blocking using 250 µg/mL poly I (black/gray bars), or in serum-free IMDM without poly I (white bars) or with poly I (white/gray bars). Graph shows mean ± SD (n = 3), ****p < 0.0001, compared to + serum within liposome group, determined by two-way ANOVA and Bonferroni's multiple comparisons tests.

DSPG-liposomes encapsulating an atherosclerosis-specific peptide significantly reduce plaque formation and increase plaque stability in atherosclerotic mice

Tolerance induction against atherosclerosis using peptides targeted against the main antigen in atherosclerosis, LDL, has yielded some success[23-28]. We hypothesized that encapsulation of an atherosclerosis-specific peptide in DSPG-liposomes would reduce atherosclerosis progression more efficiently than the free peptide, via induction of antigen-specific Tregs. The protein surrounding LDL, ApoB100, is a large protein (515 kDa in humans, 509 kDa in mice) containing several potential $CD4^+$ T cell epitopes. To identify a relevant ApoB100 peptide for immunization, we eluted MHC-II restricted peptides from BMDCs exposed to hypercholesterolemic serum. We identified several ApoB100-derived peptides using our peptidomics strategy (Table S1). Based on the predicted MHC-II binding (Table S2) we selected the peptide $ApoB100_{3500-3514}$ (p3500) and successfully loaded it into DSPG-liposomes (Table S4). $LDLr^{-/-}$ mice on a WTD were selected as a model for diet-induced atherosclerosis[12]. The mice were fed a WTD for 10 weeks, during which they were injected i.p. four times with PBS, 10 nmol of free p3500 or 10 nmol of p3500 encapsulated in DSPG-liposomes (DSPG/p3500-liposomes). Neutral lipid staining (Oil-Red-O) of the aortic valve area of the heart, which is used to quantify the lipid-rich atherosclerotic lesion, showed that treatment with p3500-loaded DSPG-

liposomes significantly reduced the lesion area by 50% (Figure 6A and B). As expected, all mice gained weight due to the WTD, but there were no differences between the groups (Figure 6C). Similarly, serum cholesterol levels were elevated in all groups because of the WTD. Interestingly, only the group of mice that received the liposomal treatment had significantly lower levels of serum cholesterol compared to the PBS control group (Figure 6D). The aortic sections were further stained for macrophage content, which is an indicator of immune activation[60]. Differences in macrophage content between the groups were not significant, although there was a trend towards lower macrophage content in the mice immunized with liposomes (Figure 6B and E), which could be (partially) responsible for the reduction in plaque size. Furthermore, there were significantly fewer $CD8^+$ T cells present in the aorta of mice injected with liposomes (Figure S7B). Levels of the inflammatory $CCR2^+Ly\text{-}6C^{hi}$ monocytes were unchanged in the blood of mice in all groups (Figure S8A), further indicating that there was no increased inflammation. Finally, the collagen content in the lesions was assessed, which is a measure of lesion stability[51]. Only the mice receiving liposomes had a higher collagen content in their lesions (Figure 6B and 6F), suggesting a more stable lesion. Total Treg levels were the same in all groups (Figure S8B). The finding that the DSPG/p3500 liposomes reduced serum cholesterol levels prompted a new atherosclerosis experiment to investigate the effect of empty DSPG liposomes. We found no differences in serum cholesterol, plaque size, or immune activation upon immunization with DSPG liposomes (Figure S9). Thus, the results suggest that DSPG/p3500-liposomes are able to reduce the growth of atherosclerotic lesions, lower serum cholesterol levels, and stabilize atherosclerotic plaques.

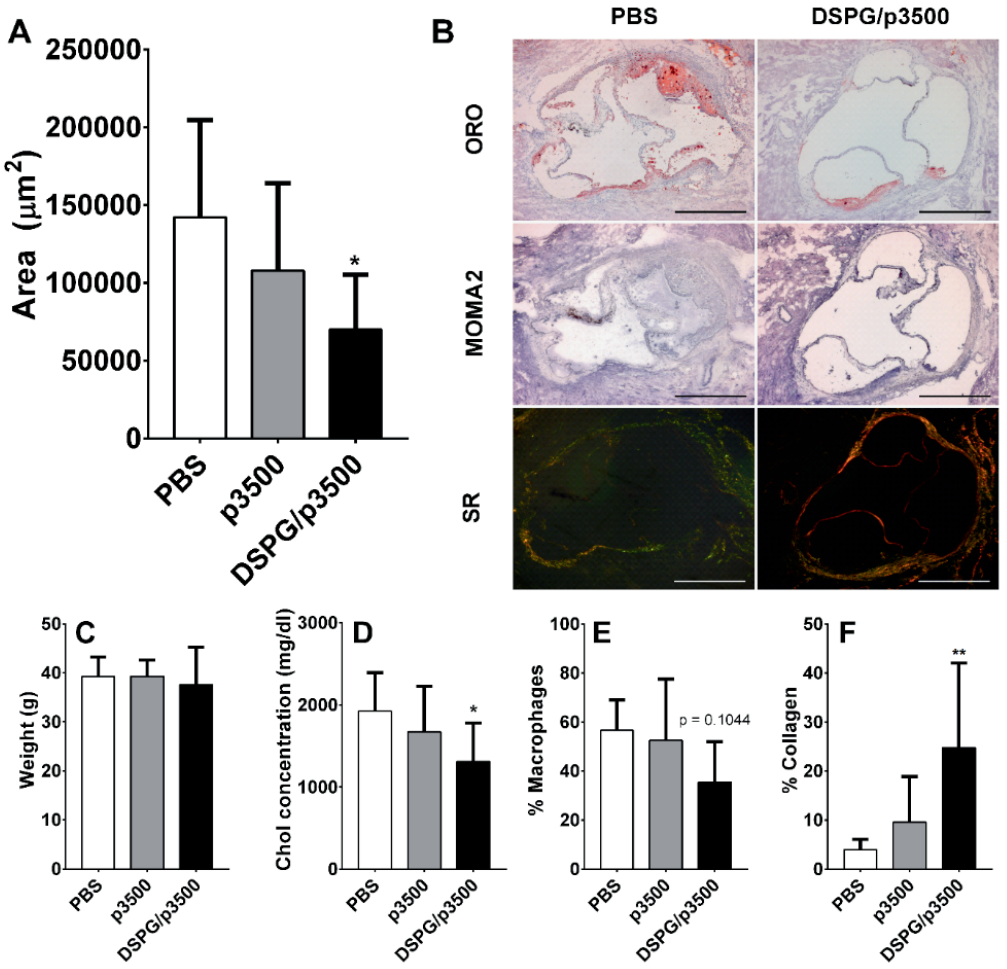


Figure 6: **Histological analysis of lesion formation in the aortic valve area of LDLr$^{-/-}$ mice.** LDLr$^{-/-}$ mice on a WTD were administered either with PBS, 10 nmol free p3500 or 10 nmol p3500 encapsulated in DSPG-liposomes via i.p. injection every 3 weeks for 10 weeks on a WTD. (A) Lesion area as determined by Oil-Red-O staining. (B) Representative images of sections of the aortic valve area in a mouse receiving PBS or DSPG/p3500-liposomes. Stainings shown are Oil-Red-O (ORO) and hematoxylin, monocyte/macrophage marker (MOMA2), and Sirius Red. In the Sirius Red staining, Type I collagen fibers are stained red, while Type III collagen fibers appear green. (C) The weight of mice at sacrifice. (D) Serum cholesterol levels of mice at sacrifice. (E) Percentage of macrophage area relative to total lesion area as determined by MOMA2 staining. (F) Percentage of collagen area relative to total lesion area as determined by Sirius Red staining. Graphs show mean ± SD (n = 9), *p < 0.05, **p < 0.01 determined by one-way ANOVA and Bonferroni's multiple comparisons tests.

Discussion & Conclusion

Atherosclerosis is the main underlying pathology for cardiovascular disease and is one of the leading causes of death worldwide[1]. While vaccination against atherosclerosis has been successful in murine models[23-28], a major challenge is the induction of antigen-specific Tregs in a safe and effective way. Here we introduce DSPG-liposomes as a peptide antigen carrier to induce regulatory T-cells and as a potential vaccine against atherosclerosis. Whereas DPTAP-liposomes can induce strong pro-inflammatory responses, we hypothesized that DSPG- and DPPS-liposomes lead to immune suppression because of their similarity to apoptotic cells. OVA323-containing liposomes were prepared with high-T_m lipids, since rigid liposomes have been shown to enhance APC uptake[61] and activation[62], and would, therefore, be more potent at inducing T cell responses compared to fluid-state liposomes. We show that all liposomes induced expansion of OVA323-specific T cells *in vivo*. The cationic liposomes induced pro-inflammatory cytokines, which we have also previously observed[42]. Only DSPG-containing liposomes induced significantly higher numbers of $CD25^+FOXP3^+CD4^+$ Tregs compared to free OVA323 in mice. This was surprising since PS-containing liposomes have been reported to induce antigen-specific Tregs in a type I diabetes model[36]. In accordance with our study, however, IL-10 and IL-4 responses were also unchanged in the diabetes model[36]. A head-to-head comparison of the effect of PS or PG liposomes complexed with Factor VIII (FVIII) *in vitro* showed that PS liposomes significantly reduced CD86 and CD40 expression, important co-activating molecules, in DCs as compared to free FVIII, while PG liposomes did not[63]. This supports our finding that DSPG liposomes have a higher potency to expand T cells. Unfortunately, T cell proliferation was only measured for PS liposomes, and Treg levels were not measured in the aforementioned study[63]. We show that DSPG-liposomes are more effectively taken up by BMDCs *in vitro* than DPPS-liposomes, which could explain their higher potency to induce Treg. Regardless, uptake of both liposomes was low (less than 30%), which has been observed previously, most likely due to unfavorable electrostatic interactions with the negatively charged cell surfac [64]. The mechanism of uptake could also be responsible for the potency of the DSPG-liposomes. *In vitro* and *in vivo*, liposomes interact with proteins in the physiological medium, resulting in the formation of a protein corona around the liposomes. Accordingly, we observed that proteins from serum attached to the liposomes and that the presence of serum was required for efficient uptake by BMDCs and subsequent Treg induction. This is in line with other studies that have shown the protein corona to be essential for the biological function of particles[65]. As mentioned above, several SRs could be responsible for anionic liposome uptake, and SR-mediated uptake may lead to immune suppression[66]. We found a significant reduction of uptake for both PG- and PS- liposomes in the presence of serum when SR-mediated uptake was blocked, which was not observed in serum-free conditions, suggesting that formation of a protein corona is required for SR interactions. PS-liposomes were entirely dependent on SR function for uptake, whereas PG-liposomes appear to have at least one additional mechanism of uptake, and could even interact directly with cells, as there was still uptake in serum-free conditions. There is evidence of binding of anionic lipids to apoptotic receptors[37,67-71]. We have so far excluded TIM4 as a receptor for PG- or PS-liposome uptake and Treg induction.

Since the serum protein C1q can bind to PS on apoptotic cells and lead to clearance

via SRs[54-56,72], we tested whether C1q present in the protein corona of the liposomes was responsible for SR-mediated uptake and Treg induction. C1q forms part of the C1 complex that is required for triggering of the classical complement pathway but can also regulate immunity[53,73]. Complement activation seems to be dependent on the structure of C1q; when it binds to IgG1, C1q has a different conformation than when it binds directly to PS exposed on the cell surface or liposomes[74]. Moreover, there is evidence of viruses binding C1q as a bridging molecule to evade the immune system and enhance infection[75-77]. C1q deficiency, either genetic[78] or via anti-C1q autoantibodies[72], can lead to symptoms almost identical to systemic lupus erythematosus (SLE). Several other autoimmune disorders have been associated with a dysregulation of the complement system and specifically C1q deficiencies, including atherosclerosis[79]. We show that C1q is present in the protein corona and binds to anionic liposomes. This is in accordance with other reports of C1q binding to PS-[70] and PG-containing liposomes[80]. The addition of C1q in serum-free conditions completely restored the uptake of both PG- and PS-liposomes. Furthermore, depletion of C1q significantly reduced uptake of PG-liposomes. Therefore, another explanation for the higher potency of DSPG-liposomes could be that they attract C1q from the circulation more efficiently than DPPS-liposomes. Since C1q cannot bind to free PS or PG[70], the density and repetitiveness of anionic head groups on liposomes may be an important parameter that affects C1q binding[81]. The molar ratios of the lipids used in this study were identical, so this would not affect binding of C1q. It has also been suggested that the electrostatic charge of the liposomes is an important parameter for binding[80,82], or that the chemical structure of the lipids is crucial[83]. In this work, the zeta-potential was the same for both liposomal formulations, leaving the structure of the lipids as the only differing factor.

Since there was a clear role for C1q in the uptake of the liposomes, we hypothesized that this may also influence Treg skewing. While we did observe that the addition of C1q increases Treg responses compared to serum-free conditions, this was not significant. Similarly, Clarke *et al.* showed that, while C1q tolerizes macrophages (increased PD-L1 and PD-L2, decreased CD40) and DCs (increased PD-L2 and decreased CD86), there was only a trend towards higher Treg responses[84]. This suggests that C1q is partially responsible for the Treg induction of both DSPG- and DPPS-liposomes, but the protein corona likely contains more components that help to induce Tregs.

Finally, we tested whether our most tolerogenic formulation was able to prevent disease progression in atherosclerosis. We immunized atherosclerotic mice with 10 nmol of our newly identified ApoB100-derived peptide (p3500), either free or encapsulated inside DSPG-liposomes. We observed a highly significant decrease in atherosclerotic lesion size of 50% only in the group that was immunized with the p3500 liposomes. Interestingly a previous study where ApoE$^{-/-}$ mice received a similar MHC-II restricted ApoB100-derived peptide ($ApoB100_{3501-3516}$) in complete Freund's adjuvant (CFA), and four booster injections in incomplete Freund's adjuvant (IFA) showed a comparable reduction in aortic plaque formation of 60%[23]. In addition, there were no changes in Treg populations upon this treatment[23], which is similar to our findings. In a more recent paper by the same group using a novel ApoB100-derived peptide and custom tetramers, antigen-specific Tregs were found[28]. This is in spite of that fact that CFA and IFA are not designed for tolerogenic responses; in fact, they generally elicit strong Th1 and Th2 responses[85]. This may explain why this previous study required a 3-fold higher peptide

dose to induce the same atheroprotective effect we report. Moreover, because of their high toxicity, use of CFA or IFA in humans is strongly discouraged[85]. Unfortunately, we were unable to measure p3500-specific Tregs in this atherosclerosis study, due to lack of specific tetramers.

We further observed a significant decrease in serum cholesterol levels in mice receiving DSPG/p3500 treatment. It has been shown that depletion of Tregs increased cholesterol levels in LDLr$^{-/-}$ mice[86], while *in vivo* Treg expansion in LDLr$^{-/-}$ mice reduced cholesterol levels[87], so this decrease in cholesterol levels could be caused by an increase in the number of antigen-specific Tregs. Finally, an increase in collagen content in the lesions of mice that received liposomes indicated more stable lesions. In accordance with this, treatment of ApoE$^{-/-}$ mice with Tregs decreased lesion size and lesion macrophage content while increasing lesion collagen content[88].

Collectively, these data show that we were able to induce high numbers of antigen-specific CD25^{+}FOXP3^{+}CD4^{+} Tregs in mice after a single injection of DSPG-containing liposomes. Furthermore, our peptidomics strategy was able to identify a novel ApoB100-derived peptide to be used for vaccination against atherosclerosis. We show that DSPG-liposomes, only when loaded with the ApoB100-derived peptide, significantly reduced lesion size, lowered serum cholesterol levels, and stabilized lesions in a murine model of atherosclerosis. Therefore, DSPG-liposomes can be a useful delivery vehicle for the induction of antigen-specific Tregs for the treatment of atherosclerosis and other autoimmune diseases.

Acknowledgments

We thank A. C. Foks, I. Bot, and R. Martins Cardoso for technical assistance during animal studies. We thank S. G. Romeijn and G. M. C. Janssen for assistance with analytical measurements.

References

1 Wang, H. *et al.* Global, regional, and national life expectancy, all-cause mortality, and cause-specific mortality for 249 causes of death, 1980–2015: a systematic analysis for the Global Burden of Disease Study 2015. *The Lancet* **388**, 1459-1544, doi:10.1016/s0140-6736(16)31012-1 (2016).

2 Pirillo, A., Norata, G. D. & Catapano, A. L. LOX-1, OxLDL, and atherosclerosis. *Mediators Inflamm* **2013**, 152786, doi:10.1155/2013/152786 (2013).

3 Libby, P. Inflammation in atherosclerosis. *Arterioscler Thromb Vasc Biol* **32**, 2045-2051, doi:10.1161/ATVBAHA.108.179705 (2012).

4 Tabas, I. & Lichtman, A. H. Monocyte-Macrophages and T Cells in Atherosclerosis. *Immunity* **47**, 621-634, doi:10.1016/j.immuni.2017.09.008 (2017).

5 Foks, A. C., Lichtman, A. H. & Kuiper, J. Treating atherosclerosis with regulatory T cells. *Arterioscler Thromb Vasc Biol* **35**, 280-287, doi:10.1161/ATVBAHA.114.303568 (2015).

6 Douna, H. & Kuiper, J. Novel B-cell subsets in atherosclerosis. *Curr Opin Lipidol* **27**, 493-498, doi:10.1097/MOL.0000000000000335 (2016).

7 Sakaguchi, S., Yamaguchi, T., Nomura, T. & Ono, M. Regulatory T cells and immune tolerance. *Cell* **133**, 775-787, doi:10.1016/j.cell.2008.05.009 (2008).

8 Mallat, Z., Ait-Oufella, H. & Tedgui, A. Regulatory T-cell immunity in atherosclerosis. *Trends Cardiovasc Med* **17**, 113-118, doi:10.1016/j.tcm.2007.03.001 (2007).

9 Keijzer, C., van der Zee, R., van Eden, W. & Broere, F. Treg inducing adjuvants for therapeutic vaccination against chronic inflammatory diseases. *Front Immunol* **4**, 245, doi:10.3389/fimmu.2013.00245 (2013).

10 Atkinson, M. A., Eisenbarth, G. S. & Michels, A. W. Type 1 diabetes. *Lancet* **383**, 69-82, doi:10.1016/S0140-6736(13)60591-7 (2014).

11 McFarland, H. F. & Martin, R. Multiple sclerosis: a complicated picture of autoimmunity. *Nat Immunol* **8**, 913-919, doi:10.1038/ni1507 (2007).

12 Hansson, G. K. & Hermansson, A. The immune system in atherosclerosis. *Nat Immunol* **12**, 204-212, doi:10.1038/ni.2001 (2011).

13 Coutinho, A. E. & Chapman, K. E. The anti-inflammatory and immunosuppressive effects of glucocorticoids, recent developments and mechanistic insights. *Mol Cell Endocrinol* **335**, 2-13, doi:10.1016/j.mce.2010.04.005 (2011).

14 Barr, T. A. *et al.* B cell depletion therapy ameliorates autoimmune disease through ablation of IL-6-producing B cells. *J Exp Med* **209**, 1001-1010, doi:10.1084/jem.20111675 (2012).

15 Chatenoud, L. & Bluestone, J. A. CD3-specific antibodies: a portal to the treatment of autoimmunity. *Nat Rev Immunol* **7**, 622-632, doi:10.1038/nri2134 (2007).

16 Shoji, T. *et al.* Inverse relationship between circulating oxidized low density lipoprotein (oxLDL) and anti-oxLDL antibody levels in healthy subjects. *Atherosclerosis* **148**, 171-177, doi:Doi 10.1016/S0021-9150(99)00218-X (2000).

17 Stemme, S. *et al.* T lymphocytes from human atherosclerotic plaques recognize oxidized low density lipoprotein. *Proc Natl Acad Sci U S A* **92**, 3893-3897, doi:10.1073/pnas.92.9.3893 (1995).

18 Fredrikson, G. N. *et al.* Identification of immune responses against aldehyde-

modified peptide sequences in apoB associated with cardiovascular disease. *Arterioscler Thromb Vasc Biol* **23**, 872-878, doi:10.1161/01.ATV.0000067935.02679.B0 (2003).

19 Sjogren, P. *et al.* High plasma concentrations of autoantibodies against native peptide 210 of apoB-100 are related to less coronary atherosclerosis and lower risk of myocardial infarction. *Eur Heart J* **29**, 2218-2226, doi:10.1093/eurheartj/ehn336 (2008).

20 Fagerberg, B., Prahl Gullberg, U., Alm, R., Nilsson, J. & Fredrikson, G. N. Circulating autoantibodies against the apolipoprotein B-100 peptides p45 and p210 in relation to the occurrence of carotid plaques in 64-year-old women. *PLoS One* **10**, e0120744, doi:10.1371/journal.pone.0120744 (2015).

21 Zhou, X., Caligiuri, G., Hamsten, A., Lefvert, A. K. & Hansson, G. K. LDL Immunization Induces T-Cell–Dependent Antibody Formation and Protection Against Atherosclerosis. *Arteriosclerosis, Thrombosis, and Vascular Biology* **21**, 108 (2001).

22 Schiopu, A. *et al.* Recombinant human antibodies against aldehyde-modified apolipoprotein B-100 peptide sequences inhibit atherosclerosis. *Circulation* **110**, 2047-2052, doi:10.1161/01.CIR.0000143162.56057.B5 (2004).

23 Tse, K. *et al.* Atheroprotective Vaccination with MHC-II Restricted Peptides from ApoB-100. *Front Immunol* **4**, 493, doi:10.3389/fimmu.2013.00493 (2013).

24 Klingenberg, R. *et al.* Intranasal immunization with an apolipoprotein B-100 fusion protein induces antigen-specific regulatory T cells and reduces atherosclerosis. *Arterioscler Thromb Vasc Biol* **30**, 946-952, doi:10.1161/ATVBAHA.109.202671 (2010).

25 Herbin, O. *et al.* Regulatory T-cell response to apolipoprotein B100-derived peptides reduces the development and progression of atherosclerosis in mice. *Arterioscler Thromb Vasc Biol* **32**, 605-612, doi:10.1161/ATVBAHA.111.242800 (2012).

26 Fredrikson, G. N. *et al.* Inhibition of atherosclerosis in apoE-null mice by immunization with apoB-100 peptide sequences. *Arterioscler Thromb Vasc Biol* **23**, 879-884, doi:10.1161/01.ATV.0000067937.93716.DB (2003).

27 Fredrikson, G. N., Bjorkbacka, H., Soderberg, I., Ljungcrantz, I. & Nilsson, J. Treatment with apo B peptide vaccines inhibits atherosclerosis in human apo B-100 transgenic mice without inducing an increase in peptide-specific antibodies. *J Intern Med* **264**, 563-570, doi:10.1111/j.1365-2796.2008.01995.x (2008).

28 Kimura, T. *et al.* Regulatory CD4(+) T Cells Recognize Major Histocompatibility Complex Class II Molecule-Restricted Peptide Epitopes of Apolipoprotein B. *Circulation* **138**, 1130-1143, doi:10.1161/CIRCULATIONAHA.117.031420 (2018).

29 van Puijvelde, G. H. *et al.* Induction of oral tolerance to oxidized low-density lipoprotein ameliorates atherosclerosis. *Circulation* **114**, 1968-1976, doi:10.1161/CIRCULATIONAHA.106.615609 (2006).

30 Frodermann, V. *et al.* Oxidized low-density lipoprotein-induced apoptotic dendritic cells as a novel therapy for atherosclerosis. *J Immunol* **194**, 2208-2218, doi:10.4049/jimmunol.1401843 (2015).

31 Hermansson, A. *et al.* Immunotherapy with tolerogenic apolipoprotein B-100-

loaded dendritic cells attenuates atherosclerosis in hypercholesterolemic mice. *Circulation* **123**, 1083-1091, doi:10.1161/CIRCULATIONAHA.110.973222 (2011).
32 Habets, K. L. *et al.* Vaccination using oxidized low-density lipoprotein-pulsed dendritic cells reduces atherosclerosis in LDL receptor-deficient mice. *Cardiovasc Res* **85**, 622-630, doi:10.1093/cvr/cvp338 (2010).
33 Raker, V. K., Domogalla, M. P. & Steinbrink, K. Tolerogenic Dendritic Cells for Regulatory T Cell Induction in Man. *Front Immunol* **6**, 569, doi:10.3389/fimmu.2015.00569 (2015).
34 Pattni, B. S., Chupin, V. V. & Torchilin, V. P. New Developments in Liposomal Drug Delivery. *Chem Rev* **115**, 10938-10966, doi:10.1021/acs.chemrev.5b00046 (2015).
35 Nagata, S., Hanayama, R. & Kawane, K. Autoimmunity and the clearance of dead cells. *Cell* **140**, 619-630, doi:10.1016/j.cell.2010.02.014 (2010).
36 Pujol-Autonell, I. *et al.* Use of autoantigen-loaded phosphatidylserine-liposomes to arrest autoimmunity in type 1 diabetes. *PLoS One* **10**, e0127057, doi:10.1371/journal.pone.0127057 (2015).
37 Ramos, G. C. *et al.* Apoptotic mimicry: phosphatidylserine liposomes reduce inflammation through activation of peroxisome proliferator-activated receptors (PPARs) in vivo. *Br J Pharmacol* **151**, 844-850, doi:10.1038/sj.bjp.0707302 (2007).
38 Hosseini, H. *et al.* Phosphatidylserine liposomes mimic apoptotic cells to attenuate atherosclerosis by expanding polyreactive IgM producing B1a lymphocytes. *Cardiovasc Res* **106**, 443-452, doi:10.1093/cvr/cvv037 (2015).
39 Varypataki, E. M., Benne, N., Bouwstra, J., Jiskoot, W. & Ossendorp, F. Efficient Eradication of Established Tumors in Mice with Cationic Liposome-Based Synthetic Long-Peptide Vaccines. *Cancer Immunol Res* **5**, 222-233, doi:10.1158/2326-6066.CIR-16-0283 (2017).
40 Barnier Quer, C., Elsharkawy, A., Romeijn, S., Kros, A. & Jiskoot, W. Cationic liposomes as adjuvants for influenza hemagglutinin: more than charge alone. *Eur J Pharm Biopharm* **81**, 294-302, doi:10.1016/j.ejpb.2012.03.013 (2012).
41 Hassan, C. *et al.* The human leukocyte antigen-presented ligandome of B lymphocytes. *Molecular & cellular proteomics : MCP* **12**, 1829-1843, doi:10.1074/mcp.M112.024810 (2013).
42 Varypataki, E. M., van der Maaden, K., Bouwstra, J., Ossendorp, F. & Jiskoot, W. Cationic liposomes loaded with a synthetic long peptide and poly(I:C): a defined adjuvanted vaccine for induction of antigen-specific T cell cytotoxicity. *AAPS J* **17**, 216-226, doi:10.1208/s12248-014-9686-4 (2015).
43 Mabrey, S. & Sturtevant, J. M. Investigation of phase transitions of lipids and lipid mixtures by sensitivity differential scanning calorimetry. *Proc Natl Acad Sci U S A* **73**, 3862-3866, doi:10.1073/pnas.73.11.3862 (1976).
44 Zhang, Y. P., Lewis, R. N. & McElhaney, R. N. Calorimetric and spectroscopic studies of the thermotropic phase behavior of the n-saturated 1,2-diacylphosphatidylglycerols. *Biophys J* **72**, 779-793, doi:10.1016/s0006-3495(97)78712-5 (1997).
45 Gaestel, M. *et al.* Lateral lipid distribution and phase transition in phosphatidylethanolamine/phosphatidylserine vesicles. A cross-linking study.

Biochim Biophys Acta **732**, 405-411, doi:10.1016/0005-2736(83)90057-3 (1983).
46 Regelin, A. E. *et al.* Biophysical and lipofection studies of DOTAP analogs. *Biochim Biophys Acta* **1464**, 151-164, doi:10.1016/s0005-2736(00)00126-7 (2000).
47 Weiss, A. C. G., Kempe, K., Forster, S. & Caruso, F. Microfluidic Examination of the "Hard" Biomolecular Corona Formed on Engineered Particles in Different Biological Milieu. *Biomacromolecules* **19**, 2580-2594, doi:10.1021/acs.biomac.8b00196 (2018).
48 Mehlem, A., Hagberg, C. E., Muhl, L., Eriksson, U. & Falkevall, A. Imaging of neutral lipids by oil red O for analyzing the metabolic status in health and disease. *Nat Protoc* **8**, 1149-1154, doi:10.1038/nprot.2013.055 (2013).
49 Kritikou, E. *et al.* Inhibition of lysophosphatidic acid receptors 1 and 3 attenuates atherosclerosis development in LDL-receptor deficient mice. *Sci Rep* **6**, 37585, doi:10.1038/srep37585 (2016).
50 Wezel, A. *et al.* Complement factor C5a induces atherosclerotic plaque disruptions. *J Cell Mol Med* **18**, 2020-2030, doi:10.1111/jcmm.12357 (2014).
51 Nadkarni, S. K. *et al.* Measurement of collagen and smooth muscle cell content in atherosclerotic plaques using polarization-sensitive optical coherence tomography. *J Am Coll Cardiol* **49**, 1474-1481, doi:10.1016/j.jacc.2006.11.040 (2007).
52 Lundqvist, M. *et al.* Nanoparticle size and surface properties determine the protein corona with possible implications for biological impacts. *Proc Natl Acad Sci U S A* **105**, 14265-14270, doi:10.1073/pnas.0805135105 (2008).
53 Merle, N. S., Church, S. E., Fremeaux-Bacchi, V. & Roumenina, L. T. Complement System Part I - Molecular Mechanisms of Activation and Regulation. *Front Immunol* **6**, 262, doi:10.3389/fimmu.2015.00262 (2015).
54 Erwig, L. P. & Henson, P. M. Clearance of apoptotic cells by phagocytes. *Cell Death Differ* **15**, 243-250, doi:10.1038/sj.cdd.4402184 (2008).
55 Patten, D. A. *et al.* SCARF-1 promotes adhesion of CD4(+) T cells to human hepatic sinusoidal endothelium under conditions of shear stress. *Sci Rep* **7**, 17600, doi:10.1038/s41598-017-17928-4 (2017).
56 Iram, T. *et al.* Megf10 Is a Receptor for C1Q That Mediates Clearance of Apoptotic Cells by Astrocytes. *J Neurosci* **36**, 5185-5192, doi:10.1523/JNEUROSCI.3850-15.2016 (2016).
57 Castellano, G. *et al.* Infiltrating dendritic cells contribute to local synthesis of C1q in murine and human lupus nephritis. *Mol Immunol* **47**, 2129-2137, doi:10.1016/j.molimm.2010.02.006 (2010).
58 Foks, A. C. *et al.* Blockade of Tim-1 and Tim-4 Enhances Atherosclerosis in Low-Density Lipoprotein Receptor-Deficient Mice. *Arterioscler Thromb Vasc Biol* **36**, 456-465, doi:10.1161/ATVBAHA.115.306860 (2016).
59 van Oosten, M., van Amersfoort, E. S., van Berkel, T. J. & Kuiper, J. Scavenger receptor-like receptors for the binding of lipopolysaccharide and lipoteichoic acid to liver endothelial and Kupffer cells. *J Endotoxin Res* **7**, 381-384, doi:10.1177/09680519010070050601 (2001).
60 Moore, K. J., Sheedy, F. J. & Fisher, E. A. Macrophages in atherosclerosis: a dynamic balance. *Nat Rev Immunol* **13**, 709-721, doi:10.1038/nri3520 (2013).
61 Anselmo, A. C. *et al.* Elasticity of nanoparticles influences their blood circulation,

phagocytosis, endocytosis, and targeting. *ACS Nano* **9**, 3169-3177, doi:10.1021/acsnano.5b00147 (2015).

62 Christensen, D. *et al.* A cationic vaccine adjuvant based on a saturated quaternary ammonium lipid have different in vivo distribution kinetics and display a distinct CD4 T cell-inducing capacity compared to its unsaturated analog. *J Control Release* **160**, 468-476, doi:10.1016/j.jconrel.2012.03.016 (2012).

63 Gaitonde, P., Peng, A., Straubinger, R. M., Bankert, R. B. & Balu-Iyer, S. V. Phosphatidylserine reduces immune response against human recombinant Factor VIII in Hemophilia A mice by regulation of dendritic cell function. *Clin Immunol* **138**, 135-145, doi:10.1016/j.clim.2010.10.006 (2011).

64 Foged, C. *et al.* Interaction of dendritic cells with antigen-containing liposomes: effect of bilayer composition. *Vaccine* **22**, 1903-1913, doi:10.1016/j.vaccine.2003.11.008 (2004).

65 Ritz, S. *et al.* Protein corona of nanoparticles: distinct proteins regulate the cellular uptake. *Biomacromolecules* **16**, 1311-1321, doi:10.1021/acs.biomac.5b00108 (2015).

66 Wang, D. *et al.* Role of scavenger receptors in dendritic cell function. *Hum Immunol* **76**, 442-446, doi:10.1016/j.humimm.2015.03.012 (2015).

67 Miyanishi, M. *et al.* Identification of Tim4 as a phosphatidylserine receptor. *Nature* **450**, 435-439, doi:10.1038/nature06307 (2007).

68 Kobayashi, N. *et al.* TIM-1 and TIM-4 glycoproteins bind phosphatidylserine and mediate uptake of apoptotic cells. *Immunity* **27**, 927-940, doi:10.1016/j.immuni.2007.11.011 (2007).

69 He, M. *et al.* Receptor for advanced glycation end products binds to phosphatidylserine and assists in the clearance of apoptotic cells. *EMBO Rep* **12**, 358-364, doi:10.1038/embor.2011.28 (2011).

70 Ramirez-Ortiz, Z. G. *et al.* The scavenger receptor SCARF1 mediates the clearance of apoptotic cells and prevents autoimmunity. *Nat Immunol* **14**, 917-926, doi:10.1038/ni.2670 (2013).

71 Choi, S. C. *et al.* Cutting edge: mouse CD300f (CMRF-35-like molecule-1) recognizes outer membrane-exposed phosphatidylserine and can promote phagocytosis. *J Immunol* **187**, 3483-3487, doi:10.4049/jimmunol.1101549 (2011).

72 Bigler, C., Schaller, M., Perahud, I., Osthoff, M. & Trendelenburg, M. Autoantibodies against complement C1q specifically target C1q bound on early apoptotic cells. *J Immunol* **183**, 3512-3521, doi:10.4049/jimmunol.0803573 (2009).

73 Son, M., Diamond, B. & Santiago-Schwarz, F. Fundamental role of C1q in autoimmunity and inflammation. *Immunol Res* **63**, 101-106, doi:10.1007/s12026-015-8705-6 (2015).

74 Ugurlar, D. *et al.* Structures of C1-IgG1 provide insights into how danger pattern recognition activates complement. *Science* **359**, 794-797, doi:10.1126/science.aao4988 (2018).

75 von Kietzell, K. *et al.* Antibody-mediated enhancement of parvovirus B19 uptake into endothelial cells mediated by a receptor for complement factor C1q. *J Virol* **88**, 8102-8115, doi:10.1128/JVI.00649-14 (2014).

76 Prohaszka, Z. *et al.* Two parallel routes of the complement-mediated

antibody-dependent enhancement of HIV-1 infection. *AIDS* **11**, 949-958, doi:10.1097/00002030-199708000-00002 (1997).

77 Takada, A., Feldmann, H., Ksiazek, T. G. & Kawaoka, Y. Antibody-dependent enhancement of Ebola virus infection. *J Virol* **77**, 7539-7544, doi:10.1128/jvi.77.13.7539-7544.2003 (2003).

78 Walport, M. J., Davies, K. A. & Botto, M. C1q and systemic lupus erythematosus. *Immunobiology* **199**, 265-285, doi:10.1016/S0171-2985(98)80032-6 (1998).

79 Bhatia, V. K. *et al.* Complement C1q reduces early atherosclerosis in low-density lipoprotein receptor-deficient mice. *Am J Pathol* **170**, 416-426, doi:10.2353/ajpath.2007.060406 (2007).

80 Bradley, A. J., Maurer-Spurej, E., Brooks, D. E. & Devine, D. V. Unusual electrostatic effects on binding of C1q to anionic liposomes: role of anionic phospholipid domains and their line tension. *Biochemistry* **38**, 8112-8123, doi:10.1021/bi990480a (1999).

81 Bachmann, M. F. & Jennings, G. T. Vaccine delivery: a matter of size, geometry, kinetics and molecular patterns. *Nat Rev Immunol* **10**, 787-796, doi:10.1038/nri2868 (2010).

82 Bradley, A. J., Brooks, D. E., Norris-Jones, R. & Devine, D. V. C1q binding to liposomes is surface charge dependent and is inhibited by peptides consisting of residues 14-26 of the human C1qA chain in a sequence independent manner. *Biochim Biophys Acta* **1418**, 19-30, doi:10.1016/s0005-2736(99)00013-9 (1999).

83 Sou, K. & Tsuchida, E. Electrostatic interactions and complement activation on the surface of phospholipid vesicle containing acidic lipids: effect of the structure of acidic groups. *Biochim Biophys Acta* **1778**, 1035-1041, doi:10.1016/j.bbamem.2008.01.006 (2008).

84 Clarke, E. V., Weist, B. M., Walsh, C. M. & Tenner, A. J. Complement protein C1q bound to apoptotic cells suppresses human macrophage and dendritic cell-mediated Th17 and Th1 T cell subset proliferation. *J Leukoc Biol* **97**, 147-160, doi:10.1189/jlb.3A0614-278R (2015).

85 Stills, H. F., Jr. Adjuvants and antibody production: dispelling the myths associated with Freund's complete and other adjuvants. *ILAR J* **46**, 280-293, doi:10.1093/ilar.46.3.280 (2005).

86 Klingenberg, R. *et al.* Depletion of FOXP3+ regulatory T cells promotes hypercholesterolemia and atherosclerosis. *J Clin Invest* **123**, 1323-1334, doi:10.1172/JCI63891 (2013).

87 Foks, A. C. *et al.* Differential effects of regulatory T cells on the initiation and regression of atherosclerosis. *Atherosclerosis* **218**, 53-60, doi:10.1016/j.atherosclerosis.2011.04.029 (2011).

88 Meng, X. *et al.* Regulatory T cells prevent plaque disruption in apolipoprotein E-knockout mice. *Int J Cardiol* **168**, 2684-2692, doi:10.1016/j.ijcard.2013.03.026 (2013).

Supplements

Table S1: Identification of relevant ApoB100 peptides for immunization by MHC-II restricted peptide elution from LDLr$^{-/-}$ serum exposed BMDC and detection by immunoprecipitation followed by peptide elution and detection by mass spectrometry.

Sequence	ApoB100
LSQEYSGSVANEAN	3500-3513
IVSHDYKGSTSHSLPY	1942-1952
HDYKGSTSHSLPY	1945-1952
VSHDYKGSTSHSLPY	1943-1957
IVSHDYKGSTSHSLPYE	1942-1958
VSHDYKGSTSHSLP	1943-1956

Table S2: Predicted binding of ApoB100 peptides identified and screened *in silico* (www.IEDB.org) for their ability to bind to MHC-II.

Peptide	Method	Percentile_Rank
LSQEYSGSVANEANV	Consensus (smm/nn)	0.23
FLSQEYSGSVANEAN	Consensus (smm/nn)	0.24
SFLSQEYSGSVANEA	Consensus (smm/nn)	0.26
SQEYSGSVANEANVY	Consensus (smm/nn)	0.62
QEYSGSVANEANVYL	Consensus (smm/nn)	0.64

Table S3: Physicochemical properties of liposomes composed of 4:1:2 molar ratio DSPC:charged lipid:chol with 0.5 mol% DSPC replaced with DPPE-Rho.

Charged lipid	Z_{ave} (nm)[a]	PDI	Zeta-potential (mV)	% LE[b]
DSPG	166.8 ± 0.5	0.07 ± 0.05	-55.9 ± 4.0	10.6 ± 3.9
DPPS	165.0 ± 4.1	0.06 ± 0.04	-51.4 ± 2.3	15.2 ± 5.0

[a] Mean ± SD (n = 6).

[b] %LE was calculated as the total amount of peptide before extrusion/total amount of peptide after purification * 100%

Table S4: Physicochemical properties of p3500-containing DSPG liposomes or empty DSPG liposomes composed of 4:1:2 molar ratio DSPC:DSPG:chol.

Z_{ave} (nm)[a]	PDI	Zeta-potential (mV)	% LE[b]
168.9 ± 2.1	0.04 ± 0.03	-55.9 ± 2.0	14.3 ± 4.2
164.5 ± 10.3	0.08 ± 0.02	-45.7 ± 5.9	-

[a] Mean ± SD (n = 6).

[b] %LE was calculated as the total amount of peptide before extrusion/total amount of peptide after purification * 100%

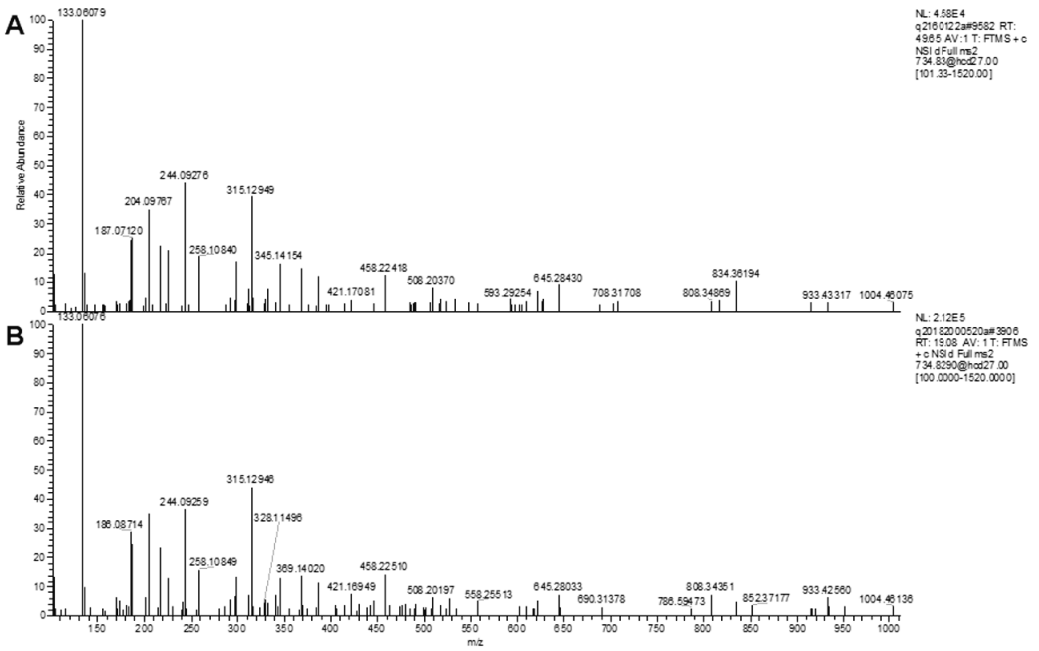


Figure S1: Matching of MS/MS spectrum eluted and synthesized ApoB100$_{3500\text{-}3513}$ peptide. (A) MS/MS spectrum of eluted ApoB100$_{3500\text{-}3513}$ peptide. (B) MS/MS spectrum of synthesized ApoB100$_{3500\text{-}3513}$ peptide.

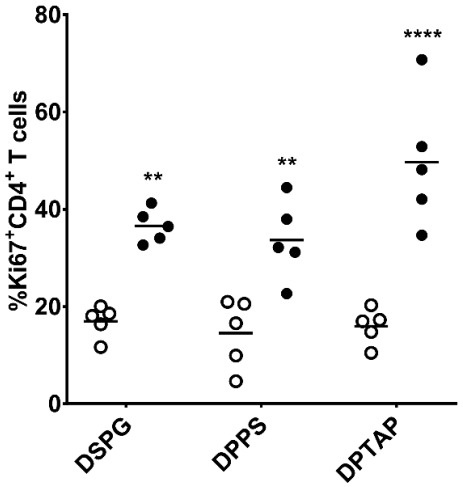


Figure S2: Proliferation of antigen-specific and total CD4$^+$ T cells in spleens of mice 8 days after i.v. injection of OVA323-containing liposomes. Ki67$^+$CD45.1$^-$CD4$^+$ (open circles) and Ki67$^+$CD45.1$^+$CD4$^+$ T cells (black circles) in spleens of WT mice after adoptive transfer of OT-II splenocytes and immunization with DSPG,- DPPS,- or DPTAP-liposomes containing OVA323 peptide detected by flow cytometry. ** $p < 0.01$, **** $p < 0.0001$ comparing CD45.1$^+$ to CD45.1$^-$ cells determined by two-way ANOVA and Bonferroni's multiple comparisons test.

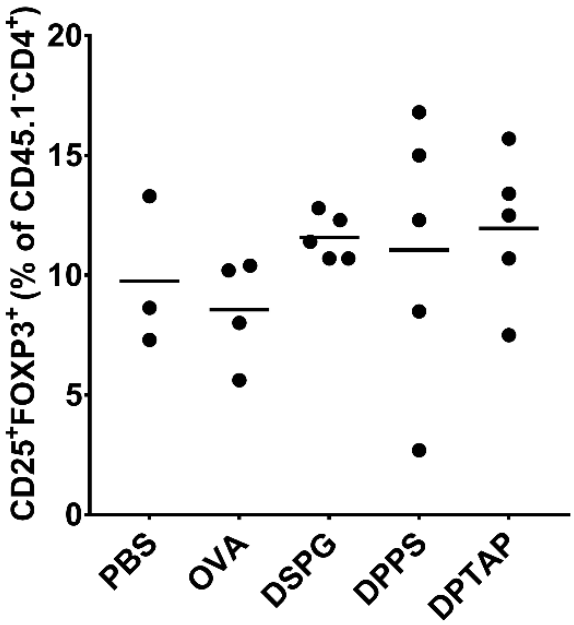


Figure S3: Total Treg percentage in iLNs of mice 8 days after i.v. injection of OVA323-containing liposomes. $CD45.1^{-}CD25^{+}FOXP3^{+}CD4^{+}$ T cells in iLNs of WT mice after immunization with PBS, free OVA323, or DSPG,- DPPS- or DPTAP-liposomes containing OVA323 peptide detected by flow cytometry. Graph shows mean, no significant differences between groups found by one-way ANOVA and Bonferroni's multiple comparisons tests. Representative results of 2 independent experiments.

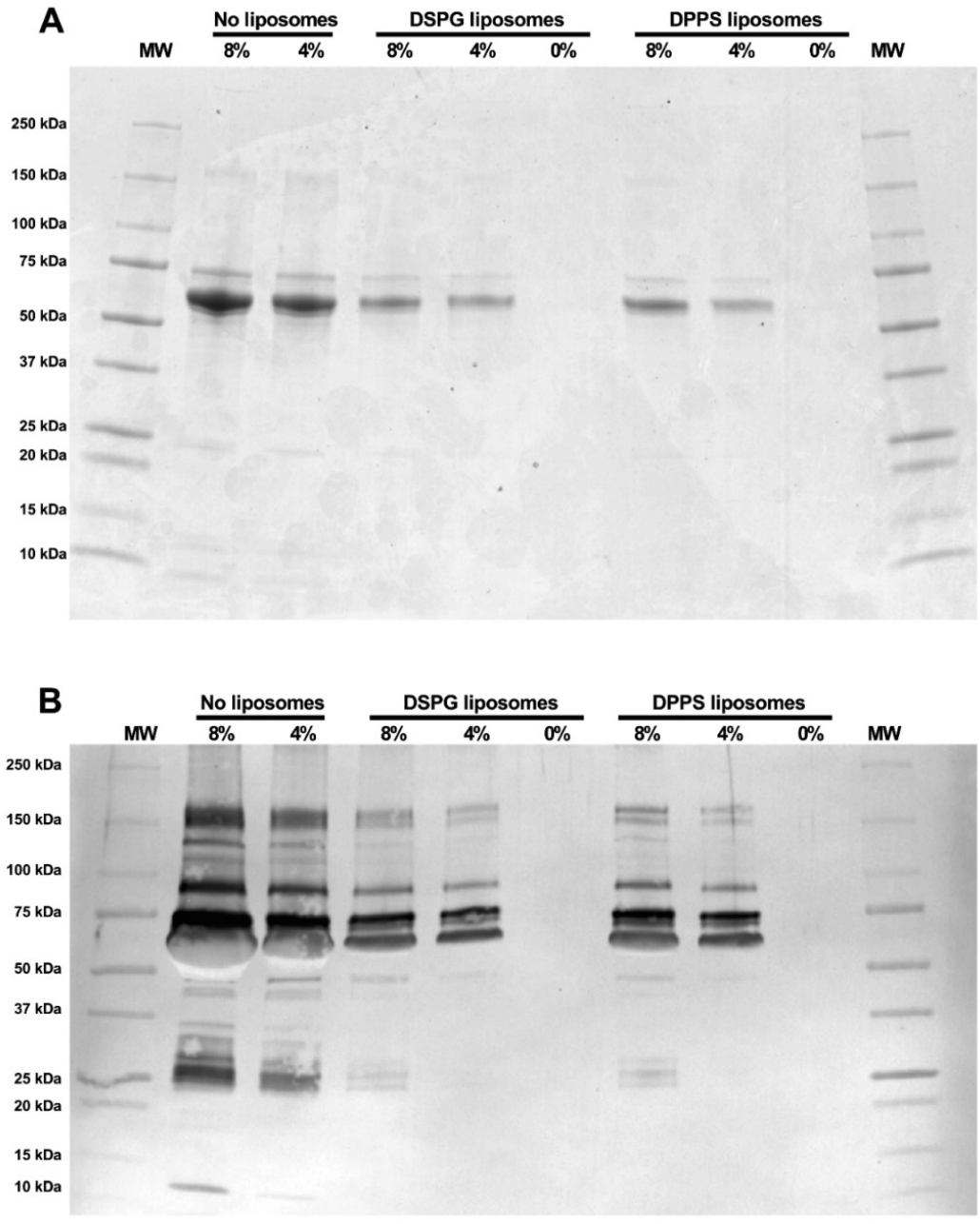


Figure S4: SDS-PAGE (reducing conditions) of protein corona formation on liposomes incubated with FCS and corresponding Western blot (WB) stained for C1q. To obtain a protein corona, liposomes were incubated with FCS/PB for 1 hour at 37°C and subsequently washed thoroughly with PB to remove all unbound proteins, leaving only the protein corona. FCS diluted in PB (not washed) was included as a control. (A) Coomassie Blue staining of SDS-PAGE gel, (B) WB for C1q (MW around 25 kDa). Percentages indicate the concentration (v/v) of FCS in PB.

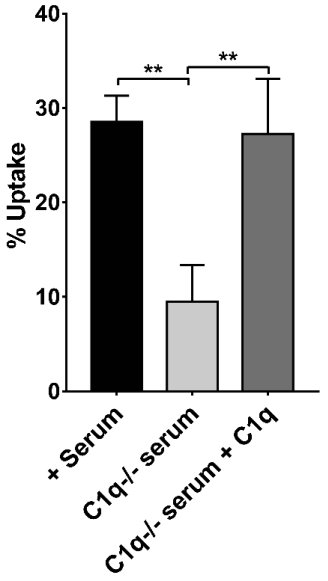


Figure S5: Effect of C1q depletion on *in vitro* uptake of DSPG-liposomes by BMDCs. (A) Percentage of DCs which have taken up fluorescently labeled OVA323-loaded DSPG-containing liposomes after 4 hours incubation, as measured by flow cytometry. Cells were incubated with liposomes either in normal human serum, C1q-depleted human serum, or C1q-depelted human serum supplemented with 10 µg/mL C1q. Graph shows mean ± SD (n = 3), ** $p < 0.01$ determined by one-way ANOVA and Bonferroni's multiple comparisons test.

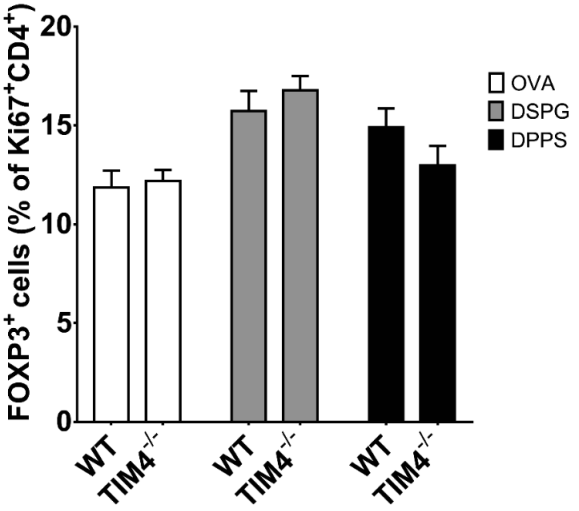


Figure S6: Effect of TIM4$^{-/-}$ on *in vitro* antigen-specific Treg induction by anionic liposomes encapsulating OVA323. FOXP3^{+}Ki67^{+}CD4^{+} T cells induced after 3 days co-culture with either WT BMDCs or TIM4$^{-/-}$ BMDCs. Graph shows mean ± SD (n = 3), no significant differences between WT and TIM4$^{-/-}$ found by two-way ANOVA and Bonferroni's multiple comparisons tests.

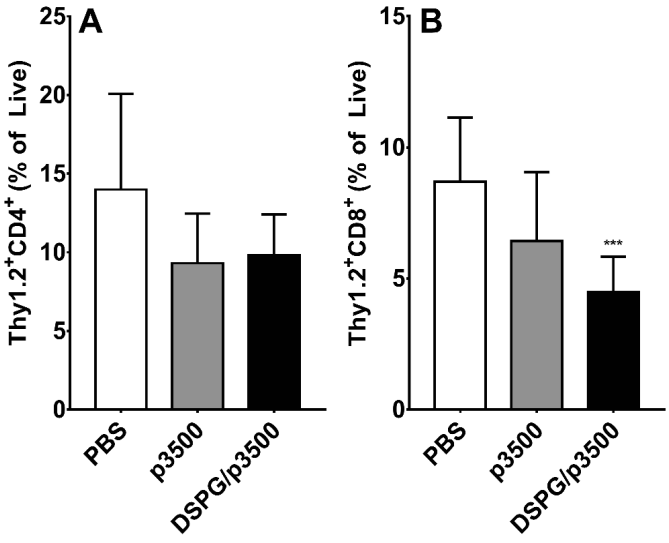


Figure S7: T cell populations in aortas of LDLr$^{-/-}$ mice immunized either with PBS, 10 nmol free p3500 or 10 nmol p3500 encapsulated in DSPG liposomes via i.p. injection every 3 weeks for 10 weeks while being fed a WTD. (A) Percentage of Thy1.2^{+}CD4^{+} T cells in the aortas of mice. (B) Percentage of Thy1.2^{+}CD8^{+} T cells in the aortas of mice. Graphs show mean ± SD (n = 9), *** p < 0.001 compared to PBS determined by one-way ANOVA and Bonferroni's multiple comparisons test.

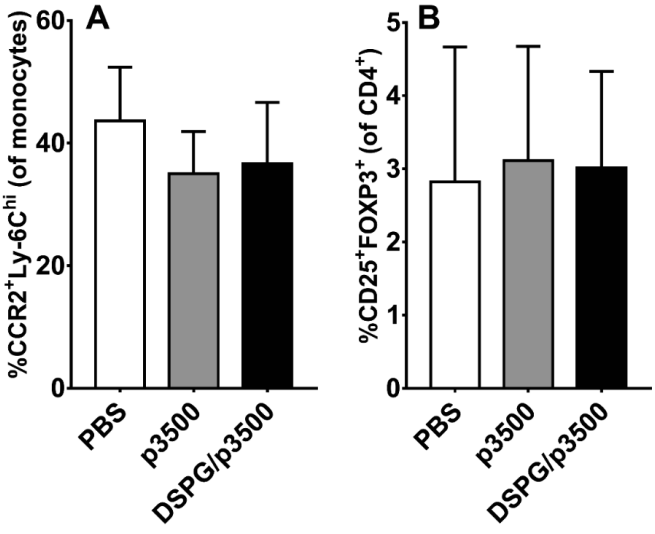


Figure S8: Leukocyte analysis in blood of LDLr$^{-/-}$ mice immunized either with PBS, 10 nmol free p3500 or 10 nmol p3500 encapsulated in DSPG liposomes via i.p. injection every 3 weeks for 10 weeks while being fed a WTD. (A) Percentage of CCR2^{+}Ly-6C^{hi} monocytes in the blood of mice. (B) Percentage of Tregs in the blood of mice. Graphs show mean ± SD (n = 9), no significant differences between groups found by one-way ANOVA and Bonferroni's multiple comparisons tests.

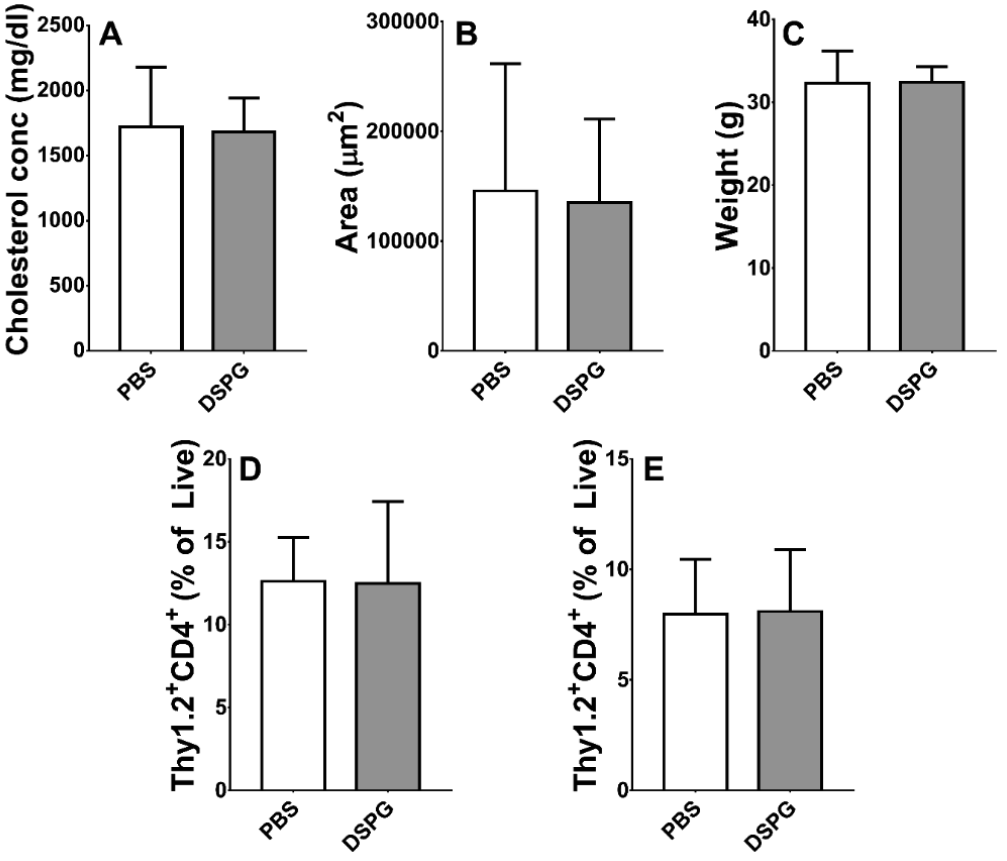


Figure S9: Analysis of atherosclerosis of LDLr$^{-/-}$ mice immunized either with PBS, or 0.5 mg DSPG liposomes via i.p. injection every 3 weeks for 10 weeks while being fed a WTD. (A) Serum cholesterol levels of mice at sacrifice. (B) Lesion area in the aortic valvee as determined by Oil-Red-O staining. (C) The weight of mice at sacrifice. (D) Percentage of Thy1.2^{+}CD4^{+} T cells in the aortas of mice. (E) Percentage of Thy1.2^{+}CD8^{+} T cells in the aortas of mice. Graphs show mean ± SD (n = 9), no significant differences between groups found by unpaired two-tailed t-test.

5

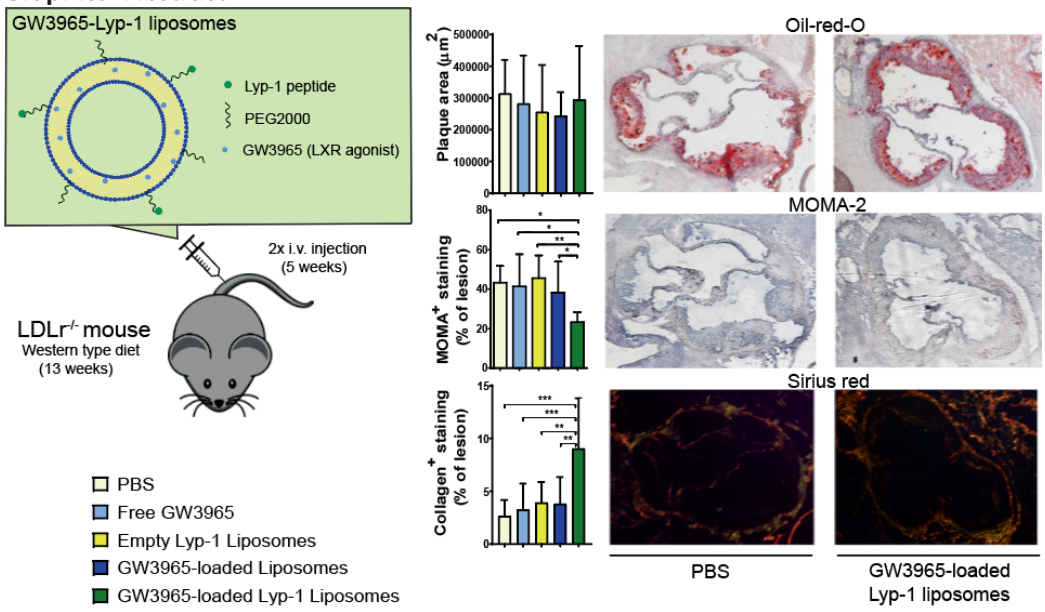
Complement Receptor Targeted Liposomes Encapsulating the Liver X Receptor Agonist GW3965 Accumulate in and Stabilize Atherosclerotic Plaques

Authors and affiliations
Naomi Benne*[1], Renata Martins Cardoso*[1], Aimee L. Boyle[2], Alexander Kros[2], Wim Jiskoot[1], Johan Kuiper[1], Joke Bouwstra[1], Miranda Van Eck[1], Bram Slütter[1]

*Both authors contributed equally
[1]Division BioTherapeutics, Leiden Academic Centre for Drug Research, Leiden University, the Netherlands
[2]Dept. Supramolecular & Biomaterials Chemistry, Leiden Institute of Chemistry, Leiden University, the Netherlands

Advanced Healthcare Materials, Volume 9, Issue 10, 24 April 2020.
doi: 10.1002/adhm.202000043

Graphical Abstract



Abstract

Atherosclerosis is the predominant underlying pathology of cardiovascular disease and is characterized by the retention of lipids, such as cholesterol, in macrophages (foam cells) in the intima of arteries. Liver X receptor agonists are promising compounds for treating atherosclerosis, since they induce reverse cholesterol transport in foam cells. However, LXR activation in the liver can lead to increased lipid levels. Therefore, in the present study we aimed to deliver LXR agonist GW3965 to atherosclerotic plaques by encapsulating it in liposomes. To increase the retention in atherosclerotic lesions, the liposomes were functionalized with the synthetic peptide Lyp-1 (CGNKRTRGC), which binds the p32 receptor on foam cells. Synthetic Lyp-1 was conjugated to DSPE-PEG2000-COOH and GW3965-containing (Lyp-1) liposomes (80 nm, PDI < 0.1, -20 mV) were prepared with nearly 100% encapsulation efficiency. Lyp-1 liposomes showed a 4-fold higher accumulation in foam cells compared to macrophages in vitro ($p < 0.05$). Moreover, in vivo targeting experiments showed significantly higher accumulation of Cy5-labeled Lyp-1 liposomes in atherosclerotic plaques compared to non-targeted liposomes, as shown by total (29-fold increase, $p < 0.01$) and relative radiant efficiency (25-fold increase, $p < 0.001$). Flow cytometric analysis demonstrated a 1.7-fold ($p < 0.05$) increase in the accumulation of Lyp-1 liposomes in atherosclerotic plaque macrophages as compared to controls. Finally, the effect of GW3965 loaded in Lyp-1 liposomes on atherosclerotic plaques was determined in low-density lipoprotein receptor knockout mice fed a western type diet for 13 weeks. Treatment with GW3965 loaded Lyp-1 liposomes twice a week for 5 weeks significantly reduced plaque macrophage content by nearly 50% ($p < 0.05$) and increased collagen content about 3-fold ($p < 0.01$) compared to PBS and free drug controls. Moreover, these changes in plaque stabilization were not accompanied by changes in plasma or hepatic lipid content. Thus, GW3965 loaded Lyp-1 liposomes successfully targeted the atherosclerotic plaque to allow plaque stabilization, in the absence of commonly observed side effects associated with the use of LXR agonists.

Introduction

Atherosclerosis is the predominant underlying pathology of cardiovascular disease and is one of the leading causes of death worldwide[1]. It is characterized by chronic inflammation in medium-and large-sized arteries caused by the subendothelial accumulation of oxidized low-density lipoprotein (oxLDL)[2].This attracts immune cells, such as monocytes, which upon differentiation into macrophages clear oxLDL via scavenger receptors and can transform into large lipid-laden foam cells[3]. These foam cells are unable to migrate out of the vessel wall, leading to a build-up at the site of inflammation and the formation of atherosclerotic plaques[4].

There is increasing evidence that the migratory capacity of foam cells out of atherosclerotic plaques can be restored after cholesterol efflux[5]. Therefore, a promising treatment strategy to reverse the formation of foam cells is to stimulate this process[6]. Lipid-laden macrophages can actively transport excess cholesterol across their membrane via the ATP-binding cassette (ABC) transporters ABCA1 and ABCG1.7 The liver X receptor (LXR) is a member of a family of nuclear transcription factors (LXRα; LXRβ) involved in the regulation of lipid homeostasis in response to altered sterol levels and controls the expression of both ABC transporters[7]. The deletion of these transcription factors in mice is associated with a remarkable increase in atherosclerotic lesions[8], implying therapeutic value of modulating LXR activity in atherosclerosis. A class of small molecules, called LXR agonists (e.g. GW3965[9]), can activate this receptor to subsequently increase the efflux of excess cholesterol from foam cells via the induction of ABCA1 and ABCG1, reducing the local lipid content and enabling subsequent clearance of these cells from the plaque[10]. Several studies have demonstrated the beneficial effects of LXR agonists on reducing atherosclerotic plaque burden[11], however, LXR expression is not restricted to macrophages. LXRα is abundantly present in the liver, intestine, adipose tissue, spleen, and kidney[12] and LXRβ is ubiquitously expressed, although at a lower level. Therefore, when administered systemically, LXR agonists may affect several organs[12]. Activation of LXRα in the liver leads to high triglyceride levels in the plasma and liver[13-15]. This unwanted effect of LXR agonism could be prevented by altering the biodistribution of the active compound, directing it away from the liver and increasing the effective dose at the target site; the atherosclerotic lesion. Encapsulation of active compounds in a drug delivery vehicle such as a nanoparticle is an effective strategy to alter their biodistribution[16]. In addition, conjugation of a targeting molecule to the drug delivery vehicle will direct the active compound to the required site of action[17]. Targeting to atherosclerotic plaques generally focuses on targeting to endothelial cells[18-22], clotted plasma proteins[23], or macrophages[24-26], by using HDL-like nanoparticles[27,28], or by passive targeting via sheer stress-mediated extravasation[29]. A common problem with many targeting strategies is lack of penetration into the plaque[22,23] or non-specificity[25,29]. The cyclic peptide Lyp-1 (CGNKRTRGC) has been identified as a valuable tool with a remarkable ability to penetrate into atherosclerotic plaques, making it superior for targeting macrophages in atherosclerotic plaques than other targeting peptides[30]. It binds to p32, also known as gC1q receptor, a receptor for the globular head domains of the complement component C1q. This receptor was originally found to be overexpressed on the cell surface of tumor cells[31] but is also expressed on foam cells in atherosclerotic plaques[32]. Nanoparticles coupled to Lyp-1 have been used for imaging of atherosclerotic plaques[33,34], but so far, no studies have been performed using Lyp-1-targeted nanoparticles as treatment against

atherosclerosis[35].

In this study, we aimed to design a particulate formulation combining the targeting properties of Lyp-1 with the therapeutic effect of an LXR agonist (GW3965) to promote cholesterol efflux from foam cells in atherosclerotic plaques to slow down atherosclerotic plaque development or reverse disease. We hypothesized that delivery of GW3965 with targeted liposomes will increase the retention of loaded particles in the atherosclerotic plaque, thereby reducing foam cell content in the plaque.

Materials and Methods

Materials and chemicals

Rat and mouse no.3 breeding chow diet and Western-type diet (WTD) contained 0.25% cholesterol and 15% cocoa butter were purchased from Special Diet Services, Essex, UK. 1,2-dioleoyl-sn-glycero-3-phosphocholine (DOPC), DOPC-cyanine 5 (DOPC-Cy5), 1,2-dioleoyl-sn-glycero-3-phospho-L-serine (DOPS), 1,2-distearoyl-sn-glycero-3-phosphoethanolamine-polyethylene glycol (DSPE-PEG2000), and DSPE-N-[carboxy(polyethylene glycol)-2000] (DSPE-PEG2000-COOH) were purchased from Avanti Polar Lipids (Alabaster, AL, USA). using O-(1H-6-chlorobenzotriazole-1-yl)-1,1,3,3-tetramethyluronium hexafluorophosphate (HCTU) and all amino acids used for synthesis were obtained from Novabiochem (Amsterdam, the Netherlands). N-N'-diisopropylethylamine (DIPEA) and Oxyma were purchased from Carl Roth (Karlsruhe, Germany). Dichloromethane (DCM) was obtained from Honeywell (Amsterdam, the Netherlands). Roswell Park Memorial Institute Medium (RPMI 1640), L-glutamine, and penicillin/streptomycin were purchased from Lonza (Basel, Switzerland). Fetal calf serum (FCS) was bought from PAA Laboratories (Ontario, Canada) and polycarbonate track-etched pore size membranes (400 nm, 200 nm and 50 nm pore size) were obtained from Whatman® NucleoporeTM, GE Healthcare (Little Chalfont, UK). 70-µm cell strainer and 96-well plates were purchased from Greiner Bio-One B.V. (Alphen aan den Rijn, the Netherlands). Monosodium phosphate (NaH2PO4), disodium phosphate (Na_2HPO_4), diethyl ether, triisopropylsilane, iodine, diisopropylcarbodiimide, GW3965, Oil-red-O, Sirius Red, hematoxylin, NonidetTM P 40 Substitute, chloroform, collagenase I, collagenase XI, DNase, and hyaluronidase were purchased from Sigma-Aldrich (Zwijndrecht, The Netherlands). Dulbecco's Modified Eagle Medium (DMEM) low glucose, non-essential amino acids, pyruvate, oxidized LDL, Pierce™ BCA Protein Assay Kit, were purchased from ThermoFisher (MA, USA). Sodium chloride (NaCl) was obtained from Boom (Meppel, The Netherlands). Trifluoroacetic acid (TFA), piperidine, dimethylformamide (DMF), potassium dihydrogen phosphate (KH_2PO_4), potassium chloride (KCl), methanol and acetonitrile were purchased from Biosolve (Valkenswaard, the Netherlands). Optimal cutting temperature formulation Tissue-Tek®O.C.T. TM was purchased from Sakura Finetek (Alphen aan den Rijn, The Netherlands). Cholesterol and triglycerides colorimetric assays were obtained from Roche Diagnostics (Almere, The Netherlands). Rat anti-mouse macrophages/monocytes antibody (MOMA2) was purchased from Bio-Rad (Veenendaal, the Netherlands). Ketamine and atropine were purchased from AUV Veterinary Services (Cuijk, the Netherlands) and xylazine from ASTFarma (Oudewater, the Netherlands). CD45-AlexaFluor700 (30-F11) was obtained from Biolegend (San Diego, CA, USA). F4/80-FITC (BM8), fixable viability dye eFluor780, and MHC-II-eFluor450 (AF6-120.1) were purchased from eBioscience (San Diego, CA, USA). All solvents used were of analytical grade.

Animals

Wild-type (WT) and LDL receptor knockout ($LDLr^{-/-}$) mice on a C57BL/6 background were purchased from Jackson Laboratory (CA, USA), bred in-house under standard laboratory conditions, and provided with food and water ad libitum. Information about the diet used for individual experiments is described in each section. The regular laboratory diet

(chow) was rat and mouse no.3 breeding diet. WTD contained 0.25 wt% cholesterol and 15 wt% cocoa butter. Animals had access to water and food ad libitum. All animal work was performed in compliance with the Dutch government guidelines and the Directive 2010/63/EU of the European Parliament. Experiments were approved by the Ethics Committee for Animal Experiments of Leiden University.

DSPE-PEG2000-Lyp-1 synthesis

The Lyp-1 peptide, GCGNKRTRGC with Cys residues protected by the non-acid-labile acetamidomethyl group, was synthesized using a Liberty Blue microwave-assisted peptide synthesizer. The synthesis was performed on a 0.1 mmol scale with a low-loading (0.18 mmol/g) tentagel R-RAM resin. Amino acid activation was achieved by using N,N'-diisopropylcarbodiimide as the activator and Oxyma as the base, while Fmoc-deprotection was achieved with 20% piperidine in DMF. Once the synthesis was complete, the resin was treated with 10 equivalents of iodine for one hour, to accommodate the concomitant deprotection and cyclization of the Cys residues. The resin was subsequently washed five times with DMF, five times with 2% acetic acid in DMF, five times with DMF and finally five times with DCM. The DSPE-PEG2000-COOH was manually coupled, on resin, to the N-terminus of an excess of the cyclized Lyp-1 by HCTU and DIPEA. The coupling reaction was left overnight, and the resin was subsequently washed with DMF and DCM. The DSPE-PEG2000-Lyp1 was cleaved from the resin by using a mixture of 97% TFA and 3% triisopropylsilane. The cleavage reaction was left to proceed for one hour, and the peptide was precipitated into ice-cold diethyl ether. The precipitate was collected by centrifugation. Levels of precipitate were low, likely due to the hydrophobic nature of the lipopeptide, therefore after centrifugation, the ether was separated from the precipitate and the ether was evaporated, leaving a white residue. This residue was combined with the original precipitate, dissolved in a mixture of acetonitrile and water, and dialyzed in a solution of 90% water and 10% acetonitrile to remove the excess uncoupled peptide and any scavengers or impurities that remained. The product was subsequently freeze-dried and analyzed using MALDI mass spectrometry to confirm the desired product had been formed.

Liposome preparation

Liposomes were prepared by using the thin film dehydration-rehydration method, as described previously[36]. Briefly, DOPC:DOPS:DSPE-PEG:DSPE-PEG-Lyp-1 in the molar ratio 76:19:4.3:0.7 were dissolved in chloroform and mixed in a round-bottom flask to obtain a final lipid concentration of 10 mg/mL. To this mixture, 2 mg of GW3965 was added. Chloroform was evaporated for 1 hour at 40°C in a rotary evaporator (Rotavapor R-210, Büchi, Switzerland). The lipid film was rehydrated with 1 mL Milli-Q water and homogenized by using glass beads and gentle swirling at room temperature (RT). The liposome dispersion was subsequently snap-frozen in liquid nitrogen, followed by freeze-drying overnight (Christ alpha 1–2 freeze-dryer, Osterode, Germany). The resulting dry lipid cake was gradually rehydrated at RT by using 10 mM phosphate buffer, pH 7.4 (PB); two volumes of 500 µL and one volume of 1000 µL PB were successively added, with intervals of 30 min between each addition. The mixture was vortexed well between each hydration step, and the resulting dispersion was kept at RT for at least 1 hour. To obtain monodisperse liposomes, the multilamellar vesicles were sized by high-pressure

extrusion at RT (LIPEX Extruder, Northern Lipids Inc., Canada). The liposome mixture was passed four times through stacked 400 nm and 200 nm polycarbonate track-etched pore size membranes and a further eight times through a 50 nm pore size membrane. To prepare fluorescently labeled liposomes, 0.1 mol% of DOPC was replaced with DOPC-Cy5. Liposomes were stored at 4°C and used for further experiments within 1 week.

Liposome characterization

The Z-average diameter and polydispersity index (PDI) of the liposomes were measured by dynamic light scattering (DLS) using a NanoZS Zetasizer (Malvern Ltd., Malvern, UK). Zeta-potential of the liposomes was determined by laser Doppler electrophoresis with the same instrument. Liposomes were diluted 100-fold in PB to a total volume of 1 mL prior to measuring. To determine the concentration of encapsulated GW3965 and Lyp-1, samples were analyzed by reversed-phase UPLC (Waters ACQUITY UPLC, Waters, MA, USA). 20 µL of the liposome dispersion was dissolved in 180 µL methanol. 10 µL of the sample was injected into a 1.7 µm BEH C18 column (2.1 x 50 mm, Waters ACQUITY UPLC, Waters, MA, USA). The column temperature and the temperature of the sample were set at 40°C and 4°C, respectively. The mobile phases were Milli-Q water with 0.1% TFA (solvent A) and acetonitrile with 0.1% TFA (solvent B). For detection, the mobile phases were applied in a linear gradient from 5% to 95% solvent B over 10.5 minutes at a flow rate of 0.370 mL/min. Lyp-1 was detected by absorbance at 220 nm using an ACQUITY UPLC TUV detector (Waters ACQUITY UPLC, Waters, MA, USA) and GW3965 was detected at 272 nm.

Bone marrow-derived macrophage (BMM) and foam cell culture

Bone marrow was isolated from the tibias and femurs of WT or LDLr$^{-/-}$ mice on a chow diet. The isolated bone marrow was passed through a 70-µm cell strainer. To differentiate the bone-marrow derived cells into macrophages, the cells were cultured in mixture of 60% complete RPMI medium (20% (v/v) FCS, 2 mM L-glutamine, 1 mM non-essential amino acids, 1 mM pyruvate, and 100 U/mL penicillin/streptavidin with 40% complete L929-conditioned DMEM low glucose medium (10% (v/v) FCS, 2 mM L-glutamine, and 100 U/mL penicillin/streptavidin) at 37˚C and 5% CO_2 for 7 days, as described previously[37]. The medium was refreshed every other day. To generate foam cells, macrophages were incubated with 75 µg/mL oxLDL for 30 hours.

Liposome association to BMMs and foam cells

BMMs and foam cells were cultured as described above. After 10 days of culture, 100,000 BMMs or foam cells were plated in 96-well plates and fluorescently labeled Lyp-1 liposomes or controls (PBS and fluorescently labeled non-targeted liposomes) were added at a concentration of 0.35 mg/mL Lyp-1 or an equivalent lipid dose. After 2 hours of incubation at 37˚C and 5% CO_2, excess liposomes were removed by washing the cells several times with medium. Cells were stained for F4/80 and viability dyes and were analyzed by flow cytometry (CytoFLEX S, Beckman Coulter, CA, USA). Data were analyzed by using FlowJo software (Treestar, OR, USA).

In vivo targeting to atherosclerotic plaques

Male LDLr$^{-/-}$ mice (6 to 10-week old) were fed WTD for 13 weeks to stimulate atherosclerotic lesion development. Subsequently, the mice were randomized into two groups (n = 10)

injected intravenously with either Cy5 fluorescently labeled non-targeting liposomes or Lyp-1 targeting liposomes (200 µL). The Lyp-1 concentration was 35 µg for Lyp-1 liposomes, and the equivalent lipid concentration was used for non-targeted liposomes. After 3 hours, the mice were anesthetized by using a mixture of ketamine (40 mg/mL), atropine (50 µg/mL), and sedazine (6.25 mg/mL) and perfused with PBS (8.13 g/L NaCl, 2.87 g/L Na_2HPO_4, 0.2 g/L KH_2PO_4, 0.19 g/L KCl, pH 7.4) via the left ventricle of the heart under physiological pressure after opening the thoracic cavity. After perfusion, the mice were imaged by using a fluorescence in vivo imaging system (IVIS, Perkin-Elmer IVIS Lumina Series III, Waltham, MA, USA) to provide information about the biodistribution of the liposomes. Afterward, spleen, lungs, liver, kidneys, hearts, and aortas were also imaged separately. Uptake by different organs was plotted as radiant efficiency and as relative radiant efficiency (%). To calculate relative radiant efficiency, the total sum of signals in organs was set to 100%, and the relative percentage per organ was calculated from this value. Aortas were further processed for flow cytometry analysis, as previously described 38. Briefly, aortas were cut into small pieces, incubated with 450 U/mL collagenase I, 250 U/mL collagenase XI, 120 U/mL DNase, and 120 U/mL hyaluronidase (30 min at 37°C under constant agitation), and strained through a 70-µm cell strainer to obtain a single-cell suspension. Cells were stained for CD45, F4/80, MHC-II, and viability and analyzed by flow cytometry.

Analysis of atherosclerosis in mice

Male $LDLr^{-/-}$ mice (6 to 10-week old) were fed WTD for 8 weeks to develop atherosclerotic lesions. Next, these mice were randomized into 5 groups (n = 10 mice) to receive intravenous injections twice a week (200 µL) of (1) PBS; (2) free GW3965; (3) empty Lyp-1 liposomes; (4) GW3965-loaded liposomes or (5) GW3965-loaded Lyp-1 liposomes. For GW3965-containing groups the dose was 6.5 mg/kg GW3965. The mice were treated for 5 weeks and continued to receive WTD during this time. After 5 weeks of treatment, the mice were anesthetized, exsanguinated and perfused, as described in the previous section. Hearts, livers, and blood were collected for further analysis. Hearts were embedded in OCT and stored at -80°C until further processing. Cryosections of the aortic root (10 µm, CM3050S cryostat, Leica, Rijswijk, the Netherlands) were collected. The sections were stained for Oil-Red-O to visualize lipid-rich plaques[39]. The largest Oil-red-O positive section of a sample and the two flanking sections were used to quantify the average plaque size. Macrophage positive area in the plaque was determined by using MOMA2 staining[40]. Macrophage positive area was calculated as the area positive for the MOMA2 staining divided by the total plaque area for the 3 largest consecutive sections. Collagen content in the plaques was measured by using Sirius Red staining[41]. Sections were visualized under polarized light[42] and the collagen content was determined by dividing the area positive for the Sirius Red staining by the total plaque area for the three largest consecutive sections. All stainings were imaged by using a Leica DM-RE microscope (Leica, Imaging Systems, UK) and analyzed using Leica QWin software.

Lipid quantification

Triglycerides were extracted from liver samples (± 50 mg tissue) homogenized with NonidetTM P 40 Substitute. To solubilize the triglycerides in the homogenate, the samples underwent two cycles of heat (90°C) and chill on ice. Subsequently, the homogenates

were centrifuged (14000 rpm) to remove insoluble material and triglycerides were measured by a colorimetric enzymatic assay[43]. The Folch method[44] was used to extract cholesterol from liver samples (ca. 50 mg tissue). Cholesterol was then quantified by using a colorimetric enzymatic assay[43]. Both triglyceride and cholesterol levels were corrected for total protein concentration. Protein concentration was determined with a Pierce™ BCA Protein Assay Kit according to the manufacturer's instructions. Non-fasted plasma levels of cholesterol and triglycerides were measured by enzymatic colorimetric assays, as previously described by Out et. al.[43]

Statistical analysis

Statistical analysis was performed by using GraphPad Prism 8 (GraphPad Software Inc., CA, USA). Data are presented as mean ± standard deviation (SD) and p values below 0.05 were considered significant. For comparison of multiple treatment groups, unpaired t-test, one-way ANOVA with Holm-Sidak post-test, or two-way ANOVA with Bonferroni's post-test were used, where appropriate.

Results

Characterization of Lyp-1 starting materials and liposomes

The coupling reaction of cyclic Lyp-1 to DSPE-PEG2000-COOH generating DSPE-PEG2000-Lyp-1 is schematically represented in Figure 1 and was confirmed by MALDI-MS (Supplementary Figure S1). All GW3965-loaded liposomes showed an encapsulation efficiency of this drug of nearly 100% (Table 1). The Z-average diameter of GW3965-loaded liposomes (ca. 75 nm) was slightly, but significantly ($p < 0.05$) smaller than that of empty liposomes (ca. 85 nm) (Table 1). The PDI was ca. 0.1 for all formulations, and the ζ-potential was about -20 mV (Table 1).

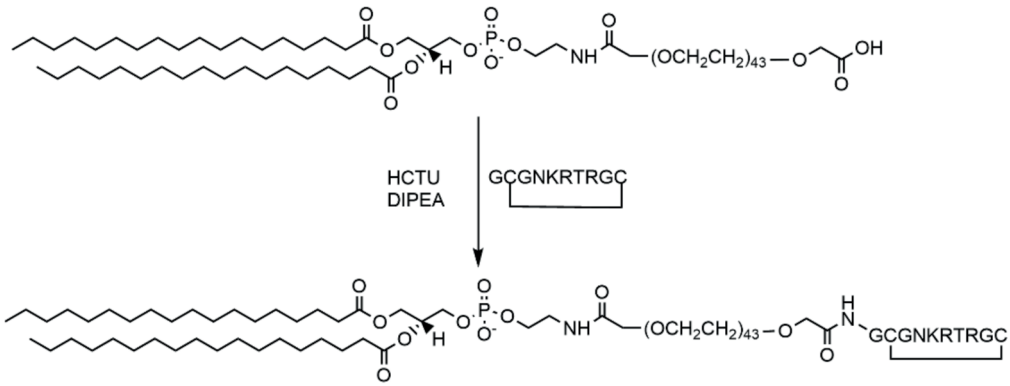


Figure 1. Synthesis of DSPE-PEG2000-Lyp-1. Schematic representation of the reaction coupling DSPE-PEG2000-COOH to cyclic peptide Lyp-1 to produce DSPE-PEG2000-Lyp-1.

Table 1: Physicochemical properties of liposomal formulations. Average particle diameter (Z_{ave}), PDI and ζ-potential were determined for all liposomal formulations. Encapsulation efficiency was calculated for liposomes loaded with GW3965 compound.

Formulation	Z_{ave} ± SD (nm)	PDI ± SD	ζ-potential ± SD (mV)	Encapsulation efficiency ± SD (%)
Empty Lyp-1 Liposomes	84.7 ± 3.9	0.09 ± 0.02	-19.3 ± 2.3	-
GW3965-loaded liposomes	73.8 ± 4.9*	0.10 ± 0.02	-19.7 ± 2.3	93.5 ± 19.9
GW3965-loaded Lyp-1 liposomes	77.5 ± 4.0*	0.09 ± 0.02	-19.5 ± 2.1	92.9 ± 22.5

*$p < 0.05$ compared to empty Lyp-1 liposomes

Lyp-1 liposomes preferentially associate with foam cells in vitro

To test the specific association of the liposomes to foam cells in vitro, fluorescently labeled liposomes were incubated with $LDLr^{-/-}$ mouse-derived non-differentiated BMMs (M0) and oxLDL-laden foam cells for 2 hours. Flow cytometric analysis showed that both non-targeted and targeted liposomes did not associate with M0 macrophages (Figure 2). Consistent with previous reports[22], foam cells showed enhanced association with both targeted and non-targeted liposomes. However, the interaction of Lyp-1 targeted liposomes was significantly increased as compared to not-targeted liposomes, marked by a higher fluorescent signal (Figure 2A and Figure 2B) and a nearly 4-fold increase in

the percentage of liposome positive foam cells ($p < 0.05$) (Figure 2C). Similar results (4-fold increase, $p < 0.01$) were observed for M0 macrophages and foam cells both derived from WT mice containing a functional LDL receptor (data not shown).

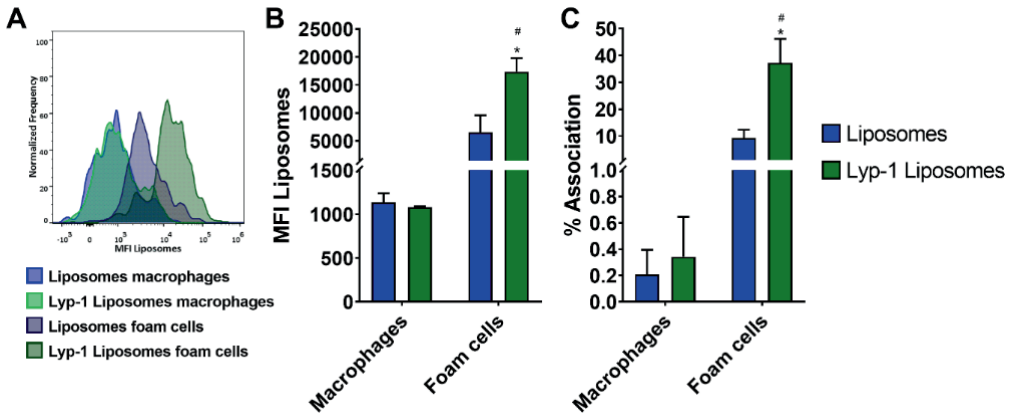


Figure 2. Preferential association of targeted Lyp-1 liposomes to foam cells in vitro. $LDLr^{-/-}$ M0 macrophages and oxLDL-laden foam cells were exposed to non-targeted liposomes or Lyp-1 liposomes labeled with DOPC-Cy5. After 2 hours of incubation, the liposomal association was determined by using flow cytometry. A) Representative MFI plots. Cell association was expressed as B) mean fluorescence intensity of the cells and C) percentage of cells positive for the fluorescent label. Graphs show means + SD of 3 independent experiments, *$p < 0.05$ comparing foam cells to M0 macrophages, #$p < 0.05$ comparing non-targeted to targeted liposomes, determined by two-way ANOVA and Bonferroni's post-test.

Lyp-1 liposomes are retained in plaque-residing foam cells of $LDLr^{-/-}$ mice

Next, we addressed the ability of the Lyp-1 liposomes to accumulate in foam cells residing in atherosclerotic plaques in vivo. $LDLr^{-/-}$ mice fed a WTD for 13 weeks were injected intravenously with fluorescently labeled Lyp-1 liposomes or non-targeted liposomes. After 3 hours, mice were anesthetized and perfused, and the biodistribution of liposomes was assessed using fluorescence imaging (see Figure 3A and 3B for representative aortas) and flow cytometry (see Figure 3C and 3D for representative plots). Lyp-1 liposomes showed a significantly higher accumulation in atherosclerotic plaques compared to non-targeted liposomes, as shown by the total radiant efficiency (29-fold increase, $p < 0.01$, Figure 3E) and the relative fluorescence signal (25-fold increase, $p < 0.001$, Figure 3F). Flow cytometric analysis confirmed a 1.7-fold ($p < 0.05$) increase in the accumulation of Lyp-1 targeted liposomes in atherosclerotic plaque foam cells as compared to non-targeted control liposomes (Figure 3G). In addition, to determine the organ distribution of the liposomes, the liver, kidneys, heart, spleen, and lungs were collected and separately imaged with IVIS. Most liposomes (both targeted and non-targeted) accumulated in the spleen, liver and kidneys, and a small amount was recovered from the lungs and hearts (Figure S2). $LDLr^{-/-}$ mice that received chow diet instead of WTD, and therefore did not develop atherosclerotic plaques, did not show any liposomal signal in aortas (data not shown).

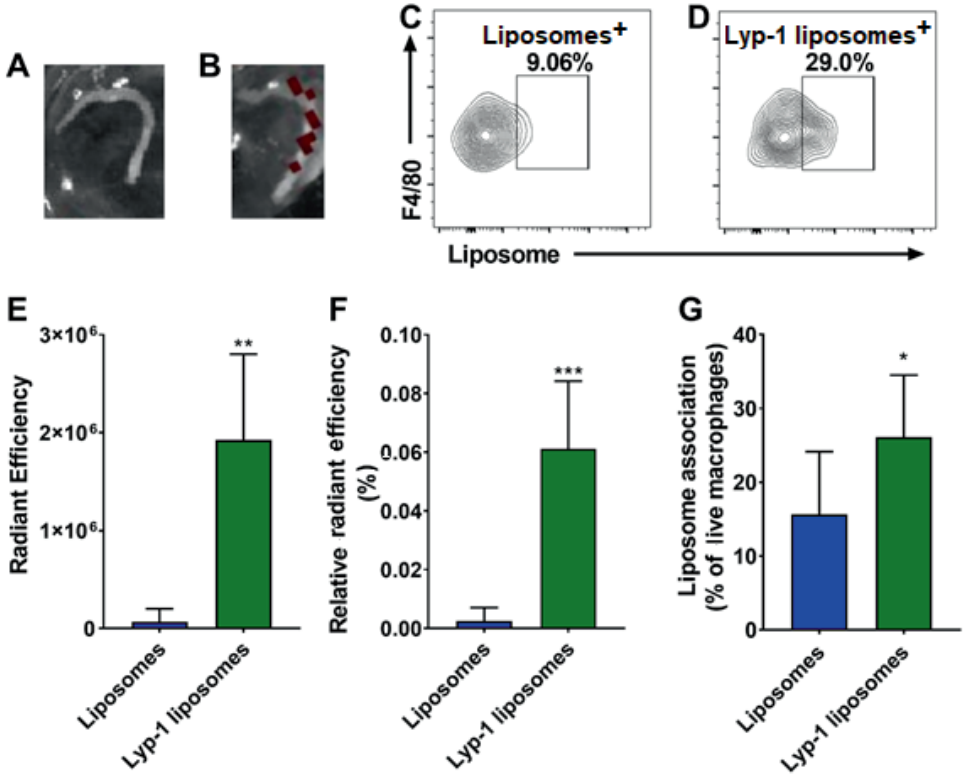


Figure 3. Association of fluorescently labeled non-targeted liposomes and Lyp-1 liposomes by plaque-residing foam cells in LDLr$^{-/-}$ mice fed WTD for 13 weeks. 3 hours after intravenous injection of liposomes, mice were perfused with PBS (pH 7.4 at RT). Representative IVIS images of descending aortas of mice that had received A) non-targeted and B) Lyp-1 liposomes. The dark brown signal indicates the presence of the Cy5 label. Representative FACS plots of pre-gated CD45^{+}MHC-II^{+}F4/80^{+} cells isolated from the aortic arch associated with C) non-targeted and D) Lyp-1 liposomes. E) Radiant efficiency of the fluorescent label in the descending aortas of mice measured by fluorescence imaging, n = 5. F) Aortic radiant efficiency as a percentage of all organs, n = 5. G) Liposomes detected in CD45^{+}MHC-II^{+}F4/80^{+} cells isolated from the aortic arch by flow cytometry, n = 8. Graphs show mean + SD, *p < 0.05, **p < 0.01, ***p < 0.001 determined by unpaired t-test.

Treatment with GW3965-loaded Lyp-1 liposomes significantly reduces the macrophage content and increases the collagen content of atherosclerotic plaques

After confirming efficient targeting of the Lyp-1 liposomes to atherosclerotic foam cells, the effect of Lyp-1 liposomal targeting of the LXR agonist GW3965 on pre-established atherosclerotic lesions was assessed. Male LDLr$^{-/-}$ mice were fed WTD for eight weeks. At this point, the average plaque size in the aortic root area was ca. 0.12 ± 0.07 mm^2, with lesion area comprising of 57.1 ± 15.2% macrophages, and 1.3 ± 1.1% collagen. Subsequently, the mice were injected intravenously twice a week with PBS, free GW3965, empty Lyp-1 liposomes, GW3965-loaded liposomes or GW3965-loaded Lyp-1 liposomes for 5 weeks, during which the WTD was maintained. Upon sacrifice, no differences were observed in atherosclerotic plaque size between any of the groups as determined in Oil-red-O stained sections of the aortic roots (Figure 4A and 4D). However,

the macrophage content, as measured with MOMA2 staining, was 2-fold ($p < 0.05$) lower in mice treated with Lyp-1 targeted GW3965-loaded liposomes compared to all other groups (Figure 4B and 4E). Previous studies have shown a positive correlation between the reduction in macrophage content and increase in collagen content in the plaque[45]. Indeed, we found that the percentage of collagen in the plaques was significantly increased (3-fold, $p < 0.01$) in mice treated with GW3965-loaded Lyp-1 liposomes as compared to all other groups (Figure 4C and 4F). Thus, foam cell delivery of GW3965 using Lyp-1 liposomes induced stabilization of established atherosclerotic plaques.

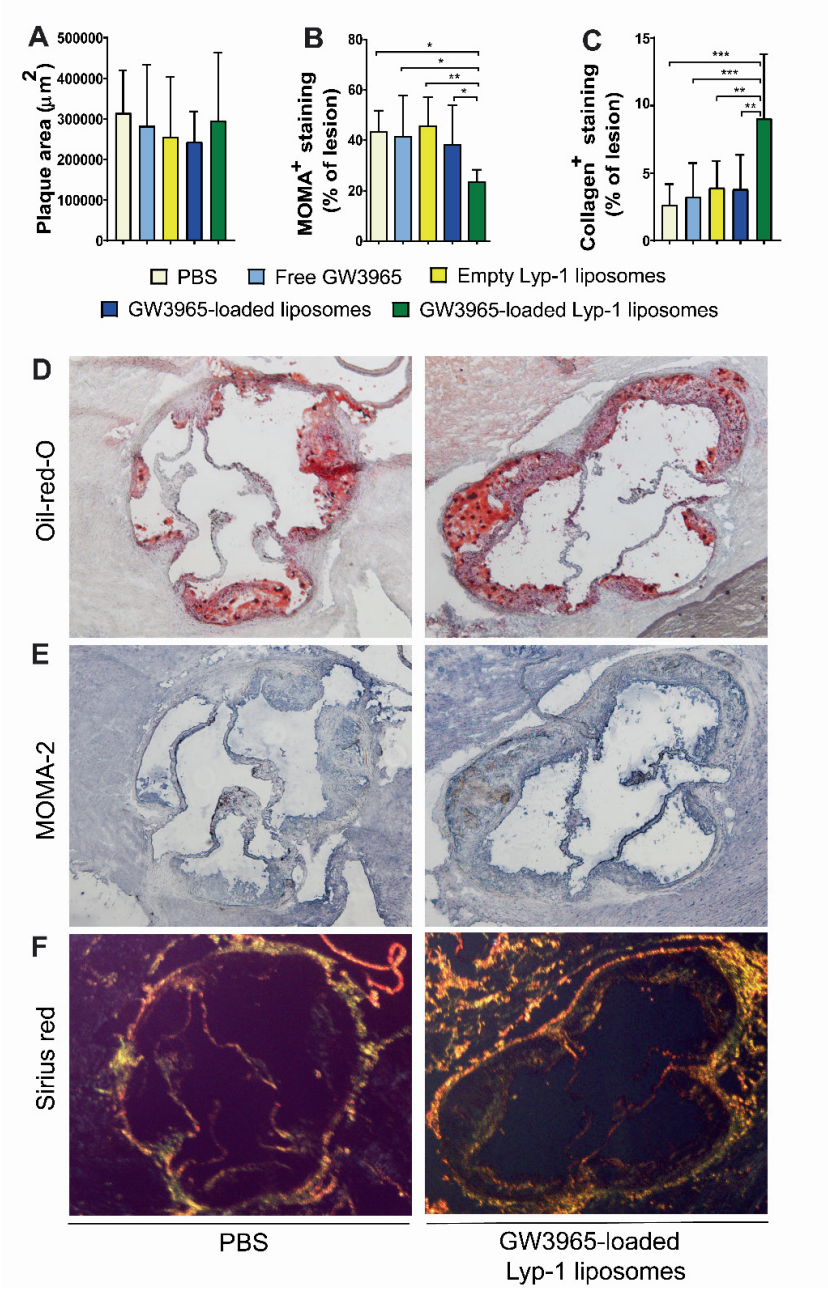


Figure 4. Effect of GW3965-loaded Lyp-1 targeted liposomes on plaque development in LDLr$^{-/-}$ mice. Mice were fed WTD for eight weeks before receiving intravenous injections of GW3965-loaded Lyp-1 liposomes or controls twice a week for five weeks while maintaining WTD. Upon sacrifice, hearts were collected and sectioned to reveal the aortic root area. Sections were stained for (A) Oil-Red-O to visualize lipids (B) MOMA2 to measure macrophage content, and (C) Sirius Red for collagen content, n = 10. Representative images of section stained for (D) Oil-red-O, (E) MOMA2 and (F) Sirius Red. Graphs show means + SD, *p < 0.05, **p < 0.01, ***p < 0.001 determined by one-way ANOVA with Holm-Sidak post-test.

Free or encapsulated GW3965 does not affect plasma and liver lipid content

Despite the positive effects of LXR activation on atherosclerosis, the use of LXR agonists, such as GW3965, has been described to alter hepatic lipid metabolism often leading to an increase in circulating triglycerides and liver steatosis[10]. Triglyceride and cholesterol content (in both plasma and liver) showed no differences between any of the groups (Figure 5), suggesting that the GW3965 treatment with Lyp-1-targeted liposomes can stabilize atherosclerotic plaques without the confounding effects on serum and liver lipid levels.

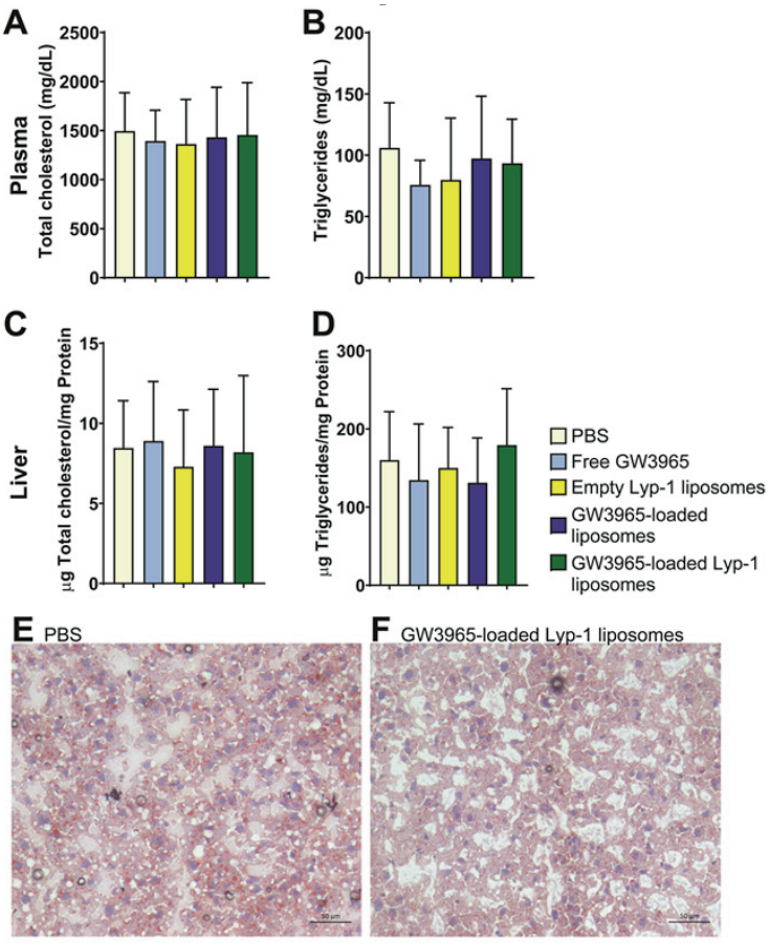


Figure 5. Effect of drug-loaded targeted liposomes and controls on lipid levels in plasma and liver of LDLr$^{-/-}$ mice on WTD. Mice received WTD for eight weeks before receiving intravenous injections of liposomes or controls twice a week for five weeks while maintaining WTD. Mice received the last injection 3 hours prior to sacrifice. Upon sacrifice, plasma and livers were collected for lipid analysis. (A) Total cholesterol and (B) triglyceride levels were measured in plasma. Livers were processed and total protein content in mg was determined. (C) Total cholesterol and (D) triglyceride levels were measured and normalized to protein content. (E) Representative image of Oil-Red-O stained liver of a mouse that received PBS, or (F) drug-loaded targeted liposomes, n = 10. Graphs show mean + SD, no significant differences found between groups were determined by one-way ANOVA with Holm-Sidak post-test.

Discussion

LXR agonists are promising compounds for the treatment of atherosclerosis, but at therapeutic doses, they increase plasma triglyceride and cholesterol levels[13-15]. In this study, we showed that loading of an LXR agonist, GW3965, in Lyp-1-bearing liposomes induces a highly relevant stabilization of pre-established atherosclerotic lesions, in contrast to free GW3965 or GW3965 encapsulated in non-targeted liposomes. This is hypothesized to be due to the migration of macrophages out of lesions after LXR-agonist-induced cholesterol efflux5. Liposomes consisting of DOPC:DOPS:DSPE-PEG:DSPE-PEG-Lyp-1 in a molar ratio of 76:19:4.3:0.7 were prepared to produce particles with fluid state membranes to improve the encapsulation of GW3965 and to prevent mononuclear phagocyte uptake upon injection into the circulation. Phosphatidylserine was added because of its anti-inflammatory properties[46-50] and reported ability to target foam cells[25]. Liposomes were PEGylated (5 mol%) to enhance their circulation time[51].

To minimize the undesired hepatic and metabolic effects, LXR agonists can be encapsulated into functionalized nanoparticles to target atherosclerotic plaques. Zhang et al. formulated GW3965 in PEGylated PLGA nanoparticles containing phosphatidylserine on the surface to target atherosclerotic foam cells. The targeted PLGA particles (10 mg/kg GW3965; administered iv 3 times per week for 2 weeks) reduced the macrophage content in the lesion compared to untreated control. However, this effect was not enhanced when compared to free drug or drug encapsulated in non-targeted liposomes and was accompanied by increased hepatic and plasma triglyceride and cholesterol levels[25]. In a different approach, Yu et al. encapsulated GW3965 in methoxy-PLA nanoparticles coated with 1,2-dilauroyl-sn-glycero-3-phosphocholine (DLPC):DSPE-PEG1000 functionalized with collagen-IV-targeting heptapeptide conjugated to DSPE-PEG2000 in the lipid layer. The GW3965-loaded collagen-targeting particles (8 mg/kg, administered intravenously 2 times per week for 5 weeks) significantly decreased the $CD68^+$ (macrophage) area in the lesion compared to free drug and non-targeted liposomes[18]. Neither of these previously described targeting approaches using collagen-IV and phosphatidylserine resulted in a reduction in total plaque size. Furthermore, the collagen content in the plaques, an important indicator of plaque stability, was not measured in these studies. It should be noted that, while in humans foam cells are mainly derived from macrophages[52], it has recently been discovered that foam cells can be derived from smooth muscle cells in the $ApoE^{-/-}$ mouse model[53]. Since the aforementioned studies and the study presented here are performed in $LDLr^{-/-}$ mice, it is unknown whether the therapeutic effect would be the same in $ApoE^{-/-}$ mice.

In this study, we made use of the interaction between the p32 receptor and Lyp-1 to target liposomes to foam cells in the plaque and deliver GW3965. Since the p32 receptor is not expressed on the surface of lipid-poor macrophages[31], the presence of Lyp-1 on the liposomal surface did not affect the in vitro association of the liposomes to undifferentiated macrophages but greatly and significantly enhanced their association to foam cells, confirming the selectivity of the targeting peptide. It should be noted that p32 has been found to be expressed in endothelial cells, foam cells, smooth muscle cells, and inflammatory cells present in the intima and media of human atherosclerotic lesions[32]. However, similarly to the Lyp-1 liposomes described here, heat shock protein cages functionalized with Lyp-1 designed by Uchida et al. showed accumulation in $Mac\text{-}3^+$ foam cells in murine ligation-induced atherosclerotic plaques[33]. Seo et al. also observed high

aortic lesion retention of Lyp-1 dendrimers 3 hours after intravenous injection in ApoE$^{-/-}$ mice[34]. Remarkably, in our study, the presence of Lyp-1 on the liposomal surface leads to enough particle retention in the aorta to allow a clear therapeutic effect of a relatively low dose of GW3965 (ca. 6.5 mg/kg/injection). For reference, the administration of a high dose of free GW3965 (10 mg/kg) orally for 12 weeks significantly reduced lesion size, but this effect was accompanied by higher serum triglycerides levels[14].

Administration of free or nanoparticle-encapsulated LXR agonist may not fully prevent unwanted effects in the plasma and in the liver[10]. In the present study, the high hepatic uptake of our GW3965-loaded Lyp-1 liposomes did not lead to the side effects typically associated with LXR agonists. Joseph et. al. showed that treatment with free GW3965 at a low dose (1 mg/kg for 12 weeks) did not result in plaque size reduction, hypertriglyceridemia or liver steatosis. The administration of a moderate dose of GW3965 (6.5 mg/kg in this study, vs 10 mg/kg by Zhang et. al.[25] and 8 mg/kg by Yu et. al.[18]) may have contributed to maintenance of hepatic and serum lipid homeostasis, as free GW3965 also did not induce these unwanted effects. The aforementioned studies along with our own study demonstrate that uptake of nanoparticles by cells in the liver is difficult to avoid, especially by Kupffer cells[54], but nanoparticles can still protect against the unwanted effects of the LXR agonist while increasing the efficiency of the drug at the site of action. Nevertheless, high hepatic particle uptake in the long-term, especially with higher doses should be avoided. Thus, other liposomal formulations or even other types of particles could be explored to reduce the undesired particle removal by the liver.

In conclusion, our work shows that functionalizing liposomes with Lyp-1 is an excellent strategy for targeting to atherosclerotic plaques. We are, to our knowledge, the first to combine this targeting approach with an LXR agonist, and we show that GW3965 loaded in targeted liposomes can reduce plaque macrophage content and increase plaque stability. These findings suggest that it is possible to increase the efficacy of this LXR agonist and may contribute to the development of better atherosclerosis therapies.

Acknowledgments
The authors thank P. J. van Santbrink, J. van Duijn, A. C. Foks, F. Lozano Vigario, R. J. T. Leboux, J. de Mol and I. Bot for their technical assistance during the animal studies.

References

1 Frostegård, J. Immunity, atherosclerosis and cardiovascular disease. BMC Med 11, 117-117, doi:10.1186/1741-7015-11-117 (2013).

2 Pirillo, A., Norata, G. D. & Catapano, A. L. LOX-1, OxLDL, and atherosclerosis. Mediators Inflamm 2013, 152786, doi:10.1155/2013/152786 (2013).

3 Chistiakov, D. A., Melnichenko, A. A., Myasoedova, V. A., Grechko, A. V. & Orekhov, A. N. Mechanisms of foam cell formation in atherosclerosis. J Mol Med (Berl) 95, 1153-1165, doi:10.1007/s00109-017-1575-8 (2017).

4 Tabas, I. Macrophage death and defective inflammation resolution in atherosclerosis. Nat Rev Immunol 10, 36-46, doi:10.1038/nri2675 (2010).

5 Luo, Y. et al. Macrophagic CD146 promotes foam cell formation and retention during atherosclerosis. Cell Research 27, 352-372, doi:10.1038/cr.2017.8 (2017).

6 Tall, A. R. Cholesterol efflux pathways and other potential mechanisms involved in the athero-protective effect of high density lipoproteins. Journal of Internal Medicine 263, 256-273, doi:10.1111/j.1365-2796.2007.01898.x (2008).

7 Venkateswaran, A. et al. Control of cellular cholesterol efflux by the nuclear oxysterol receptor LXR alpha. Proc Natl Acad Sci U S A 97, 12097-12102, doi:10.1073/pnas.200367697 (2000).

8 Bischoff, E. D. et al. Non-redundant roles for LXRα and LXRβ in atherosclerosis susceptibility in low density lipoprotein receptor knockout mice. Journal of Lipid Research 51, 900-906, doi:10.1194/jlr.M900096-JLR200 (2010).

9 Collins, J. L. et al. Identification of a Nonsteroidal Liver X Receptor Agonist through Parallel Array Synthesis of Tertiary Amines. Journal of Medicinal Chemistry 45, 1963-1966, doi:10.1021/jm0255116 (2002).

10 Kirchgessner, T. G. et al. Beneficial and Adverse Effects of an LXR Agonist on Human Lipid and Lipoprotein Metabolism and Circulating Neutrophils. Cell Metab 24, 223-233, doi:10.1016/j.cmet.2016.07.016 (2016).

11 Levin, N. et al. Macrophage liver X receptor is required for antiatherogenic activity of LXR agonists. Arteriosclerosis, thrombosis, and vascular biology 25, 135-142, doi:10.1161/01.Atv.0000150044.84012.68 (2005).

12 Wojcicka, G., Jamroz-Wisniewska, A., Horoszewicz, K. & Beltowski, J. Liver X receptors (LXRs). Part I: structure, function, regulation of activity, and role in lipid metabolism. Postepy higieny i medycyny doswiadczalnej (Online) 61, 736-759 (2007).

13 Joseph, S. B. et al. Direct and indirect mechanisms for regulation of fatty acid synthase gene expression by liver X receptors. The Journal of biological chemistry 277, 11019-11025, doi:10.1074/jbc.M111041200 (2002).

14 Joseph, S. B. et al. Synthetic LXR ligand inhibits the development of atherosclerosis in mice. Proc Natl Acad Sci U S A 99, 7604-7609, doi:10.1073/pnas.112059299 (2002).

15 Schultz, J. R. et al. Role of LXRs in control of lipogenesis. Genes & Development 14, 2831-2838, doi:10.1101/gad.850400 (2000).

16 Tibbitt, M. W., Dahlman, J. E. & Langer, R. Emerging Frontiers in Drug Delivery. J Am Chem Soc 138, 704-717, doi:10.1021/jacs.5b09974 (2016).

17 Accardo, A. & Morelli, G. Review peptide-targeted liposomes for selective

drug delivery: Advantages and problematic issues. Biopolymers 104, 462-479, doi:10.1002/bip.22678 (2015).
18 Yu, M. et al. Targeted Nanotherapeutics Encapsulating Liver X Receptor Agonist GW3965 Enhance Antiatherogenic Effects without Adverse Effects on Hepatic Lipid Metabolism in Ldlr-/- Mice. Adv Healthc Mater, doi:10.1002/adhm.201700313 (2017).
19 Kelly, K. A., Nahrendorf, M., Yu, A. M., Reynolds, F. & Weissleder, R. In Vivo Phage Display Selection Yields Atherosclerotic Plaque Targeted Peptides for Imaging. Molecular Imaging and Biology 8, 201, doi:10.1007/s11307-006-0043-6 (2006).
20 Park, K. et al. A new atherosclerotic lesion probe based on hydrophobically modified chitosan nanoparticles functionalized by the atherosclerotic plaque targeted peptides. Journal of Controlled Release 128, 217-223, doi:https://doi.org/10.1016/j.jconrel.2008.03.019 (2008).
21 Deosarkar, S. P. et al. Polymeric particles conjugated with a ligand to VCAM-1 exhibit selective, avid, and focal adhesion to sites of atherosclerosis. Biotechnol Bioeng 101, 400-407, doi:10.1002/bit.21885 (2008).
22 Namdee, K. et al. In vivo evaluation of vascular-targeted spheroidal microparticles for imaging and drug delivery application in atherosclerosis. Atherosclerosis 237, 279-286, doi:10.1016/j.atherosclerosis.2014.09.025 (2014).
23 Peters, D. et al. Targeting atherosclerosis by using modular, multifunctional micelles. Proc Natl Acad Sci U S A 106, 9815-9819, doi:10.1073/pnas.0903369106 (2009).
24 Cormode, D. P. et al. Nanocrystal Core High-Density Lipoproteins: A Multimodality Contrast Agent Platform. Nano Letters 8, 3715-3723, doi:10.1021/nl801958b (2008).
25 Zhang, X. Q. et al. Nanoparticles containing a liver X receptor agonist inhibit inflammation and atherosclerosis. Adv Healthc Mater 4, 228-236, doi:10.1002/adhm.201400337 (2015).
26 Zhaorigetu, S., Rodriguez-Aguayo, C., Sood, A. K., Lopez-Berestein, G. & Walton, B. L. Delivery of negatively charged liposomes into the atherosclerotic plaque of apolipoprotein E-deficient mouse aortic tissue. J Liposome Res 24, 182-190, doi :10.3109/08982104.2013.863208 (2014).
27 Binderup, T. et al. Imaging-assisted nanoimmunotherapy for atherosclerosis in multiple species. Science Translational Medicine 11, eaaw7736, doi:10.1126/scitranslmed.aaw7736 (2019).
28 Alaarg, A. et al. A systematic comparison of clinically viable nanomedicines targeting HMG-CoA reductase in inflammatory atherosclerosis. Journal of Controlled Release 262, 47-57, doi:https://doi.org/10.1016/j.jconrel.2017.07.013 (2017).
29 Lobatto, M. E. et al. Atherosclerotic Plaque Targeting Mechanism of Long-Circulating Nanoparticles Established by Multimodal Imaging. ACS Nano 9, 1837-1847, doi:10.1021/nn506750r (2015).
30 Hamzah, J. et al. Specific penetration and accumulation of a homing peptide within atherosclerotic plaques of apolipoprotein E-deficient mice. Proc Natl Acad Sci U S A 108, 7154-7159, doi:10.1073/pnas.1104540108 (2011).
31 Laakkonen, P., Porkka, K., Hoffman, J. A. & Ruoslahti, E. A tumor-homing peptide with a targeting specificity related to lymphatic vessels. Nat Med 8, 751-755,

doi:10.1038/nm720 (2002).
32 Peerschke, E. I. et al. Expression of gC1q-R/p33 and its major ligands in human atherosclerotic lesions. Mol Immunol 41, 759-766, doi:10.1016/j.molimm.2004.04.020 (2004).
33 Uchida, M. et al. Protein cage nanoparticles bearing the LyP-1 peptide for enhanced imaging of macrophage-rich vascular lesions. ACS Nano 5, 2493-2502, doi:10.1021/nn102863y (2011).
34 Seo, J. W. et al. (64)Cu-labeled LyP-1-dendrimer for PET-CT imaging of atherosclerotic plaque. Bioconjug Chem 25, 231-239, doi:10.1021/bc400347s (2014).
35 Song, N., Zhao, L., Zhu, M. & Zhao, J. Recent progress in LyP-1-based strategies for targeted imaging and therapy. Drug Deliv 26, 363-375, doi:10.1080/10717544.2019.1587047 (2019).
36 Benne, N. et al. Atomic force microscopy measurements of anionic liposomes reveal the effect of liposomal rigidity on antigen-specific regulatory T cell responses. Journal of Controlled Release, doi:https://doi.org/10.1016/j.jconrel.2019.12.003 (2019).
37 Marim, F. M., Silveira, T. N., Lima, D. S., Jr. & Zamboni, D. S. A Method for Generation of Bone Marrow-Derived Macrophages from Cryopreserved Mouse Bone Marrow Cells. PLOS ONE 5, e15263, doi:10.1371/journal.pone.0015263 (2010).
38 van Duijn, J. et al. $CD8^+$ T-cells contribute to lesion stabilization in advanced atherosclerosis by limiting macrophage content and $CD4^+$ T-cell responses. Cardiovascular Research 115, 729-738, doi:10.1093/cvr/cvy261 (2018).
39 Mehlem, A., Hagberg, C. E., Muhl, L., Eriksson, U. & Falkevall, A. Imaging of neutral lipids by oil red O for analyzing the metabolic status in health and disease. Nat Protoc 8, 1149-1154, doi:10.1038/nprot.2013.055 (2013).
40 Kritikou, E. et al. Inhibition of lysophosphatidic acid receptors 1 and 3 attenuates atherosclerosis development in LDL-receptor deficient mice. Sci Rep 6, 37585, doi:10.1038/srep37585 (2016).
41 Wezel, A. et al. Complement factor C5a induces atherosclerotic plaque disruptions. J Cell Mol Med 18, 2020-2030, doi:10.1111/jcmm.12357 (2014).
42 Nadkarni, S. K. et al. Measurement of collagen and smooth muscle cell content in atherosclerotic plaques using polarization-sensitive optical coherence tomography. J Am Coll Cardiol 49, 1474-1481, doi:10.1016/j.jacc.2006.11.040 (2007).
43 Out, R. et al. Macrophage ABCG1 Deletion Disrupts Lipid Homeostasis in Alveolar Macrophages and Moderately Influences Atherosclerotic Lesion Development in LDL Receptor-Deficient Mice. Arteriosclerosis, thrombosis, and vascular biology 26, 2295-2300, doi:10.1161/01.ATV.0000237629.29842.4c (2006).
44 Folch, J., Lees, M. & Sloane Stanley, G. H. A simple method for the isolation and purification of total lipides from animal tissues. The Journal of biological chemistry 226, 497-509 (1957).
45 Dickhout, J. G., Basseri, S. & Austin, R. C. Macrophage Function and Its Impact on Atherosclerotic Lesion Composition, Progression, and Stability. Arteriosclerosis, thrombosis, and vascular biology 28, 1413-1415, doi:doi:10.1161/

ATVBAHA.108.169144 (2008).
46 Rodriguez-Fernandez, S. et al. Phosphatidylserine-Liposomes Promote Tolerogenic Features on Dendritic Cells in Human Type 1 Diabetes by Apoptotic Mimicry. Front Immunol 9, 253, doi:10.3389/fimmu.2018.00253 (2018).
47 Krishna, S. M. et al. Anionic nanoliposomes reduced atherosclerosis progression in Low Density Lipoprotein Receptor (LDLR) deficient mice fed a high fat diet. J Cell Physiol, doi:10.1002/jcp.26610 (2018).
48 Hosseini, H. et al. Phosphatidylserine liposomes mimic apoptotic cells to attenuate atherosclerosis by expanding polyreactive IgM producing B1a lymphocytes. Cardiovasc Res 106, 443-452, doi:10.1093/cvr/cvv037 (2015).
49 Benne, N. et al. Anionic 1,2-distearoyl-sn-glycero-3-phosphoglycerol (DSPG) liposomes induce antigen-specific regulatory T cells and prevent atherosclerosis in mice. J Control Release 291, 135-146, doi:10.1016/j.jconrel.2018.10.028 (2018).
50 Pujol-Autonell, I. et al. Use of autoantigen-loaded phosphatidylserine-liposomes to arrest autoimmunity in type 1 diabetes. PLoS One 10, e0127057, doi:10.1371/journal.pone.0127057 (2015).
51 Abuchowski, A., McCoy, J. R., Palczuk, N. C., van Es, T. & Davis, F. F. Effect of covalent attachment of polyethylene glycol on immunogenicity and circulating life of bovine liver catalase. The Journal of biological chemistry 252, 3582-3586 (1977).
52 Fernandez, D. M. et al. Single-cell immune landscape of human atherosclerotic plaques. Nature Medicine 25, 1576-1588, doi:10.1038/s41591-019-0590-4 (2019).
53 Wang, Y. et al. Smooth Muscle Cells Contribute the Majority of Foam Cells in ApoE (Apolipoprotein E)-Deficient Mouse Atherosclerosis. Arteriosclerosis, thrombosis, and vascular biology 39, 876-887, doi:10.1161/atvbaha.119.312434 (2019).
54 Bieghs, V. et al. Internalization of modified lipids by CD36 and SR-A leads to hepatic inflammation and lysosomal cholesterol storage in Kupffer cells. PLoS One 7, e34378, doi:10.1371/journal.pone.0034378 (2012).

Supplementary figures

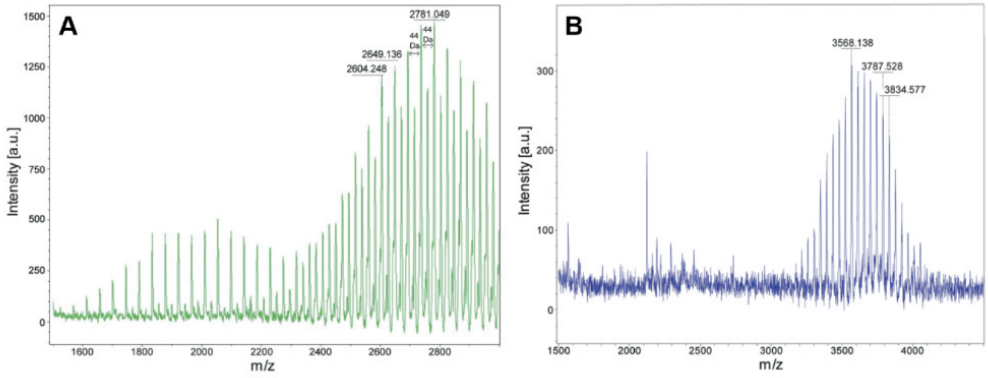


Figure S1: MALDI-MS spectra showing the coupling of DSPE-PEG2000-COOH to cyclic peptide Lyp-1. DSPE-PEG2000-COOH (A) was coupled to cyclic peptide Lyp-1 to produce DSPE-PEG2000-Lyp-1 (B). The mass change between the two spectra corresponds to the successful coupling of the peptide to the lipid.

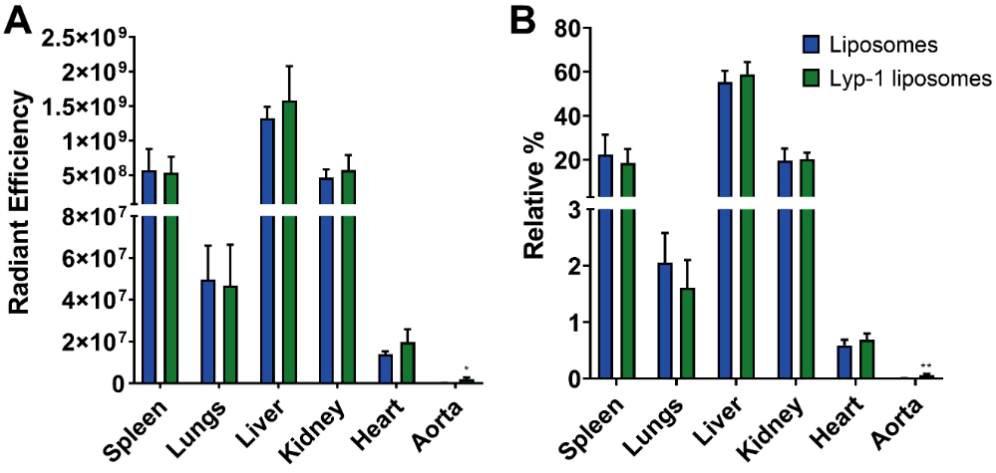


Figure S2: Absolute and relative radiant efficiency of liposomal signal in selected organs in LDLr$^{-/-}$ mice on WTD for 13 weeks, 3 hours after iv injection of non-targeted or Lyp-1 targeted liposomes. Radiant efficiency was measured in spleens, lungs, liver, kidneys, heart, and aorta. (A) Absolute radiant efficient values per organ. (B) The total sum of signals in organs was set to 100%, and the relative radiant efficiency was calculated from this value, n = 5. Graph shows mean + SD, *p < 0.05, ***p < 0.001 comparing Lyp-1 liposomes to non-targeted liposomes, determined by unpaired t-test.

6

An Accelerated Prime-Boost Strategy with cdiGMP-Containing Liposomes Induces Large and Long-Lasting CD8 T Cell Responses Against Neoepitopes and Eliminates Tumors in Mice

Authors and affiliations
Naomi Benne[a1], Dmitrij Ostroumov[b1], Bram Slütter[a], Thomas Wirth[b]
[a] Division of BioTherapeutics, Leiden Academic Centre for Drug Research, Leiden, the Netherlands
[b] Department of Gastroenterology, Hepatology and Endocrinology, Medical School Hannover, Hannover, Germany

[1] Authors contributed equally

Manuscript in preparation

Abstract

The immune system is known to be involved in the resolution of cancer and many cells, including T cells, are important for suppressing tumor growth. Antigen-specific vaccination to prime T cells against tumor cells is an attractive treatment strategy for tumors. One possibility to elicit antigen-specific T cells is by injecting dendritic cells (DCs), loaded with neoantigens *ex vivo* and boosting with a mix of an agonistic anti-CD40 antibody (Co), antigen (A) and a TLR3 ligand (T) Poly I:C. While DC-CoAT vaccination does lead to strong immune responses, *ex vivo* priming of DCs is very labor-intensive and expensive, prohibiting widespread use. Using a delivery system to encapsulate a neoantigen, such as nanoparticles, can deliver the antigen to DCs *in situ* in an "off-the-shelf" approach. Here, we present a vaccination strategy using cationic liposomes composed of distearoylphosphatidylcholine (DSPC), dipalmitoyltrimethylammoniumpropane (DPTAP) and cholesterol (CHOL) as a platform for encapsulating neoantigens and TLR ligands. Vaccination effectiveness was tested by priming mice with liposomes and boosting with CoAT (LS-CoAT), and restimulating blood *ex vivo* with neoantigens. The resulting IFNγ production by $CD8^+$ and $CD4^+$ T cells indicated the magnitude of the antigen-specific immune response. We show using this strategy that the STING agonist cyclic-di-guanosine monophosphate (cdiGMP) is the best adjuvant for enhancing antigen-specific $CD8^+$ T cell responses against the neoepitope $Adpgk_{mut}$, and we report extremely high levels (60%) of antigen-specific $CD8^+$ T cells. Moreover, cdiGMP liposomes also induced high and long-lasting $CD8^+$ T-cell responses against another neoepitope, $Alg8_{mut}$, with around 12% and 4% of $CD8^+$ T cells still recognizing $Alg8_{mut}$ and $Adpgk_{mut}$, respectively, after 83 days. Furthermore, we evaluated whether co-administering $CD8^+$ and $CD4^+$ epitopes in cdiGMP liposomes would boost antigen-specific $CD8^+$ T cell responses. We found no additional benefit of the $CD4^+$ epitope MTAG85B. Finally, LS-CoAT with $Adpgk_{mut}$ was tested in a tumor mouse model. Mice were inoculated with the MC-38 cells and received LS-priming after 4 days of tumor growth, followed by CoAT-boosting one week later. We observed high antigen-specific responses to the antigen combined with tumor regression within 30 days and 100% survival. In conclusion, we show that our LS-CoAT strategy can induce extremely high frequencies of antigen-specific $CD8^+$ T cells to at least two neoepitopes in a short time and that these T cells are very long-lasting. This allowed for rapid and complete tumor elimination in an MC-38 mouse tumor model.

Introduction

The immune system is known to be involved in the resolution of cancer. Many cells, including T cells, are important for suppressing tumor growth from the early stages of tumor development[1]. While the main focus for tumor suppression is $CD8^+$ T cells[2], $CD4^+$ T cells have also been shown to be important[3]. Antigen-specific vaccination to prime $CD8^+$ and $CD4^+$ T cells against tumor cells is an attractive treatment strategy for tumors. In order for T cells to distinguish healthy cells from tumor cells, T cells detect surface expression of tumor antigens[4]. These can be tumor-associated antigens, which are epitopes that are expressed on healthy cells but over-expressed on tumor cells. However, vaccinating against these epitopes can lead to unwanted side effects when T cells attack healthy tissues[5]. The second class of tumor antigens is neoantigens. These result from non-synonymous somatic mutations that encode new peptides that can be presented on the cell surface. Since they are not expressed in healthy cells, they are highly immunogenic and a safer target for vaccination[6]. T cells are activated by antigen-presenting cells (APCs) that have taken up and processed an antigen. The antigen is presented on major histocompatibility complex (MHC)-I or MHC-II molecules to $CD8^+$ and $CD4^+$ T cells, respectively, and together with a costimulatory signal directs T cell differentiation and activation[7]. A strategy to elicit antigen-specific T cells is by injecting dendritic cells (DCs), a type of APC, loaded with neoantigens. Hereby, DCs are isolated and pulsed with antigens *ex vivo*, and subsequently reinjected[8]. These DCs can then present the tumor-specific epitopes to T cells and prime them to destroy the cancer cells. However, this response is often quite weak without the use of an adjuvant, so DCs are typically primed *ex vivo*[9]. APCs generally become activated upon recognition of danger signals via pattern recognition receptors (PRRs) such as Toll-like receptors (TLRs) and stimulator of interferon (IFN) genes (STING)[10]. Therefore, after priming with antigen-loaded DCs, boosting with a mix of an agonistic anti-CD40 antibody (Co), antigen (A) and a TLR ligand (T) Poly I:C, greatly enhances antigen-specific $CD8^+$ and $CD4^+$ T cell responses[11]. Furthermore, this CoAT vaccination strategy could control tumor growth in an MC-38 tumor mouse model[12]. While DC-CoAT vaccination does lead to strong immune responses, *ex vivo* priming of DCs is very labor-intensive and expensive, prohibiting widespread use[8]. Using a delivery system to encapsulate a neoantigen, such as nanoparticles, can deliver the antigen to DCs *in situ* in a simpler way[13]. Liposomes are a type of nanoparticle composed of phospholipids which form a bilayer around an aqueous core[14]. A major advantage of liposomes is that they can encapsulate one or multiple antigens and adjuvants, such as TLR ligands[15,16] or STING agonists[17], to further enhance the immune response. We and others have shown that cationic liposomes by themselves or formulated with a TLR ligand such as Poly I:C[16,18-20] can induce strong antigen-specific pro-inflammatory $CD8^+$ and $CD4^+$ T cells responses. Furthermore, it is evident that liposomes with high rigidity can further enhance these responses[21-23].

We hypothesize that cationic liposomes can replace DC priming in DC-CoAT vaccination, providing a more broadly applicable vaccination strategy against neoepitopes. Here, we present a vaccination strategy using cationic liposomes composed of distearoylphosphatidylcholine (DSPC), dipalmitoyltrimethylammoniumpropane (DPTAP) and cholesterol (CHOL) as a platform for encapsulating neoantigens and TLR ligands. We show that the STING agonist cyclic-di-guanosine monophosphate (cdiGMP) is the best adjuvant for enhancing antigen-specific $CD8^+$ T cell responses using the

neoepitope $Adpgk_{mut}$ in a liposome-CoAT (LS-CoAT) vaccination strategy. In a head-to-head comparison, cdiGMP liposomes performed as well as DCs. Furthermore, cdiGMP liposomes also induced high and long-lasting $CD8^+$ T-cell responses against another neoepitope, $Alg8_{mut}$. Moreover, we evaluated whether co-administering $CD8^+$ and $CD4^+$ epitopes in cdiGMP liposomes would boost antigen-specific $CD8^+$ T cell responses. Finally, LS-CoAT with $Adpgk_{mut}$ eliminated established MC-38 tumors in mice.

Methods

Liposome preparation

Cationic liposomes were prepared by the thin film dehydration-rehydration method, as described before[23]. Briefly, DSPC, DPTAP, and CHOL were dissolved in chloroform and mixed in a 50 mL round-bottom flask at a molar ratio of 4:1:2, to a final lipid concentration of 10 mg/mL. The chloroform was evaporated under vacuum at 40°C for 30 min using a rotary evaporator (Rotavapor R-210, Büchi, Switzerland). The resulting lipid film was rehydrated with 1 mg peptide (Adpgk$_{mut}$: ASMTNMELM, Alg8$_{mut}$: ITYTWTRL, Adpgk$_{mut}$ long: TGIPVHLELASMTNMELMSSIVH, MTAG85B: KFQDAYNAAGGHNAVF, Adpgk$_{mut}$ long/MTAG85B fused: TGIPVHLELASMTNMELMSSIVHKFQDAYNAAGGHNAVF, all purchased from ProImmune, Oxford, UK) dissolved in 1 mL 1:1 ACN/MilliQ (v/v) + 0.04% NH_4OH (w/v), or 1 mL 1:1 ACN/MilliQ (v/v) + 0.04% NH_4OH (w/v) for empty liposomes. To incorporate cdiGMP, 150 µg cdiGMP was dissolved in methanol and added to the lipid film before evaporation. For liposomes containing monophosphoryl lipid A (MPLA), 80 nmol MPLA was dissolved and added to the lipid mixture before evaporation. For Poly I:C liposomes, 99.5 µg Poly I:C and 0.5 µg Poly I:C-Rhodamine were dissolved in MilliQ at a concentration of 1 mg/mL and added dropwise to the lipid/peptide or lipid/MilliQ mix. After rehydration, glass beads were added and the suspension was homogenized for 30 minutes at 60°C. The dispersion was subsequently snap-frozen in liquid nitrogen and freeze-dried overnight (Christ alpha 1–2 freeze-dryer, Osterode, Germany). The resulting lipid cake was slowly rehydrated using 10 mM sodium phosphate buffer (PB), pH 7.4 at 60°C. Two volumes of 500 µL and one volume of 1,000 µL PB were successively added, with intervals of 30 min between each addition. The mixture was vortexed well between each hydration step, and the resulting dispersion was left to rehydrate for at least 1 hour. Sizing of the liposomes was performed using high-pressure extrusion at 60°C (LIPEX Extruder, Northern Lipids Inc., Canada) by passing the dispersion four times through stacked 400-nm and 200-nm pore size polycarbonate track-etched membranes (Whatman® NucleporeTM, GE Healthcare, Little Chalfont, UK). To separate non-encapsulated peptide and/or adjuvants, the dispersion was washed several times using a Vivaspin 2 centrifuge membrane concentrator (MWCO 300 kDa, Sartorius, Göttingen, Germany) by centrifugation at 1500 rpm and 4°C.

Liposome characterization

The Z-average diameter and polydispersity index (PDI) of the liposomes were measured by dynamic light scattering (DLS) using a NanoZS Zetasizer (Malvern Ltd., Malvern, UK). The same instrument was used to measure ζ-potential by laser Doppler electrophoresis. The liposomes were diluted 100-fold in PB to a total volume of 1 mL for measurement. To determine the concentration of encapsulated peptide and cdiGMP, samples were analyzed by reversed-phase UPLC (Waters ACQUITY UPLC, Waters, MA, USA). 20 µL of the liposome dispersion was dissolved in 180 µL methanol. 10 µL of this was injected into a 1.7 µm BEH C18 column (2.1 × 50 mm, Waters ACQUITY UPLC, Waters, MA, USA). The column temperature was 40°C. The mobile phases were Milli-Q water with 0.1% TFA (solvent A) and acetonitrile with 0.1% TFA (solvent B). For separation, the mobile phases were applied in a linear gradient from 20% to 100% solvent B over 6 minutes at a flow rate of 0.25 mL/min. Peptides were detected by absorbance at 220 nm using an ACQUITY

UPLC TUV detector (Waters ACQUITY UPLC, Waters, MA, USA). cdiGMP was detected by absorbance at 254 nm. Poly I:C content was determined by fluorescence (Ex: 546 nm, Em: 576 nm) using a TECAN plate-reader (Salzburg, Austria). MPLA integrates readily into the lipid bilayer, so loading was assumed to be 100%[24].

Animals

6- to 8-week old C57BL6/J mice were bred at the Animal Care Facility of the Hannover Medical School, Germany. During experiments, mice were housed in the Animal Care Facility of the Hannover Medical School according to the required biosafety level. All animal experiments were performed according to German legal guidelines for animal care and experimentation (TierSchG) and were approved by institutional and governmental boards (LAVES).

DC-CoAT and LS-CoAT vaccinations

For DC-CoAT vaccination, splenic DCs were isolated from donor mice that received a subcutaneous injection of 5×10^6 B16 cells expressing Flt3L resuspended in 100 µL PBS, as described previously[25]. After DC harvest, cells were maturated in vitro with LPS (0.5 µg/ml) and incubated in the presence of peptides (2 µg/ml) for approximately 2 hours. For vaccination, $1x10^6$ DCs resuspended in 100 µL PBS were injected intravenously into the mice. CoAT immunizations were performed as described previously[12]. Briefly, individual mice received intravenous injection of 100 µg soluble peptides (thinkpeptides, Oxford, UK), 200 µg Poly I:C (Invivogen, San Diego, CA, USA) and 100 µg of agonistic anti-CD40 antibody (clone 1C10, hybridoma kindly provided by Frances Lund, Department of Microbiology, University of Alabama at Birmingham, AL, USA). For LS-CoAT vaccinations, mice were injected intravenously with 100 µL of 10 nmol peptide encapsulated in liposomes. CoAT boosting was the same as described above for both particles.

Quantification and phenotypic analysis of antigen-specific T-cells.

The magnitude of the epitope-specific $CD8^+$ T-cell response was determined by IFNγ staining as described before[26]. For antibody or tetramer staining, a small volume (~50 µL) of blood was collected via submandibular bleeding. Extracellular antibody and intracellular cytokine staining were performed according to standard protocols. Intracellular cytokine staining for IFNγ was performed in total splenocytes and tumors of sacrificed mice. Mice were sacrificed and subjected to cardiac perfusion with PBS (Gibco, Germany) prior to harvesting the spleens. In order to obtain single-cell suspensions spleens were forced through 40 µm cell strainers (Falcon, Colorado Springs, CO, USA) prior to extracellular antibody and intracellular cytokine staining. For preparation of cells from subcutaneous tumors, mice were euthanized and tumors were removed. Then tumor tissue was mechanically separated using a scalpel and afterwards enzymatically digested for 30 min at 37°C and 200 rpm. The digestion medium contained RPMI + GlutaMAX (Gibco), supplemented with 10% fetal calf serum (FCS, Biowest), 1% Penicillin-Streptomycin (100 U/ml Penicillin, 100 µg/ml Streptomycin, Biochrom), Hyaluronidase (0.2 mg/ml), DNAseI (0.2 mg/ml), collagenase type IA (0.2 mg/ml), and collagenase type IV (0.2 mg/ml) (Sigma-Aldrich). Digestion was arrested by addition of RPMI + GlutaMAX supplemented with 10% FCS and 1% Penicillin-Streptomycin, and cell suspensions were passed through 40 µm cell strainers and washed once with RPMI + GlutaMAX supplemented with 10%

FCS and 1% Penicillin-Streptomycin prior to extracellular antibody and intracellular cytokine staining. Antibodies used for FACS analysis were CD8 (53-6.7), CD4 (GK1.5), IFNγ (XMG1.2), CD90.2 (53-2.1) (eBioscience, San Diego, CA, USA), TruStain FcX™ (anti-mouse CD16/32) (Biolegend, San Diego, CA, USA), and appropriate isotype controls.

Induction of subcutaneous tumors

Subcutaneous tumors in C57BL6/J mice were generated by subcutaneous injection with 5×10^6 MC-38 cells per mouse resuspended in 100 µL PBS. MC-38 is a colon carcinoma cell line (kindly provided by Michael Neumaier, University of Mannheim, Germany). The growth of subcutaneous tumors was monitored three times a week and mice were sacrificed when tumor diameter exceeded 1.5 cm^3 or when tumors exulcerated considerably. Tumor volume was determined by the formula 0.5 × length (mm) × (width (mm))^2, which was published previously[27].

Statistical analysis

Statistical analysis was performed using GraphPad Prism v8. All experiments were repeated at least once to ensure reproducibility. Asterisks indicate levels of significance: *$p < 0.05$, **$p < 0.01$, ***$p < 0.001$, ****$p < 0.0001$.

Results

cdiGMP is a superior liposomal adjuvant for vaccination in combination with CoAT

DSPC:DPTAP:CHOL (mol ratio 4:1:2) encapsulating the neoepitope $Adpgk_{mut}$ were prepared using the dehydration-rehydration method. Without adjuvant, liposomes are around 200 nm in size and cationic. The loading efficiency of $Adpgk_{mut}$ was 40% (Table 1). Inclusion of poly I:C increased the size of the liposomes and decreased the ζ-potential to 27 mV. The inclusion of MPLA resulted in a small reduction in size to around 180 nm. Liposomes adjuvanted with cdiGMP did not alter in size compared to non-adjuvanted liposomes, but ζ-potential decreased slightly to 32 mV. This formulation showed a 50% reduction in antigen loading efficiency (Table 1), suggesting competition of the antigen and adjuvant. To test whether liposomes encapsulating the neoepitope $Adpgk_{mut}$ and different adjuvants could induce antigen-specific $CD8^+$ T cell responses, mice were injected with $Adpgk_{mut}$ liposomes (10 nmol peptide concentration), either without adjuvant or with Poly I:C, MPLA or cdiGMP. As controls, mice received empty liposomes or free $Adpgk_{mut}$ (10 nmol). 6 days after injection, blood was collected from mice and restimulated with $Adpgk_{mut}$, and IFNγ production by $CD8^+$ T cells was measured. 7 days after prime, all mice received the CoAT boost, and 7 days after boost IFNγ production by $CD8^+$ T cells was determined (Figure 1A). Only mice receiving liposomes with cdiGMP showed measurable IFNγ responses before CoAT (Figure 1B). The CoAT boost enhanced IFNγ responses for all groups except the free peptide group, showing liposomal delivery significantly enhances the effect of CoAT boosting. The levels of IFNγ production are in fact among the highest ever reported for this peptide[12,28,29]. All liposomal formulations with peptide, except for Poly I:C liposomes, showed significantly higher production of IFNγ compared to empty liposomes or free peptide (Figure 1C). There was no significant difference between adjuvant-free liposomes, MPLA liposomes, and cdiGMP liposomes. Importantly, mice showed no signs of distress due to vaccination. Since cdiGMP liposomes already elicited a response after prime and outperformed the other adjuvanted liposomes, we decided to continue with this formulation in combination with CoAT boosting, hereafter referred to as LS-CoAT.

Table 1: Physicochemical properties of DSPC:DPTAP:CHOL liposomes encapsulating $Adpgk_{mut}$ and different adjuvants.

Adjuvant	Size (nm)	PDI	Z-potential (mV)	LE $Adpgk_{mut}$ (%)	LE adjuvant (%)
None	209.2	0.158	39.4	40.8	-
Poly I:C	394.6	0.264	27.2	39.5	8.8
MPLA	178.7	0.281	36.6	57.8	Assumed 100%
cdiGMP	210.2	0.119	31.6	19.2	39.3

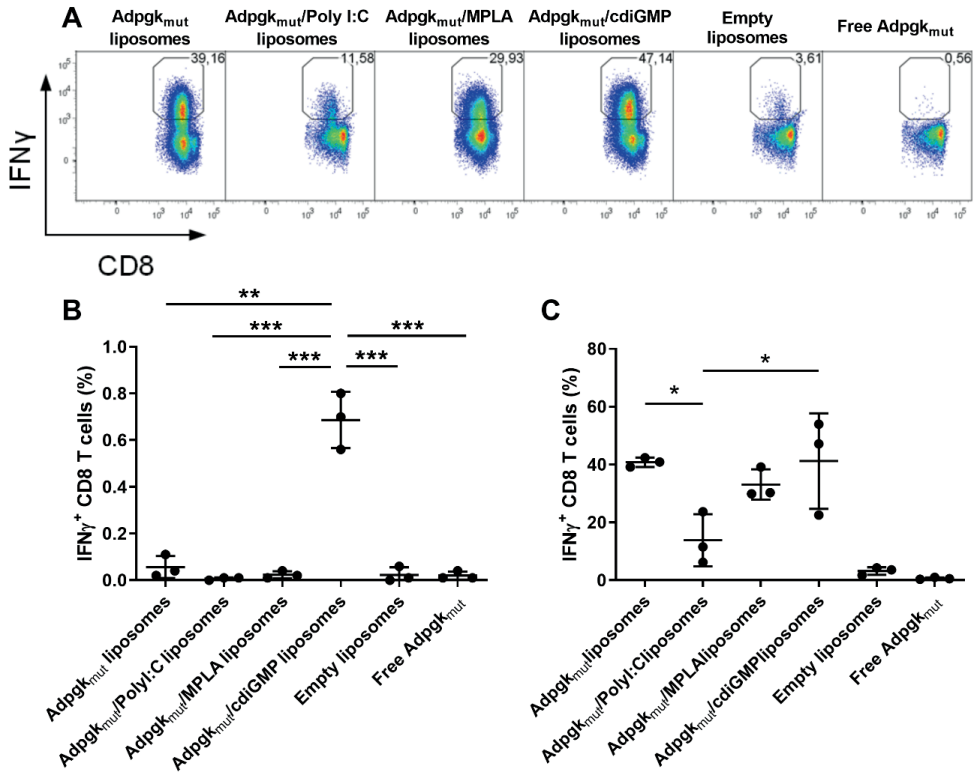


Figure 1: Effect of liposomal adjuvant on Adpgk$_{mut}$-specific CD8$^+$ T cell responses *in vivo*. Mice were injected with Adpgk$_{mut}$-containing liposomes (10 nmol peptide concentration), either without adjuvant or with Poly I:C, MPLA or cdiGMP. As controls, some mice received empty liposomes or free Adpgk$_{mut}$ (10 nmol). All mice received a CoAT boost on day 7. (A) Representative FACS plots of blood restimulated with Adpgk$_{mut}$ 7 days after boost. IFNγ production by CD8$^+$ T cells upon restimulation with Adpgk$_{mut}$ was measured in the blood (B) 6 days after prime and (C) 7 days after boost. Graphs show mean ± SD, *p < 0.05, **p < 0.01, ***p < 0.001 determined by one-way ANOVA with Tukey's multiple comparisons test.

cdiGMP liposome vaccination performs as well as DC-CoAT vaccination

As stated above, DC-CoAT vaccination is currently one of the best methods for inducing high numbers of antigen-specific CD8$^+$ T cells. To test whether cdiGMP liposomes are a viable replacement for *ex vivo* primed DCs, we performed a direct comparison between cdiGMP liposome-CoAT and DC-CoAT vaccination. Non-adjuvanted DPTAP liposomes were used as control. Mice were injected with the different groups, and 6 days after prime, blood was collected and restimulated with Adpgk$_{mut}$ to measure IFNγ production by CD8$^+$ T cells. We observed a significantly higher production of IFNγ in mice injected with cdiGMP liposomes compared to the other groups (Figure 2A). One day later, all mice received a CoAT boost and the immune response was measured in blood again after 7 days. Here, we saw that DC-CoAT and cdiGMP LS-CoAT significantly increased IFNγ production in mice compared to non-adjuvanted liposomes (Figure 2B).

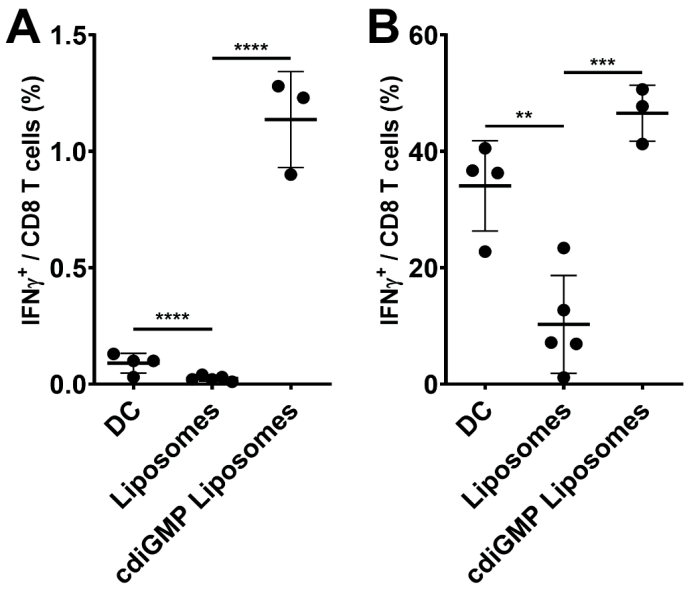


Figure 2: Comparison of liposomal formulations to DC-CoAT vaccination *in vivo*. Mice were injected with Adpgk$_{mut}$-pulsed DCs, Adpgk$_{mut}$ liposomes, or Adpgk$_{mut}$ cdiGMP liposomes. All mice received a CoAT boost on day 7. IFNγ production by CD8$^+$ T cells upon restimulation with Adpgk$_{mut}$ was measured in the blood (A) 6 days after prime, and (B) 7 days after boost. Graphs show mean ± SD, **p < 0.01, ***p < 0.001, ****p < 0.0001 determined by one-way ANOVA with Tukey's multiple comparisons test.

LS-CoAT induces high, long-lasting antigen-specific CD8$^+$ T cell responses against Adpgk$_{mut}$ and Alg8$_{mut}$

Next, we aimed to assess whether the LS-CoAT could also induce responses against other neoepitopes, such as Alg8$_{mut}$, and how long these responses would be sustained. For good anti-tumor responses, it is important that CD8$^+$ T cells persist over a long time. Furthermore, different tumor cells will have different antigens, so it is important to test the LS-CoAT approach for another neoepitope. We prepared Alg8$_{mut}$ liposomes, Adpgk$_{mut}$ liposomes, Alg8$_{mut}$/cdiGMP liposomes, and Adpgk$_{mut}$/cdiGMP liposomes (Table 2), and injected these in mice. 6 days after prime, blood was collected and restimulated with either Alg8$_{mut}$ or Adpgk$_{mut}$. Again, we observed a measurable antigen-specific IFNγ response in CD8$^+$ T cells, only for mice that received cdiGMP-adjuvanted liposomes (Figure 3A). 7 days after prime mice were boosted with CoAT, and responses were measured again after 7 days. For both non-adjuvanted liposomes, the IFNγ response was around 6%. Incorporation of cdiGMP enhanced this response significantly to around 30% for Alg8$_{mut}$, and 45% for Adpgk$_{mut}$ (Figure 3B). This response was very long-lasting, and after 83 days (the last time-point for the experiment), we measured 12% IFNγ$^+$ CD8$^+$ T cells for mice injected with Alg8$_{mut}$/cdiGMP liposomes, and 4% for Adpgk$_{mut}$/cdiGMP liposomes (Figure 3C). Non-adjuvanted liposomes showed shorter-lasting responses and lower peak numbers of around 1% on day 7 (Figure 3C).

Table 2: Physicochemical properties of DSPC:DPTAP:CHOL liposomes encapsulating $Alg8_{mut}$ with and without cdiGMP.

Liposome	Size (nm)	PDI	Z-potential (mV)	LE $Alg8_{mut}$ (%)	LE cdiGMP (%)
$Alg8_{mut}$	178.1	0.078	38.6	60.0	-
$Alg8_{mut}$/cdiGMP	166.8	0.081	40	53.7	67.6

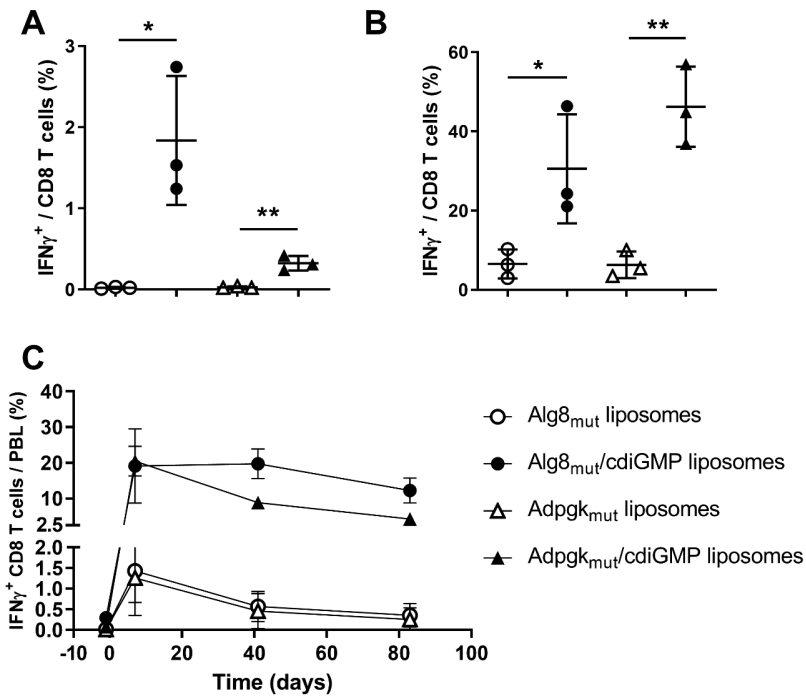


Figure 3: Long-lasting antigen-specific responses after LS/CoAT with $Adpgk_{mut}$ and $Alg8_{mut}$. Mice were injected with $Alg8_{mut}$- or $Adpgk_{mut}$-containing liposomes (10 nmol peptide, circles, and triangles, respectively), with or without cdiGMP (black and open symbols, respectively). All mice received a CoAT boost after 7 days. IFNγ production by $CD8^+$ T cells upon restimulation with $Alg8_{mut}$ or $Adpgk_{mut}$ was measured in the blood (A) 6 days after prime, and (B) 7 days after boost. (C) Antigen-specific $CD8^+$ T cells in the PBLs were followed over a period of 83 days. Graphs show mean ± SD, *$p < 0.05$, **$p < 0.01$, determined by one-way ANOVA with Tukey's multiple comparisons test.

Mixing $Adpgk_{mut}$ and MTAG85B liposomes enhance $CD8^+$ T cell responses in LS-CoAT vaccination

$CD4^+$ T cell help is pivotal for $CD8^+$ T cell expansion and acquisition of effector function, so the addition of MHCII restricted peptides may improve the $CD8^+$ T-cell response[3]. Moreover, long peptides (LP) have been shown to exhibit stronger $CD8^+$ T cell activation than short peptides (SP), due to the need for LP to undergo endosomal processing[30]. Therefore, we tested whether exchanging the $Adpgk_{mut}$ SP for LP would enhance the immune response. We also assessed whether mixing $Adpgk_{mut}$ SP or LP cdiGMP liposomes with cdiGMP liposomes encapsulating the $CD4^+$ epitope MTAG85B,

or cdiGMP liposomes containing a fused $Adpgk_{mut}$ LP/MTAG85B peptide would increase the $CD8^+$ T cell response (Table 3). Mice were primed with either $Adpgk_{mut}$ SP/cdiGMP liposomes, $Adpgk_{mut}$ LP/cdiGMP liposomes, a mixture of $Adpgk_{mut}$ SP/cdiGMP liposomes and MTAG85B/cdiGMP liposomes, a mixture of $Adpgk_{mut}$ LP/cdiGMP liposomes or $Adpgk_{mut}$ LP/MTAG85B fusion peptide/cdiGMP liposomes. In all cases, peptide dose was 10 nmol. 6 days after priming, IFNγ production by $CD8^+$ T cells in the blood was measured after restimulation with $Adpgk_{mut}$ SP (Figure 4A), and $Adpgk_{mut}$ LP (Figure 4B) for mice receiving $Adpgk_{mut}$ LP. IFNγ production by $CD4^+$ T cells was analyzed after MTAG85B restimulation in the mice receiving MTAG85B (Figure 4C). 7 days after priming mice were injected with CoAT with the corresponding peptide(s), and 7 days later, IFNγ production in $CD8^+$ and $CD4^+$ T cells was measured again in the blood (Figure 4D, E, and F). To measure long-term $CD4^+$ and $CD8^+$ T cell stimulation, the same responses were measured after 92 days (Figure 4G, H, and I). Before boosting, IFNγ responses after restimulation with $Adpgk_{mut}$ SP or MTAG85B were not altered between any of the groups, but IFNγ production by $CD8^+$ T cells was significantly higher for mice injected with cdiGMP liposomes encapsulating the fused $Adpgk_{mut}$ LP/MTAG85B peptide compared to $Adpgk_{mut}$ LP alone (Figure 4B). One week after boosting, $CD8^+$ T cell responses were unchanged between any of the groups, but $CD4^+$ T cells had a significantly higher production of IFNγ after injection with fused peptide liposomes compared to a mix of cdiGMP/$Adpgk_{mut}$ LP liposomes and cdiGMP/MTAG85B liposomes (Figure 4F). This persisted until day 92 (Figure 4I). Using LS-CoAT in combination with $CD4^+$ epitopes induces potent $CD4^+$ T cell responses, and for this, the fused peptide is more effective. However, for $CD8^+$ T cell responses against the minimal $Adpgk_{mut}$ epitope, the $CD4^+$ epitope has no benefit.

Table 3: Physicochemical properties of cdiGMP-adjuvanted DSPC:DPTAP:CHOL liposomes encapsulating different peptides

Peptide	Size (nm)	PDI	Z-potential (mV)	LE peptide (%)	LE cdiGMP (%)
$Adpgk_{mut}$ LP	213.1	0.180	35.7	35.4	76.7
MTAG85B	217.2	0.119	34.9	12.8	33.8
Fused $Adpgk_{mut}$ LP/ MTAG85B	235.1	0.210	36.5	28.4	58.8

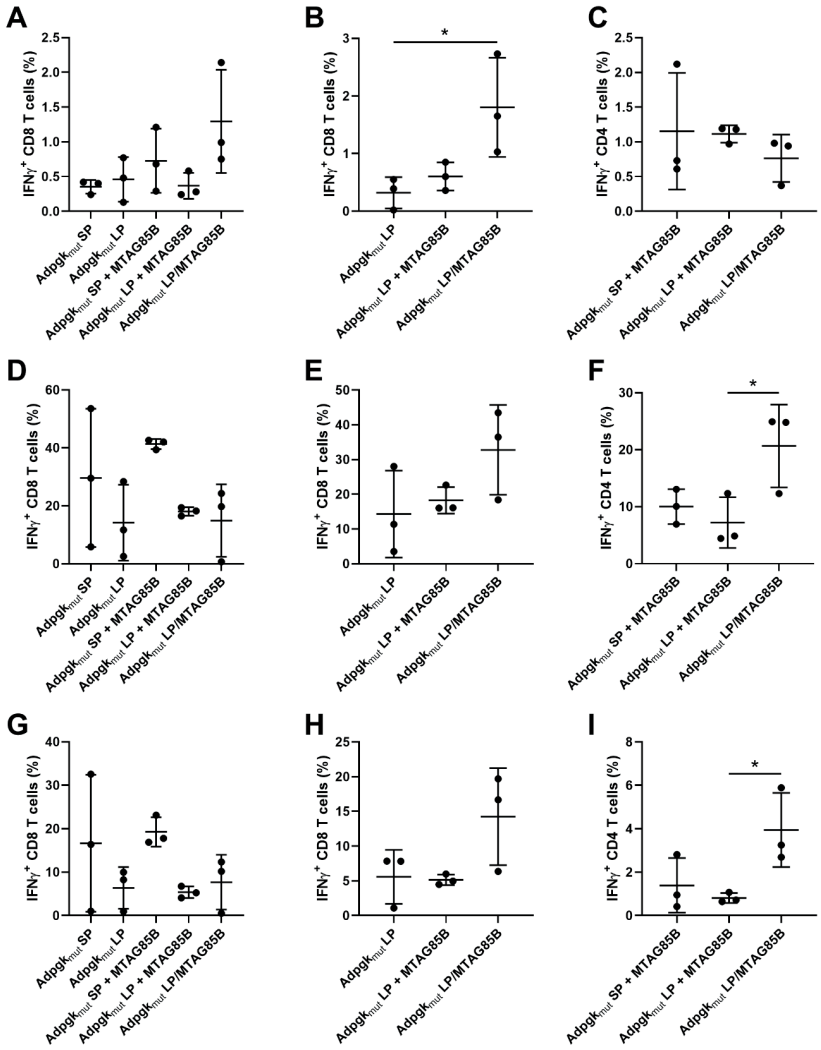


Figure 4: Effect of long and short Adpgkmut peptides, and the CD4+ epitope MTAG85B on antigen-specific CD8+ and CD4+ T cell responses in vivo. Mice were injected with liposomes encapsulating Adpgkmut SP or LP, a mix of Adpgkmut SP and MTAG85B liposomes, a mix of Adpgkmut LP and MTAG85B liposomes, or liposomes containing a fused Adpgk¬mut LP/MTAG85B peptide (10 nmol peptide concentration). All liposomes were adjuvanted with cdiGMP. All mice received a CoAT boost with the corresponding peptide(s) on day 7. Blood was collected at different time points. One day before boost, IFNγ production by CD8+ T cells in the blood was measured after restimulation with (A) Adpgkmut SP, and (B) Adpgkmut LP. (C) CD4+ T cell responses were measured after restimulation with MTAG85B. 7 days after boost IFNγ production by CD8+ T cells in the blood was measured after restimulation with (D) Adpgkmut SP, and (E) Adpgkmut LP. (F) CD4+ T cell responses were measured after restimulation with MTAG85B. 92 days after boost IFNγ production by CD8+ T cells in the blood was measured after restimulation with (G) Adpgkmut SP, and (H) Adpgkmut LP. (I) CD4+ T cell responses were measured after restimulation with MTAG85B. Graphs show mean ± SD, *$p < 0.05$, determined by one-way ANOVA with Tukey's multiple comparisons test.

LS-CoAT and LS-CoT eliminate tumors in an MC38 tumor model

Since the Adpgkmut-loaded cdiGMP liposomes elicited strong antigen-specific CD8+ T cell responses, we address their potential to treat tumors. Mice were inoculated with MC-38 tumor cells and injected 4 days later with liposomes. As controls, mice were injected with antigen-free cdiGMP liposomes (Table 4), or untreated tumor-bearing mice. The tumor-free control mice also received Adpgkmut/cdiGMP liposomes. 6 days after prime, blood was collected and IFNγ responses were measured after restimulation of CD8+ T cells with Adpgkmut. Mice that received Adpgkmut/cdiGMP liposomes showed a significantly higher number of IFNγ+ CD8+ T cells compared to unvaccinated controls, reaching more than 60% of the total CD8+ T-cell population (Figure 5A). On day 11 mice that received Adpgkmut/cdiGMP liposomes were boosted with CoAT, and mice that received cdiGMP liposomes without antigen were boosted with CoT, that only contained agonistic CD40 antibody and Poly I:C, and no peptide antigen. After the boost immunization mice that received LS-CoT had only a small but still measurable CD8= T cell response against Adpgkmut, while mice receiving LS-CoAT had significantly high IFNγ responses of around 60% (Figure 5B). There were no differences between the tumor-inoculated and the tumor-free control mice, suggesting the CD8 T-cell response was not impeded by the tumor. Interestingly, LS-CoT produced significantly high IFNγ production by CD8+ T cells upon restimulation with MC38 cells (Figure 5C). Tumor size and mouse mortality were monitored for 40 days, starting from tumor inoculation. After treatment with LS-CoAT or LS-CoT, tumor size shrank, and tumors disappeared within 26 days for all mice in these groups (Figure 5D and E). The untreated control mice had massive outgrowth of the tumors and all had to be sacrificed according to humane end-points within 36 days after tumor inoculation (Figure 5F). All mice receiving LS-CoAT or LS-CoT survived until the end of the experiment (Figure 5G). We also observed high endogenous Adpgkmut responses in tumor cells of untreated tumor-bearing mice (Figure 6).

Table 4: Physicochemical properties of antigen-free cdiGMP-containing DSPC:DPTAP:CHOL liposomes

Size (nm)	PDI	Z-potential (mV)	LE cdiGMP (%)
217.4	0.075	31.5	41.6

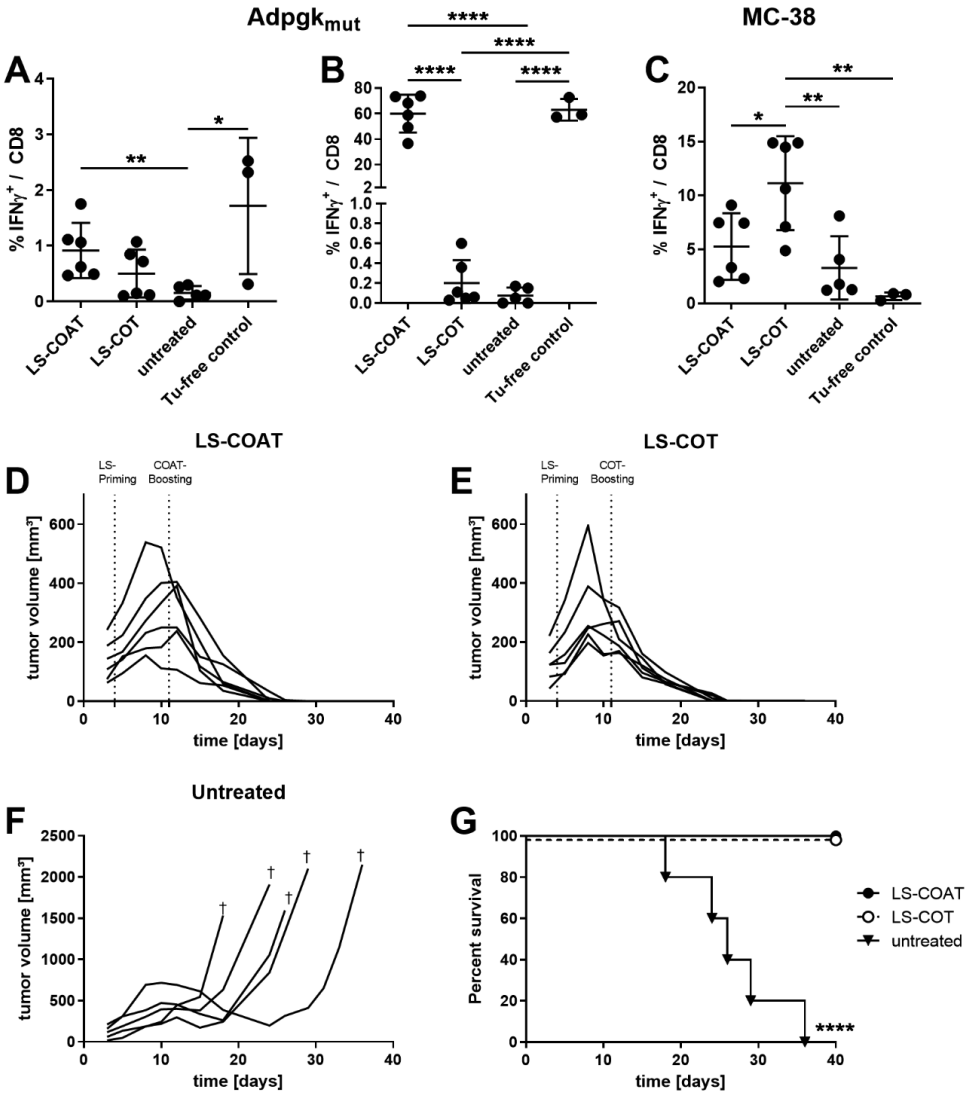


Figure 5: Tumor growth inhibition by cdiGMP liposomes with or without antigen. Mice were inoculated with 5 x 106 MC-38 cells, and tumors were allowed to grow for 4 days. One group did not receive tumor cells. Mice were primed with Adpgkmut-containing cdiGMP liposomes (tumor and tumor-free mice), antigen-free cdiGMP liposomes or untreated. After 7 days, mice were boosted with CoAT, CoT or untreated. IFNγ production by CD8+ T cells upon restimulation with Adpgkmut was measured in the blood (A) 6 days after prime, and (B) 7 days after boost. (C) IFNγ production by CD8+ T cells upon restimulation with MC-38 cells was measured in blood 7 days after boost. Tumor growth was measured during treatment with (D) LS-CoAT, (E) LS-CoT, and (F) untreated. (G) Survival of mice during tumor experiment. Graphs (A-C) show mean ± SD, *p < 0.05, **p < 0.01, ****p < 0.0001 determined by one-way ANOVA with Tukey's multiple comparisons test. (G) ***p < 0.0001 as determined by log-rank Mantel-Cox test.

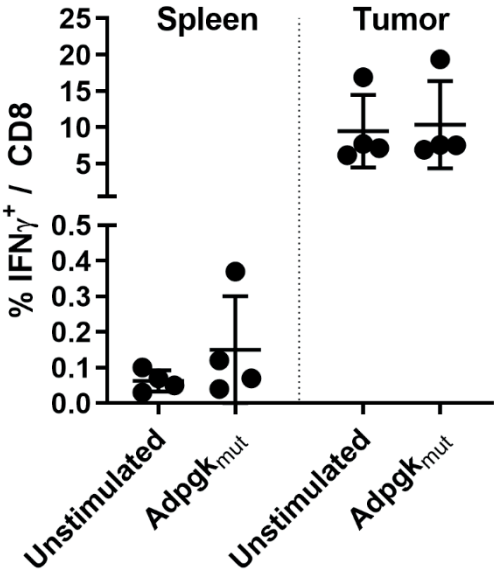


Figure 6: Endogenous CD8+ T cell responses in spleens and tumors of mice inoculated with MC-38 cells.

Discussion

Previously, DC-CoAT vaccination against the neoepitope Adpgkmut elicited around 20-60% IFNγ production by CD8+ T cells after restimulation with the peptide in a very short time period (2 weeks). Furthermore, DC-CoAT vaccination-induced tumor regression within 2 weeks in an MC-38 subcutaneous cancer model and eliminated tumors within 50 days12. However, ex vivo priming of DCs is very labor-intensive and expensive8. Therefore, we aimed to replace the DC priming in the DC-CoAT vaccination scheme with liposomes. Cationic and rigid liposomes are known to elicit pro-inflammatory responses required for anti-tumor effects20,21. Liposomes can be formulated with adjuvants to enhance this response. We compared non-adjuvanted Adpgkmut liposomes with liposomes containing the TLR3 ligand Poly I:C, the TLR4 agonist MPLA or the STING agonist cdiGMP (Figure 1), as all of these have been shown to be effective in cancer treatment15-17. Interestingly, LS/cdiGMP priming already induced a measurable response (Figure 1A). Targeting the STING pathway is especially interesting since it has been found to be the major pathway for APC activation in tumors10. STING can directly bind cyclic dinucleotides, such as cdiGMP, leading to the production of pro-inflammatory cytokines and type 1 IFNs, which are important for the activation of pro-inflammatory T cells31,32. STING agonists have been used effectively as an adjuvant in liposomes for cancer vaccination33,34. After boosting with CoAT, non-adjuvanted liposomes, MPLA liposomes, and cdiGMP liposomes had higher IFNγ responses compared to empty liposomes or free peptide (Figure 1B), approaching the high response seen with DC-CoAT vaccination. Non-adjuvanted liposomes had extremely high responses in this experiment (~40%); however, this response was not consistent among different experiments (Figures 2 and 3). Poly I:C liposomes showed much lower responses; this was probably because the poly I:C liposomes were much larger than the other liposomes (around 400 nm vs 200 nm, Table 1). Since poly I:C is negatively charged, it may aggregate with the cationic liposomes. Inclusion of cdiGMP in the liposomes reduced the antigen load by about a half; there is likely competition between the antigen and cdiGMP for loading. We minimized competition by loading cdiGMP in the lipid bilayer, but the loss of antigen could not be completely avoided. Due to the success of the cdiGMP liposomes and the interesting effects of cdiGMP reported in literature, we continued with this formulation in further experiments. Crucially, in a direct comparison between DC-CoAT and LS-CoAT with cdiGMP liposomes, liposomes performed as well as DCs (Figure 2).

For a more widely applicable tumor vaccination strategy, we aim to address whether the cdiGMP liposomes could elicit CD8+ T cell responses against another peptide. Therefore, we encapsulated the neoepitope Alg8mut in the same liposomes to test the responses. Both neoepitopes have a high affinity for MHC-I (predicted affinity of Adpgkmut = 2 nM35, and Alg8mut = 3 nM36), and they showed comparable levels of IFNγ production by CD8+ T cells after restimulation (Figure 3). For both peptides, incorporation of cdiGMP in the liposomes clearly boosted the immune response and led to very long-lasting responses, which were similar to those achieved with DC-CoAT12.

Next, we wanted to improve our vaccination by eliciting CD4+ T cell help3 and selecting a long version of Adpgkmut peptide30. Vaccination with long peptides to trigger CD8+ T cell responses is generally very potent [ref]. In our experiment, the long peptide did not enhance the CD8+ T cell response against the minimal epitope

(Figure 4). However, it may still be useful to vaccinate with longer epitopes, since it is not prerequisite to know what the minimal epitope is [ref]. Furthermore, long peptides lead to processing by DCs and cross-presentation, which is important in the context of peptide presentation by tumor cells [ref]. We also saw no evidence of the MTAG85B-induced CD4+ T cell activation boosting the CD8+ responses (Figure 4), so it seems in this case that CD4+ T cell activation and using a long peptide has no additional value. It may be that the liposomes and/or cdiGMP direct the response away from CD4+ T cells to CD8+ T cells, and already enhance potency so much so as to abolish the potential benefits of a long peptide. In addition, the potent effects of the boost containing agonistic anti-CD40 antibody may eliminate the need for CD4+ T cell help, since it mimics CD40L and can thereby replace the function of CD4+ T cells37. Due to the lack of improvement of the Adpgkmut responses with the addition of a CD4+ T cell epitope or a long peptide, we decided to perform a tumor study using only the minimal Adpgkmut peptide in cdiGMP liposomes.

In the MC-38 tumor model, we again observed high antigen-specific responses to the antigen with or without tumor inoculation (Figure 5A and 4B), and we saw tumor regression within 30 days and 100% survival in mice receiving the LS-CoAT vaccination (Figure 5D and 5G). Interestingly, tumor regression started in most mice before boost at around 6 days after priming with liposomes. Wang and Celis studied the effect of cdiGMP in a slightly altered CoAT vaccination approach as presented here. Mice were inoculated with B16-F10 cells and primed on day 8 with an iv injection of 100 µg peptide, 50 µg anti-CD40 antibody, 25 µg Poly I:C, and 100 µg cdiGMP followed by a boost 9 days later with an iv injection of 100 µg peptide, 25 µg anti-CD40 antibody, 25 µg Poly I:C, and 100 µg cdiGMP. They report high levels of tetramer+ CD8+ T cells after boost (up to 80%), and significant halting, but not the elimination of tumor progression compared to controls in a B16 melanoma model38. Koshy et al. encapsulated cyclic guanosine monophosphate-adenosine monophosphate (cGAMP) in DOTAP:CHOL:DSPE-PEG liposomes as a treatment in the B16-F10 melanoma model. Mice were inoculated with cells and injected intratumoral on days 7, 9, 14, and 16 with a dose of 1 µg cGAMP in liposomes. They observed tumor elimination in 50% of the mice. At day 60, the surviving mice were challenged with B16-F10 cells, which resulted in 100% survival, indicating long-lasting immunity. They also showed high retention of cGAMP in the tumor site 24 hours after injection of liposomes, which was mostly co-localized with MHC-II-expressing cells39. Surprisingly, we saw complete tumor regression and mouse survival for mice receiving LS-CoT (Figure 5E and 5G), and this vaccination strategy was the only one to produce significantly higher IFNγ upon restimulation with MC-38 cells compared to untreated control (Figure 5C). Free STING agonists have been shown to significantly reduce tumor growth after iv injection24,40 and even eliminate tumors after intratumoral injection39,41. However, these studies required many injections of high doses of STING agonist (up to 500 µg/mouse/injection). Encapsulating compounds in liposomes leads to targeting immune cells and reduction of the number of injections and dosage42. We provided a single liposomal injection followed by a boost, and the cdiGMP dose was 2 µg/mouse. Other types of cationic formulations encapsulating STING agonists can display long-lasting protection after intratumoral injection39,43 and iv injection44, also compared to free STING agonists. In all aforementioned studies, it seems that the efficacy of the STING agonist in the absence of antigen is due to effects in the tumor

microenvironment. However, it may be that for other tumor models than the one tested here, antigen-specific therapy is necessary. Indeed, we saw high endogenous Adpgkmut responses in tumor cells of untreated tumor-bearing mice (Figure 6), supporting the hypothesis that the MC-38 tumor model is highly susceptible to immunotherapy.

In conclusion, we have developed an extremely potent cationic liposomal formulation adjuvanted with cdiGMP that performs as well as DC-CoAT at inducing antigen-specific CD8+ T cell responses. The generated immune response after liposome vaccination is very long-lasting and thereby enables the elimination of established tumors. In future, it would be interesting to test the LS-CoAT strategy in other tumor models in order to evaluate the wider application of the liposomes.

References

1 Ostroumov, D., Fekete-Drimusz, N., Saborowski, M., Kuhnel, F. & Woller, N. CD4 and CD8 T lymphocyte interplay in controlling tumor growth. Cell Mol Life Sci 75, 689-713, doi:10.1007/s00018-017-2686-7 (2018).

2 Appay, V., Douek, D. C. & Price, D. A. CD8+ T cell efficacy in vaccination and disease. Nat Med 14, 623-628, doi:10.1038/nm.f.1774 (2008).

3 Shankaran, V. et al. IFNgamma and lymphocytes prevent primary tumour development and shape tumour immunogenicity. Nature 410, 1107-1111, doi:10.1038/35074122 (2001).

4 Coulie, P. G., Van den Eynde, B. J., van der Bruggen, P. & Boon, T. Tumour antigens recognized by T lymphocytes: at the core of cancer immunotherapy. Nat Rev Cancer 14, 135-146, doi:10.1038/nrc3670 (2014).

5 Johnson, L. A. et al. Gene therapy with human and mouse T-cell receptors mediates cancer regression and targets normal tissues expressing cognate antigen. Blood 114, 535-546, doi:10.1182/blood-2009-03-211714 (2009).

6 Lu, Y. C. & Robbins, P. F. Cancer immunotherapy targeting neoantigens. Semin Immunol 28, 22-27, doi:10.1016/j.smim.2015.11.002 (2016).

7 Guermonprez, P., Valladeau, J., Zitvogel, L., Thery, C. & Amigorena, S. Antigen presentation and T cell stimulation by dendritic cells. Annu Rev Immunol 20, 621-667, doi:10.1146/annurev.immunol.20.100301.064828 (2002).

8 Chen, P. et al. Dendritic cell targeted vaccines: Recent progresses and challenges. Hum Vaccin Immunother 12, 612-622, doi:10.1080/21645515.2015.1105415 (2016).

9 Bol, K. F. et al. The clinical application of cancer immunotherapy based on naturally circulating dendritic cells. Journal for immunotherapy of cancer 7, 109, doi:10.1186/s40425-019-0580-6 (2019).

10 Corrales, L., McWhirter, S. M., Dubensky, T. W., Jr. & Gajewski, T. F. The host STING pathway at the interface of cancer and immunity. J Clin Invest 126, 2404-2411, doi:10.1172/JCI86892 (2016).

11 Llopiz, D. et al. Combined immunization with adjuvant molecules poly(I:C) and anti-CD40 plus a tumor antigen has potent prophylactic and therapeutic antitumor effects. Cancer Immunology, Immunotherapy 57, 19-29, doi:10.1007/s00262-007-0346-8 (2008).

12 Nimanong, S. et al. CD40 Signaling Drives Potent Cellular Immune Responses in Heterologous Cancer Vaccinations. Cancer Res 77, 1918-1926, doi:10.1158/0008-5472.CAN-16-2089 (2017).

13 Jia, J. et al. Interactions Between Nanoparticles and Dendritic Cells: From the Perspective of Cancer Immunotherapy. Front Oncol 8, 404, doi:10.3389/fonc.2018.00404 (2018).

14 Pattni, B. S., Chupin, V. V. & Torchilin, V. P. New Developments in Liposomal Drug Delivery. Chem Rev 115, 10938-10966, doi:10.1021/acs.chemrev.5b00046 (2015).

15 Boks, M. A. et al. MPLA incorporation into DC-targeting glycoliposomes favours anti-tumour T cell responses. J Control Release 216, 37-46, doi:10.1016/j.jconrel.2015.06.033 (2015).

16 Varypataki, E. M., van der Maaden, K., Bouwstra, J., Ossendorp, F. & Jiskoot, W. Cationic liposomes loaded with a synthetic long peptide and poly(I:C): a defined adjuvanted vaccine for induction of antigen-specific T cell cytotoxicity. AAPS J 17, 216-226, doi:10.1208/s12248-014-9686-4 (2015).
17 Nakamura, T. et al. Liposomes loaded with a STING pathway ligand, cyclic di-GMP, enhance cancer immunotherapy against metastatic melanoma. J Control Release 216, 149-157, doi:10.1016/j.jconrel.2015.08.026 (2015).
18 Korsholm, K. S. et al. Induction of CD8+ T-cell responses against subunit antigens by the novel cationic liposomal CAF09 adjuvant. Vaccine 32, 3927-3935, doi:10.1016/j.vaccine.2014.05.050 (2014).
19 Varypataki, E. M., Benne, N., Bouwstra, J., Jiskoot, W. & Ossendorp, F. Efficient Eradication of Established Tumors in Mice with Cationic Liposome-Based Synthetic Long-Peptide Vaccines. Cancer Immunol Res 5, 222-233, doi:10.1158/2326-6066.CIR-16-0283 (2017).
20 Heuts, J. et al. Cationic Liposomes: A Flexible Vaccine Delivery System for Physicochemically Diverse Antigenic Peptides. Pharm Res 35, 207, doi:10.1007/s11095-018-2490-6 (2018).
21 Benne, N., van Duijn, J., Kuiper, J., Jiskoot, W. & Slutter, B. Orchestrating immune responses: How size, shape and rigidity affect the immunogenicity of particulate vaccines. J Control Release 234, 124-134, doi:10.1016/j.jconrel.2016.05.033 (2016).
22 Anselmo, A. C. & Mitragotri, S. Impact of particle elasticity on particle-based drug delivery systems. Adv Drug Deliv Rev 108, 51-67, doi:10.1016/j.addr.2016.01.007 (2017).
23 Benne, N. et al. Anionic 1,2-distearoyl-sn-glycero-3-phosphoglycerol (DSPG) liposomes induce antigen-specific regulatory T cells and prevent atherosclerosis in mice. J Control Release 291, 135-146, doi:10.1016/j.jconrel.2018.10.028 (2018).
24 Alving, C. R., Rao, M., Steers, N. J., Matyas, G. R. & Mayorov, A. V. Liposomes containing lipid A: an effective, safe, generic adjuvant system for synthetic vaccines. Expert Rev Vaccines 11, 733-744, doi:10.1586/erv.12.35 (2012).
25 Schmidt, N. W. et al. Memory CD8 T cell responses exceeding a large but definable threshold provide long-term immunity to malaria. Proc Natl Acad Sci U S A 105, 14017-14022, doi:10.1073/pnas.0805452105 (2008).
26 Badovinac, V. P., Messingham, K. A., Jabbari, A., Haring, J. S. & Harty, J. T. Accelerated CD8+ T-cell memory and prime-boost response after dendritic-cell vaccination. Nat Med 11, 748-756, doi:10.1038/nm1257 (2005).
27 Tomayko, M. M. & Reynolds, C. P. Determination of subcutaneous tumor size in athymic (nude) mice. Cancer chemotherapy and pharmacology 24, 148-154, doi:10.1007/bf00300234 (1989).
28 Aurisicchio, L. et al. Poly-specific neoantigen-targeted cancer vaccines delay patient derived tumor growth. Journal of Experimental & Clinical Cancer Research 38, 78, doi:10.1186/s13046-019-1084-4 (2019).
29 Menares, E. et al. Tissue-resident memory CD8+ T cells amplify anti-tumor immunity by triggering antigen spreading through dendritic cells. Nature Communications 10, 4401, doi:10.1038/s41467-019-12319-x (2019).

30 Melief, C. J. & van der Burg, S. H. Immunotherapy of established (pre)malignant disease by synthetic long peptide vaccines. Nat Rev Cancer 8, 351-360, doi:10.1038/nrc2373 (2008).
31 Woo, S. R. et al. STING-dependent cytosolic DNA sensing mediates innate immune recognition of immunogenic tumors. Immunity 41, 830-842, doi:10.1016/j.immuni.2014.10.017 (2014).
32 Barber, G. N. STING: infection, inflammation and cancer. Nat Rev Immunol 15, 760-770, doi:10.1038/nri3921 (2015).
33 Hanson, M. C. et al. Nanoparticulate STING agonists are potent lymph node-targeted vaccine adjuvants. J Clin Invest 125, 2532-2546, doi:10.1172/JCI79915 (2015).
34 Miyabe, H. et al. A new adjuvant delivery system ‚cyclic di-GMP/YSK05 liposome' for cancer immunotherapy. J Control Release 184, 20-27, doi:10.1016/j.jconrel.2014.04.004 (2014).
35 Yadav, M. et al. Predicting immunogenic tumour mutations by combining mass spectrometry and exome sequencing. Nature 515, 572-576, doi:10.1038/nature14001 (2014).
36 Matsushita, H. et al. Cancer exome analysis reveals a T-cell-dependent mechanism of cancer immunoediting. Nature 482, 400-404, doi:10.1038/nature10755 (2012).
37 Schoenberger, S. P., Toes, R. E., van der Voort, E. I., Offringa, R. & Melief, C. J. T-cell help for cytotoxic T lymphocytes is mediated by CD40-CD40L interactions. Nature 393, 480-483, doi:10.1038/31002 (1998).
38 Wang, Z. & Celis, E. STING activator c-di-GMP enhances the anti-tumor effects of peptide vaccines in melanoma-bearing mice. Cancer Immunol Immunother 64, 1057-1066, doi:10.1007/s00262-015-1713-5 (2015).
39 Koshy, S. T., Cheung, A. S., Gu, L., Graveline, A. R. & Mooney, D. J. Liposomal Delivery Enhances Immune Activation by STING Agonists for Cancer Immunotherapy. Adv Biosyst 1, doi:10.1002/adbi.201600013 (2017).
40 Li, T. et al. Antitumor Activity of cGAMP via Stimulation of cGAS-cGAMP-STING-IRF3 Mediated Innate Immune Response. Sci Rep 6, 19049, doi:10.1038/srep19049 (2016).
41 Corrales, L. et al. Direct Activation of STING in the Tumor Microenvironment Leads to Potent and Systemic Tumor Regression and Immunity. Cell Rep 11, 1018-1030, doi:10.1016/j.celrep.2015.04.031 (2015).
42 Schwendener, R. A. Liposomes as vaccine delivery systems: a review of the recent advances. Ther Adv Vaccines 2, 159-182, doi:10.1177/2051013614541440 (2014).
43 Demaria, O. et al. STING activation of tumor endothelial cells initiates spontaneous and therapeutic antitumor immunity. Proc Natl Acad Sci U S A 112, 15408-15413, doi:10.1073/pnas.1512832112 (2015).
44 Cheng, N. et al. A nanoparticle-incorporated STING activator enhances antitumor immunity in PD-L1-insensitive models of triple-negative breast cancer. JCI Insight 3, doi:10.1172/jci.insight.120638 (2018).

7

General Summary and Perspectives

The immune system is our body's defense against infections. However, it can also be involved in diseases such as autoimmune diseases[1-3] or cancer[4,5]. T cells are vital for the homeostasis of the immune system, and therefore are a target for treating such diseases[6-8]. In this thesis, we have focused on the treatment of diseases in which T cells are too active (atherosclerosis) or not sufficiently activated (cancer) and propose new treatment strategies using liposomes, which is introduced in **chapter 1**.

Liposomes are versatile vesicle-like structures, that can be engineered into various physical forms. In **chapter 2** we reviewed how particle size, shape, and rigidity of particulate vaccines affect biodistribution, cellular uptake, antigen presentation and the resulting immune response. While there are trends that can be observed between the physicochemical parameters of such vaccines and the resulting immune responses, it is often very difficult to alter just one parameter without affecting others. However, it is clear that a rational design approach is necessary to optimize a vaccine for a specific use; the physicochemical parameters for optimal antigen-presenting cell (APC) uptake may not be ideal for eliciting the desired immune response. In later chapters, this is always considered and studied in detail when designing the liposomes.

In **chapter 3** we aimed to understand the effect of liposomal rigidity, one of the most over-looked parameters for nanoparticles, on antigen-specific T cell responses. One of the reasons that rigidity has not been studied as extensively as other physicochemical parameters is the difficulty in accurately measuring it[9-14], and a lack of standardization in the literature. We used atomic force microscopy (AFM) to accurately measure the rigidity of individual anionic liposomes containing an ovalbumin-derived $CD4^+$ T cell epitope. The surface charge, phospholipid head group composition, antigen content and size of the liposomes were controlled in order to minimize alterations in other physicochemical parameters. We found that the incorporation of cholesterol in the lipid bilayer decreases the rigidity of gel-state liposomes and increases that of fluid-state ones. Furthermore, the transition temperature of the phospholipids influenced the overall liposome rigidity. Interestingly, almost all formulations showed a positive correlation between liposomal rigidity and APC association. However, dioleoylphosphatidylcholine (DOPC):dioleoylphosphatidylglycerol (DOPG) liposomes showed the highest association to dendritic cells (DCs) of all tested formulations despite having the lowest rigidity, indicating that liposomal rigidity alone does not control APC uptake. We did observe a significant correlation between the rigidity of the liposomes and the regulatory T cell (Treg) responses they elicited *in vitro* and in *vivo*. Our findings may contribute to a better understanding of the factors driving Treg responses, and support a rational design of liposomal as well as other nanoparticulate vaccine formulations aiming to enhance antigen-specific Treg responses for the treatment of autoimmune diseases.

Building upon the information presented in **chapters 2** and **3**, **chapters 4** and **5** focus on using liposomes to treat atherosclerosis. Atherosclerosis is the predominant underlying pathology of cardiovascular disease, which affects millions of people worldwide[15]. Lipids in the form of low-density lipoprotein (LDL) accumulate in the subendothelial space in medium- and large-sized arteries, which leads to chronic inflammation[16]. LDL can modify to form oxidized LDL (oxLDL), which attracts immune cells, continuing the inflammation[16]. Some of these immune cells, such as monocytes, can differentiate into macrophages which can phagocytose oxLDL, leading to foam cell formation[17]. Manipulation of immune cells, especially T cells[2,18] or foam cells[19], can be an effective way to treat

atherosclerosis. In **chapter 4** we designed liposomes that can induce Tregs. Liposomes were composed of distearoylphosphatidylcholine (DSPC):distearoylphosphatidylglycerol (DSPG):cholesterol (CHOL) (also one of the most rigid and potent formulations in **chapter 3**) and were loaded with an ovalbumin-derived $CD4^+$ T cell epitope. These liposomes were shown to elicit high production of antigen-specific Tregs *in vitro* and *in vivo* in mice as compared to free antigen, DSPC:dipalmitoylphosphatidylserine (DPPS):CHOL, and DSPC:dipalmitoyltrimethylammoniumpropane (DPTAP):CHOL liposomes. As an atherosclerosis-specific antigen, we turned to ApoB100, the protein component of oxLDL, which was already shown to be a relevant antigen[20-31]. We identified a major-histocompatibility complex (MHC)-II-restricted ApoB100-derived peptide, referred to as p3500, using a peptidomics strategy. When encapsulating p3500 in DSPG-liposomes it successfully reduced atherosclerotic plaque formation, as measured by a reduction in total plaque size, and an increase in plaque stability.

We also described the mechanism behind the potency of the DSPG-liposomes. Interestingly, it has been shown that anionic liposomes composed of PS resemble apoptotic cells, since PS becomes exposed on the surface of apoptotic cells[32]. Through scavenger receptor (SR)-mediated uptake by APCs, PS-containing liposomes can mediate an anti-inflammatory effect[33,34]. We show that DSPG-liposomes are more effectively taken up by DCs *in vitro* than DPPS-liposomes. We also demonstrate a role for the protein corona in Treg induction via SRs. *In vitro* and *in vivo*, liposomes interact with proteins in the physiological medium, resulting in the formation of a protein corona around the liposomes[35]. We found a significant reduction of uptake for both PG- and PS- liposomes in the presence of serum when SR-mediated uptake by DCs was blocked, which was not observed in serum-free conditions, suggesting that formation of a protein corona is required for liposome-SR interactions. We concentrated on the serum protein complement component 1 Q (C1q), since it was shown to bind to PS on apoptotic cells and lead to clearance via SRs[36-39]. Interestingly, C1q is also involved in the pathology of atherosclerosis[40]. We showed that C1q is present in the protein corona and binds to anionic liposomes. The addition of C1q in serum-free conditions completely restored the uptake of both PG- and PS-liposomes, while specific depletion of C1q in serum significantly reduced uptake of PG-liposomes. We further observed that the addition of C1q increases Treg responses compared to serum-free conditions, but not significantly. This suggests that C1q is partially responsible for the Treg induction of both DSPG- and DPPS-liposomes, but the protein corona likely contains more components that help to induce Tregs. Furthermore, it would be very interesting to study whether there is a relationship between liposomal rigidity and the protein corona, which is something we have not studied.

C1q does not only interact with SRs, but also binds to other proteins, such as the C1q-binding protein, also known as p32. This receptor is aberrantly expressed in plaque-resident macrophages[41]. As mentioned above, macrophages play an important role in the pathogenesis of atherosclerosis, since they can phagocytose lipids and become large lipid-rich foam cells[42]. These foam cells are unable to migrate out of the vessel wall, leading to a build-up at the site of the inflammation and formation of a plaque[43]. Therefore, a suitable treatment strategy would be to prevent and/or reverse the formation of foam cells[19], which was our goal in **chapter 5**. Macrophages are able to reverse cholesterol transport across their membrane via ATP-binding cassette (ABC) transporters ABCA1 and

ABCG1[44]. The expression of both of these transporters is controlled by the liver X receptor (LXR). A class of small molecules, called LXR agonists (*e.g.*, GW3965), can activate this receptor to induce reverse cholesterol transport in foam cells, allowing for migration of these cells from the plaque[45]. Unfortunately, when administered systemically at therapeutic doses, LXR agonists have effects in other organs, such as the liver, leading to high triglyceride levels in the plasma or liver[46-48]. Encapsulation of the LXR agonist in a drug delivery vehicle such as liposomes can overcome this problem[49]. The cyclic peptide Lyp-1 (CGNKRTRGC) binds to p32 and can therefore be used to target macrophages in atherosclerotic lesions[50,51]. For this purpose, we designed a particulate formulation that combines the targeting properties of the cyclic peptide Lyp-1 with the therapeutic effect of an LXR agonist (GW3965) and promotes reverse cholesterol transport in foam cells to stabilize atherosclerotic plaques. We used the knowledge gained from **chapter 2**, **chapter 3** and **chapter 4** to formulate liposomes with long circulation time, minimal APC uptake, and minimal immune effects. We then functionalized the liposomes with Lyp-1, and this led to greatly enhanced association to foam cells *in vitro*, while having limited affinity for macrophages. *In vivo* we saw retention of liposomes in atherosclerotic plaques, and we confirmed that the plaque-resident foam cells had taken up the targeted liposomes. We showed that using a low dose of GW3965 encapsulated in Lyp-1 liposomes can reduce plaque macrophage content and increase plaque stability while avoiding an increase in lipids in the serum and liver. These findings demonstrate that it is possible to increase the therapeutic window of LXR agonists, and may contribute to the design of other atherosclerosis therapies. In particular, Lyp-1-functionalized liposomes could be used as a platform to deliver other compounds, such as anti-inflammatory drugs, to foam cells.

The final research chapter of this thesis (**chapter 6**) focuses on using liposomes to treat cancer, which is another major health concern[52]. Cancer encompasses a group of diseases involving abnormal sustained cell proliferation, replication, and survival[53]. T cells are also involved in cancer, since they can recognize tumor-associated antigens[4,5], however in contrast to atherosclerosis, T cell responses in cancer are not effective and suffer from exhaustion[54]. As we have shown in **chapter 4**, DSPC:DPTAP:CHOL liposomes are potent at inducing antigen-specific pro-inflammatory T cells and may provide the type of immune response required to kill a tumor. In **chapter 6** we aimed to repurpose DSPC:DPTAP:CHOL liposomes with tumor neoepitopes as a therapeutic cancer vaccine. Neoepitopes are very interesting for treatment; they result from non-synonymous somatic mutations that encode new amino acid residues, leading to novel peptides that can be presented on the cell surface of tumor cells[55]. The Hannover Medical School previously showed that inducing strong pro-inflammatory T cell responses against $Adpgk_{mut}$ (a neoepitope) could eliminate established cancers[56]. This was achieved by isolating DCs from mice, pulsing them with antigen and adjuvants *ex vivo*, and reinjecting them[57]. These DCs can then present the tumor-specific epitopes to T cells and prime them to destroy the cancer cells[58]. To boost $CD8^+$ T cell responses, mice were injected after some time with a mix of an agonistic anti-CD40 antibody (Co), antigen (A) and a toll-like receptor (TLR) ligand (T) Poly I:C[59]. Unfortunately, *ex vivo* priming of DCs is very labor-intensive and expensive, prohibiting wide-spread use[57]. We propose DSPC:DPTAP:CHOL liposomes as a delivery system to deliver the antigen to DCs *in situ* in a simpler way[60]. First, we compared non-adjuvanted $Adpgk_{mut}$ liposomes with liposomes containing the TLR3 ligand poly(I:C), the TLR4 agonist MPLA, or the

STING agonist cdiGMP. Mice were primed with liposomes and boosted with CoAT. The cdiGMP liposomes induced the strongest antigen-specific $CD8^+$ T cell response, so we continued with this formulation in further experiments. In a direct comparison, cdiGMP liposomes performed as good as DC-CoAT vaccination. We also tested the suitability of the liposomes with another neoepitope, $Alg8_{mut}$. Similar to $Adpgk_{mut}$, encapsulation of the antigen in cdiGMP liposomes greatly boosted the immune response and led to very long-lasting responses which were similar to those achieved with DC-CoAT[56]. Next, we aimed to improve our vaccination protocol by eliciting $CD4^+$ T cell help with the $CD4^+$ epitope MTAG85B[61] and selecting a long version of $Adpgk_{mut}$ peptide[62]. The long peptide did not enhance the $CD8^+$ T cell response against the minimal epitope. We also saw no evidence of the MTAG85B-induced $CD4^+$ T cell activation boosting the $CD8^+$ responses. Due to the lack of improvement of the $Adpgk_{mut}$ responses with the addition of a $CD4^+$ T cell epitope or a long peptide, we decided to perform a tumor study using only the minimal $Adpgk_{mut}$ peptide in cdiGMP liposomes. Here, we observed extremely high antigen-specific responses to the antigen (up to 60% of all $CD8^+$ T cells responded to the antigen by producing IFNγ). We observed tumor regression within 30 days and 100% survival in mice receiving the LS-CoAT vaccination. Overall, this work shows that cdiGMP liposomes are a very powerful platform for encapsulating tumor neoepitopes to induce strong antigen-specific $CD8^+$ T cells and eliminate established tumors.

Perspectives

While we presented several different treatment strategies for different diseases, liposomes were used in all cases. We used liposomes to deliver a drug to plaque-resident macrophages by using a targeted approach. We also manipulated the physicochemical properties of liposomes to induce anti-inflammatory or pro-inflammatory T cell responses. These studies further add to the evidence that liposomes are extremely versatile drug delivery particles[63].

In **chapter 5** we explored a method for treating atherosclerosis by using targeted liposomes to deliver a drug. Aside from targeting to atherosclerotic plaques, targeted liposomes have been applied in the treatment of cancer[64], and to cross the blood-brain barrier to treat neurological diseases such as Alzheimer's[65]. Several liposomal formulations, including PEGylated liposomes, have already been shown to be safe and are FDA and EMA approved[66]. Furthermore, PEGylated liposomes have been used to passively deliver prednisolone (an anti-inflammatory drug) to atherosclerotic plaques in humans, indicating that there is some translation from animals to humans[67].

We have emphasized the importance of designing liposomes with specific physicochemical parameters, and summarized the significance of size, shape and rigidity in **chapter 2**. Liposomal rigidity was intriguing since we could not find a substantial amount of literature concerning this parameter. Therefore, we aimed to enhance our understanding of this parameter and performed a detailed study examining the relationship between liposomal rigidity and Treg responses in **chapter 3**. For this, we presented an optimized protocol for measuring the rigidity of liposomes using AFM, which can also be applied to other particulate vaccines and drug delivery systems. Both of these chapters contribute to the understanding of the effect of physicochemical parameters of liposomes on the immune responses, and could help others with the design of liposomal vaccines. It should also be noted that liposomes are by nature relatively soft particles, so it is unknown

whether the immune effects we observed apply to a wider range of rigidities. The exact mechanism of why rigidity affects the immune response is still not fully understood, and future studies examining this in more detail would be very valuable.

The induction of antigen-specific Tregs are a focus of **chapters 3** and **4**. We identified a peptide derived from murine ApoB100 for vaccination, but human ApoB100 epitopes have been identified which were successful at reducing atherosclerosis in humanized mice[68]. These peptides can be encapsulated in liposomes to enhance their effects and safety. Unfortunately, so far, no clinical studies have been performed using ApoB100-derived epitopes, so there is still a question about the translation of these studies to a clinical setting[69]. Since many people suffering from atherosclerosis use statins to control their disease, the interaction between statins and peptides and/or liposomes needs to be studied as well. For instance, combined use of statins and LDL-mimicking liposomes led to the liposomes crossing the blood-brain barrier in an *in vitro* culture model[70], which could be dangerous. Furthermore, using fluorescence anisotropy, it has been shown that some statins interact with the bilayer of liposomes and can alter their fluidity[71], and thereby their immunogenicity. As opposed to our study with Lyp-1 liposomes, the tolerogenic liposomes in **chapter 4** were administered at the same time as starting the western-type diet; it would be more clinically relevant to administer the liposomes in mice with established atherosclerosis.

Tregs are not only important in the treatment of atherosclerosis, but are involved in many other diseases, grouped under the term autoimmune diseases[72]. We found a role for serum-derived C1q in the interaction of liposomes and SRs, and it would be interesting to study this mechanism in more detail. Autoimmune diseases include diseases such as Crohn's diseases, diabetes, multiple sclerosis and rheumatoid arthritis, and affect an estimated 7.6–9.4% of the population, with women being at a higher risk[73]. There is currently no cure for any of the autoimmune diseases, and treatment focuses on systemic suppression of inflammation with anti-inflammatory drugs. However, these therapies can result in severe side effects and susceptibility to infection, especially upon long-term treatment[74-76], emphasizing the need for more specific therapies. While we have only studied the effects of Treg-inducing liposomes on atherosclerosis, other studies have been performed with tolerogenic liposomes treating diabetes[33] and rheumatoid arthritis[77]. All of this work is vital for developing a possible treatment for autoimmune diseases.

Immunomodulation was also the focus of **chapter 6**, but instead of suppressing the immune response to an antigen, we aimed to enhance it by the use of cationic liposomes. Cancer immunotherapy via DCs[78] or T cells[79], and immunotherapy against neoantigens[80] has been studied for several years. We argue that immunotherapy via liposomes is a faster, more cost-effective treatment strategy. Indeed, nanoparticles, including liposomes, have been shown to be effective in cancer therapy[81], and our work contributes to this evidence. Tools to identify antigens specific to autoimmune diseases[82,83], including the atherosclerosis antigen p3500 identified in this thesis, and cancer[84] are improving. Combined with the ability of liposomes to encapsulate a wide range of epitopes, liposomes could be an important player in the future of personalized therapies[85]. It should be noted that, while we observed no toxicity in our animal studies, at high doses cationic phospholipids induce toxicity in *in vivo* animal models[86] and *in vitro* human cells[87]. Therefore, further development of these liposomes should always

strive for minimizing the dose of the cationic phospholipids in the liposomes. In order to progress to clinical trials, more toxicity studies need to be performed in animal models to test whether the liposomes are safe to use, either in the short-term or long-term.

Aside from the need to test the safety of the liposomes for clinical use, testing in humans requires large amounts of liposomes and the encapsulated contents (drug, peptide, adjuvant). Scale-up is not only potentially very costly (although encapsulation of a compound in a (targeted) nanoparticle greatly decreases the required dose, and therefore cost[88]), but it can alter the liposomes' physicochemical properties. This is also true for the GMP production of liposomes. Methods such as micro-fluidics[89] and ethanol injection[90,91] are proven to be able to reproducibly manufacture large amounts of liposomes under GMP conditions. However, a detailed evaluation of the effect of production method on liposomal properties should be performed. Despite this, there are a substantial number of liposomes that are already approved for humans, or in clinical trials[66], so the potential for further developing the treatments presented here is promising.

References

1 Clemente-Casares, X. *et al.* Expanding antigen-specific regulatory networks to treat autoimmunity. *Nature* **530**, 434-440, doi:10.1038/nature16962 (2016).

2 Foks, A. C., Lichtman, A. H. & Kuiper, J. Treating atherosclerosis with regulatory T cells. *Arterioscler Thromb Vasc Biol* **35**, 280-287, doi:10.1161/ATVBAHA.114.303568 (2015).

3 van Herwijnen, M. J. *et al.* Regulatory T cells that recognize a ubiquitous stress-inducible self-antigen are long-lived suppressors of autoimmune arthritis. *Proc Natl Acad Sci U S A* **109**, 14134-14139, doi:10.1073/pnas.1206803109 (2012).

4 Grivennikov, S. I., Greten, F. R. & Karin, M. Immunity, inflammation, and cancer. *Cell* **140**, 883-899, doi:10.1016/j.cell.2010.01.025 (2010).

5 Coulie, P. G., Van den Eynde, B. J., van der Bruggen, P. & Boon, T. Tumour antigens recognized by T lymphocytes: at the core of cancer immunotherapy. *Nat Rev Cancer* **14**, 135-146, doi:10.1038/nrc3670 (2014).

6 Raphael, I., Nalawade, S., Eagar, T. N. & Forsthuber, T. G. T cell subsets and their signature cytokines in autoimmune and inflammatory diseases. *Cytokine* **74**, 5-17, doi:10.1016/j.cyto.2014.09.011 (2015).

7 Naran, K., Nundalall, T., Chetty, S. & Barth, S. Principles of Immunotherapy: Implications for Treatment Strategies in Cancer and Infectious Diseases. *Front Microbiol* **9**, 3158, doi:10.3389/fmicb.2018.03158 (2018).

8 Feldmann, M. & Steinman, L. Design of effective immunotherapy for human autoimmunity. *Nature* **435**, 612-619, doi:10.1038/nature03727 (2005).

9 Matsingou, C. & Demetzos, C. Calorimetric study on the induction of interdigitated phase in hydrated DPPC bilayers by bioactive labdanes and correlation to their liposome stability: The role of chemical structure. *Chem Phys Lipids* **145**, 45-62, doi:10.1016/j.chemphyslip.2006.10.004 (2007).

10 Altunayar, C., Sahin, I. & Kazanci, N. A comparative study of the effects of cholesterol and desmosterol on zwitterionic DPPC model membranes. *Chem Phys Lipids* **188**, 37-45, doi:10.1016/j.chemphyslip.2015.03.006 (2015).

11 Takechi-Haraya, Y., Sakai-Kato, K. & Goda, Y. Membrane Rigidity Determined by Atomic Force Microscopy Is a Parameter of the Permeability of Liposomal Membranes to the Hydrophilic Compound Calcein. *AAPS PharmSciTech* **18**, 1887-1893, doi:10.1208/s12249-016-0624-x (2017).

12 Zhao, L., Feng, S. S., Kocherginsky, N. & Kostetski, I. DSC and EPR investigations on effects of cholesterol component on molecular interactions between paclitaxel and phospholipid within lipid bilayer membrane. *Int J Pharm* **338**, 258-266, doi:10.1016/j.ijpharm.2007.01.045 (2007).

13 Eloy, J. O. *et al.* Co-loaded paclitaxel/rapamycin liposomes: Development, characterization and in vitro and in vivo evaluation for breast cancer therapy. *Colloids Surf B Biointerfaces* **141**, 74-82, doi:10.1016/j.colsurfb.2016.01.032 (2016).

14 Toyran, N. & Severcan, F. Interaction between vitamin D2 and magnesium in liposomes: Differential scanning calorimetry and FTIR spectroscopy studies. *Journal of Molecular Structure* **839**, 19-27, doi:10.1016/j.molstruc.2006.11.005 (2007).

15 Wang, H. *et al.* Global, regional, and national life expectancy, all-cause mortality, and cause-specific mortality for 249 causes of death, 1980–2015: a systematic analysis for the Global Burden of Disease Study 2015. *The Lancet* **388**, 1459-1544, doi:10.1016/s0140-6736(16)31012-1 (2016).
16 Pirillo, A., Norata, G. D. & Catapano, A. L. LOX-1, OxLDL, and atherosclerosis. *Mediators Inflamm* **2013**, 152786, doi:10.1155/2013/152786 (2013).
17 Tabas, I. & Lichtman, A. H. Monocyte-Macrophages and T Cells in Atherosclerosis. *Immunity* **47**, 621-634, doi:10.1016/j.immuni.2017.09.008 (2017).
18 Douna, H. & Kuiper, J. Novel B-cell subsets in atherosclerosis. *Curr Opin Lipidol* **27**, 493-498, doi:10.1097/MOL.0000000000000335 (2016).
19 Tall, A. R. Cholesterol efflux pathways and other potential mechanisms involved in the athero-protective effect of high density lipoproteins. *Journal of Internal Medicine* **263**, 256-273, doi:10.1111/j.1365-2796.2007.01898.x (2008).
20 Stemme, S. *et al.* T lymphocytes from human atherosclerotic plaques recognize oxidized low density lipoprotein. *Proc Natl Acad Sci U S A* **92**, 3893-3897 (1995).
21 Fredrikson, G. N. *et al.* Identification of immune responses against aldehyde-modified peptide sequences in apoB associated with cardiovascular disease. *Arterioscler Thromb Vasc Biol* **23**, 872-878, doi:10.1161/01.ATV.0000067935.02679.B0 (2003).
22 Sjogren, P. *et al.* High plasma concentrations of autoantibodies against native peptide 210 of apoB-100 are related to less coronary atherosclerosis and lower risk of myocardial infarction. *Eur Heart J* **29**, 2218-2226, doi:10.1093/eurheartj/ehn336 (2008).
23 Fagerberg, B., Prahl Gullberg, U., Alm, R., Nilsson, J. & Fredrikson, G. N. Circulating autoantibodies against the apolipoprotein B-100 peptides p45 and p210 in relation to the occurrence of carotid plaques in 64-year-old women. *PLoS One* **10**, e0120744, doi:10.1371/journal.pone.0120744 (2015).
24 Zhou, X., Caligiuri, G., Hamsten, A., Lefvert, A. K. & Hansson, G. K. LDL Immunization Induces T-Cell–Dependent Antibody Formation and Protection Against Atherosclerosis. *Arteriosclerosis, Thrombosis, and Vascular Biology* **21**, 108 (2001).
25 Schiopu, A. *et al.* Recombinant human antibodies against aldehyde-modified apolipoprotein B-100 peptide sequences inhibit atherosclerosis. *Circulation* **110**, 2047-2052, doi:10.1161/01.CIR.0000143162.56057.B5 (2004).
26 Tse, K. *et al.* Atheroprotective Vaccination with MHC-II Restricted Peptides from ApoB-100. *Front Immunol* **4**, 493, doi:10.3389/fimmu.2013.00493 (2013).
27 Klingenberg, R. *et al.* Intranasal immunization with an apolipoprotein B-100 fusion protein induces antigen-specific regulatory T cells and reduces atherosclerosis. *Arterioscler Thromb Vasc Biol* **30**, 946-952, doi:10.1161/ATVBAHA.109.202671 (2010).
28 Herbin, O. *et al.* Regulatory T-cell response to apolipoprotein B100-derived peptides reduces the development and progression of atherosclerosis in mice. *Arterioscler Thromb Vasc Biol* **32**, 605-612, doi:10.1161/ATVBAHA.111.242800 (2012).

29 Fredrikson, G. N. *et al.* Inhibition of atherosclerosis in apoE-null mice by immunization with apoB-100 peptide sequences. *Arterioscler Thromb Vasc Biol* **23**, 879-884, doi:10.1161/01.ATV.0000067937.93716.DB (2003).
30 Fredrikson, G. N., Bjorkbacka, H., Soderberg, I., Ljungcrantz, I. & Nilsson, J. Treatment with apo B peptide vaccines inhibits atherosclerosis in human apo B-100 transgenic mice without inducing an increase in peptide-specific antibodies. *J Intern Med* **264**, 563-570, doi:10.1111/j.1365-2796.2008.01995.x (2008).
31 Kimura, T. *et al.* Regulatory CD4(+) T Cells Recognize MHC-II-Restricted Peptide Epitopes of Apolipoprotein B. *Circulation* **138**, 13, doi:10.1161/CIRCULATIONAHA.117.031420 (2018).
32 Nagata, S., Hanayama, R. & Kawane, K. Autoimmunity and the clearance of dead cells. *Cell* **140**, 619-630, doi:10.1016/j.cell.2010.02.014 (2010).
33 Pujol-Autonell, I. *et al.* Use of autoantigen-loaded phosphatidylserine-liposomes to arrest autoimmunity in type 1 diabetes. *PLoS One* **10**, e0127057, doi:10.1371/journal.pone.0127057 (2015).
34 Ramos, G. C. *et al.* Apoptotic mimicry: phosphatidylserine liposomes reduce inflammation through activation of peroxisome proliferator-activated receptors (PPARs) in vivo. *British Journal of Pharmacology* **151**, 844-850, doi:10.1038/sj.bjp.0707302 (2007).
35 Ritz, S. *et al.* Protein corona of nanoparticles: distinct proteins regulate the cellular uptake. *Biomacromolecules* **16**, 1311-1321, doi:10.1021/acs.biomac.5b00108 (2015).
36 Bigler, C., Schaller, M., Perahud, I., Osthoff, M. & Trendelenburg, M. Autoantibodies against complement C1q specifically target C1q bound on early apoptotic cells. *J Immunol* **183**, 3512-3521, doi:10.4049/jimmunol.0803573 (2009).
37 Erwig, L. P. & Henson, P. M. Clearance of apoptotic cells by phagocytes. *Cell Death Differ* **15**, 243-250 (2007).
38 Patten, D. A. *et al.* SCARF-1 promotes adhesion of CD4(+) T cells to human hepatic sinusoidal endothelium under conditions of shear stress. *Sci Rep* **7**, 17600, doi:10.1038/s41598-017-17928-4 (2017).
39 Iram, T. *et al.* Megf10 Is a Receptor for C1Q That Mediates Clearance of Apoptotic Cells by Astrocytes. *J Neurosci* **36**, 5185-5192, doi:10.1523/JNEUROSCI.3850-15.2016 (2016).
40 Bhatia, V. K. *et al.* Complement C1q reduces early atherosclerosis in low-density lipoprotein receptor-deficient mice. *Am J Pathol* **170**, 416-426, doi:10.2353/ajpath.2007.060406 (2007).
41 Peerschke, E. I. *et al.* Expression of gC1q-R/p33 and its major ligands in human atherosclerotic lesions. *Mol Immunol* **41**, 759-766, doi:10.1016/j.molimm.2004.04.020 (2004).
42 Chistiakov, D. A., Melnichenko, A. A., Myasoedova, V. A., Grechko, A. V. & Orekhov, A. N. Mechanisms of foam cell formation in atherosclerosis. *J Mol Med (Berl)* **95**, 1153-1165, doi:10.1007/s00109-017-1575-8 (2017).
43 Tabas, I. Macrophage death and defective inflammation resolution in atherosclerosis. *Nat Rev Immunol* **10**, 36-46, doi:10.1038/nri2675 (2010).

44 Venkateswaran, A. *et al.* Control of cellular cholesterol efflux by the nuclear oxysterol receptor LXR alpha. *Proceedings of the National Academy of Sciences of the United States of America* **97**, 12097-12102, doi:10.1073/pnas.200367697 (2000).
45 Kirchgessner, T. G. *et al.* Beneficial and Adverse Effects of an LXR Agonist on Human Lipid and Lipoprotein Metabolism and Circulating Neutrophils. *Cell Metab* **24**, 223-233, doi:10.1016/j.cmet.2016.07.016 (2016).
46 Joseph, S. B. *et al.* Direct and indirect mechanisms for regulation of fatty acid synthase gene expression by liver X receptors. *J Biol Chem* **277**, 11019-11025, doi:10.1074/jbc.M111041200 (2002).
47 Joseph, S. B. *et al.* Synthetic LXR ligand inhibits the development of atherosclerosis in mice. *Proc Natl Acad Sci U S A* **99**, 7604-7609, doi:10.1073/pnas.112059299 (2002).
48 Schultz, J. R. *et al.* Role of LXRs in control of lipogenesis. *Genes & Development* **14**, 2831-2838, doi:10.1101/gad.850400 (2000).
49 Tibbitt, M. W., Dahlman, J. E. & Langer, R. Emerging Frontiers in Drug Delivery. *J Am Chem Soc* **138**, 704-717, doi:10.1021/jacs.5b09974 (2016).
50 Uchida, M. *et al.* Protein cage nanoparticles bearing the LyP-1 peptide for enhanced imaging of macrophage-rich vascular lesions. *ACS Nano* **5**, 2493-2502, doi:10.1021/nn102863y (2011).
51 Seo, J. W. *et al.* (64)Cu-labeled LyP-1-dendrimer for PET-CT imaging of atherosclerotic plaque. *Bioconjug Chem* **25**, 231-239, doi:10.1021/bc400347s (2014).
52 Siegel, R. L., Miller, K. D. & Jemal, A. Cancer statistics, 2019. *CA Cancer J Clin* **69**, 7-34, doi:10.3322/caac.21551 (2019).
53 Hanahan, D. & Weinberg, R. A. Hallmarks of cancer: the next generation. *Cell* **144**, 646-674, doi:10.1016/j.cell.2011.02.013 (2011).
54 Whiteside, T. L. Inhibiting the inhibitors: evaluating agents targeting cancer immunosuppression. *Expert Opin Biol Ther* **10**, 1019-1035, doi:10.1517/14712598.2010.482207 (2010).
55 Lu, Y. C. & Robbins, P. F. Cancer immunotherapy targeting neoantigens. *Semin Immunol* **28**, 22-27, doi:10.1016/j.smim.2015.11.002 (2016).
56 Nimanong, S. *et al.* CD40 Signaling Drives Potent Cellular Immune Responses in Heterologous Cancer Vaccinations. *Cancer Res* **77**, 1918-1926, doi:10.1158/0008-5472.CAN-16-2089 (2017).
57 Chen, P. *et al.* Dendritic cell targeted vaccines: Recent progresses and challenges. *Hum Vaccin Immunother* **12**, 612-622, doi:10.1080/21645515.2015.1105415 (2016).
58 Bol, K. F. *et al.* The clinical application of cancer immunotherapy based on naturally circulating dendritic cells. *Journal for immunotherapy of cancer* **7**, 109, doi:10.1186/s40425-019-0580-6 (2019).
59 Llopiz, D. *et al.* Combined immunization with adjuvant molecules poly(I:C) and anti-CD40 plus a tumor antigen has potent prophylactic and therapeutic antitumor effects. *Cancer Immunology, Immunotherapy* **57**, 19-29, doi:10.1007/s00262-007-0346-8 (2008).
60 Jia, J. *et al.* Interactions Between Nanoparticles and Dendritic Cells: From

the Perspective of Cancer Immunotherapy. *Front Oncol* **8**, 404, doi:10.3389/fonc.2018.00404 (2018).
61 Shankaran, V. *et al.* IFNgamma and lymphocytes prevent primary tumour development and shape tumour immunogenicity. *Nature* **410**, 1107-1111, doi:10.1038/35074122 (2001).
62 Melief, C. J. & van der Burg, S. H. Immunotherapy of established (pre)malignant disease by synthetic long peptide vaccines. *Nat Rev Cancer* **8**, 351-360, doi:10.1038/nrc2373 (2008).
63 Pattni, B. S., Chupin, V. V. & Torchilin, V. P. New Developments in Liposomal Drug Delivery. *Chem Rev* **115**, 10938-10966, doi:10.1021/acs.chemrev.5b00046 (2015).
64 Deshpande, P. P., Biswas, S. & Torchilin, V. P. Current trends in the use of liposomes for tumor targeting. *Nanomedicine* **8**, 1509-1528, doi:10.2217/nnm.13.118 (2013).
65 Agrawal, M. *et al.* Recent advancements in liposomes targeting strategies to cross blood-brain barrier (BBB) for the treatment of Alzheimer's disease. *Journal of Controlled Release* **260**, 61-77, doi:https://doi.org/10.1016/j.jconrel.2017.05.019 (2017).
66 Anselmo, A. C. & Mitragotri, S. Nanoparticles in the clinic. *Bioengineering & Translational Medicine* **1**, 10-29, doi:10.1002/btm2.10003 (2016).
67 van der Valk, F. M. *et al.* Prednisolone-containing liposomes accumulate in human atherosclerotic macrophages upon intravenous administration. *Nanomedicine* **11**, 1039-1046, doi:10.1016/j.nano.2015.02.021 (2015).
68 Gisterå, A. *et al.* Vaccination against T-cell epitopes of native ApoB100 reduces vascular inflammation and disease in a humanized mouse model of atherosclerosis. *Journal of Internal Medicine* **281**, 383-397, doi:10.1111/joim.12589 (2017).
69 Chyu, K.-Y. & Shah Prediman, K. In Pursuit of an Atherosclerosis Vaccine. *Circulation Research* **123**, 1121-1123, doi:10.1161/CIRCRESAHA.118.313842 (2018).
70 Pinzón-Daza, M. L. *et al.* The association of statins plus LDL receptor-targeted liposome-encapsulated doxorubicin increases in vitro drug delivery across blood–brain barrier cells. *British Journal of Pharmacology* **167**, 1431-1447, doi:10.1111/j.1476-5381.2012.02103.x (2012).
71 Bhandary, S., Basu, R., Das, S. & Nandy, P. Effect of some statin group of drugs on the phase profile of liposomal membrane – a fluorescence anisotropy study. *Phase Transitions* **82**, 821-830, doi:10.1080/01411590903432616 (2009).
72 Dominguez-Villar, M. & Hafler, D. A. Regulatory T cells in autoimmune disease. *Nat Immunol* **19**, 665-673, doi:10.1038/s41590-018-0120-4 (2018).
73 Cooper, G. S., Bynum, M. L. K. & Somers, E. C. Recent insights in the epidemiology of autoimmune diseases: improved prevalence estimates and understanding of clustering of diseases. *Journal of autoimmunity* **33**, 197-207, doi:10.1016/j.jaut.2009.09.008 (2009).
74 Coutinho, A. E. & Chapman, K. E. The anti-inflammatory and immunosuppressive effects of glucocorticoids, recent developments and mechanistic insights. *Mol Cell Endocrinol* **335**, 2-13, doi:10.1016/j.

mce.2010.04.005 (2011).
75 Barr, T. A. *et al.* B cell depletion therapy ameliorates autoimmune disease through ablation of IL-6-producing B cells. *J Exp Med* **209**, 1001-1010, doi:10.1084/jem.20111675 (2012).
76 Chatenoud, L. & Bluestone, J. A. CD3-specific antibodies: a portal to the treatment of autoimmunity. *Nat Rev Immunol* **7**, 622-632, doi:10.1038/nri2134 (2007).
77 Capini, C. *et al.* Antigen-specific suppression of inflammatory arthritis using liposomes. *J Immunol* **182**, 3556-3565, doi:10.4049/jimmunol.0802972 (2009).
78 Palucka, K. & Banchereau, J. Cancer immunotherapy via dendritic cells. *Nat Rev Cancer* **12**, 265-277, doi:10.1038/nrc3258 (2012).
79 Bonifant, C. L., Jackson, H. J., Brentjens, R. J. & Curran, K. J. Toxicity and management in CAR T-cell therapy. *Molecular Therapy - Oncolytics* **3**, 16011, doi:https://doi.org/10.1038/mto.2016.11 (2016).
80 Schumacher, T. N. & Schreiber, R. D. Neoantigens in cancer immunotherapy. *Science* **348**, 69, doi:10.1126/science.aaa4971 (2015).
81 Yan, S., Zhao, P., Yu, T. & Gu, N. Current applications and future prospects of nanotechnology in cancer immunotherapy. *Cancer biology & medicine* **16**, 486-497, doi:10.20892/j.issn.2095-3941.2018.0493 (2019).
82 Riedhammer, C. & Weissert, R. Antigen Presentation, Autoantigens, and Immune Regulation in Multiple Sclerosis and Other Autoimmune Diseases. *Frontiers in Immunology* **6**, doi:10.3389/fimmu.2015.00322 (2015).
83 van Eden, W. *et al.* Heat Shock Proteins Can Be Surrogate Autoantigens for Induction of Antigen Specific Therapeutic Tolerance in Rheumatoid Arthritis. *Frontiers in Immunology* **10**, doi:10.3389/fimmu.2019.00279 (2019).
84 Vigneron, N. Human Tumor Antigens and Cancer Immunotherapy. *BioMed research international* **2015**, 948501, doi:10.1155/2015/948501 (2015).
85 Herrmann, I. K. & Rösslein, M. Personalized medicine: the enabling role of nanotechnology. *Nanomedicine* **11**, 1-3, doi:10.2217/nnm.15.152 (2015).
86 Knudsen, K. B. *et al.* In vivo toxicity of cationic micelles and liposomes. *Nanomedicine: Nanotechnology, Biology and Medicine* **11**, 467-477, doi:https://doi.org/10.1016/j.nano.2014.08.004 (2015).
87 Roursgaard, M. *et al.* In vitro toxicity of cationic micelles and liposomes in cultured human hepatocyte (HepG2) and lung epithelial (A549) cell lines. *Toxicology in Vitro* **36**, 164-171, doi:https://doi.org/10.1016/j.tiv.2016.08.002 (2016).
88 Cheng, Z., Al Zakaaaaaai, A., Hui, J. Z., Muzykantov, V. R. & Tsourkas, A. Multifunctional nanoparticles: cost versus benefit of adding targeting and imaging capabilities. *Science (New York, N.Y.)* **338**, 903-910, doi:10.1126/science.1226338 (2012).
89 Zhong, J. *et al.* Large scale preparation of midkine antisense oligonucleotides nanoliposomes by a cross-flow injection technique combined with ultrafiltration and high-pressure extrusion procedures. *Int J Pharm* **441**, 712-720, doi:10.1016/j.ijpharm.2012.10.023 (2013).
90 Charcosset, C., Juban, A., Valour, J.-P., Urbaniak, S. & Fessi, H. Preparation of liposomes at large scale using the ethanol injection method: Effect of scale-up

and injection devices. *Chemical Engineering Research and Design* **94**, 508-515, doi:https://doi.org/10.1016/j.cherd.2014.09.008 (2015).
91 Wagner, A. *et al.* GMP Production of Liposomes—A New Industrial Approach. *Journal of Liposome Research* **16**, 311-319, doi:10.1080/08982100600851086 (2006).

Appendix

Nederlandse Samenvatting

Curriculum vitae

List of Publications

Nederlandse Samenvatting

Het immuunsysteem is de afweer van ons lichaam tegen infecties. Het kan echter ook betrokken zijn bij ziekten zoals auto-immuunziekten of kanker. T-cellen zijn van belang voor de homeostase van het immuunsysteem en zijn daarom een doelwit voor de behandeling van dergelijke ziekten. In dit proefschrift hebben we ons gericht op de behandeling van ziekten waarbij T-cellen te actief zijn (atherosclerose) of niet voldoende geactiveerd zijn (kanker) en stellen we nieuwe behandelstrategieën voor met behulp van liposomen, die in **hoofdstuk 1** werden geïntroduceerd.

In **hoofdstuk 3** wilden we het effect bestuderen van liposomale rigiditeit, één van de minst bestudeerde parameters voor nanodeeltjes, op antigeenspecifieke T-celresponsen. Eén van de redenen dat rigiditeit niet zo uitgebreid is bestudeerd als andere fysicochemische parameters, is de moeite om het nauwkeurig te meten en een gebrek aan standaardisatie in de literatuur. We gebruikten atomic force microscopy (AFM) om de rigiditeit van individuele anionische liposomen nauwkeurig te meten. De oppervlaktelading, fosfolipide kopgroepsamenstelling, antigeengehalte en grootte van de liposomen werden gecontroleerd om veranderingen in andere fysicochemische parameters te minimaliseren. We vonden dat cholesterol in de lipide dubbellaag de rigiditeit van liposomen in de gel-toestand vermindert en die in vloeibare toestand verhoogt. Bovendien beïnvloedde de overgangstemperatuur van de fosfolipiden de algehele liposoomstijfheid. Interessant genoeg vertoonden bijna alle formuleringen een positieve correlatie tussen liposomale rigiditeit en dendritische cel (DC)-associatie. Dioleoylfosfatidylcholine (DOPC):dioleoylfosfatidylglycerol (DOPG) liposomen vertoonden echter de hoogste associatie met DC's van alle geteste formuleringen ondanks de laagste rigiditeit, hetgeen aangeeft dat liposomale rigiditeit alleen de DC-opname niet bepaalt. We hebben een significante correlatie waargenomen tussen de rigiditeit van de liposomen en de regulatoire T-cel (Treg)-responsen *in vitro* en *in vivo*. Onze bevindingen kunnen bijdragen tot een beter begrip van de factoren die de Treg-reacties beïnvloeden, en ondersteunen een rationeel ontwerp van liposomale en andere nanodeeltjes vaccinformuleringen die gericht zijn op het verbeteren van antigeenspecifieke Treg-reacties voor de behandeling van auto-immuunziekten.

Voortbouwend op de informatie in de **hoofdstukken 2 en 3**, richten de **hoofdstukken 4 en 5** zich op het gebruik van liposomen om atherosclerose te behandelen. Atherosclerose is de overheersende onderliggende pathologie van hart- en vaatziekten, waarvan wereldwijd miljoenen mensen lijden. Lipiden in de vorm van Lagedichtheidlipoproteïne (LDL) hopen zich op in de binnenste laag van middelgrote en grote slagaders, wat leidt tot chronische ontsteking. LDL kan zich modificeren om geoxideerd LDL (oxLDL) te vormen, dat immuuncellen aantrekt en de ontsteking voortzet. Sommige van deze immuuncellen, zoals monocyten, kunnen differentiëren tot macrofagen die oxLDL kunnen fagocyteren, wat leidt tot schuimcelvorming. Manipulatie van immuuncellen, met name T-cellen of schuimcellen, kan een effectieve manier zijn om atherosclerose te behandelen. In **hoofdstuk 4** hebben we liposomen ontworpen die Tregs kunnen induceren. Liposomen waren samengesteld uit distearoylfosfatidylcholine (DSPC):distearoylfosfatidylglycerol (DSPG):cholesterol (één van de meest rigide en krachtige formuleringen in **hoofdstuk 3**) en waren geladen met een van ovalbumine afgeleide $CD4^+$ T-celepitoop. Deze liposomen bleken *in vitro* en in muizen een hoge productie van antigeenspecifieke Tregs op te wekken in vergelijking met vrij antigeen, DSPC:dipalmitoylfosfatidylserine

(DPPS):cholesterol en DSPC:dipalmitoyltrimethylammoniumpropaan (DPTAP):cholesterol liposomen. Als een atherosclerose-specifiek antigeen hebben we ApoB100 gebruikt, het eiwitcomponent van oxLDL, waarvan al werd aangetoond dat het een relevant antigeen was voor vaccinatie tegen atherosclerose. We identificeerden een major histocompatibility complex (MHC)-II-beperkt ApoB100-afgeleid peptide, aangeduid als p3500, met behulp van een peptidomics-strategie. Het laden van p3500 in DSPG-liposomen verminderde de vorming van atherosclerotische plaques, zoals gemeten door een vermindering van de totale plaquegrootte en een toename van de plaquestabiliteit.

We beschreven ook het mechanisme achter de werking van de DSPG-liposomen. Interessant is dat anionische liposomen samengesteld uit PS lijken op apoptotische cellen, aangezien PS wordt blootgesteld op het oppervlak van apoptotische cellen. Door middel van scavenger receptoren (SR)-gemedieerde opname door APC's, kunnen PS-bevattende liposomen een ontstekingsremmend effect bemiddelen. We laten zien dat DSPG-liposomen nog effectiever worden opgenomen door DC's *in vitro* dan DPPS-liposomen. We demonstreren ook een rol voor de eiwitcorona bij Treg-inductie via SR's. In fysiologische medium *in vitro* en *in vivo* vormen eiwitten een corona om liposomen heen. We vonden een significante vermindering van opname voor zowel PG- als PS-liposomen in aanwezigheid van serum wanneer SR-gemedieerde opname door DC's werd geblokkeerd, wat niet werd waargenomen in serumvrije omstandigheden, wat suggereert dat de vorming van een eiwitcorona nodig is voor liposoom-SR interacties. We hebben ons geconcentreerd op serumproteïne-complementcomponent 1 Q (C1q), omdat is aangetoond dat het aan PS in apoptotische cellen bindt en leidt tot klaring via SRs. Interessant is dat C1q ook betrokken is bij de pathologie van atherosclerose. We hebben aangetoond dat C1q aanwezig is in het eiwit corona en bindt aan anionische liposomen. De toevoeging van C1q in serumvrije omstandigheden herstelde de opname van zowel PG- als PS-liposomen volledig, terwijl specifieke depletie van C1q in serum de opname van PG-liposomen aanzienlijk verminderde. We hebben verder waargenomen dat de toevoeging van C1q de Treg-reacties verhoogt in vergelijking met serumvrije omstandigheden, maar dit effect was niet significant. Dit suggereert dat C1q gedeeltelijk verantwoordelijk is voor de Treg-inductie van zowel DSPG- als DPPS-liposomen, maar de eiwitcorona bevat waarschijnlijk meer componenten die helpen bij het induceren van Tregs. Verder zou het heel interessant zijn om te onderzoeken of er een verband bestaat tussen liposomale rigiditeit en de eiwitcorona, iets dat we niet hebben bestudeerd.

C1q bindt niet alleen SR's, maar bindt ook aan andere eiwitten, zoals het C1q-bindende eiwit, ook bekend als p32. Deze receptor komt afwijkend tot expressie in macrofagen die in de atherosclerotische plaque aanwezig zijn. Zoals hierboven vermeld, spelen macrofagen een belangrijke rol bij de pathogenese van atherosclerose, omdat ze lipiden kunnen fagocyteren en grote lipide-rijke schuimcellen kunnen worden. Deze schuimcellen kunnen niet uit de vaatwand migreren, wat leidt tot een ophoping op de plaats van de ontsteking en de vorming van een plaque. Daarom zou een geschikte behandelingsstrategie de vorming van schuimcellen voorkomen en/of omkeren, wat ons doel was in **hoofdstuk 5**. Macrofagen kunnen cholesteroltransport over hun membraan omkeren via de ATP-binding cassette (ABC) transporters ABCA1 en ABCG1. De expressie van beide transporters wordt geregeld door de lever X-receptor (LXR). Een klasse van kleine moleculen, LXR-agonisten (bijv. GW3965), kan deze receptor activeren cholesterol uit schuimcellen te pompen, waardoor migratie van deze cellen uit de plaque mogelijk

wordt. Helaas, wanneer systemisch toegediend in therapeutische doses, hebben LXR-agonisten effecten in andere organen, zoals de lever, wat leidt tot hoge triglycerideniveaus in het plasma of de lever. Lading van het LXR-agonist in liposomen kan dit probleem voorkomen. Het cyclische peptide Lyp-1 (CGNKRTRGC) bindt aan p32 en kan daarom worden gebruikt voor het targeting naar macrofagen in atherosclerotische plaques. Voor dit doel hebben we een deeltjesformulering ontwikkeld die het cyclische peptide Lyp-1 combineert met een LXR-agonist (GW3965). We hebben de kennis uit **hoofdstuk 2, 3 en 4** gebruikt om liposomen te formuleren met een lange circulatietijd en minimale immuuneffecten. Vervolgens hebben we de liposomen gefunctionaliseerd met Lyp-1, en dit leidde tot een sterk verbeterde associatie met schuimcellen *in vitro*, terwijl ze een beperkte affiniteit hadden voor macrofagen. *In vivo* zagen we retentie van liposomen in atherosclerotische plaques, en we bevestigden dat de schuimcellen in de plaques de liposomen opnemen. We hebben aangetoond dat het gebruik van een lage dosis GW3965 geladen in Lyp-1-liposomen het gehalte aan schuimcellen kan verminderen en de stabiliteit van de plaque kan verhogen, terwijl een toename van lipiden in het serum en de lever wordt vermeden. Deze bevindingen tonen aan dat het mogelijk is om het therapeutisch venster van LXR-agonisten te vergroten en kan bijdragen aan het ontwerp van andere therapieën voor atherosclerose. In het bijzonder zouden Lyp-1 gefunctionaliseerde liposomen kunnen worden gebruikt als een platform voor het afgeven van andere geneesmiddelen aan schuimcellen, zoals ontstekingsremmende geneesmiddelen.

Het laatste onderzoekshoofdstuk van dit proefschrift (**hoofdstuk 6**) richt zich op het gebruik van liposomen om kanker te behandelen, wat ook een belangrijk gezondheidsprobleem is. Kanker omvat een groep ziekten met abnormale aanhoudende celproliferatie, replicatie en overleving. T-cellen zijn ook betrokken bij kanker, omdat ze tumor-geassocieerde antigenen kunnen herkennen, echter, in tegenstelling tot atherosclerose, zijn T-celreacties bij kanker niet effectief en lijden ze aan uitputting. Zoals we in **hoofdstuk 4** hebben aangetoond, zijn DSPC:DPTAP:cholesterol liposomen effectief in het induceren van antigeenspecifieke pro-inflammatoire T-cellen en kunnen de immuunrespons leveren dat nodig is om een tumor te verwijderen. In **hoofdstuk 6** wilden we deze DSPC:DPTAP:cholesterol liposomen combineren met tumorneoepitopen als een therapeutisch vaccin tegen kanker. Neoepitopen zijn zeer interessant voor behandeling; ze zijn het gevolg van niet-synonieme somatische mutaties die coderen voor nieuwe aminozuurresiduen, wat leidt tot nieuwe peptiden die kunnen worden gepresenteerd op het celoppervlak van tumorcellen. De Hannover Medical School toonde eerder aan dat het induceren van sterke pro-inflammatoire T-celreacties tegen $Adpgk_{mut}$ (een neoepitoop) gerichte kankers kon elimineren. Dit werd bereikt door DC's van muizen te isoleren, ze *ex vivo* te pulseren met antigeen en adjuvantia en ze opnieuw te injecteren. Deze DC's kunnen vervolgens de tumorspecifieke epitopen presenteren aan T-cellen en deze primen om de kankercellen te vernietigen. Om $CD8^+$ T-celreacties te stimuleren, werden muizen na enige tijd geïnjecteerd met een mengsel van een agonistisch anti-CD40-antilichaam (Co), antigeen (A) en een toll-like receptor (TLR) ligand (T) Poly I:C. Helaas is *ex vivo* priming van DC's zeer arbeidsintensief en duur en verhindert toegankelijkheid. We stelden voor dat DSPC:DPTAP:cholesterol het antigeen op een eenvoudige manier *in situ* aan DC's kan afleveren. Eerst hebben we kale $Adpgk_{mut}$-liposomen vergeleken met liposomen die het TLR3-ligand poly (I:C), de TLR4-agonist MPLA of de stimulator of interferon genes (STING)-agonist cdiGMP bevatten. Muizen werden geprimed met

liposomen en gestimuleerd met CoAT. De cdiGMP-liposomen induceerden de sterkste antigeenspecifieke $CD8^+$ T-celrespons, dus gingen we door met deze formulering in verdere experimenten. In een directe vergelijking presteerden cdiGMP-liposomen net zo goed als DC-CoAT-vaccinatie. We hebben ook de geschiktheid van de liposomen getest met een andere neoepitoop, $Alg8_{mut}$. Net als bij $Adpgk_{mut}$ verhoogde lading van $Alg8_{mut}$ in cdiGMP-liposomen de immuunrespons aanzienlijk en leidde dit tot zeer langdurige responsen die vergelijkbaar waren met die welke werden bereikt met DC-CoAT. Vervolgens streefden we ernaar ons vaccinatieprotocol te verbeteren door $CD4^+$ T-cellen te induceren door toevoeging van het $CD4^+$ T celepitoop MTAG85B. We wilden ook het effect bestuderen van een lange versie van het $Adpgk_{mut}$ peptide op $CD8^+$ T-celresponsen. Het lange peptide verhoogde de $CD8^+$ T-celrespons tegen het minimale epitoop niet. Er was ook geen bewijs dat de door MTAG85B geïnduceerde $CD4^+$ T-celactivatie de $CD8^+$ T-celreacties stimuleerde. Vanwege het gebrek aan verbetering van de $Adpgk_{mut}$-reacties met de toevoeging van een $CD4^+$ T-celepitoop of een lang peptide, hebben we besloten een tumorstudie uit te voeren met alleen het minimale $Adpgk_{mut}$-peptide in cdiGMP-liposomen. Hier hebben we extreem hoge antigeen-specifieke responsen op het antigeen waargenomen (tot 60% van alle $CD8^+$ T-cellen reageerden op het antigeen door IFNy te produceren). We zagen tumorregressie binnen 30 dagen en 100% overleving bij muizen die de LS-CoAT-vaccinatie ontvingen. In het algemeen toont dit werk aan dat cdiGMP-liposomen een zeer krachtig platform zijn voor het laden van tumorneoepitopen om sterke antigeenspecifieke $CD8^+$ T-cellen te induceren en gevestigde tumoren te elimineren.

Toekomstperspectief

In **hoofdstuk 5** hebben we een methode onderzocht om atherosclerose te behandelen door gerichte liposomen te gebruiken om een medicijn af te leveren. In de literatuur zijn gerichte liposomen toegepast bij de behandeling van kanker en om de bloed-hersenbarrière te passeren om neurologische ziekten zoals Alzheimer te behandelen. Verschillende liposomale formuleringen, waaronder gePEGyleerde liposomen, zijn al veilig gebleken en zijn FDA- en EMA-goedgekeurd. Bovendien zijn gePEGyleerde liposomen gebruikt om prednisolon (een ontstekingsremmend medicijn) passief af te leveren aan atherosclerotische plaques bij mensen, wat aangeeft dat er enige vertaling is van dieren naar mensen.

We hebben het belang van het ontwerpen van liposomen met specifieke fysicochemische parameters benadrukt en het effect van grootte, vorm en rigiditeit samengevat in **hoofdstuk 2**. Liposomale rigiditeit was intrigerend omdat we geen substantiële literatuur over deze parameter konden vinden. Daarom wilden we ons begrip van deze parameter vergroten en een gedetailleerd onderzoek uitvoeren naar de relatie tussen liposomale rigiditeit en Treg-responsen in **hoofdstuk 3**. Hiervoor hebben we een geoptimaliseerd protocol gepresenteerd voor het meten van de rigiditeit van liposomen met behulp van AFM. Beide hoofdstukken dragen bij aan het begrip van het effect van fysicochemische parameters van liposomen op de immuunresponsen en kunnen anderen helpen bij het ontwerpen van liposomale vaccins. Er moet ook worden opgemerkt dat liposomen van nature relatief zachte deeltjes zijn, dus het is onbekend of de waargenomen immuuneffecten van toepassing zijn op een bredere reeks van rigiditeiten. Het exacte mechanisme hoe rigiditeit de immuunrespons beïnvloedt, is nog steeds niet volledig bekend en toekomstige studies die dit in meer detail onderzoeken zouden zeer

waardevol zijn.

De inductie van antigeenspecifieke Tregs is een focus van **hoofdstukken 3 en 4**. We identificeerden een peptide afgeleid van muizen-ApoB100 voor vaccinatie, maar menselijke ApoB100 epitopen zijn beschreven door anderen, en waren succesvol tegen atherosclerose in gehumaniseerde muizen. Deze peptiden kunnen geladen worden in liposomen om hun effecten en veiligheid te verbeteren. Helaas zijn er tot nu toe geen klinische studies uitgevoerd met behulp van ApoB100-afgeleide epitopen, dus er is nog steeds een vraag over de vertaling van deze studies naar een klinische setting. Omdat veel patiënten die lijden aan atherosclerose statines gebruiken, moet ook de interactie tussen statines en peptiden en/of liposomen worden bestudeerd. Het is al gedemonstreerd dat gecombineerd gebruik van statines en LDL-nabootsende liposomen ernaar leiden dat liposomen de bloed-hersenbarrière overschreden in een *in vitro* kweekmodel, wat gevaarlijk kan zijn. Verder is met behulp van fluorescentie-anisotropie aangetoond dat sommige statines een interactie aangaan met de bilaag van liposomen en hun vloeibaarheid kunnen veranderen, en daarmee hun immunogeniciteit. In tegenstelling tot onze studie met Lyp-1 liposomen, werden de tolerogene liposomen in **hoofdstuk 4** ingevoerd terwijl atherosclerose werd geïnduceerd in de muizen; het zou klinisch relevant zijn om de liposomen toe te dienen bij muizen die al atherosclerose hebben.

Immuunmodulatie was ook de focus van **hoofdstuk 6**, maar in plaats van de immuunrespons op een antigeen te onderdrukken, wilden we het juist verbeteren door het gebruik van kationische liposomen. Immunotherapie tegen kanker via DC's of T-cellen en immunotherapie tegen neoantigenen is al enkele jaren onderzocht. Wij stellen dat immuuntherapie via liposomen een snellere, goedkopere behandelingsstrategie is. Nanodeeltjes, waaronder liposomen, zijn inderdaad al effectief gebleken bij kankertherapie en ons werk draagt bij aan dit bewijs. Technieken om antigenen te identificeren die specifiek zijn voor ziekten, inclusief het in dit proefschrift geïdentificeerde atherosclerose-antigeen p3500, zijn in de laatste jaren verbeterd. In combinatie met het vermogen van liposomen om een breed scala aan epitopen te laden, zouden liposomen een belangrijke speler kunnen zijn in de toekomst van gepersonaliseerde therapieën. Het moet gemeld worden dat, hoewel we geen toxiciteit hebben waargenomen in onze dierstudies, kationische fosfolipiden bij hoge doses toxiciteit induceren in *in vivo* diermodellen en *in vitro* menselijke cellen. Daarom moet de verdere ontwikkeling van deze liposomen er altijd naar streven de dosis van de kationische fosfolipiden in de liposomen te minimaliseren. Om door te gaan naar klinische proeven moeten meer toxiciteitsstudies worden uitgevoerd in diermodellen om te testen of de liposomen veilig zijn om te gebruiken, op korte of lange termijn.

Afgezien van de noodzaak om de veiligheid van de liposomen voor klinisch gebruik te testen, vereist testen bij mensen grote hoeveelheden liposomen en de geladen inhoud (medicijn, peptide, adjuvans). Schaalvergroting is niet alleen potentieel duur (hoewel inkapseling van een verbinding in een (gericht) nanodeeltje de vereiste dosis en dus kosten sterk verlaagt), maar het kan de fysicochemische eigenschappen van de liposomen veranderen. Dit geldt ook voor de GMP-productie van liposomen. Het is aangetoond dat methoden zoals micro-fluidics en ethanolinjectie reproduceerbaar grote hoeveelheden liposomen kunnen produceren onder GMP-omstandigheden. Er moet echter een gedetailleerde evaluatie van het effect van de productiemethode op liposomale eigenschappen worden uitgevoerd.

Curriculum Vitae

Naomi Benne was born on the 12th of March, 1993 in Heemskerk, the Netherlands. She obtained a bilingual International Baccalaureate diploma (English and German) from the International School Rheintal in Buchs, St. Gallen, Switzerland in 2010. She obtained a BSc diploma in Bio-Pharmaceutical Sciences from Leiden University in 2013, where she performed her bachelor project titled "Incorporation of TLR Ligands in Liposomes to Improve Dendritic Cell Activation in a Therapeutic Peptide Vaccine" at the Division of Drug Delivery Technology under the supervision of Eleni Varypataki. She continued this project during her 9 months master internship, writing the thesis "Development, Characterisation and Evaluation of Synthetic Long Peptide-Based Liposomal Formulations". She performed her 6 months master internship at Octoplus in Leiden, and wrote a thesis titled "A Novel Formulation Process for the Preparation of Surface Eroding PLGA-Based Microparticles Using an Ultrasonic Nozzle". She obtained her MSc diploma in Bio-Pharmaceutical Sciences in 2015. In August 2015 she started her PhD project titled "Vaccination and Targeted Therapy Using Liposomes; Opportunities for Treatment of Atherosclerosis and Cancer" under the supervision of Dr. Bram Slütter, Prof. Dr. Wim Jiskoot and Prof. Dr. Johan Kuiper at the Division of Biotherapeutics at the Leiden Academic Center for Drug Research. In December 2019, she started as a postdoctoral researcher in the group of Prof. Dr. Femke Broere at the Division of Immunology, Department of Infectious Diseases and Immunology, Faculty of Veterinary Medicine, Utrecht University, working on developing tolerogenic vaccines to treat rheumatoid arthritis.

List of Publications

Benne, N., van Duijn, J., Kuiper, J., Jiskoot, W. & Slütter, B. Orchestrating immune responses: How size, shape and rigidity affect the immunogenicity of particulate vaccines. J Control Release 234, 124-134, (2016).

Varypataki, E. M., **Benne, N**., Bouwstra, J., Jiskoot, W. & Ossendorp, F. Efficient eradication of established tumors in mice with cationic liposome-based synthetic long-peptide vaccines. Cancer Immunology Research 5, 222-233, (2017).

Benne, N., van Duijn, J., Lozano Vigario, F., Leboux, R. J. T., van Veelen, P., Kuiper, J., Jiskoot, W. & Slütter, B. Anionic 1,2-distearoyl-sn-glycero-3-phosphoglycerol (DSPG) liposomes induce antigen-specific regulatory T cells and prevent atherosclerosis in mice. J Control Release 291, 135-146, (2018).

van Duijn, J., Kritikou, E., **Benne, N**., van der Heijden, T., van Puijvelde, G. H., Kröner, M. J., Schaftenaar, F. H., Foks, A. C., Wezel, A., Smeets, H., Yagita, H., Bot, I., Jiskoot, W., Kuiper, J. & Slütter, B. CD8+ T-cells contribute to lesion stabilization in advanced atherosclerosis by limiting macrophage content and CD4+ T-cell responses. Cardiovascular Research 115, (2018).

van Duijn, J., van Elsas, M., **Benne, N**., Depuydt, M., Wezel, A., Smeets, H., Bot, I., Jiskoot, W., Kuiper, J. & Slütter, B. CD39 identifies a microenvironment-specific anti-inflammatory CD8+ T-cell population in atherosclerotic lesions. Atherosclerosis 285, 71-78, (2019).

Benne, N., Leboux, R. J. T., Glandrup, M., van Duijn, J., Vigario, F. L., Neustrup, M. A., Romeijn, S., Galli, F., Kuiper, J., Jiskoot, W. & Slütter, B. Atomic force microscopy measurements of anionic liposomes reveal the effect of liposomal rigidity on antigen-specific regulatory T cell responses. Journal of Controlled Release 318, 246-55, (2020).

Benne, N., Martins Cardoso, R., Boyle, A. L., Kros, A., Jiskoot, W., Kuiper, J., Bouwstra, J., van Eck, M. & Slütter, B. Complement receptor targeted liposomes encapsulating the liver X receptor agonist GW3965 accumulate in and stabilize atherosclerotic plaques. Advanced Healthcare Materials, 9, (2020).